

SECONDARY NATURAL GAS RECOVERY: TARGETED TECHNOLOGY APPLICATIONS FOR
INFIELD RESERVE GROWTH IN FLUVIAL RESERVOIRS IN THE FRIO FORMATION,
SEELIGSON FIELD, SOUTH TEXAS

TOPICAL REPORT

(September 1988 - December 1991)

Prepared by

William A. Ambrose, Jeffry D. Grigsby, Bob A. Hardage, Lee A. Jirik, and Raymond A. Levey

Bureau of Economic Geology

W.L. Fisher, Director

The University of Texas at Austin

Austin, Texas 78713-7508

and

R. E. Collins and Mark Sippel

Research and Engineering Consultants, Inc.

and

W. E. Howard and Jose Vidal

ResTech, Inc.

for

GAS RESEARCH INSTITUTE

Contract No. 5088-212-1718

Bruce C. Smith, GRI Project Manager

January 1992

DISCLAIMER

LEGAL NOTICE This report was prepared by the Bureau of Economic Geology as an account of work sponsored by the Gas Research Institute (GRI). Neither GRI, members of GRI, nor any person acting on behalf of either:

- a. Makes any warranty or representation, expressed or implied, with respect to the accuracy, completeness, or usefulness of the information contained in this report, or that the use of any apparatus, method, or process disclosed in this report may not infringe privately owned rights; or
- b. Assumes any liability with respect to the use of, or for damages from the use of, any information, apparatus, method, or process disclosed in this report.

RESEARCH SUMMARY

- Title** Secondary natural gas recovery: targeted technology applications for infield reserve growth in fluvial reservoirs in the Frio Formation, Seeligson field, South Texas
- Contractor** Bureau of Economic Geology, The University of Texas at Austin, GRI Contract No. 5088-212-1718, entitled "Secondary Natural Gas Recovery: Targeted Technology Applications for Infield Reserve Growth."
- Principal Investigator** Robert J. Finley, Edgar Guevara, and Raymond A. Levey
- Report Period** September 1988 - December 1991
- Objectives** The objective of this report is to better enable natural gas producers to develop additional natural gas resources in fields with conventional porosity and permeability by describing and evaluating the effect of reservoir heterogeneities in a mature gas field (Seeligson field) of the Oligocene middle Frio Formation in the Frio Fluvial/Deltaic Sandstone along the Vicksburg Fault Zone (FR-4) play in South Texas.
- Technical Perspective** A major goal of the Infield Natural Gas Reserve Growth Joint Venture project is to assess the potential for increasing recoverable reserves of natural gas, mainly in reservoirs with conventional porosity and permeability. These reservoirs commonly contain incompletely drained compartments that are defined primarily by depositional facies heterogeneity and secondarily by structural heterogeneity and local variations in porosity and permeability. At Seeligson field and in other fields in the FR-4 play, complex fluvial reservoirs contain opportunities for identifying potentially undrained reservoir compartments. Remaining natural gas in these compartments can be contacted either by recompletion of old wells that have bypassed these compartments or by infill wells that contact compartments not drained by current well spacing. Exploration for compartments or bypassed gas zones in old fields can be improved using detailed geologic studies that integrate engineering and petrophysical methods.
- Results** This report summarizes the results of a 3-yr research program including results from a project experiment site in fluvial reservoirs in Seeligson field. These reservoirs consist of channel-fill and crevasse-splay sandstones, levee siltstones, and floodplain siltstones and mudstones. Although Seeligson field contains poorly contacted reservoir compartments, its potential for secondary gas recovery in the middle Frio Formation is less than that of other fields in the FR-4 play. Seeligson field contains well-connected fluvial sandstones that have been effectively drained by relatively greater numbers of completions. In contrast, many other fields in the play (Stratton and Agua Dulce) contain less intensively completed, isolated fluvial sandstones that represent uncontacted reservoir compartments. Differences in fluvial reservoir architecture and completion practices must be considered as an important part of any infield exploration program for fields in the FR-4 play and in other gas plays.

Bypassed gas zones were identified by reservoir-characterization methods and state-of-the-art petrophysical techniques. The reserve-growth potential of bypassed and untapped zones was evaluated using an advanced cased-hole logging program. Pulsed-neutron, gamma-ray, and acoustic logs were recorded in selected cased holes and interpreted using new techniques that demonstrate their effectiveness in identifying gas-bearing zones. Five successful recompletions were made in two zones (14B and 19B) that have produced more than 1.4 Bcf of additional gas from poorly drained reservoir compartments in approximately 18 mo. Poorly drained compartments in the 14B and 19B reservoirs occur in sandstones bounded by channel-on-channel contacts where partial permeability barriers are inferred to exist along mudstone-intraclast zones.

Other reservoir zones at Seeligson field are stratigraphically complex but were initially developed as homogeneous reservoirs. For example, the Zone 15 and 19C reservoirs appear to be relatively continuous but have a high degree of internal architectural complexity and contain a limited number of compartments with uncontacted gas reserves. Anomalous bottom-hole pressures occur in recompleted wells in Zone 15 that contact incompletely drained channel-fill deposits. Although there appear to be few compartments between closely spaced wells (200 to 1,000 ft [61 to 305 m]) in the Zone 15 reservoir, even between wells in different facies (for example, proximal splay and channel fill), compartments may be recognizable at a larger scale (for example, in channel-fill complexes that are separated from each other by thousands of feet of mudstone-rich floodplain and distal-splay deposits). Drainage in the Zone 15 reservoir has occurred between (1) small splay compartments that are well connected to channel-fill compartments and (2) along depositional axes of channel-fill complexes. However, well-separated channel-fill complexes should be targeted for recompletions or infill wells because these complexes have been poorly drained by wells in other channel-fill complexes thousands of feet away, even though the distant completions are at the same stratigraphic level.

Technical Approach

The research integrated advanced geologic mapping, petrophysical techniques, engineering analysis, and geophysical measurements to evaluate controls of both interreservoir and intrareservoir heterogeneity on the recovery of incremental gas. A total of eight tasks were undertaken to meet the major project objectives. Tasks (1) through (4) were undertaken in an early phase of the research that was conducted as part of a GRI co-production study, whereas tasks (5) through (8) were undertaken later as part of the secondary-gas recovery project. These tasks were:

- (1) To evaluate fields and reservoirs in the FR-4 play that have potential for containing bypassed gas-bearing zones and uncontacted compartments.
- (2) To select a field in the play for study and to develop a cooperative relationship with the field operator to facilitate data acquisition and to formulate recompletion strategies.
- (3) To provide a detailed geological characterization of selected gas reservoirs in the field and to describe depositional and diagenetic controls on reservoir geometry.

(4) To identify potential reservoir compartments containing uncontacted or bypassed gas and to recommend these recompletion targets to the field operator for evaluation with cased-hole logging.

(5) To use the results of cased-hole logging to evaluate reserve additions in bypassed zones in the field.

(6) To select a site in the field to conduct an experiment from which reservoir heterogeneity could be inferred from pressure-communication tests.

(7) To characterize and contrast different scales of reservoir heterogeneity in the field from seismic, geologic, engineering, and petrographic data.

(8) To evaluate the gas-reserve growth potential of Seeligson field by comparing and contrasting completion and production data in the field to other fields in the FR-4 play.

Implications

CONTENTS

EXECUTIVE SUMMARY	1
OBJECTIVES.....	3
INTRODUCTION.....	4
GEOLOGIC SETTING.....	11
Frio Fluvial/Deltaic Sandstone along the Vicksburg Fault Zone (FR-4) Play.....	11
Structural Framework.....	15
Stratigraphic Framework.....	18
Nonunit Reservoirs (Upper Vicksburg and Lower Frio Formations).....	20
Unit Reservoirs (Middle Frio Formation).....	20
Fluvial Facies	23
Channel Fill.....	23
Splay.....	25
Levee.....	26
Floodplain	28
Subsurface Mapping of Fluvial Deposits.....	29
RESERVOIR INVESTIGATIONS	30
Reservoir Nomenclature.....	30
Zone 19C Reservoir.....	31
Depositional Environments.....	31
Potential for Reservoir Compartments.....	39
Pressure Data.....	43
Rate Data.....	46
Well Tests	46
Results	49
Zone 19B Reservoir.....	50

Depositional Environments.....	50
Potential for Reservoir Compartments.....	50
Zone 18A Reservoir.....	56
Depositional Environments.....	56
Potential for Reservoir Compartments.....	56
Zone 17 Reservoir.....	59
Depositional Environments.....	59
Potential for Reservoir Compartments.....	59
Zone 15 Reservoir.....	62
Depositional Environments.....	62
Potential for Reservoir Compartments.....	68
Pressure Data.....	68
Rate Data.....	68
Well Tests.....	72
Results.....	80
Zone 14B Reservoir.....	81
Depositional Environments.....	81
Potential for Reservoir Compartments.....	83
Summary of Facies-Related Production Performance.....	83
Facies-Related Permeability.....	86
Effective Drainage Area.....	86
Drainage Volumes of Gas Completions in the Zone 15 and 19C Reservoirs.....	88
RESERVOIR SANDSTONE COMPOSITION AND POROSITY DISTRIBUTION.....	88
Sandstone Composition.....	88
Detrital Framework Mineralogy.....	89
Authigenic Mineralogy.....	91
Reservoir Quality.....	95

Porosity Distribution	100
Methods	102
Total and Effective Porosity from Core.....	102
Humidity-Dried Samples.....	102
Capillary Pressure.....	104
Cation Exchange Capacity	106
Total and Effective Porosity from Logs	110
Discussion.....	111
PETROPHYSICAL RESEARCH	115
Open-Hole Petrophysical Research.....	116
Data Acquisition	116
Development of the Petrophysical Model.....	119
Core Mineralogy.....	120
Determination of Shale Volume	120
Determination of Porosity	120
Determination of Formation Water Resistivity	121
Cementation Exponent "m" and Saturation Exponent "n"	122
Determination of Formation Water Saturation.....	122
Application.....	122
Quick-Evaluation Techniques.....	123
Problems Encountered.....	128
Pressure Prediction from Pulsed-Neutron Logs.....	130
Cased-Hole Petrophysical Research.....	133
Previous Research	133
Oryx Three-Well Project	135
Determination of Shale Volume and Lithology.....	139
Determination of Porosity	139

Gas Indicators.....	140
Water Saturation.....	142
Borehole Gravity Survey.....	142
Temperature, CET, and Noise Log.....	144
Limitations.....	147
Results of Petrophysical Research.....	147
THREE-DIMENSIONAL SEISMIC PROGRAM.....	149
Introduction.....	149
Three-Dimensional Seismic Amplitude Maps.....	149
AVO Maps.....	151
Fundamental Assumptions and Approximations.....	152
Field Geometries Used in the Seeligson Three-Dimensional Seismic Survey.....	154
Receiver Lines.....	154
Receiver Arrays.....	155
Recording System.....	155
Source Arrays.....	155
Analysis of the Three-Dimensional Receiver and Source Array Responses.....	160
Source Radiation Patterns.....	161
Receiver Antenna Patterns.....	167
Common Midpoint Coverage.....	168
Stacking Fold.....	168
Data Processing.....	171
Surface-Consistent Processes.....	172
Dip Moveout.....	177
GAS RESERVOIR HETEROGENEITY AND RESERVE GROWTH POTENTIAL.....	178
Stratigraphic Architecture.....	178
Scales of Heterogeneity.....	183

Secondary Gas Recovery Potential of Seeligson Field and Related Fluvial-Deltaic Reservoirs.....	189
CONCLUSIONS.....	196
ACKNOWLEDGMENTS.....	198
REFERENCES.....	199
APPENDICES	
1. Evaluation of results.....	206
2. Seeligson No. 1-89 well borehole gravity log analysis and interpretation.....	207

Figures

1. Location and extent of Seeligson field.....	5
2. Center of Seeligson field, showing well numbers, cored wells, three-dimensional seismic grid, and map area of the 14B and 19B reservoirs in the east-central part of the field.....	6
3. Major types of reservoir compartments.....	8
4. Location of fields in the FR-4 play.....	9
5. Frio depositional systems in the Texas Gulf Coast.....	12
6. Three-dimensional facies relationships and characteristic SP log responses in middle and upper Frio fluvial reservoirs in Seeligson field.....	13
7. Structure map of Seeligson field.....	16
8. Structural seismic dip section E-E' across Seeligson field with zero-offset VSP through the Mobil No. 248 Seeligson well.....	17
9. Structural dip section G-G' in Seeligson field.....	19
10. Cross section A-A' in Seeligson field.....	21
11. Type log in Seeligson field.....	22
12. Core description and SP and resistivity log response of the Zone 15 reservoir in the Sun No. 141 P. Canales well.....	24
13. Core description and porosity and permeability profiles in the Zone 20B reservoir in the Sun No. 16-125 A. A. Seeligson well.....	27
14. Stratigraphic cross section in the Zone 19C reservoir in north Seeligson field.....	32

15.	SP log-facies map of the lower Zone 19C genetic unit in north-central Seeligson field.....	33
16.	SP log-facies map of the middle Zone 19C genetic unit in north-central Seeligson field.....	34
17.	Net-sandstone thickness map of the upper Zone 19C genetic unit in north-central Seeligson field.....	35
18.	SP log-facies map of the upper Zone 19C genetic unit in north-central Seeligson field.....	37
19.	Three-dimensional seismic map of the upper Zone 19C genetic unit in north-central Seeligson field.....	38
20.	Topology of positive AVO response near the level of the Zone 19C reservoir.....	40
21.	VSP images extending away from the Mobil No. 247 Seeligson well on cross section F-F'.....	41
22.	Production data for wells in the Zone 19C reservoir in Tract 1 in north Seeligson field.....	42
23.	Location of wells completed in the Zone 19C reservoir in Tract 1 in north Seeligson field.....	44
24.	Pressure data in wells in the Zone 19C reservoir in Tract 1 in north Seeligson field.....	45
25.	Stratigraphic cross section D-D' in the undivided Zone 19C reservoir in north Seeligson field.....	47
26.	Net-sandstone thickness map of the lower Zone 19B genetic unit in east-central Seeligson field.....	51
27.	Net-sandstone thickness map of the middle Zone 19B genetic unit in east-central Seeligson field.....	52
28.	Stratigraphic dip section B-B' in the lower and middle Zone 19B genetic units in east-central Seeligson field.....	53
29.	Combined cased-hole log suite, Oryx No. 1-168 Seeligson well.....	54
30.	Net-sandstone thickness map of the Zone 18A reservoir in east-central Seeligson field.....	57
31.	Inferred depositional environments in the Zone 18A reservoir in east-central Seeligson field.....	58
32.	Net-sandstone thickness map of the Zone 17 reservoir in east-central Seeligson field.....	60
33.	SP log-facies map of the Zone 17 reservoir in east-central Seeligson field.....	61
34.	Fence diagram of the Zone 15 reservoir in central Seeligson field.....	63

35.	Net-sandstone thickness map of the Zone 15B genetic unit in north-central Seeligson field.....	64
36.	SP log-facies map of the Zone 15B genetic unit in north-central Seeligson field.....	65
37.	Net-sandstone thickness map of the Zone 15C genetic unit in north-central Seeligson field.....	66
38.	SP log-facies map of the Zone 15C genetic unit in north-central Seeligson field.....	67
39.	Completions in the Zone 15 reservoir in Tract 1 in north Seeligson field.....	69
40.	Pressure versus cumulative production and pressure-decline plot for the undivided Zone 15 reservoir.....	70
41.	Production rate versus time and pressure versus cumulative production for wells in the Zone 15 reservoir.....	71
42.	Gas-production rate versus time in Tract 1 wells in the Zone 15 reservoir and pressure versus time in the Oryx No. 1-100 well.....	73
43.	SP log-facies map of the undivided Zone 15 reservoir in north-central Seeligson field.....	74
44.	Interval with wireline RFT measurements in the undivided Zone 15 reservoir in the Mobil No. 248 A. A. Seeligson well.....	76
45.	Cross section C-C' in the Zone 15 reservoir.....	77
46.	Bottom-hole pressure versus time for 11 wells that have produced from the Zone 15 reservoir at Seeligson field.....	79
47.	SP log-facies and net-sandstone thickness map of the Zone 14B genetic unit in east-central Seeligson field.....	82
48.	Combined logging suite of pulsed-neutron log and sonic log in the Oryx No. 1-168 Seeligson well and combined cased-hole log suite in the Oryx No. 1-94 Seeligson well.....	84
49.	Detrital composition of middle Frio sandstones in Seeligson field.....	90
50.	Photomicrograph of pedogenic calcite cement.....	92
51.	Photomicrograph of sparry calcite cement.....	93
52.	Photomicrograph showing the development of oversized, op, and intragranular, ip, secondary pores in middle Frio sandstones.....	94
53.	Photomicrograph of kaolinite, k, filling secondary pores.....	96
54.	Generalized diagenetic sequence in middle Frio sandstones in Seeligson field.....	97
55.	Cross plot of log permeability versus porosimeter porosity for sandstones of the middle Frio Formation.....	98

56.	Cross plot of calcite cement versus porosimeter porosity and log permeability for middle Frio sandstones in Seeligson field.....	99
57.	Distribution of porosity and minerals beginning with rock consisting of a clay-free sandstone reservoir and progressing to clay-rich shale.....	101
58.	Comparison of capillary pressure data for air brine and air mercury in one of the sandstone samples	107
59.	Comparison of capillary pressure data for air brine and air mercury in one of the shale samples	108
60.	Total porosity, effective porosity, and clay content measured on cores and computed from log analysis	113
61.	Total porosity, effective porosity computed from logs.....	114
62.	Induction log from the pay interval of the Mobil No. 247 Seeligson well.....	117
63.	Illustration of R_{wa} interpretation in the Sun No. 141 Canales well.....	125
64.	Gas effect from density-neutron logs in the Zone 15 reservoir in the Sun No. 141 Canales well	126
65.	Gas effect from neutron-sonic log in the Zone 15 reservoir in the Sun No. 141 Canales well	127
66.	Full waveform sonic log of the Mobil No. 247 Seeligson well	129
67.	Sequential formation pressure tests taken at 7,323 ft in the Mobil No. 247 Seeligson well.....	131
68.	Formation pressure test at 7,341 ft in the Mobil No. 247 Seeligson well	132
69.	Relationship between pulsed-neutron and formation pressure in the Mobil No. 248 Seeligson well	134
70.	The Zone 15 reservoir is gas bearing in the 1-89 well, as indicated by porosity logs and borehole gravity survey and pulsed-neutron count rates.....	137
71.	Pressure prediction from pulsed-neutron count rates indicates that the Zone 15 reservoir may be partly depleted in the 1-89 well.....	138
72.	Reliable compressional travel times obtained through casing.....	141
73.	The CET acoustic caliper, showing casing damage from 5,165 to 5,210 ft in the 1-89 well.....	145
74.	The CET cement evaluation log showing that the perforated and squeezed interval from 5,165 to 5,210 ft is adequate but marginal above and below the squeeze.....	146
75.	Field geometry used to record a three-dimensional surface seismic grid in part of Seeligson field, Jim Wells County.....	150

76.	The fundamental source assumption involved in three-dimensional seismic data acquisition and the fundamental receiver assumption.....	153
77.	Geometrical parameters used to construct individual source and receiver lines in the Seeligson three-dimensional seismic data grid.....	156
78.	Distribution of vibrator sweep energy as a function of frequency and the nonlinear time functions controlling the pad frequency and the hydraulic drive level that produces the frequency-dependent energy distribution.....	159
79.	Mathematical models used to investigate the three-dimensional directional properties of the Seeligson receiver and source arrays.....	162
80.	Shape of radiation pattern produced by the four-vibrator source array used for the Seeligson three-dimensional seismic program.....	163
81.	The shape of the 10-Hz antenna pattern provided by the twelve-element receiver arrays.....	164
82.	The shape of the 40-Hz antenna pattern provided by the twelve-element receiver array.....	165
83.	The shape of the 70-Hz antenna pattern provided by the twelve-element receiver arrays.....	166
84.	Simplified picture of the maximum stacking fold achieved in the Seeligson three-dimensional seismic survey.....	169
85.	Black and white copy of the original color display of stacking fold within the Seeligson grid.....	170
86.	Wavefield recorded by all 504 Seeligson receiver arrays when the vibrators were positioned at the westernmost source point of the data grid.....	174
87.	Wavefield recorded by all 504 Seeligson receiver arrays when the vibrators were positioned at the center source point of the data grid.....	175
88.	Wavefield recorded by all 504 Seeligson receiver arrays when the vibrators were positioned at the easternmost source point of the data grid.....	176
89.	Fluvial architectural styles in the middle Frio Formation in the FR-4 play.....	179
90.	Comparison of fluvial architectural style between Seeligson and Stratton fields.....	182
91.	Four scales of reservoir heterogeneity.....	184
92.	Six-fold hierarchy of heterogeneity in fluvial systems.....	185
93.	Distribution of thickness of individual sandstones in Stratton and Seeligson fields.....	190
94.	Generalized illustration of field- and reservoir-development parameters.....	192
95.	Distribution of individual-sandstone thickness and composite-sandstone thickness in selected middle Frio reservoirs in Seeligson field.....	193

96. Reservoir nomenclature at Stratton field in the FR-4 play.....194

Tables

1. Successful recompletions in the Zone 14B and 19B reservoirs in east-central Seeligson field.....55

2. Permeability measurements in the Zone 15 and 19C reservoirs87

3. Humidity-dried and convection-dried core porosity results from shale samples, beginning with sample no. 1S103

4. Summary of average bulk volumes for the cored interval.....105

5. Comparison of humidity-dried porosity with effective porosity from capillary pressure, including the resulting bulk volume mercury and air.....109

6. Parameters utilized for computation of the well logs.....112

7. Log types available for the 1-85, 1-89, and 1-171 wells at Seeligson field.....118

8. Data processing sequence used to produce three-dimensional imagery at Seeligson field.....173

9. Range of scales of reservoir heterogeneities in fluvial sandstones illustrated in figure 91.....186

10. Field-size, drilling, completion, and production data from the major fields in the FR-4 play195

EXECUTIVE SUMMARY

The Lower-48 States contain approximately 800 Tcf of technically recoverable natural gas resources in reservoirs with conventional porosity and permeability (Finley and others, 1988). Many of these reservoirs have incompletely drained compartments that are defined primarily by depositional facies heterogeneity and secondarily by structural heterogeneity and local variations in porosity and permeability. Additional natural gas in these compartments can be contacted and economically produced by recompleting old wells that have bypassed these compartments or by infill wells that contact compartments undrained by current well and completion spacing. Infield exploration in mature gas fields can be improved using a combination of detailed geologic studies that integrate engineering, petrophysics and reservoir geophysics.

This report summarizes the results of a 3-yr research program including results from a project experiment site in fluvial gas reservoirs in Seeligson field, in the productive Frio Fluvial/Deltaic Sandstone along the Vicksburg Fault Zone play in South Texas. A great potential for secondary recovery of gas resources exists in the South Texas Gulf Coast, where stratigraphically complex Tertiary strata contain hundreds of lenticular sandstone reservoirs interbedded with mudstone. Seeligson field produces gas from multiple, stacked fluvial sandstones. The field provides an excellent opportunity for studying heterogeneous fluvial reservoirs and for integrating geological reservoir characterization and cased-hole log-evaluation techniques to identify potentially bypassed-gas zones and poorly drained reservoir compartments.

Bypassed-gas zones in Seeligson field were identified with advanced reservoir-characterization methods and state-of-the-art petrophysical techniques. Recompletion opportunities exist in poorly drained compartments in channel-fill sandstones that are bounded vertically by channel-on-channel contacts, where potential permeability barriers are inferred along clay mudstone-intraclast zones and laterally where lenticular belts of channel-fill sandstones are separated from each other by thousands of feet of low-permeability floodplain mudstone. Five successful recompletions were made in two reservoirs (Zones 14B and 19B) that

were identified as gas saturated from cased-hole logs. The recompleted wells together produced more than 1.4 Bcf of additional gas in approximately 18 mo. In addition, anomalously high bottom-hole pressures (928 to 1,111 psi; 2 to 3 times as high as the fieldwide average) were observed in some recompleted wells in the Zone 15 reservoir, which contains incompletely drained channel-fill deposits, laterally separated by other channel-fill deposits by thousands of feet of floodplain mudstone. Two of these wells each produced approximately 1 Bcf after they were recompleted. The Zone 15 reservoir has been drained between (1) small splay compartments that are well connected to channel-fill compartments and (2) along depositional axes of channel-fill complexes. However, well-separated channel-fill complexes can be successfully targeted for recompletions or infill wells because these complexes have been poorly drained by wells in other channel-fill complexes thousands of feet away, even though the distant completions are at the same stratigraphic level.

Seismic techniques for advanced reservoir characterization include three-dimensional seismic maps that help resolve the shape and extent of reservoir compartments and allow strategic positioning of development wells. Three-dimensional slices of reflection amplitude and positive AVO response across gas horizons indicate that individual channel-fill deposits and reservoir compartments in Seeligson field are less laterally extensive than previously inferred from net-sandstone and log-facies maps from well log data. Three-dimensional seismic maps in Seeligson and other fields should help better define reservoir compartments.

Although Seeligson field contains poorly contacted reservoir compartments, its potential for secondary gas recovery in the middle Frio Formation is less than that of other fields in the Frio fluvial-deltaic play. Seeligson field contains well-connected fluvial sandstones that have been effectively drained by relatively greater numbers of completions. In contrast, many other fields in the play (Stratton and Agua Dulce) contain less intensively completed, isolated fluvial sandstones that represent uncontacted reservoir compartments. Differences in fluvial reservoir architecture and completion practices must be considered as an important part of any infield exploration program for fields in the Frio fluvial-deltaic play and in other gas plays.

OBJECTIVES

This report summarizes three years of research of Frio gas reservoirs at Seeligson field. The objectives of this research were to identify recompletion targets in heterogeneous reservoirs in a major gas play, the Frio Fluvial/Deltaic Sandstone along the Vicksburg Fault Zone (FR-4) play in South Texas, and characterize the potential for contacting bypassed gas and poorly drained reservoir compartments in these reservoirs. Eight critical tasks were chosen to meet these objectives. Tasks (1) through (4) were undertaken in an early phase of the research (Jirik and others, 1989) that was conducted as part of a Gas Research Institute (GRI) co-production study, whereas tasks (5) through (8) were later undertaken as part of a GRI secondary-gas study. These tasks were:

- (1) To evaluate fields and reservoirs in the FR-4 play that have potential for containing bypassed gas-bearing zones and uncontacted compartments.
- (2) To select a field in the play for study and to develop a cooperative relationship with the field operator to facilitate data acquisition and to formulate recompletion strategies.
- (3) To provide a detailed geological characterization of selected gas reservoirs in the field and to describe depositional and diagenetic controls on reservoir geometry.
- (4) To identify potential reservoir compartments containing uncontacted or bypassed gas and to recommend these recompletion targets to the field operator for evaluation using cased-hole logging.
- (5) To use the results of cased-hole logging to evaluate reserve additions in bypassed zones in the field.
- (6) To select a site in the field to conduct an experiment from which reservoir heterogeneity could be inferred from pressure-communication tests.

- (7) To characterize and contrast different scales of reservoir heterogeneity in the field from seismic, geologic, engineering, and petrographic data.
- (8) To evaluate the gas-reserve growth potential of Seeligson field by comparing and contrasting completion and production data in the field to other fields in the FR-4 play.

INTRODUCTION

More than 200 gas fields in South Texas were evaluated as potential study areas. South Texas leads the state in nonassociated-gas production, which is from multiple, stacked, heterogeneous fluvial and deltaic Tertiary reservoirs in regional growth-fault zones. Data from the Railroad Commission of Texas (RRC) and commercial sources were compiled to determine field location and size, reservoir age, and cumulative production. Seeligson field was selected because of its geologic setting, stratigraphic and structural framework, production history, and availability of data. The middle Frio Formation in Seeligson field was selected because it is highly productive and possesses lithologic heterogeneity sufficient to result in bypassed gas zones and untapped or incompletely drained reservoir compartments. The willingness of Oryx Energy Company and Mobil Exploration and Producing U.S., Inc., to participate in the cooperative program also played an important part in the selection.

Seeligson field is located in Jim Wells and Kleberg Counties, South Texas, north of the town of Premont (fig. 1). The field encompasses more than 40 mi² (102 km²) and contains more than 1,000 wells. Cumulative production totals more than 2.5 Tcf of gas from 130 Frio and Vicksburg fluvial and deltaic sandstone reservoirs. This study focused primarily on unitized Frio reservoirs from an 8.5-mi² (22.0-km²) area in the field (figs. 1 and 2).

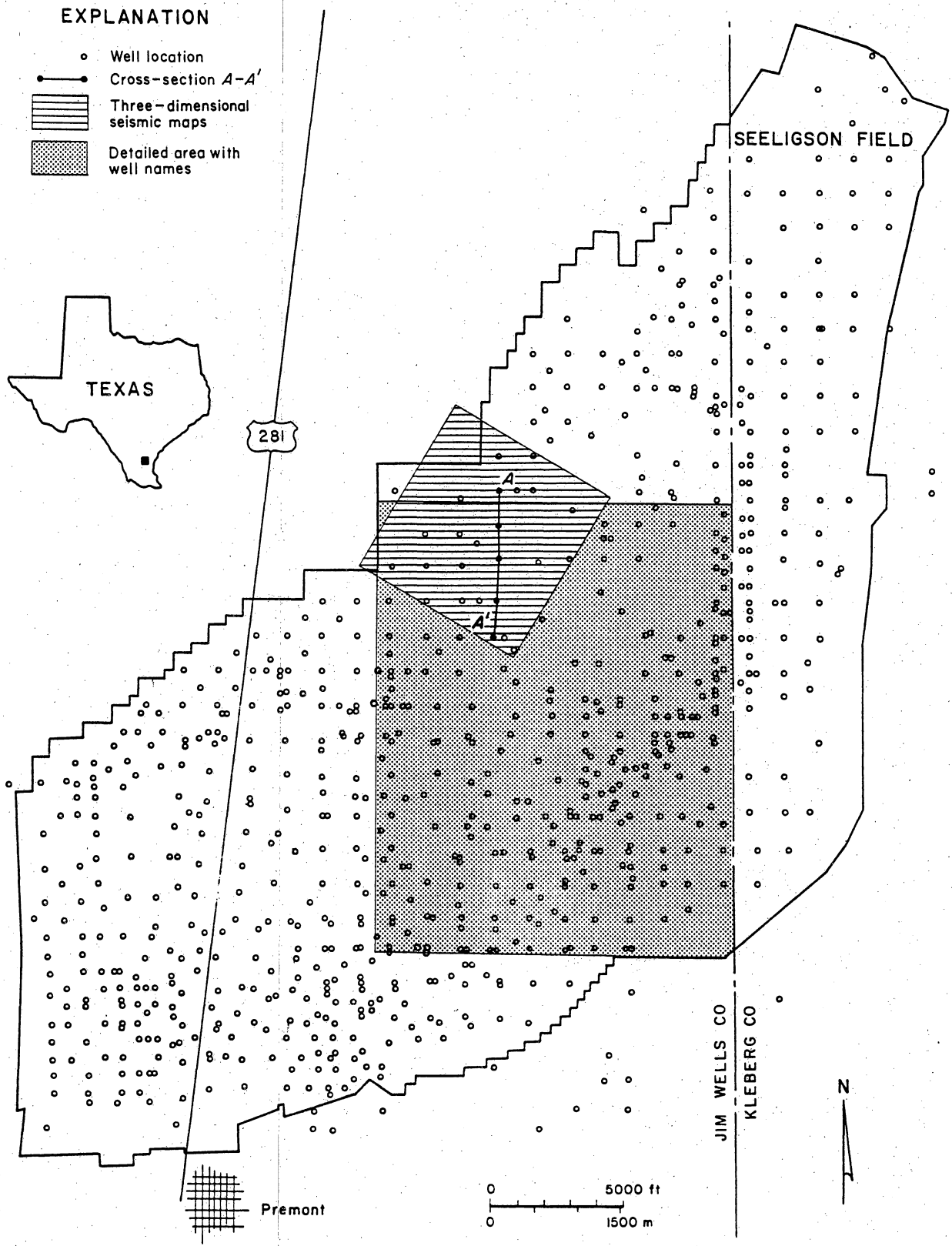
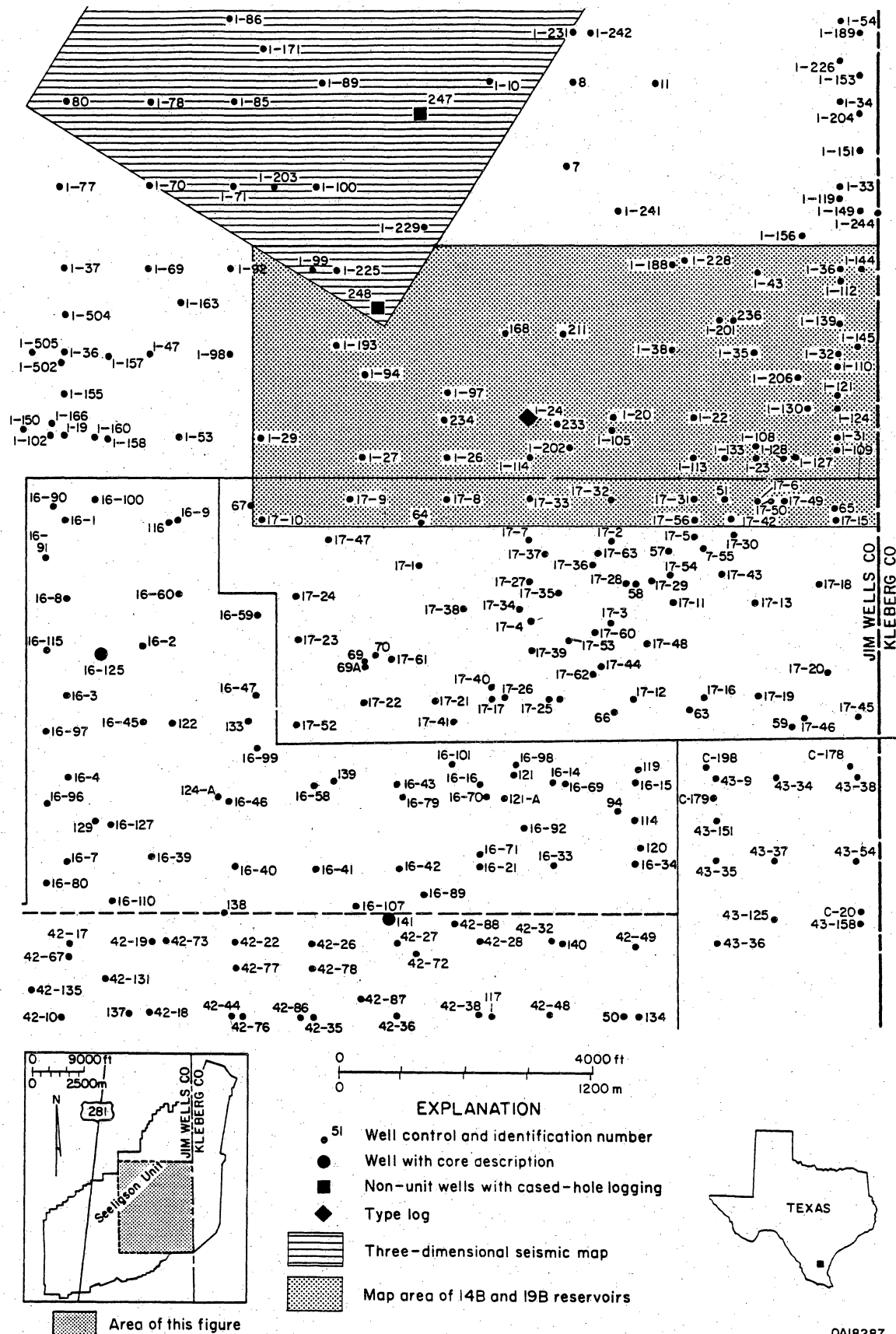


Figure 1. Location and extent of Seeligson field. Cross section A-A' shown in figure 10. Modified from Finley and others (1990).



QA18287

Figure 2. Center of Seeligson field, showing well numbers, cored wells, three-dimensional seismic grid, and map area of the 14B and 19B reservoirs in the east-central part of the field (figs. 26, 27, and 47). Outline of Seeligson field shown in figure 1. Type log is figure 11. Modified from Jirik and others (1989).

Secondary gas recovery from recompletions in existing wells or infill drilling in mature fields can be an effective source of reserve additions. Reserve additions from old fields benefit from investments already made in reservoir development and production infrastructure. These incremental-gas reserves exist in bypassed gas reservoirs or untapped and poorly drained compartments (fig. 3). Bypassed gas reservoirs have been contacted by existing wells but have not been produced because they were considered to be uneconomic or nonproductive on the basis of previous log evaluation. Uncontacted reservoirs occur in zones of multiple gas reservoirs that have not been penetrated by existing wells. Poorly drained compartments occur in heterogeneous reservoirs that are segmented by permeability barriers that result from boundaries between depositional facies, variations in diagenesis, or complex structures.

Bypassed gas zones can be identified and developed by integrating advanced geologic methods and petrophysical techniques. Since 1988, the Gas Research Institute (GRI) has supported cooperative field research programs that develop and test methods that can improve ultimate recovery of gas from conventional reservoirs. These methods, which include state-of-the-art logging tools and new techniques for interpretation, are used to evaluate bypassed gas-bearing zones either above or within producing intervals.

A great potential for secondary recovery of bypassed-gas resources exists in the south Texas Gulf Coast, where complex Tertiary strata contain hundreds of lenticular sandstone reservoirs interbedded with mudstone. For example, an additional 10 to 23 percent of postcycling gas-in-place can potentially be contacted through infill drilling and well recompletion in some mature Frio gas reservoirs (Jackson and Ambrose, 1989) in the FR-4 play (Kosters and others, 1989) in South Texas (fig. 4). A play is defined as a set of reservoirs in a structural province that produce from similar depositional settings (Kosters and others, 1989). Seeligson field is located in the FR-4 play and produces gas from multiple, stacked fluvial sandstones. The field provides an excellent opportunity for studying heterogeneous fluvial reservoirs and for integrating geological reservoir

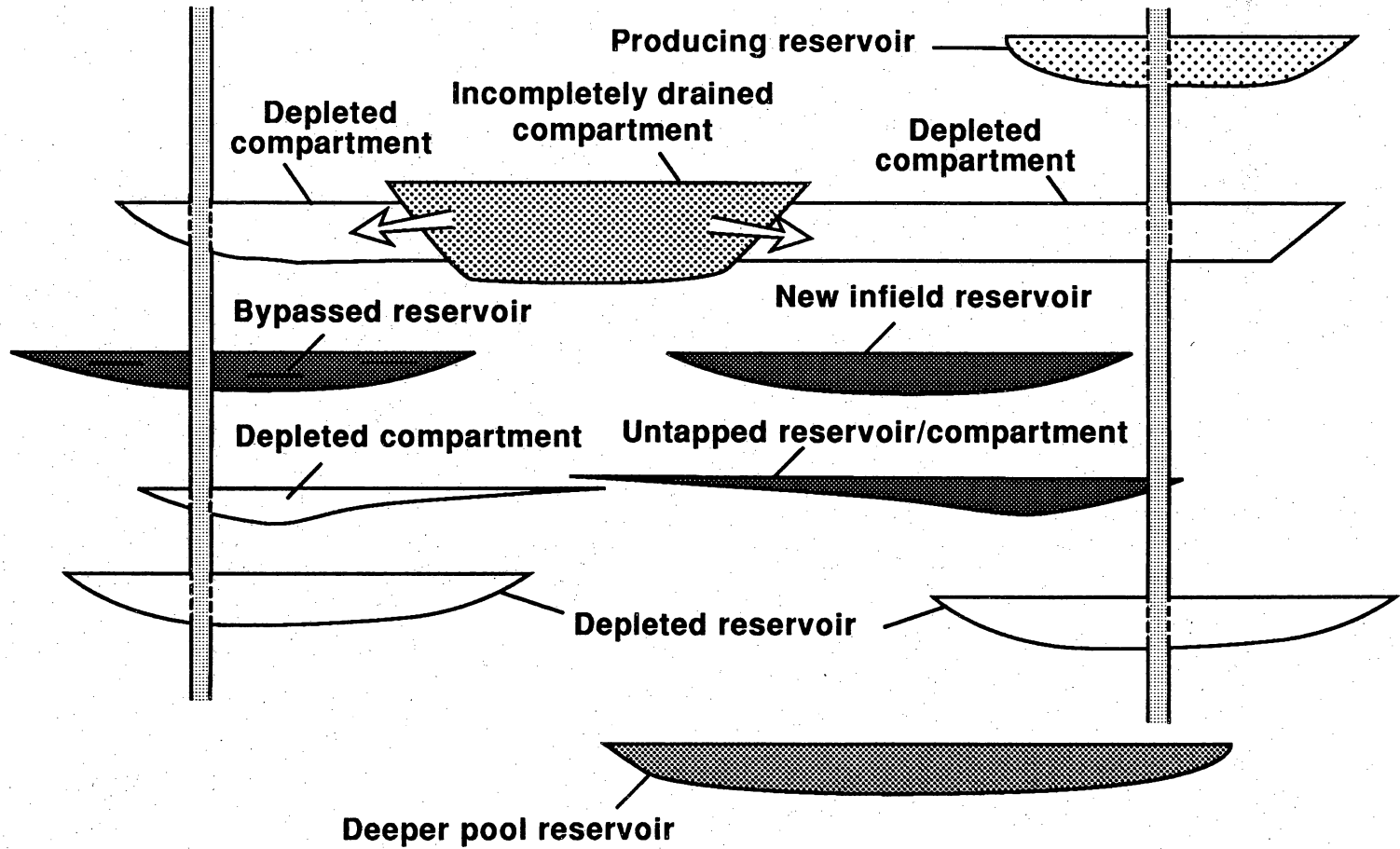
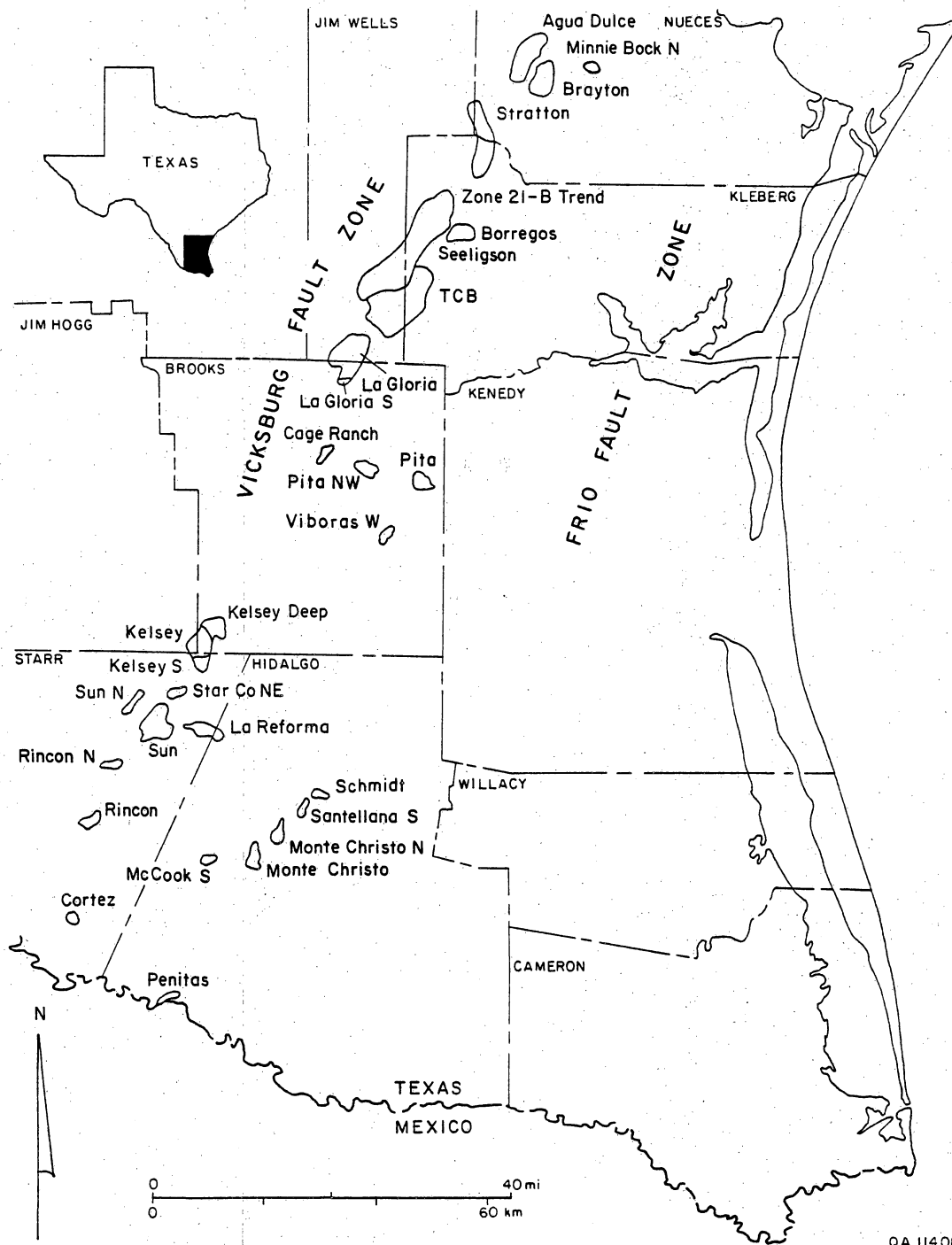


Figure 3. Major types of reservoir compartments. From Levey (1991).



QA 11408

Figure 4. Location of fields in the FR-4 play (Frio Fluvial/Deltaic Sandstone along the Vicksburg Fault Zone). Field outline includes oil rim. From Kosters and others (1989).

characterization and cased-hole log-evaluation techniques to identify potentially bypassed gas zones and poorly drained reservoir compartments.

Oryx Energy Company (formerly Sun Exploration and Production Company), the primary operator of unitized middle Frio reservoirs in Seeligson field, was systematically evaluating recompletion opportunities in the late 1980's using pulsed-neutron logs in temporarily abandoned wells. Studies funded by GRI (Jirik and others, 1989; Finley and others, 1990; Jirik, 1990; Jirik and others, 1991), jointly undertaken by the Bureau of Economic Geology (BEG), ResTech Houston, and, later, Research & Engineering Consultants, Inc. (REC), suggested additional recompletion candidates to Oryx. The initial research effort of these studies in late 1987 focused on an area encompassing approximately 4 mi² (10 km²) in the east-central part of the field (figs. 1 and 2). Oryx offered BEG and ResTech Houston the opportunity to recommend recompletion candidates, which, together with Oryx's own evaluations, resulted in five successful well recompletions. Total cumulative production in an 18-mo period ending in March 1990 for the recompleted zones was more than 1.4 Bcf of gas. The recompletions were made in zones identified as containing bypassed gas opportunities or in reservoir compartments in structurally higher parts of the field. ResTech Houston estimated reserves at 4.2 Bcf for the five recompleted wells from initial production data. Using the net value of the gas (\$1.80/Mcf at 1990 prices) and dividing by the approximate costs of the project (\$476,000), an undiscounted rate of return on investment was estimated to be 10 to 1. A more conservative estimate of 3 Bcf of reserves yielded a 4-to-1 rate of return (Jirik and others, 1991).

GEOLOGIC SETTING

Frio Fluvial/Deltaic Sandstone along the Vicksburg Fault Zone (FR-4) Play

Seeligson field is located in the prolific FR-4 play (Kosters and others, 1989), which extends from Nueces County to Starr and Hidalgo Counties in South Texas (fig. 4). The fields are located on the downthrown side of growth faults in the regionally continuous Vicksburg fault zone. These faults mainly offset the Vicksburg Formation but also affect the overlying Frio Formation. The FR-4 play is the largest of the onshore Texas Gulf Coast nonassociated-gas plays and had produced 11.8 Tcf of gas as of January 1, 1987, of which an unknown amount is recycled gas. The play is mature and has probably been depleted by more than 90 percent through conventional production methods (Galloway and others, 1982). Most discoveries were made between the 1940's and early 1960's. Most of the reservoirs in the FR-4 play produce nonassociated gas, as do most of the middle Frio reservoirs at Seeligson field. However, some reservoirs in the play have a thin oil rim; drive mechanisms commonly are a combination of gas-cap expansion, solution gas, and water drive.

The FR-4 play corresponds to the downdip margin of the Gueydan fluvial system, a major river system that occupied the Rio Grande Embayment during the Catahoula-Frio (Oligocene) depositional episode (Galloway, 1977). Seeligson field is located at the downdip edge of the Gueydan fluvial system, where it grades into the Norias delta system, (fig. 5). Nanz (1954) described the dip-oriented, lenticular Zone 19B reservoir at Seeligson field as the delta-plain deposit of an Oligocene river, probably an ancestral Rio Grande. The Gueydan fluvial system consists of channel-fill and point-bar sandstones that were deposited by mixed-load, slightly sinuous streams having broad natural levees (fig. 6). The channel-fill deposits are flanked by thinner, widespread crevasse-splay deposits and floodplain mudstones and siltstones. Individual channel-fill sequences are

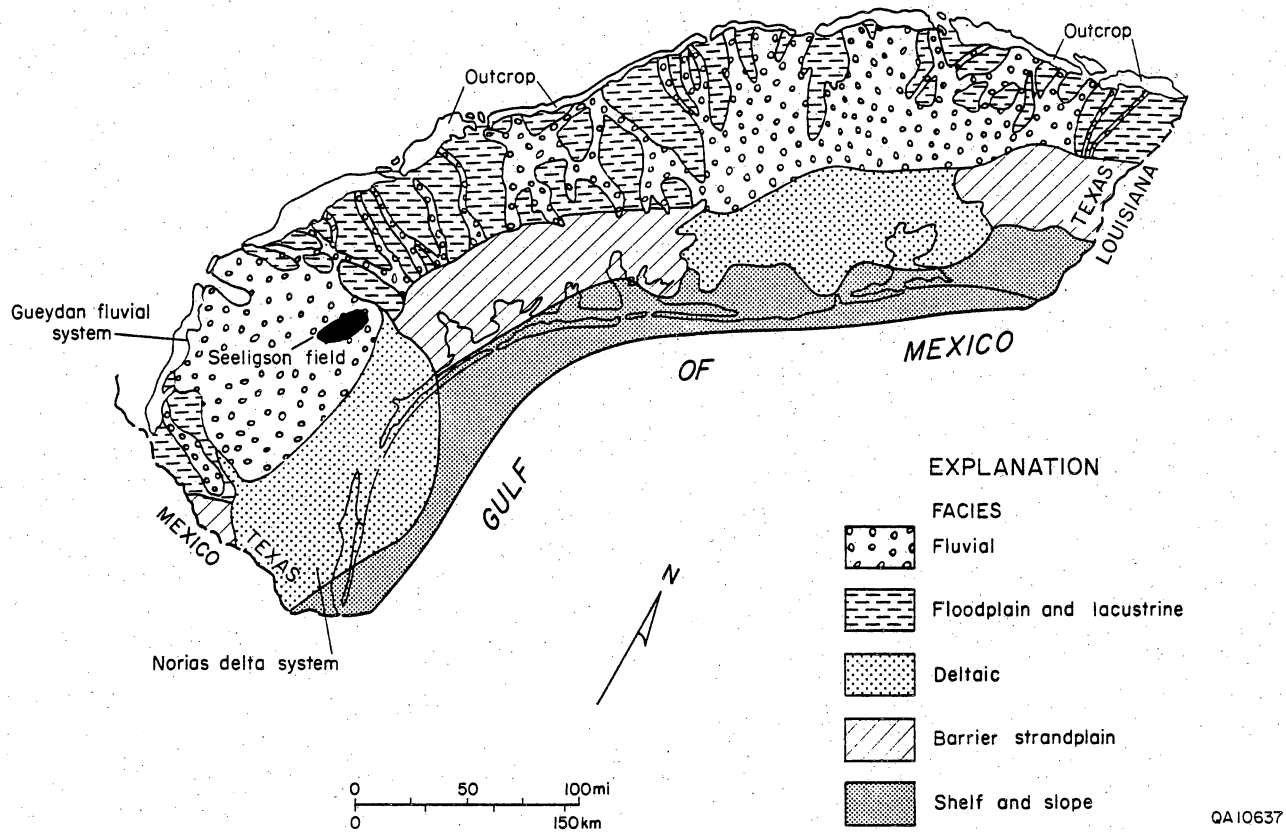


Figure 5. Frio depositional systems in the Texas Gulf Coast. Middle and upper Frio sediments were deposited in the Gueydan fluvial system, in which low-sinuosity, bed-load stream deposits grade basinward into high-sinuosity, mixed-load stream deposits. Modified from Galloway and others (1982).

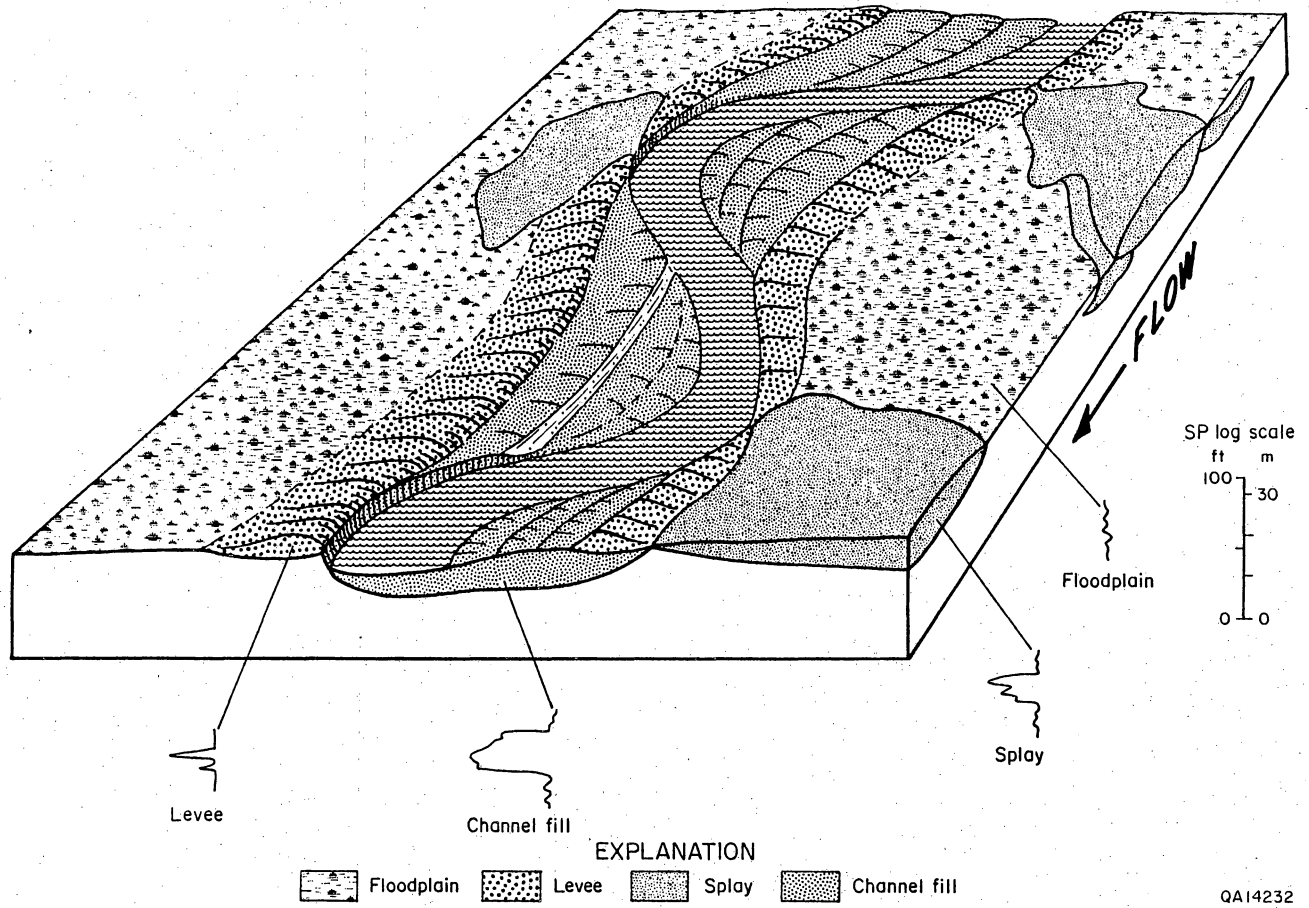


Figure 6. Three-dimensional facies relationships and characteristic SP log responses in middle and upper Frio fluvial reservoirs in Seeligson field. Modified from Galloway (1977).

10 to 30 ft (3 to 9 m) thick but are commonly stacked into composite units as thick as 100 ft (30 m). Individual channel-fill deposits are approximately 2,500 ft (762 m) wide, but where they coalesce, their combined width is commonly more than 1 mi (1.6 km) (Galloway, 1982). Splay deposits as much as 20 ft (6 m) thick proximal to channel-fill deposits can extend laterally for more than 4,000 ft (1,220 m).

Channel-fill and splay sandstones, the reservoir facies, have porosities averaging 20 percent and permeabilities ranging from 10's to 100's of millidarcys. Floodplain mudstones and silty levee deposits are both lateral and vertical barriers to gas flow. Other vertical barriers occur between channel-fill sandstones where low-permeability (1.0 to 0.01 md) mud-intraclast zones exist at channel-on-channel contacts.

Both structure and stratigraphy control production in the FR-4 play. Hydrocarbon traps occur in broad rollover anticlines on the downthrown side of the main Vicksburg fault. Middle Frio reservoirs, which are internally complex, can be offset by minor, subsidiary faults. Sandstones in these reservoirs exhibit varying degrees of stratigraphic complexity. Although each zone is generally less than 100 ft (30 m) thick, the majority are composite intervals of several positionally controlled genetic units. Aggregate net-sandstone thickness trends are dominantly dip parallel, indicating fluvial environments (Jirik and others, 1989).

Fluvial reservoirs in the FR-4 play are discontinuous and commonly contain internal permeability differences that segment reservoirs into compartments that may contain bypassed or compartmentalized gas resources. More than one-third of the production in the play may be from stratigraphic traps (Galloway and others, 1982). Detailed three-dimensional facies mapping, as part of an advanced reservoir characterization program, can provide a basis for designing infill wells and recompletions that target isolated, poorly drained compartments in these reservoirs (Ambrose and Jackson, 1989; Jirik and others, 1989).

Structural Framework

Seeligson field is bounded on the northwest by a major growth fault in the northeast-trending Vicksburg fault zone (fig. 7). A subregional, two-dimensional reflection seismic profile (fig. 8) illustrates the position of the major Vicksburg growth fault relative to Seeligson field. In addition, stratigraphic control from a well with a zero-offset VSP (vertical seismic profile) illustrates the relatively simple structure associated with the Frio Formation compared with that of the deeper Vicksburg Formation.

Minor synthetic and antithetic faults offset Vicksburg and Frio strata in the field. Although upper Vicksburg and lower Frio strata are offset up to several hundred feet, middle Frio strata are offset by <100 ft (<30 m). The east, downdip boundary of the field is defined primarily by the limits of production because no significant bounding faults segment the field into a well-defined block. Most of the gas is trapped in fluvial and deltaic sandstones located over the crest of a broad, northeast-trending rollover anticline associated with the growth fault. Structural relief of reservoirs is commonly <400 ft (<120 m). Secondary structurally high areas occur along the northeast-trending crest of the primary rollover anticline.

Structure of upper Vicksburg and lower Frio strata is complex and related to the main Vicksburg growth fault. Northeast-trending faults that offset these strata are approximately parallel to the main segment of the regional Vicksburg growth fault. Restoration of lower Frio throw across these faults indicates that fault movement occurred before Frio deposition but that the faults were briefly reactivated after lower Frio deposition.

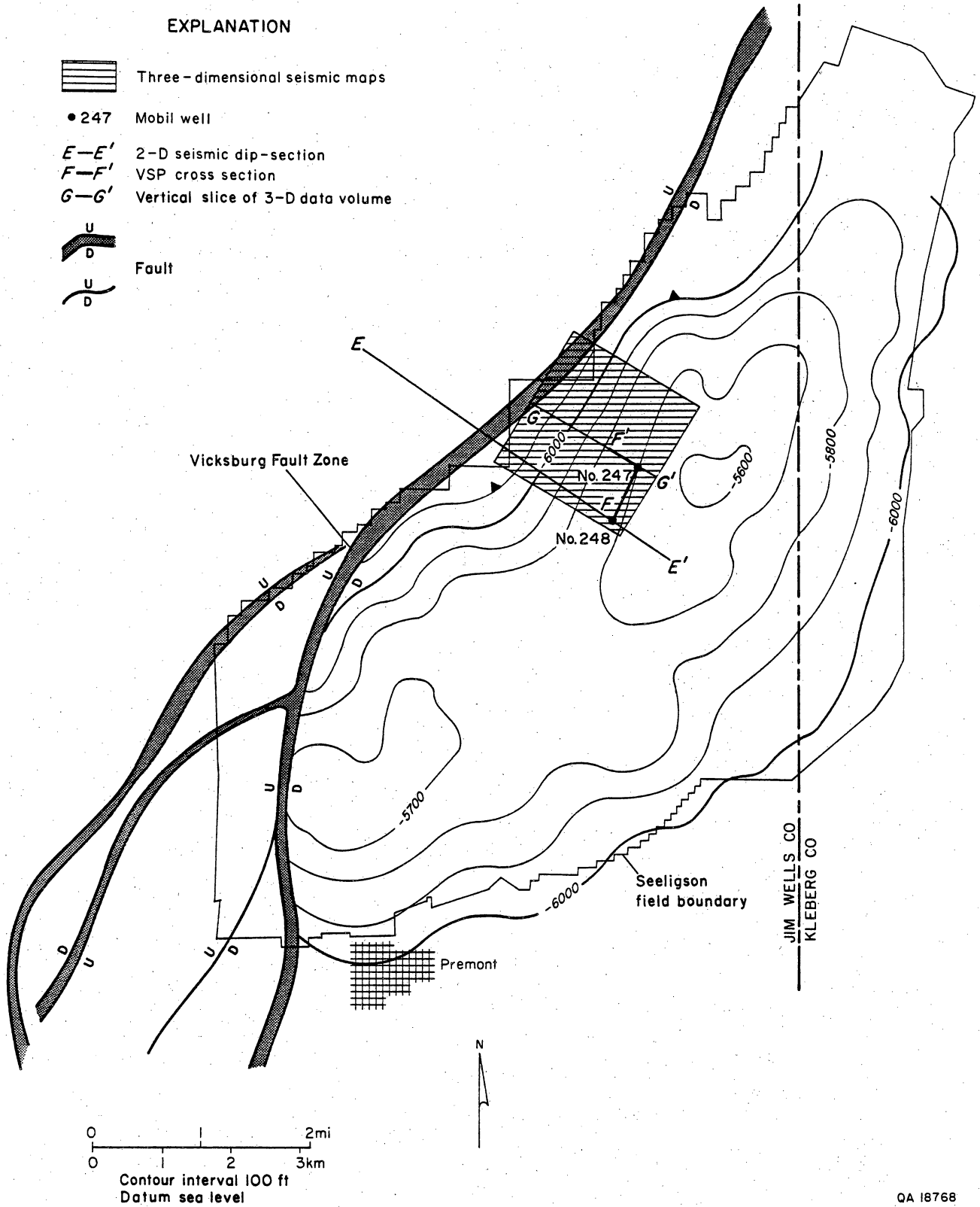
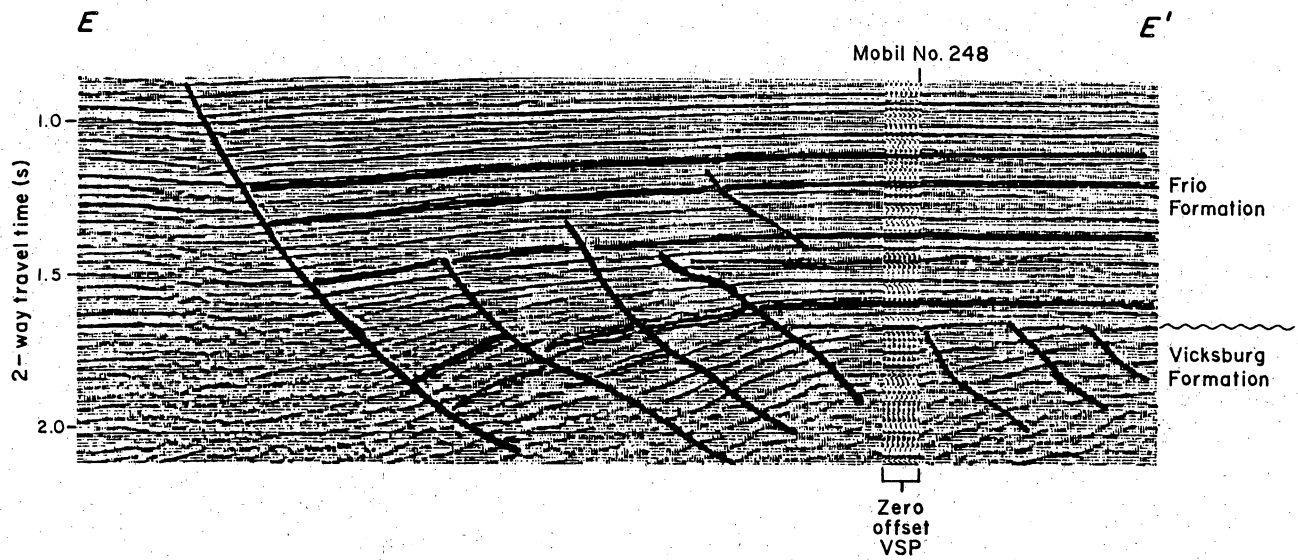


Figure 7. Structure map of Seeligson field, contoured on the *Textularia mississippiensis* (lower Frio) biozone. The principal growth fault offsets Vicksburg and Frio strata from 300 to 1,700 ft (91 to 518 m) and forms the west boundary of the field. Cross sections E-E', F-F', and G-G' are located in figures 8, 21, and 9, respectively. Modified from Jirik and others (1989).



QA18767

Figure 8 . Structural seismic dip section E-E' across Seeligson field with zero-offset VSP through the Mobil No. 248 Seeligson well. Line of section shown in figure 7.

Stratigraphic Framework

At Seeligson field, the Frio and upper Vicksburg Formations are informally divided into four stratigraphic units. In ascending order, these stratigraphic units are: (1) upper Vicksburg Formation, (2) lower Frio Formation, (3) middle Frio Formation, and (4) upper Frio Formation. The upper Vicksburg and lower Frio Formations together comprise nonunit reservoirs in Seeligson field, whereas unit reservoirs, operated by Oryx, occur in the middle Frio Formation.

Figure 9 (cross section G-G') illustrates a vertical slice through the three-dimensional surface seismic grid in north Seeligson field, located in figure 7. The intensity of faulting decreases in the shallower horizons on this cross section, especially ascending from stratigraphic unit 2 to unit 3.

The upper Vicksburg Formation consists of thick progradational deltaic sandstone deposits (Han and Scott, 1981). Upper Vicksburg sandstones are 50 to 150 ft (15 to 46 m) thick and occur as progradational wedges typically separated by 50- to 100-ft (15- to 30-m) thick mudstones. Correlations in the structurally complex upper Vicksburg Formation are difficult, and reservoir compartments in this lower section of the field are mainly controlled by faults, as well as stratigraphic heterogeneity.

The lower Frio Formation is separated from the underlying upper Vicksburg Formation by an angular unconformity, which is recognized in dipmeter logs, changes in resistivity and density-log responses, seismic sections, and in electric log correlations. The lower Frio Formation, which contains the *Textularia warreni* biozone, consists of laterally continuous strandplain sandstones interbedded with lower coastal-plain and inner-shelf mudstones.

The middle Frio Formation contains predominantly fluvial sandstones and floodplain mudstones. Middle Frio sandstones at Seeligson field are typical of those of

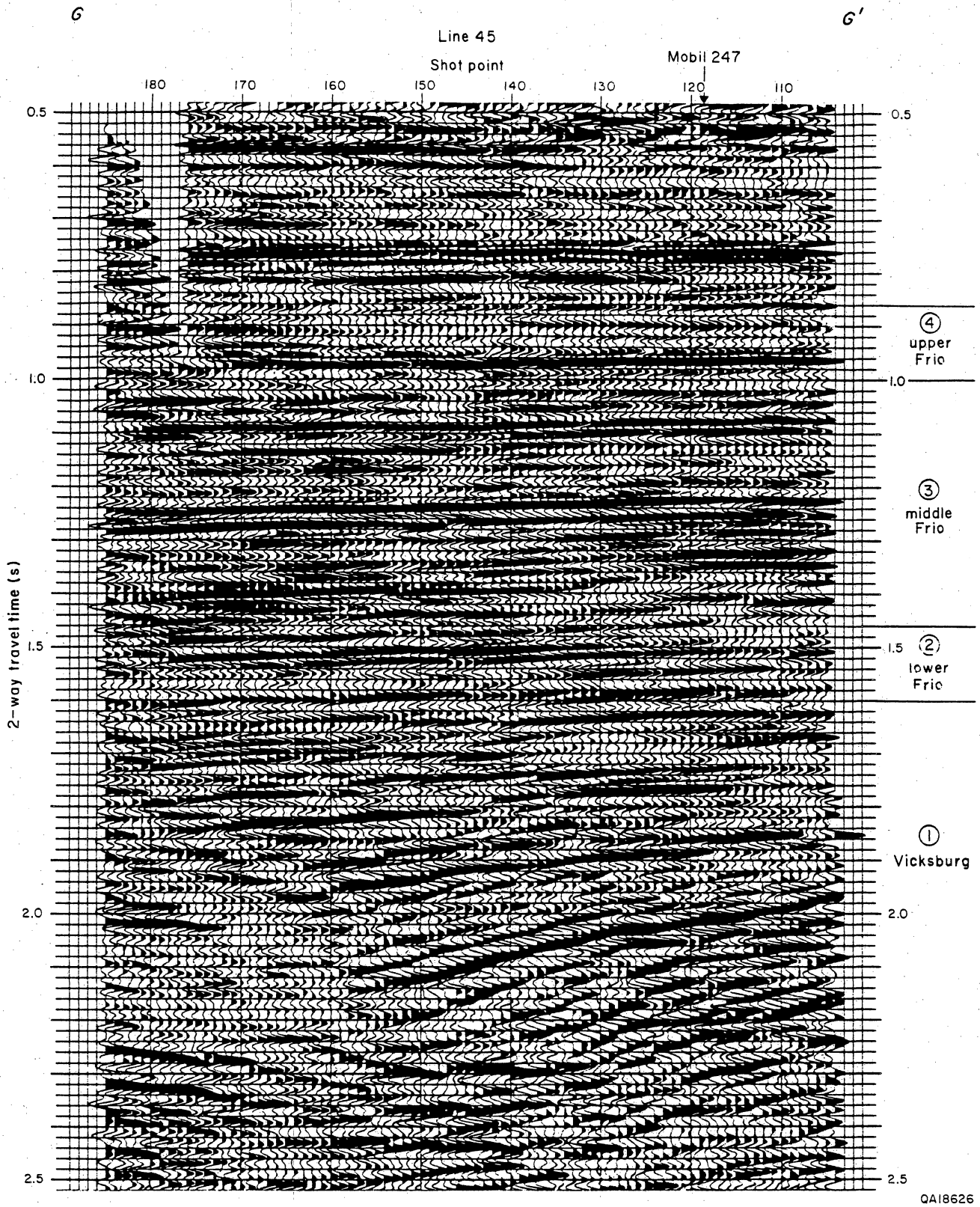


Figure 9. Structural dip section G-G', which is a vertical slice from the three-dimensional seismic grid in north Seeligson field. Line of section shown in figure 7.

the Gueydan fluvial system. Individual channel-fill deposits, which are flanked by widespread crevasse-splay deposits, are approximately 35 to 50 ft (10 to 15 m) thick and are approximately 2,500 ft (762 m) wide.

Although the contact with the upper and middle Frio Formation is gradational, locally it is erosional where channel-fill sandstones truncate middle Frio strata. The upper Frio Formation contains laterally continuous strandplain sandstones and lower coastal-plain mudstones, with isolated fluvial or thin back-barrier sandstones commonly referred to as the *Heterostegina-Marginulina* sandstones. Upper Frio strata consist of retrogradational shoreline sandstones that are overlain by shelf mudstones of the Anahuac Shale, which was deposited during a major transgression in the Gulf Coast structural province.

Nonunit Reservoirs (Upper Vicksburg and Lower Frio Formations)

Nonunit reservoirs in Seeligson field, operated by Mobil, are in the upper Vicksburg and lower Frio Formations and extend from below Frio 20C reservoirs (approximately 6,200 ft [1,890 m] deep) to the base of the upper Vicksburg Formation (8,000 to 10,000 ft [2,439 to 3,049 m] deep (fig. 10). These reservoirs vary in depth because they are offset by hundreds of feet by faults. Nonunit reservoirs in the upper Vicksburg Formation are continuous and occur in thick (50 to 150 ft [15 to 46 m]) progradational, upward-coarsening sandstones that are separated by continuous mudstones that are 50 to 100 ft (15 to 30 m) thick. Lower Frio nonunit reservoirs are continuous but only 10 to 50 ft (3 to 15 m) thick.

Unit Reservoirs (Middle Frio Formation)

Unit reservoirs in Seeligson field, operated primarily by Oryx, occur in the middle Frio Formation and include Zones 7 through 20C (figs. 10 and 11). These reservoirs

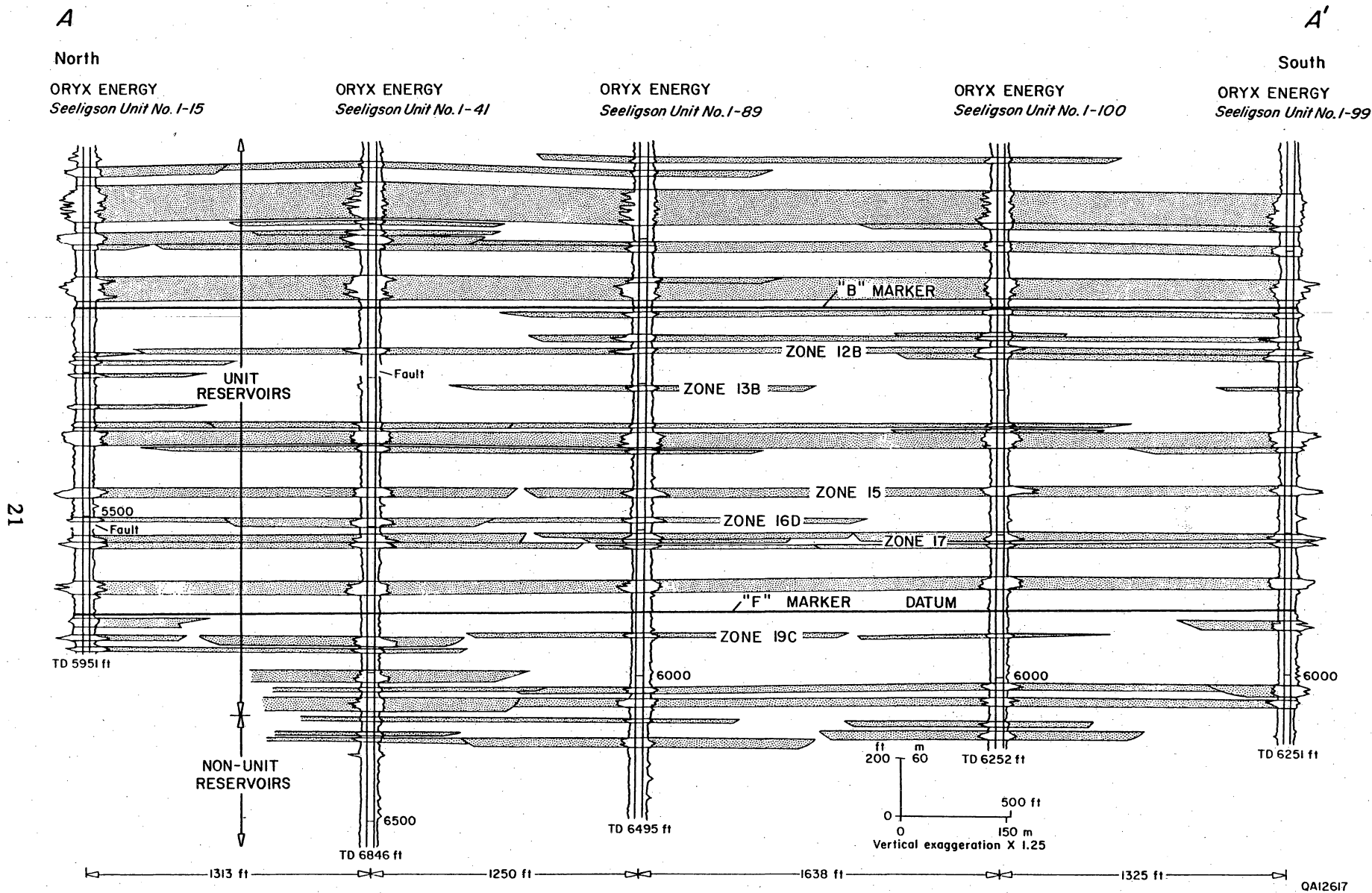


Figure 10. Cross section A-A', showing extent of lower Frio nonunit and middle Frio unitized reservoirs in Seeligson field. The B and F resistivity markers are continuous throughout the field. Line of section shown in figure 1. From Jirik (1990).

MAGNOLIA
A. A. Seeligson No. 24 (1-24)
Jim Wells County, Texas

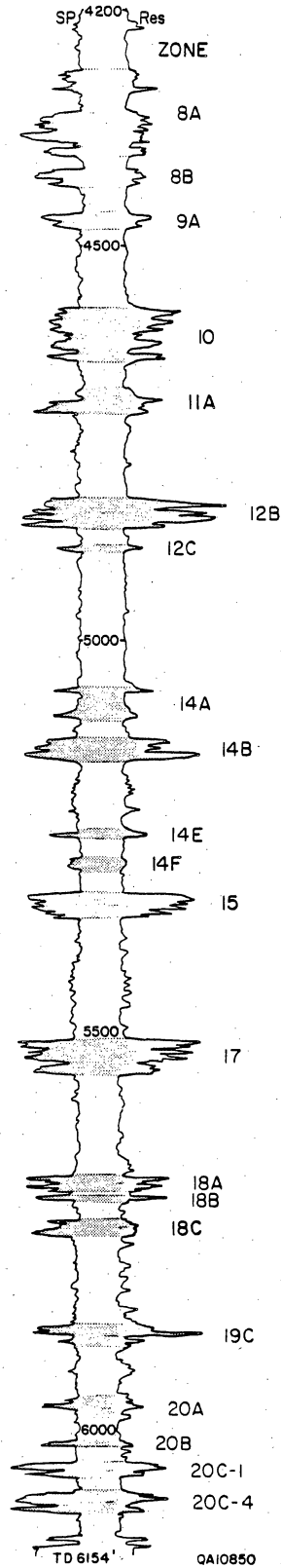


Figure 11. Type log (Magnolia No. 1-24 A. A. Seeligson) in Seeligson field, showing more than 20 middle Frio reservoirs in thin (typically <30-ft [<9 -m] thick) fluvial reservoirs. Log located in figure 2. From Jirik and others (1989).

range from approximately 4,000 to 6,200 ft (1,220 to 1,890 m) in depth. Unit reservoirs are typical of the Gueydan Fluvial System (Galloway, 1982). Dip-elongate channel-fill and point-bar sandstones, crevasse-splay sandstones, and levee and overbank siltstones and mudstones are characteristic lithofacies of Seeligson unit reservoirs (Jirik and others, 1989). Other unit reservoirs exhibit strike-elongate (northeast-trending) net-sandstone patterns, suggesting local variation in the orientation of meanderbelt systems.

Fluvial Facies

Four main facies (channel-fill, splay, levee, and floodplain) occur in middle Frio reservoirs at Seeligson field as well as the nearby Stratton field, which is also in the FR-4 play (fig. 6). These facies are identified from cores, well-log interpretations, and net-sandstone and log-facies maps (Jirik, 1990; Kerr, 1990; Kerr and Jirik, 1990).

Channel Fill

The channel-fill facies occurs mainly as dip-elongate belts of sandstone that individually attain a maximum thickness of 20 to 30 ft (6 to 9 m) at Seeligson field. These channel-fill belts are typically 2,000 to 2,500 ft (610 to 762 m) wide. Thalwegs (channel pathways), inferred from net-sandstone maps, were moderately sinuous. However, three-dimensional seismic maps suggest that channel pathways were highly sinuous. Channel-fill facies at Seeligson and Stratton fields are divided into three subfacies (lower, middle, and upper). The overall succession of sedimentary structures and textures from the lower to upper channel-fill subfacies is typical of multitiered, lateral-accretion bar deposits (Connolly and others, 1986). Lower channel-fill subfacies consist of clay-clast conglomerates and crossbedded medium sandstones that have thin mud layers draped on foreset strata (for example, fig. 12; 5,426 ft [1,654 m]). Middle channel fill subfacies contain plane-bedded and ripple-laminated fine sandstones (for

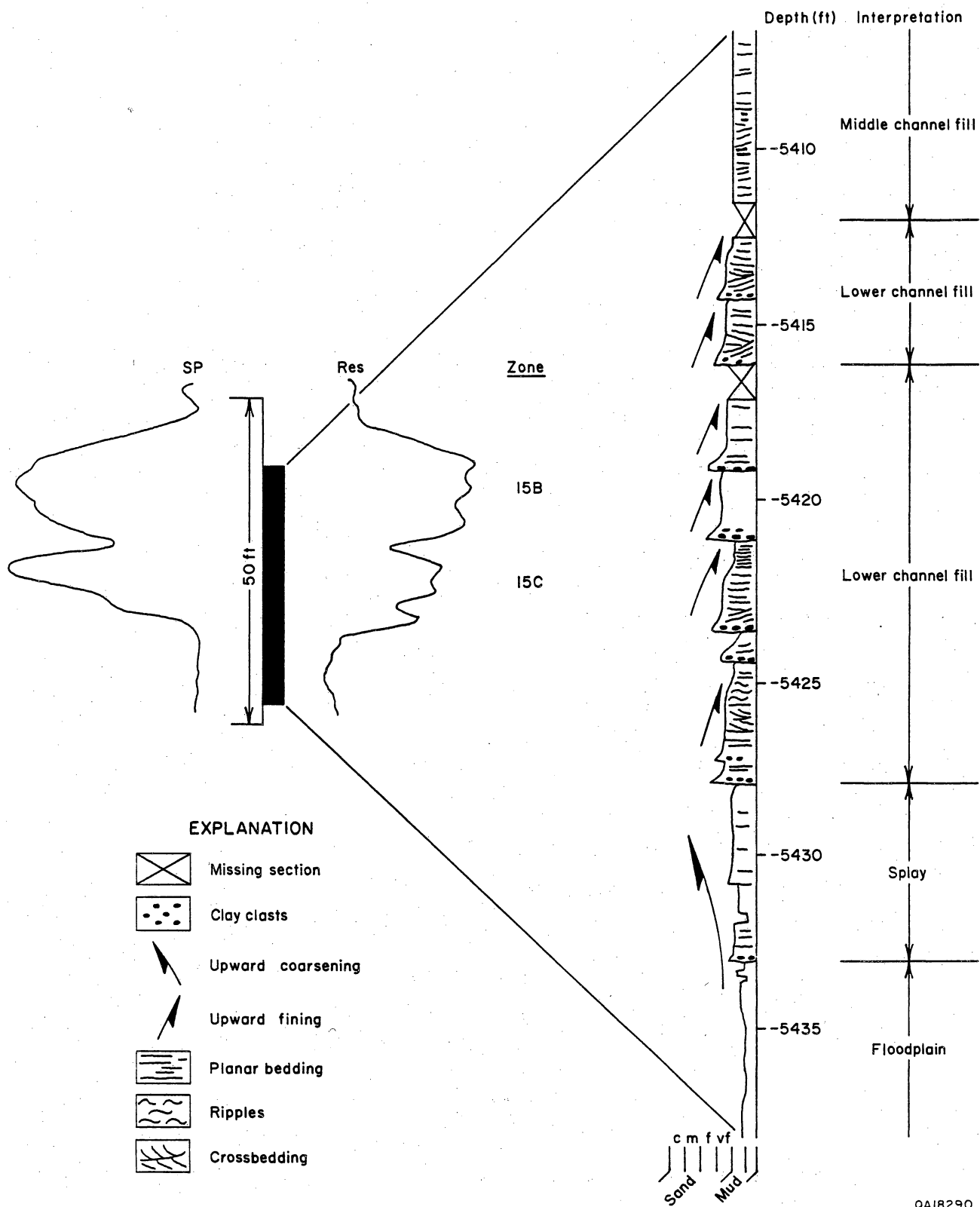


Figure 12. Core description and SP and resistivity log response of the Zone 15 reservoir in the Sun No. 141 P. Canales well at Seeligson field. Well located in figure 2.

example, fig. 12; 5,410 ft [1,649 m]). The middle channel fill also contains mud-draped, low-angle surfaces that represent lateral accretion surfaces. Upper channel-fill subfacies, present in core from Stratton field, consist of structureless, fine sandstones and mudstones having carbonate nodules, desiccation cracks, and root mottling that indicates soil-forming environments.

The channel-fill facies at Seeligson field is inferred from blocky or upward-fining (upward-right deflection) SP responses, consistent with expected upward increase in clay content in point-bar deposits (fig. 6). However, concentration of mudstone intraclasts at the base of the channel-fill facies may suppress the SP log response, although the resistivity response is commonly not suppressed. The upper limit of channel-fill facies is interpreted to occur at the top of the broad shoulder developed in the resistivity curve.

Vertical changes in porosity and permeability in the channel-fill facies are related to variations in texture and sedimentary structures. The intraclast-rich channel-lag deposits have low porosity and permeability values (5 to 20 percent and 0.01 to 10.0 md, respectively). In contrast, the large-scale crossbedded, medium to fine sandstones contain higher values (20 to 30 percent; 100 to 500 md). Plane-bedded and ripple-laminated, fine to very fine sandstones have large variations in porosity and permeability vertically over a few feet (15 to 20 percent; 1 to 200 md). These data indicate that flow barriers, controlled by small-scale lithologic heterogeneities, may exist in apparently continuous, homogeneous sandstones as inferred from conventional wireline logs.

Splay

At Seeligson field, splay facies flank the channel-fill facies, where they are as much as 20 ft (6 m) thick. They pinch out over a distance of thousands of feet, to as much as

2 mi (3.2 km) away from the inferred crevasse break. The splay facies consists of several sandstone beds that collectively represent multiple flood events from a single crevasse or merging of splay complexes from different crevasse breaks. Net-sandstone thickness patterns of the splay facies commonly have a fan or lobate shape. However, because most splay deposits occur as complexes composed of the deposits of multiple flood events, irregular net-sandstone thicknesses also occur.

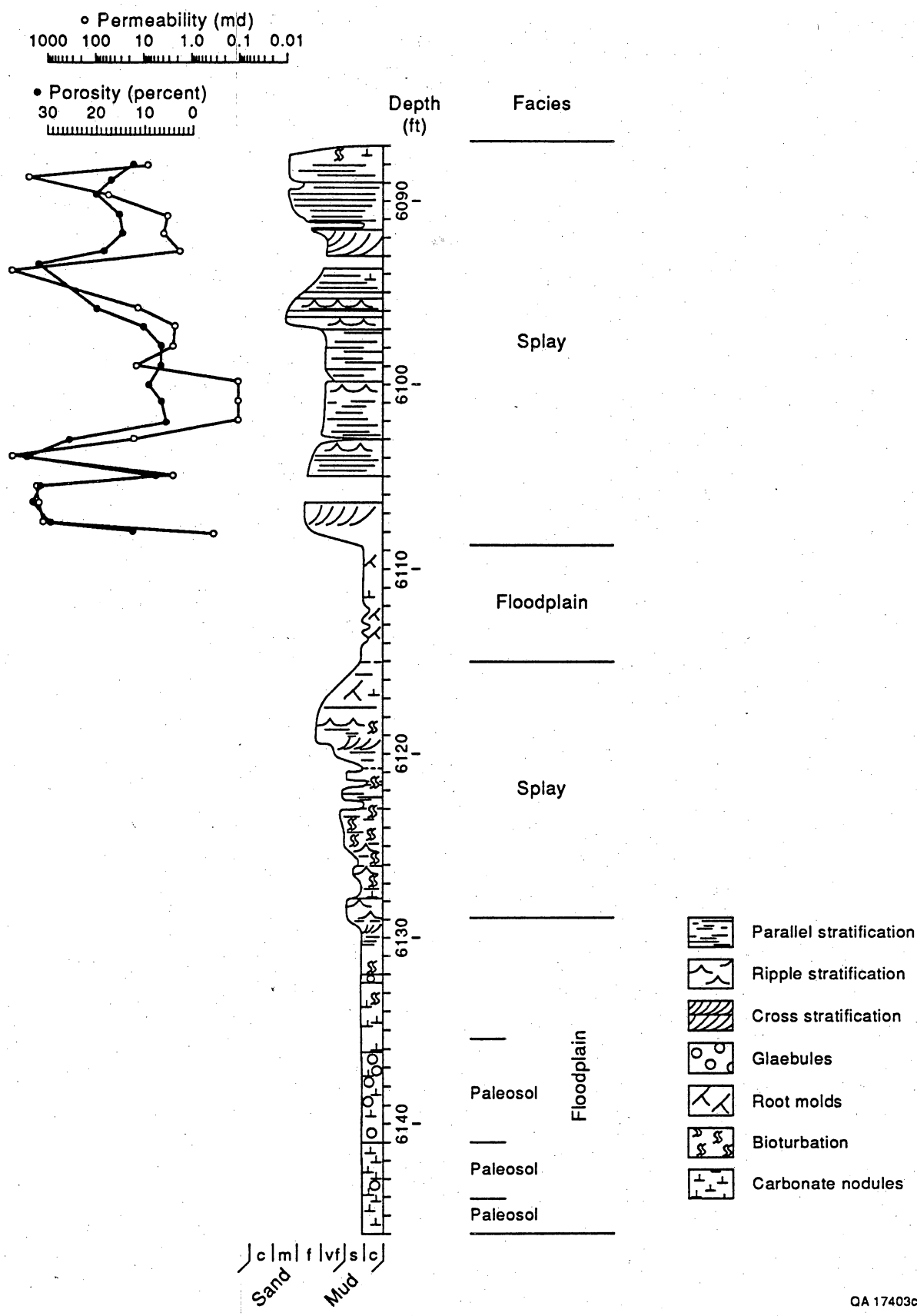
The splay facies consists of fine and very fine sandstone with medium-scale cross-stratification and parallel and ripple stratification (fig. 13). Some splay sandstones contain root mottling and soft-sediment deformation caused by dewatering. These structures and presence of infiltrated mud and siltstone suggest deposition in standing water (small lakes or ponds) in the interfluvial area.

The log profile of the splay facies is typically upward coarsening (upward-left deflection on the SP curve), reflecting progradation of the splay lobe in the interchannel area (fig. 6). However, this pattern can be complex in splay deposits that consist of several superimposed lobes from different sources. Additionally, upward-fining and blocky SP responses indicate splay-channel deposits proximal to the channel fill.

Porosity and permeability values in splay sandstones vary widely (5 to 30 percent; 0.1 to 500 md, respectively) at Seeligson field (fig. 13), reflecting the wide range of hydraulic conditions of sandstones deposited from proximal- to distal-splay environments. The marked contrast in permeability suggests that flow barriers may exist between individual sandstone beds within a splay complex.

Levee

The levee facies consists of narrow wedges (<500 ft [<152 m] wide) that flank channel-fill facies (fig. 6). Although levee deposits are locally thick where they are adjacent to channel-fill deposits, they pinch out over short distances (100 to 150 ft [30



QA 17403c

Figure 13. Core description and porosity and permeability profiles in the Zone 20B reservoir in the Sun No. 16-125 A. A. Seeligson well at Seeligson field. Well located in figure 2. From Levey and others (1991).

to 46 m]) (Kerr, 1990). Additionally, levee deposits may not occur along the entire length of the channel system. The levee facies consists of interbedded sandstones and mudstones that commonly contain low-angle laminae, slump structures, root traces, and paleosol fabrics. The SP response of the levee facies is subdued, baseline, or spiky. However, the resistivity response is commonly spiky, which suggests thin sandstone beds interbedded with mudstone. Porosity and permeability data are unavailable for the levee facies. However, this facies probably has low permeability and is therefore inferred to be a poor conductor of fluids between reservoirs.

Floodplain

Floodplain facies occurs over wide areas and separates channel-fill and splay facies both vertically and laterally (fig. 6). Vertical separation of floodplain and channel-fill and/or splay facies ranges from less than 5 ft (1.5 m) to as much as 200 ft (61 ft). Lateral extent of the floodplain facies is also highly variable, depending on the extent of channel migration.

The floodplain facies at Seeligson field consists of mudstones (siltstones, claystones) and silty sandstones (fig. 13). These rocks vary in color and are green, red, purple, or variegated. Variations in the value and chroma of red and green hues indicate differences in the oxidation state of iron-oxide and hydrous-iron-oxide minerals and, to a lesser extent, differences in organic carbon content. The fine sediments of the floodplain facies are structureless or poorly laminated; ripple lamination is uncommon but present in some siltstone beds. Sediment-filled root molds and carbonized root filaments with reduction halos are also present. Vertisol-type paleosols contain several pedogenic fabrics in the mottled intervals of the floodplain mudstone facies. Slickensides, which are clearly unrelated to coring processes, are present in the claystones. Carbonate nodules and ped structures are also common.

The floodplain facies is identified by a baseline SP response on the basis of inferred high clay content. Accurate porosity and permeability data are unavailable for this facies. Like the levee facies, the floodplain mudstone facies probably has low permeability and is also inferred to be a poor conductor of fluids between reservoirs.

Subsurface Mapping of Fluvial Deposits

A detailed stratigraphic analysis of each selected reservoir was made to define discrete stratigraphic intervals composed of genetically related facies and to infer the existence of potential lateral or vertical reservoir compartments. Cross sections and detailed correlations of sandstones and resistivity and conductivity markers in shales were made to establish the stratigraphic framework of the reservoirs. Amalgamated sandstone bodies were subdivided into discrete genetic units (facies deposited approximately contemporaneously) through detailed correlation of SP and resistivity curves.

The lateral and vertical extents of sandstone bodies were inferred from net-sandstone thickness maps and cross sections constructed with closely spaced wells (<3,000 ft [<915 m] apart). Net-sandstone thickness was inferred by measuring thickness of SP deflections along a vertical line drawn at one-third the distance from the shale baseline to the line of maximum (negative) deflection. The extent of sandstone bodies was determined from cross sections in the oil-producing parts of the field, where well spacings are 500 to 1,000 ft (152 to 305 m) and extrapolated to the more sparsely drilled gas cap. Depositional environments and facies associations were inferred from core descriptions and comparison of net-sandstone and log-facies maps.

RESERVOIR INVESTIGATIONS

Reservoir Nomenclature

At Seeligson field, the nomenclature of gas-productive horizons in the middle Frio Formation is a numerical system in which reservoirs are grouped into zones numbered from 7 through 20 in a descending stratigraphic order (fig. 10). Individual reservoirs in these zones, which are commonly identified with an alphabetic subscript (for example, Zone 19C), are defined by vertical lengths of perforations and are the basic interval in which production is reported to regulatory agencies. Each individual reservoir may contain multiple sandstone beds that represent discrete genetic units corresponding to depositional facies (for example, Zone 19C lower, middle, and upper). Recompletion targets and heterogeneity in Seeligson reservoirs are identified and discussed at the level of genetic depositional units that are illustrated by net-sandstone, log-facies, and three-dimensional seiscrop maps.

The data base consisted of approximately 250 well logs in the center of the field (fig. 2). Additional data, provided by Oryx, included modern log suites (sonic, neutron density, thermal decay time [TDT]), repeat-formation test data, and bottom-hole pressure (BHP) data for selected wells. Well-history summaries were used for more than 100 wells. Approximately 270 ft (82 m) of whole core from two wells (Sun No. 16-125 Seeligson and Sun No. 141 P. Canales, located in fig. 2) was used to perform petrophysical and petrographic analyses, to characterize facies, and to calibrate log responses. Numerous mineralogical and core analyses provided porosity and permeability information. Mobil Exploration and Producing U.S., Inc. (Mobil), provided similar data for nonunitized lower Frio and upper Vicksburg wells. Open- and cased-hole log data in two wells (Mobil No. 247 and No. 248 A. A. Seeligson, located in fig. 2) were used to evaluate additional uncontacted gas in lower Frio and upper Vicksburg reservoirs.

Vertical-seismic-profile and three-dimensional surface seismic data were analyzed to further determine the areal extent and continuity of middle Frio reservoir sandstones and to identify any overprint of Vicksburg structural features on the relatively structurally simple middle Frio reservoir section.

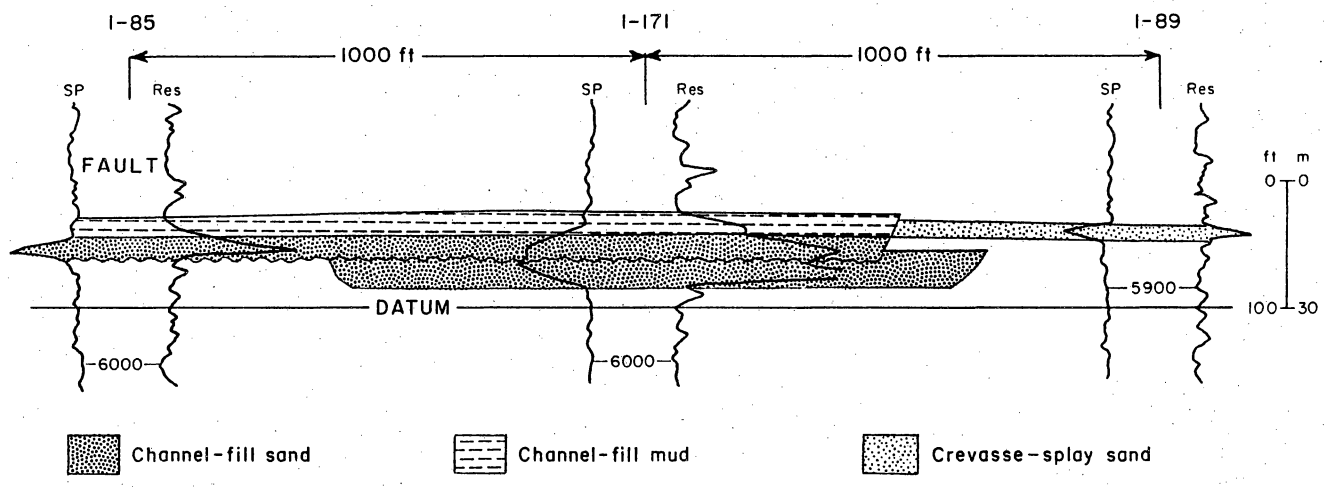
Zone 19C Reservoir

The Zone 19C reservoir occurs at depths ranging from 5,600 to 5,900 ft (1,680 to 1,770 m) at Seeligson field. Zone 19C is a complex, amalgamated reservoir that contains three major genetic units (upper, middle, and lower [fig. 14]). The Zone 19C reservoir was chosen for study because vertical seismic profiles and variations in pressure data from wells were initially thought to indicate changes in net-sandstone thickness over short distances between wells.

Depositional Environments

The lower and middle 19C genetic units are each composed of single-channel systems. The lower Zone 19C genetic unit is composed of two dip-oriented channel-fill deposits approximately 20 ft (6 m) thick and less than 2,000 ft (610 m) wide, flanked by widespread crevasse-splay deposits (fig. 15). The middle Zone 19C genetic unit contains dip-oriented channel-fill sandstones approximately 20 ft (6 m) thick. Width of these channel-fill deposits varies little from 2,000 ft (610 m). Areas of truncation by overlying channel-fill sandstones occur locally in the field (fig. 16).

The upper Zone 19C genetic unit is composed of three superimposed channel-fill systems that were mapped as one undivided body (Jirik and others, 1991). Depositional axes in the upper Zone 19C genetic unit are defined by two straight to slightly sinuous northeast-trending belts of more than 20 ft (6 m) of net sandstone that vary in width from 1,500 to 4,000 ft (457 to 1,220 m) (fig. 17). Locally, these depositional axes contain



QA18505

Figure 14. Stratigraphic cross section in the Zone 19C reservoir in north Seeligson field. Zone 19C is a composite of three genetic sandstones, each <20 ft (<6 m) thick. Wells in cross section located in figure 2.

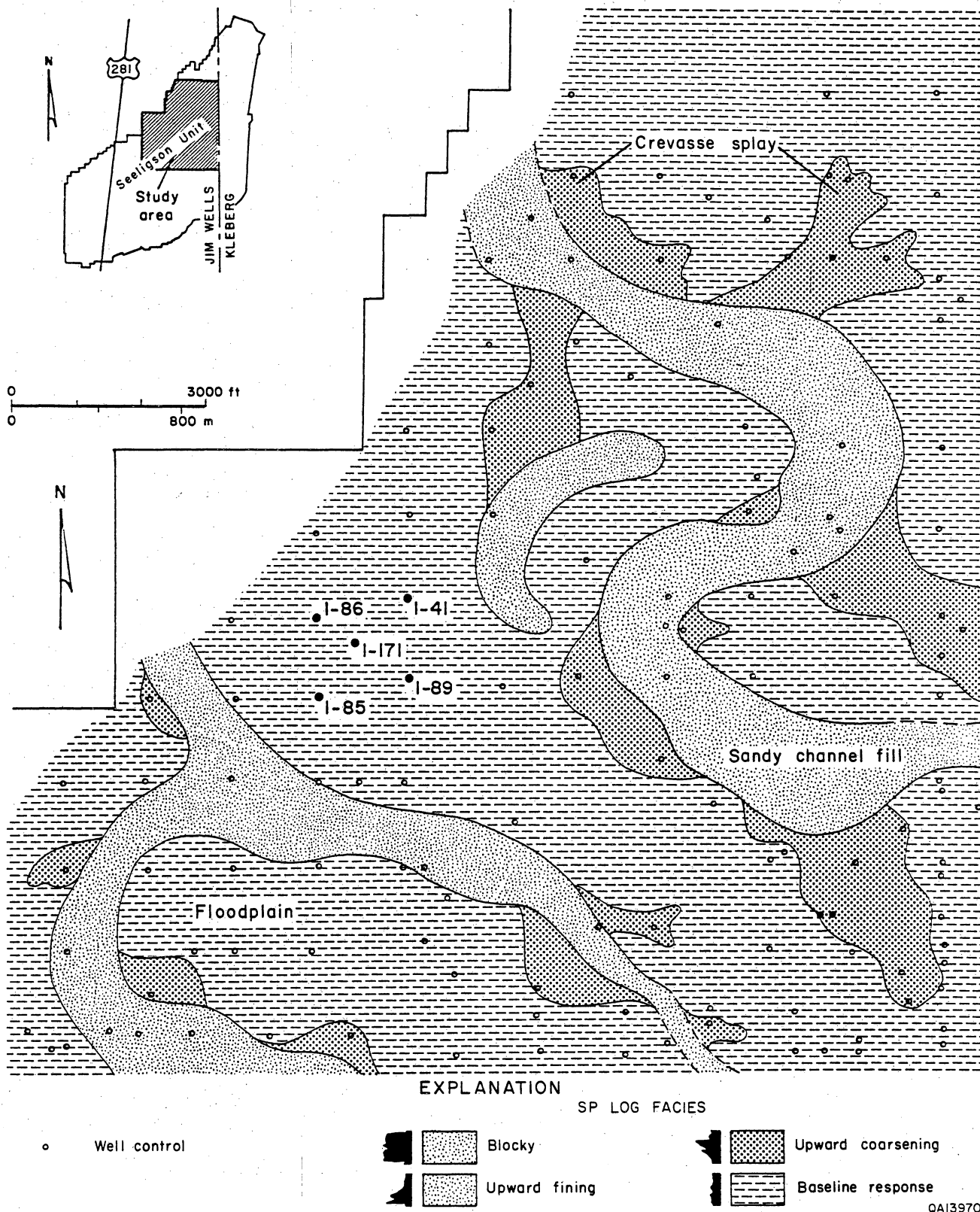


Figure 15. SP log-facies map of the lower Zone 19C genetic unit in north-central Seeligson field. Two narrow channel-fill deposits flanked by crevasse-splay deposits compose this genetic unit. Modified from Jirik (1990).

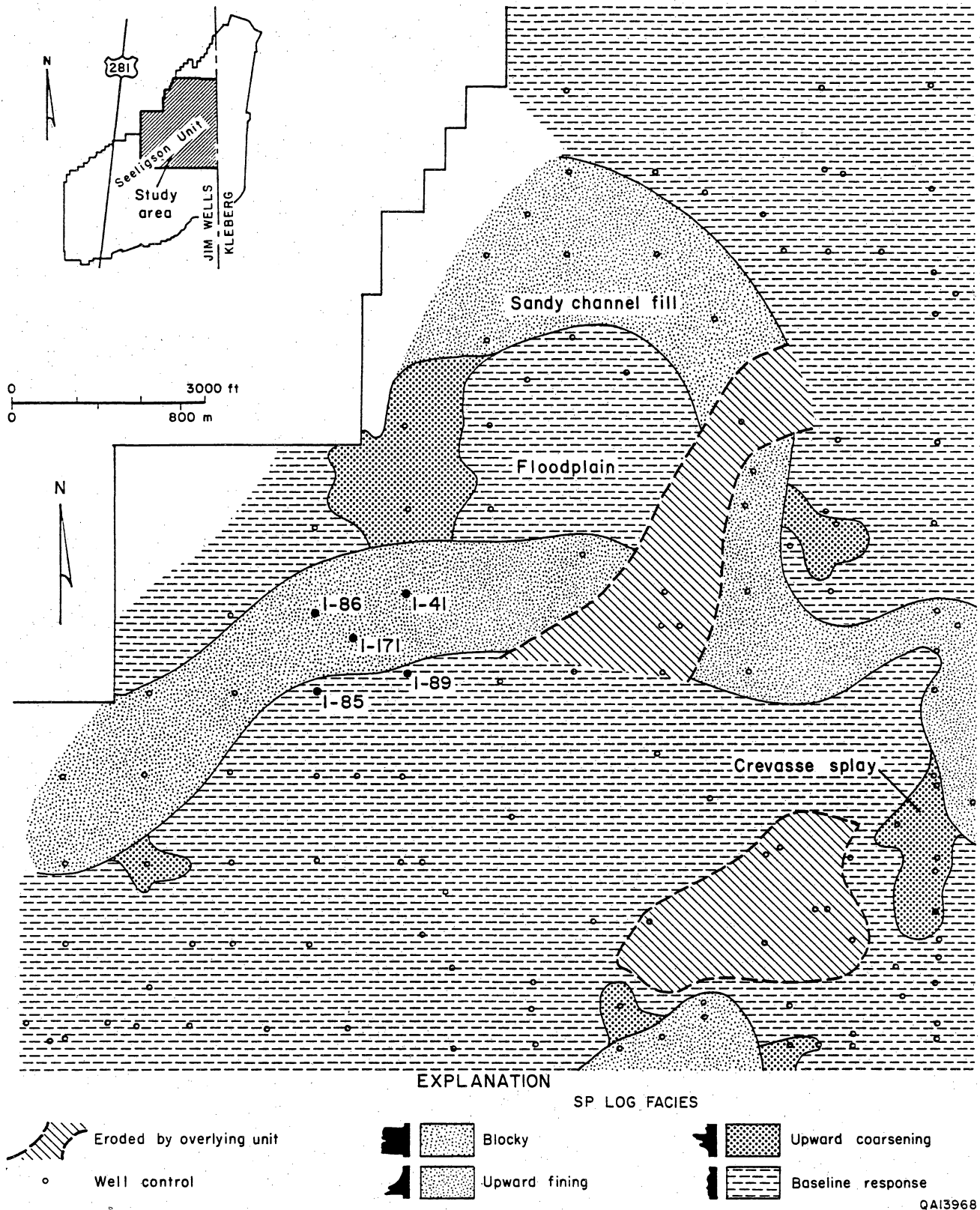


Figure 16. SP log-facies map of the middle Zone 19C genetic unit in north-central Seeligson field, showing two converging channel-fill deposits flanked by minor crevasse-splay deposits. Modified from Jirik (1990).

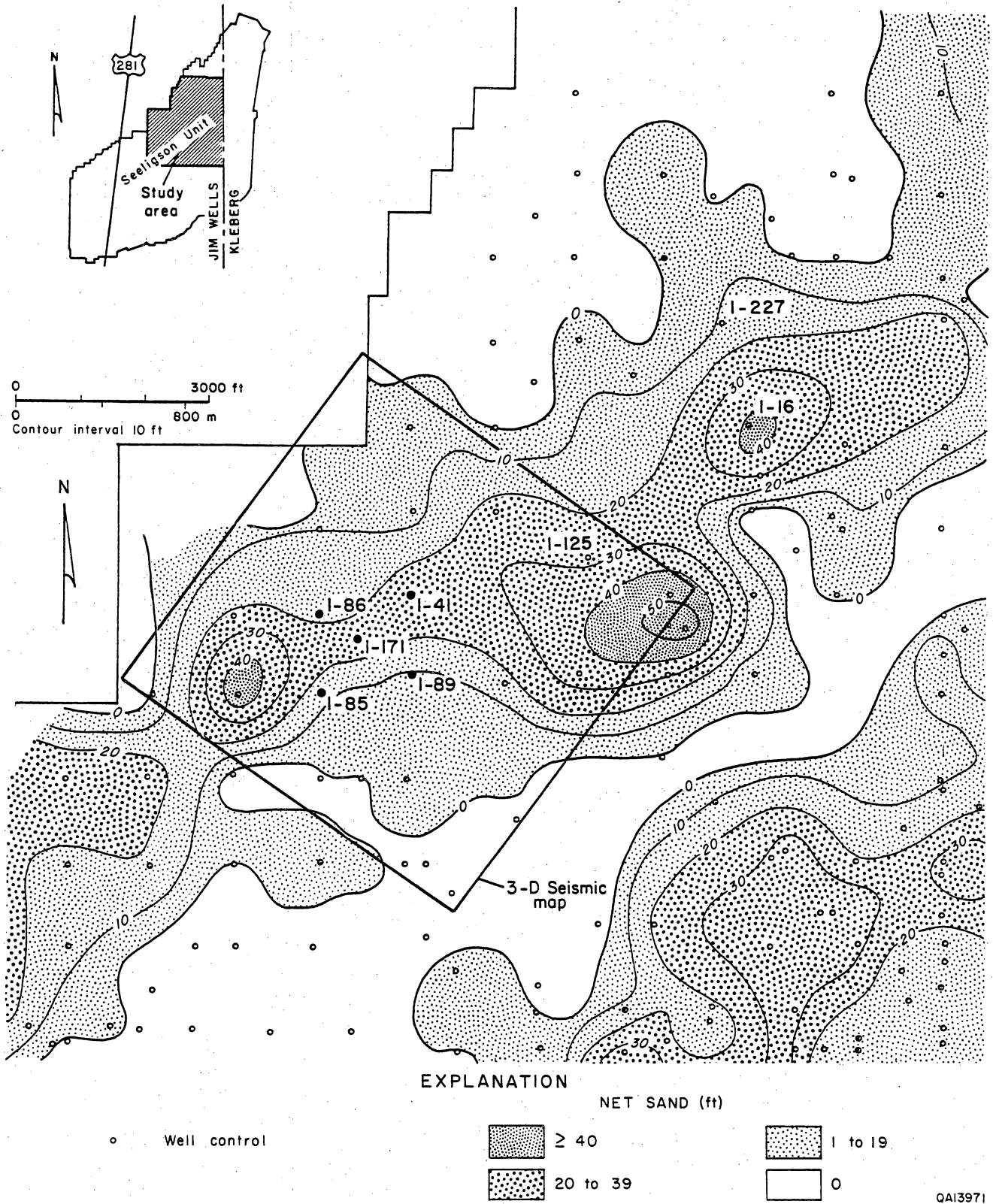


Figure 17. Net-sandstone thickness map of the upper Zone 19C genetic unit in north-central Seeligson field. Two northeast-trending depositional axes, defined by more than 20 ft (6 m) of net sandstone, occur in this part of the field. Three-dimensional seismic map shown in figure 19. Modified from Jirik (1990).

more than 40 ft (12 m) of net sandstone. The northeast-trending belts of sandstone reflect a locally occurring, strike-oriented section of a meanderbelt containing accretion-bar complexes flanked by crevasse-splay and floodplain deposits (fig. 18).

A three-dimensional seismic map of the upper Zone 19C genetic unit (fig. 19) suggests that individual channel-fill deposits in Seeligson field are less extensive laterally than previously inferred from net-sandstone and log-facies maps from well log data (figs. 17 and 18). The conventional net-sandstone and log-facies maps indicate that channel-fill deposits in the field occur in straight to slightly sinuous belts that are 1,500 to 4,000 ft (457 to 1,220 m) wide (Jirik, 1990), whereas the three-dimensional seismic map indicates highly sinuous channel-fill sandstones that were deposited in meanderbelt systems with an average wavelength of approximately 2,700 ft (823 m) and widths ranging from only 500 to 1,000 ft (152 to 305 m). Comparisons between the three-dimensional seismic and the net-sandstone and log-facies maps suggest that reservoir compartments may be smaller than previously inferred and therefore poorly contacted at present well spacing.

The potential impact in utilizing three-dimensional seismic data in a fluvial reservoir is illustrated by the calculated difference in channel sinuosity between inferred geology using well control and seismic-defined topology from three-dimensional imaging. Using net-sandstone thickness to define the thalweg position on the basis of well control indicates the channel sinuosity in the upper Zone 19C genetic unit to be approximately 1.1 (fig. 19a). In contrast, the three-dimensional reflection amplitude anomaly indicates that the probable channel sinuosity is significantly higher and approaches 1.9 (fig. 19b). In the simplest case, advance knowledge of sinuosity and of the thickest reservoir areas would allow strategic positioning of development wells in the reservoir. In field redevelopment the impact might be greatest in screening which wells have the greatest access to laterally extensive reservoirs or might be potentially separated from other reservoir compartments in the same reservoir.

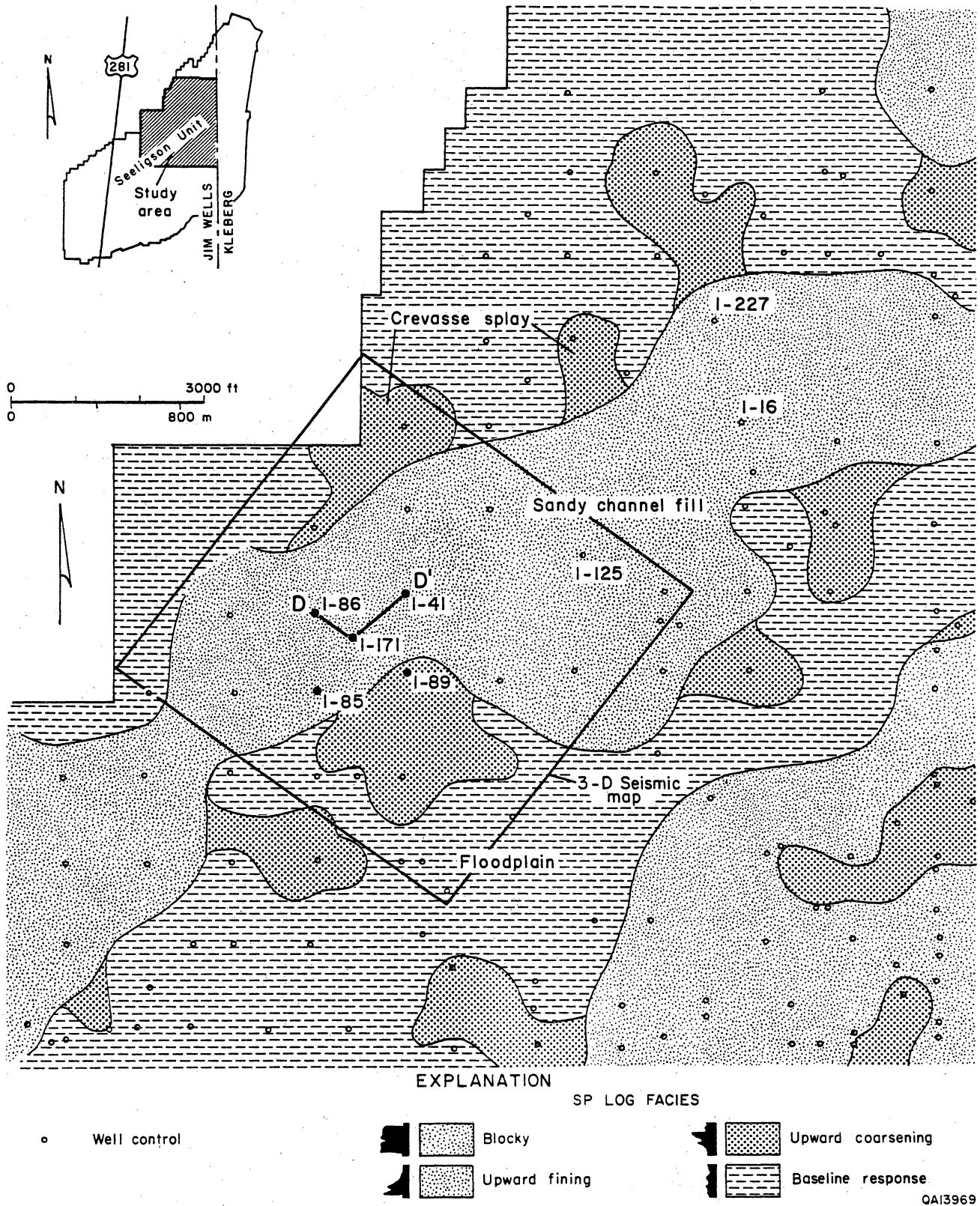
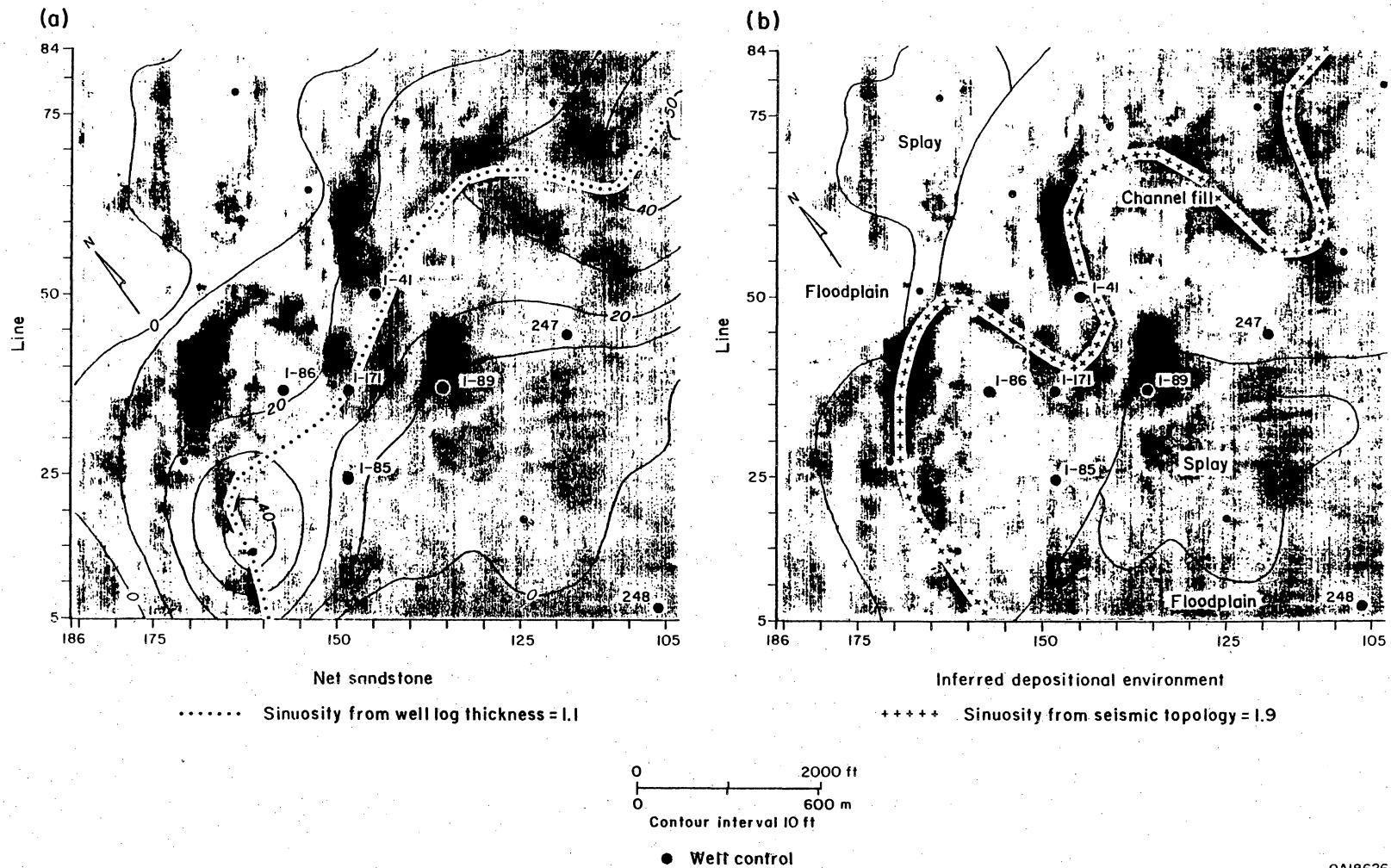


Figure 18. SP log-facies map of the upper Zone 19C genetic unit in north-central Seeligson field. Three-dimensional seismic map shown in figure 19. Cross section D-D' shown in figure 25. Modified from Jirik (1990).



QA18626

Figure 19. Three-dimensional seismic map of the upper Zone 19C genetic unit in north-central Seeligson field, indicating narrow (<1,000 ft [<305 m] wide), sinuous channel-fill deposits. (a) Net-sandstone contours superimposed from figure 17. (b) SP log-facies superimposed from figure 18. Sinuosity is defined as the horizontal distance along the channel thalweg divided by the distance along the channel meanderbelt.

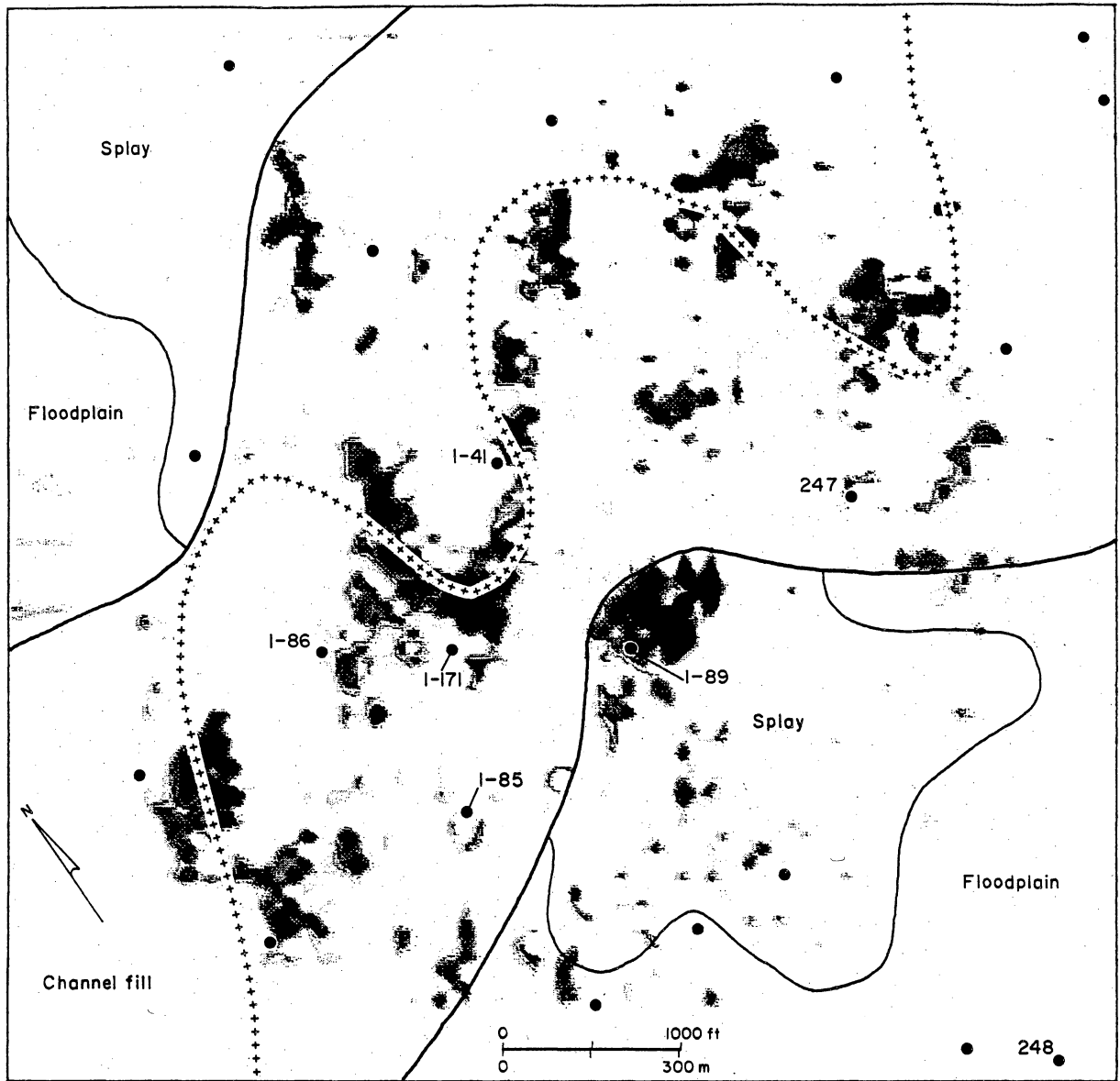
Figure 20 shows a seiscrop map of the amplitude versus offset (AVO) near the level of the Zone 19C reservoir. Comparison with figure 19 illustrates a close correspondence of both reflection amplitude and the positive AVO response. Strong coherence of the relative position of seismic anomalies between these two types of images suggests that both seismic reflection amplitude and saturation response may be affected by similar or related factors. Both images show a similar topology that strongly suggests a sinuous pattern typical of a fluvial depositional system.

Figure 21 illustrates two offset VSP images in the nonunit reservoirs in the middle Frio Formation. A high intensity of interwell variability is inferred from the rapid and strong changes in waveform character away from the 247 well. Rapid lateral changes are commonly associated with fluvial depositional systems where highly sinuous channel patterns dominate.

Potential for Reservoir Compartments

The gas cap in the Zone 19C reservoir has expanded significantly because it was used for recycling and pressure maintenance of an oil rim. According to operator records, the cumulative gas production from 12 wells in the gas cap was 40 Bcf, and the cumulative injection volume was 47.4 Bcf. The negative net production is explained by the expansion of the gas cap and gas production from wells in the oil rim. Since 1974, cumulative gas produced was 19.6 Bcf, with 7.9 Bcf as injected gas. The original reservoir pressure was 2,789 psi, and in 1991 it had declined to about 200 psi.

The gas-recycling project for the Zone 19C reservoir used two wells for injection until 1977, when the reservoir pressure in the gas cap was about 1,250 psi. Gas withdrawals were modest from 1977 until 1984, when workovers and recompletions in the Zone 19C reservoir resulted in a significant increase in producing rate (fig. 22a



EXPLANATION

***** Meanderbelt axis inferred from seiscrop map

● Well control

QA18602

Figure 20. Topology of positive AVO response near the level of the Zone 19C reservoir. Location of three-dimensional seismic grid shown in figure 2.

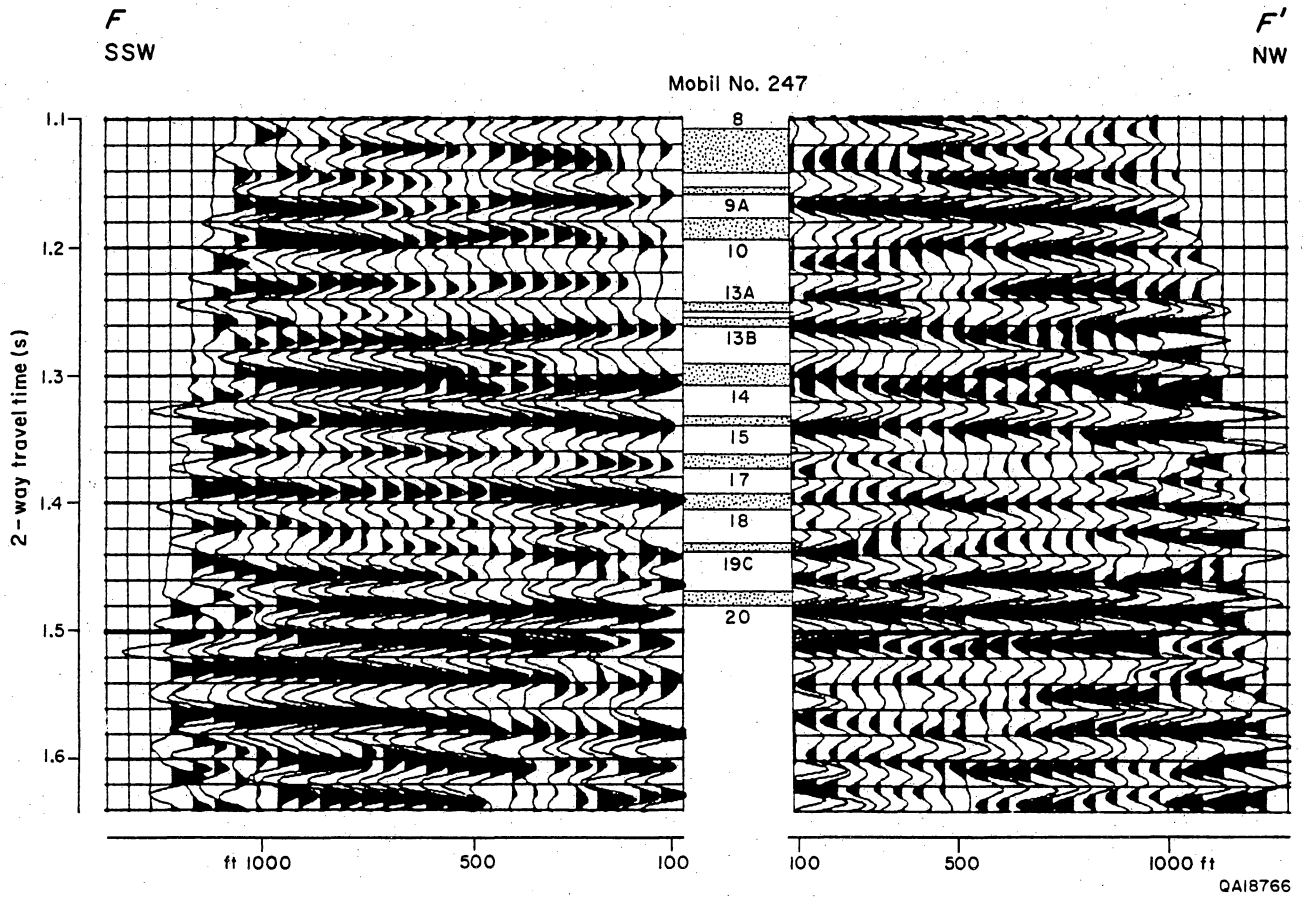


Figure 21. VSP images extending away from the Mobil No. 247 Seeligson well on cross section F-F'. Variable waveform character indicates a high probability of stratigraphic variation away from the well bore. Locations of VSP profiles shown in figure 7.

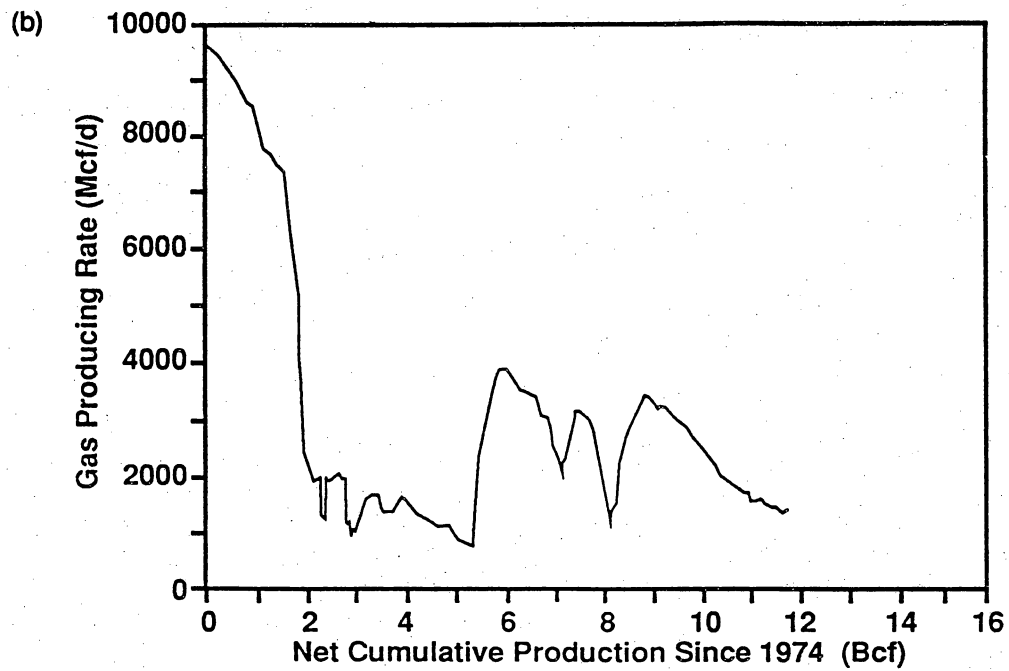
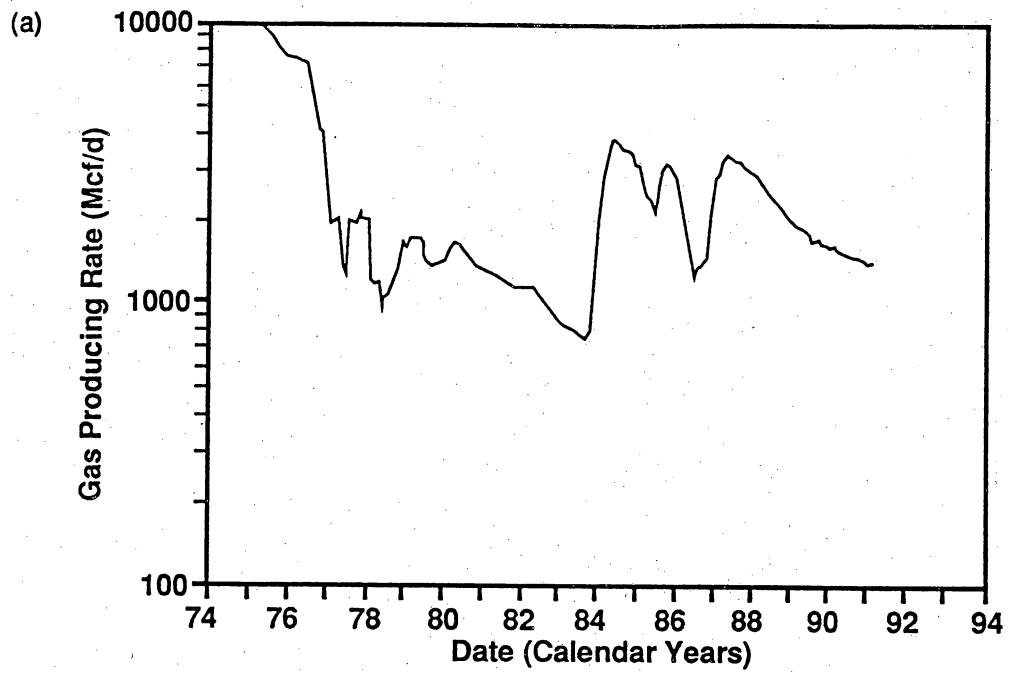


Figure 22. Production data for wells in the Zone 19C reservoir in Tract 1 in north Seeligson field. (a) Semilog plot of daily producing rate versus time. (b) Daily producing rate with cumulative production.

and b). This increase in rate suggested that incompletely drained reservoir compartments with relatively high pressure existed in the Zone 19C reservoir.

The Zone 19C reservoir was selected for study because of five wells (1-41, 1-85, 1-86, 1-89, and 1-171 [fig. 18]) at close proximity for interference testing and borehole seismic tomography. It was hoped that transient well tests would compliment the geophysical data acquisition. The concepts to be examined in this reservoir were potential splay-channel barriers and vertical heterogeneity of channel sandstones.

Production from completions located in the north part of the field (fig. 23) were evaluated for evidence of reservoir compartments. The monthly production data were from 1974, when monthly records started, to 1990. The trend of the pressure data indicates that average reservoir pressure was about 1,450 psi in 1974 and had declined to about 200 psi by 1991 (fig. 24a and b). The cumulative production since recycling operations ceased in 1977 for these completions was about 11.7 Bcf through 1990. A plot of pressure versus composite cumulative indicates a straight-line trend, indicating a volumetric depletion of the wells in a common reservoir without pressure support.

Pressure Data

The pressure data from the gas wells in figure 23 were averaged to obtain annual pressures and establish trends. The cumulative production from the completions were added to give a composite cumulative production. The historical pressure data for the wells consists of shut-in wellhead pressures converted to bottom-hole pressures. Many of these reported data appear to be unreliable. The average annual pressure data since 1974 plot as a straight-line trend with cumulative production (fig. 24a and b). Any reserve growth from the completion additions made later would have caused a flattening of the trend. Therefore, the pressure data probably do not suggest reservoir compartments or reserve growth for the Zone 19C reservoir.

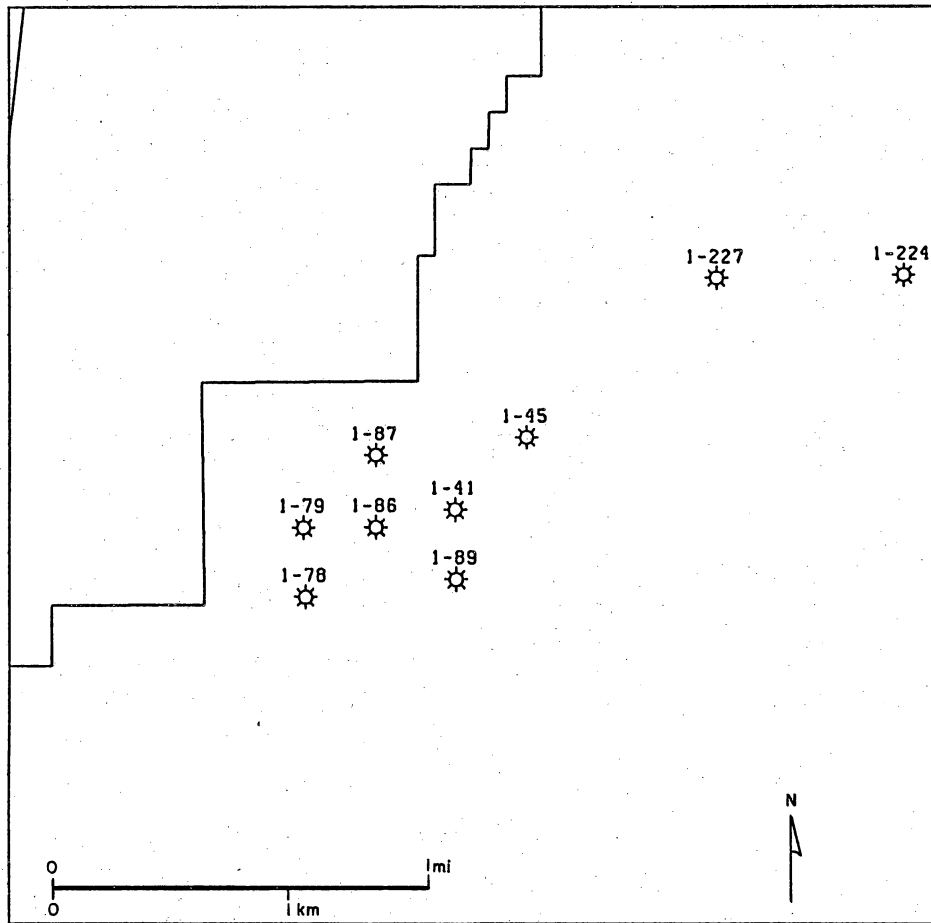


Figure 23. Location of wells completed in the Zone 19C reservoir in Tract 1 in north Seeligson field. Wells 1-78, 1-86, and 1-89 located in figure 2.

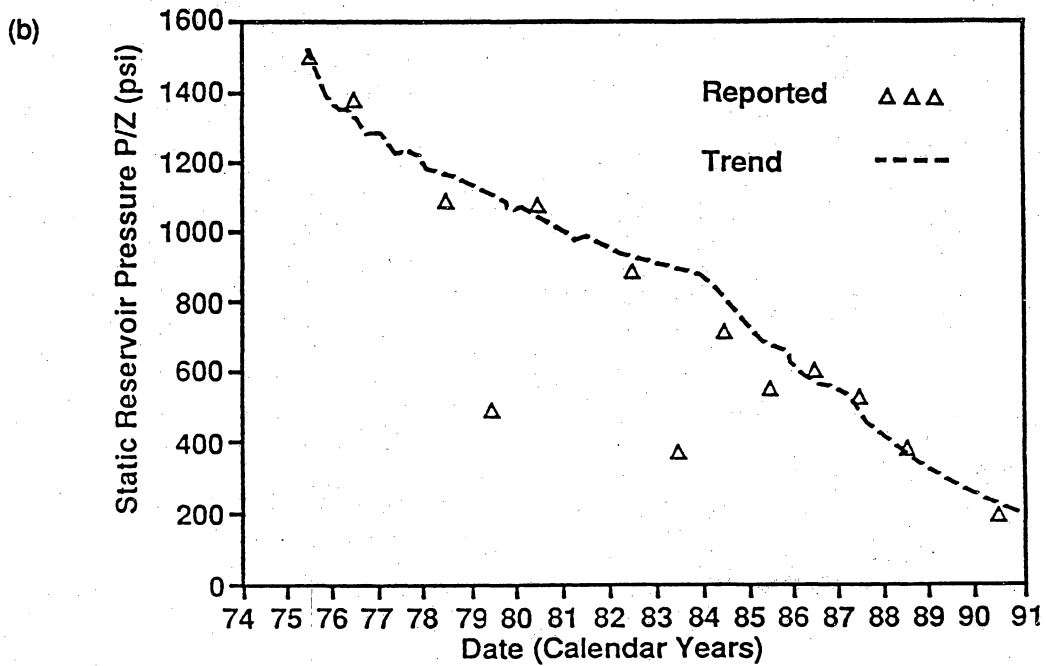
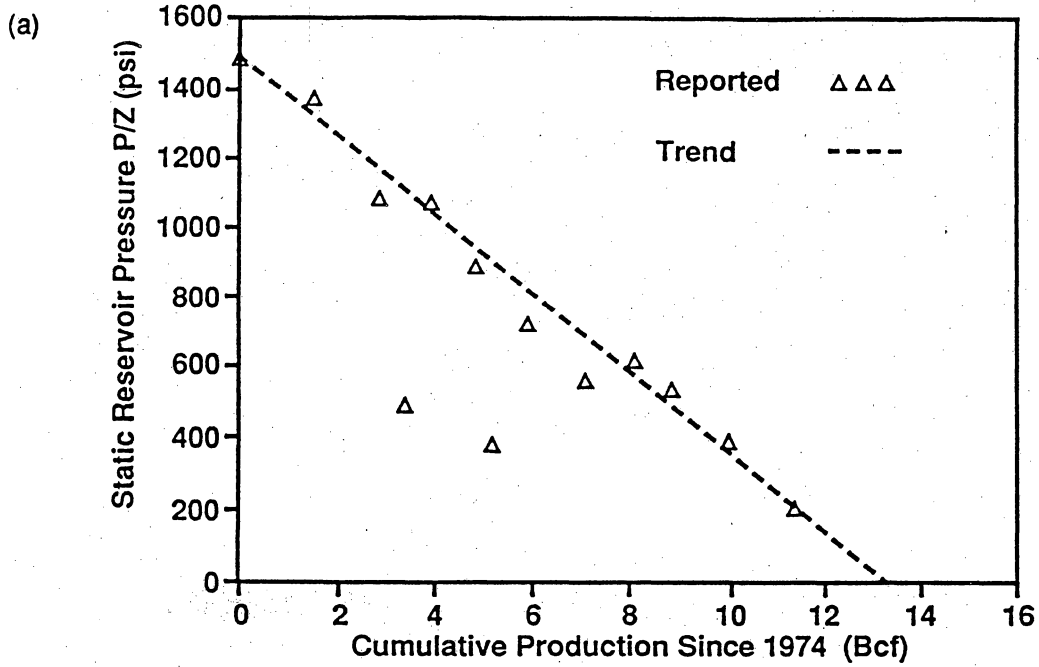


Figure 24. Pressure data in wells in the Zone 19C reservoir in Tract 1 in north Seeligson field. (a) Average reservoir pressure with cumulative production since 1974. (b) Average reservoir pressure versus time.

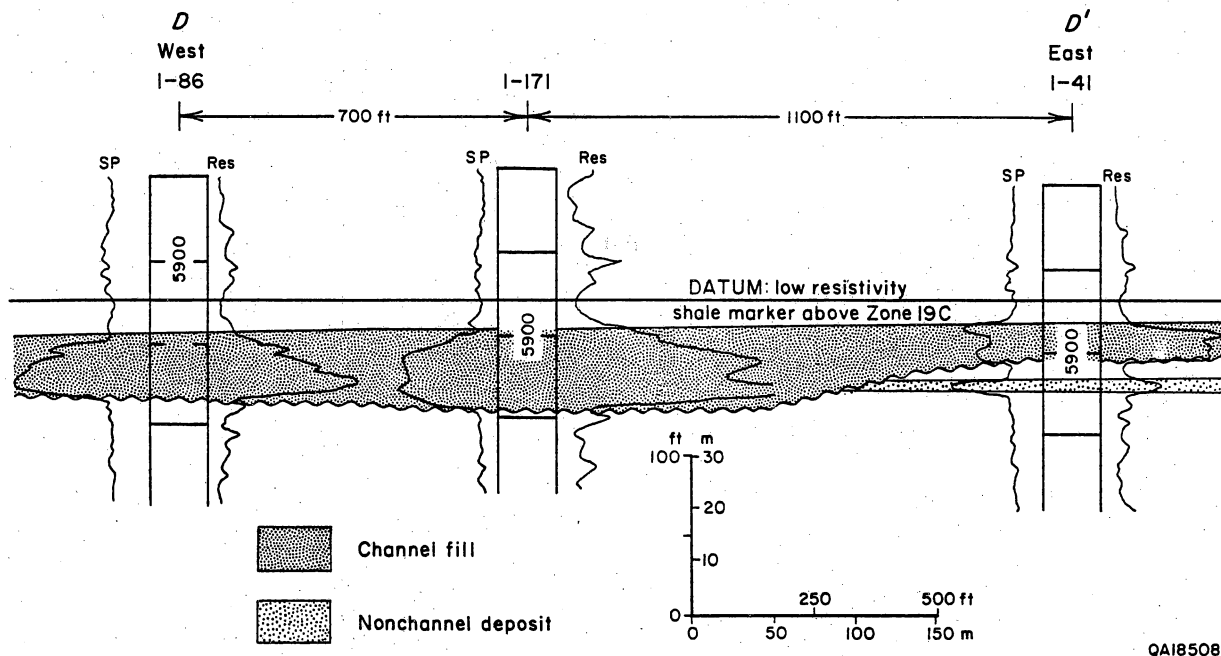
Rate Data

The historical production data from the gas wells are plotted from 1974 through 1990 in figure 22. The sharp drop in producing rate at the end of 1976 follows the end of injection and the simultaneous abandonment of two primary producing wells in the reservoir. The increase in producing rate after 1984 is the result of completions and workovers. The production plots for these wells suggest reserve growth had occurred. However, the pressure data and the composite pressure versus cumulative production indicate that significant reserve growth did not result from these additional completions in the reservoir. The observed rate increase after 1984 is probably the result of repairing damaged wells and increasing the producing well count.

Well Tests

The objectives of well testing in middle Frio reservoirs were to describe potential heterogeneity between channel-fill and splay facies and to quantify reservoir performance characteristics in these facies. Five wells, shown in figure 18, were identified for inclusion in a test plan, which would have observed pressure pulses from two producing wells at three observation wells. Two of the wells, the 1-41 and 1-86, are currently producing from the Zone 19C reservoir. The other three wells were to be recompleted in Zone 19C and tested. The 1-89 well was important because it was completed in a proximal-splay deposit.

Two channel-fill completions (1-41 and 1-86 wells in fig. 25) in the Zone 19C reservoir were tested by pressure buildup in November 1990. The 1-86 well was flowing 430 Mcf/d, with a bottom-hole flowing pressure of 124 psia before shut-in. Calculations from the pressure buildup data yield a permeability of 280 md for the 21 ft (6.4 m) of net reservoir thickness. The extrapolated pressure was determined to be 182 psia at reservoir depth. The 1-41 well was flowing 402 Mcf/d, with a bottom-hole pressure of 151 psia before shut-in. A permeability of 169 md was calculated from the buildup data



QA18508

Figure 25. Stratigraphic cross section D-D' in the undivided Zone 19C reservoir in north Seeligson field. The wells in this cross section are in channel-fill deposits and in pressure communication. Line of section D-D' shown in figure 18.

using a net reservoir thickness of 26 ft (7.9 m). The extrapolated pressure was determined to be 205 psia at reservoir depth. The 27 psia difference between the wells is insignificant and is partly the result of extrapolating the pressure at gauge depth to reservoir depth. The pressure recorders were placed at the bottom of the tubing, which was 120 to 140 ft (36.6 to 42.7 m) above the perforation depths. The 1-89 well was recompleted in Zone 19C, and the reservoir pressure was measured using an electronic gauge, which was left on the bottom for 24 hr in May 1991. The static pressure of Zone 19C was found to be a constant 216 psia at reservoir depth over the 24-hr test period. The 1-171 well was tested for the purpose of a central pressure-observation well an interference test plan. The bottom-hole pressure was 525 psia and rising. This pressure was concluded to be the result of communication with another zone through a channel behind pipe. That well was found unsuitable for well tests and evaluation of the Zone 19C reservoir. A completion was also made in the 1-85 well. Unfortunately, a pressure leak of the casing liner in the well did not allow a determination of the static reservoir pressure of Zone 19C in this well.

The low reservoir pressure and mechanical problems of key wells prevented the execution of the planned interference test for the Zone 19C reservoir. However, the splay facies sandstone in the 1-89 well had a pressure consistent with the static pressures measured in the offsetting channel-fill completions. A review of the Zone 19C production history of the 1-89 well shows that the well was an excellent producer during the time of gas recycling. The gas injection well was completed in a thick portion of the channel-fill facies. We infer that (1) no effective channel-splay barrier isolates the 1-89 from the main channel complex and (2) the splay sandstone has a permeability comparable to that of the channel-fill facies.

Results

The postinjection pressure (P/Z) trend versus cumulative production plots as a straight line, indicating that the completions and workovers did not develop incremental reserves that were trapped in incompletely drained compartments. The productive capacity of the splay completion in the 1-89 well suggests that proximal-splay facies have permeability and deliverability equal to or superior to that of channel-fill facies completions. The large cumulative production attributed to the 1-89 well indicates that it was in excellent communication with the main channel complex.

Pressure measurements in the Zone 19C reservoir confirm a geologic hypothesis of reservoir communication between proximal-splay and channel-fill deposits in this reservoir. Proximal-splay and channel-fill sandstones are commonly well connected physically and contain similar rock properties (average grain size, mudstone content) because they are deposited in similar high- to moderate-energy settings and flow regimes. Gas-producing wells in channel-fill deposits are therefore expected to produce gas from nearby proximal-splay deposits. Future pressure-buildup studies in other fields should be conducted in well pairs in distal-splay and channel-fill deposits, rather than in well pairs in proximal-splay and channel-fill deposits. Unlike proximal-splay and channel-fill deposits, which are commonly well connected and separated by only hundreds of feet, distal-splay and channel-fill deposits are commonly separated laterally by thousands of feet and may contain permeability barriers where thin distal-splay sandstones pinch out into floodplain mudstones.

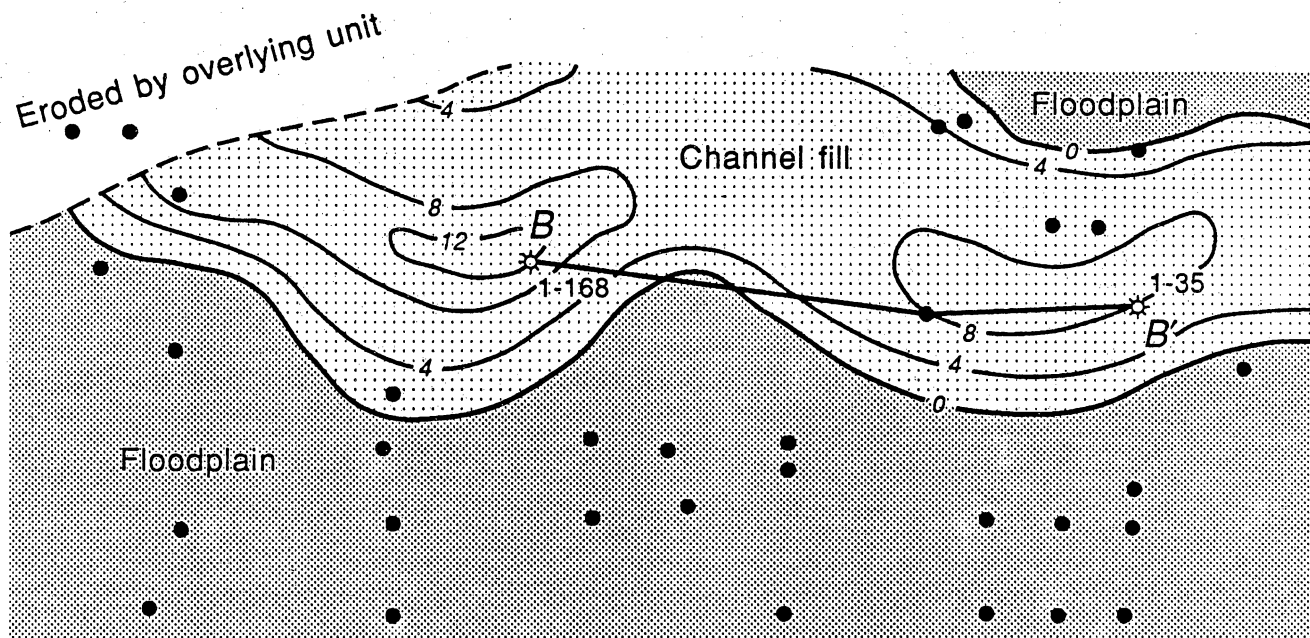
Zone 19B Reservoir

Depositional Environments

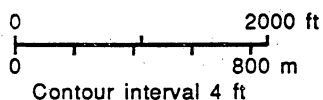
The Zone 19B reservoir is composed of three genetic units (lower, middle, and upper) of which only the lower and middle units are herein described. The lower Zone 19B genetic unit is composed primarily of channel-fill sandstones that average 2,000 ft (610 m) in width (fig. 26) (Jirik and others, 1991). Greatest net-sandstone thickness in the lower Zone 19B genetic unit is only 12 ft (3.7 m), reflecting truncation by the overlying middle Zone 19B genetic unit. The lower Zone 19B genetic unit is completely truncated in the northwest corner of the map area (fig. 26). In contrast, the middle Zone 19B genetic unit contains channel-fill and crevasse-splay sandstones as thick as 27 ft (8.2 m) and thin levee deposits in the northeast corner of the map area (fig. 27).

Potential for Reservoir Compartments

The Oryx No. 1-168 Seeligson well, shown in figures 26 and 27, was recompleted in channel-fill sandstones in the lower Zone 19B genetic unit (fig. 28) (Jirik and others, 1991). Open- and cased-hole water saturation values were similar, and indications of gas-saturated sandstones were observed on logs (fig. 29). In addition, a successful recompletion was made in channel-fill sandstones from both the lower and middle Zone 19B genetic units in the Oryx No. 1-35 Seeligson well (fig. 28 and table 1). These successful recompletions were from reservoir compartments bounded by channel-on-channel contacts, where partial permeability barriers are inferred to exist along mudstone-intraclast zones. The middle and lower Zone 19B sandstones are in erosional contact throughout most of the east-central part of the field, and therefore may be separated by partial permeability barriers.



Log - Facies and Net Sandstone 19B



⊛ Successful new completion

● Well control

QA18350c

Figure 26. Net-sandstone thickness map of the lower Zone 19B genetic unit in east-central Seeligson field. Area of map shown in figure 2. Cross section B-B' shown in figure 28. Modified from Jirik and others (1991).

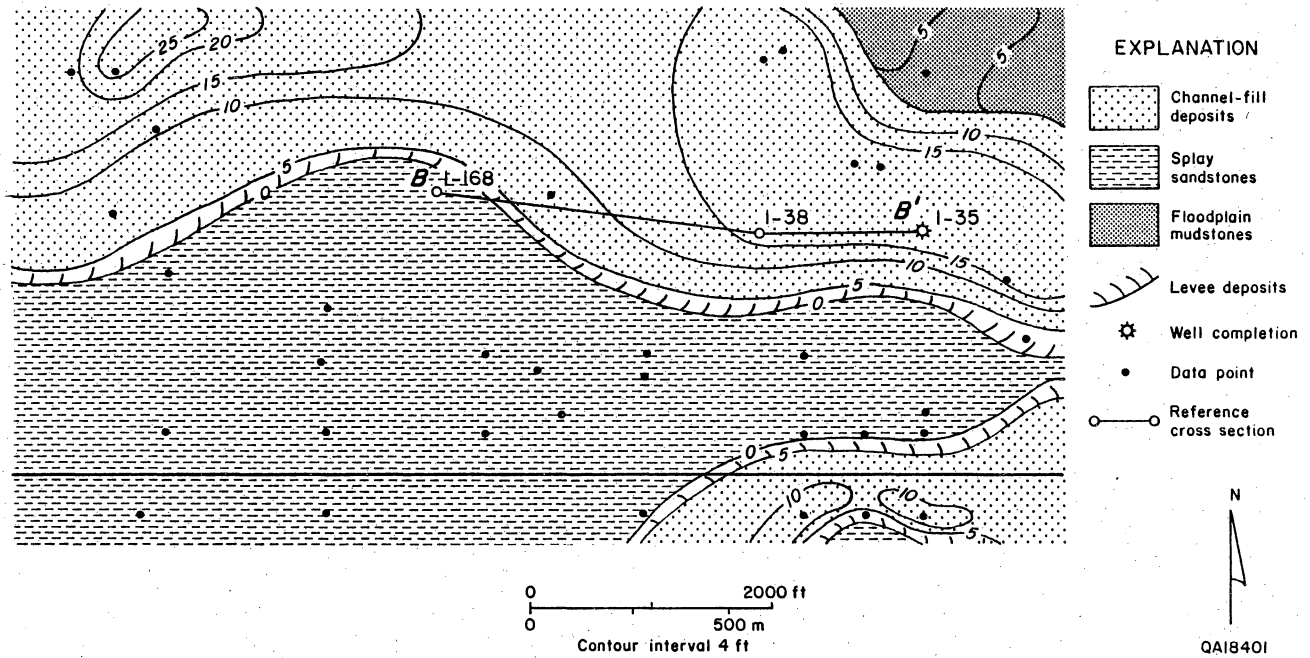
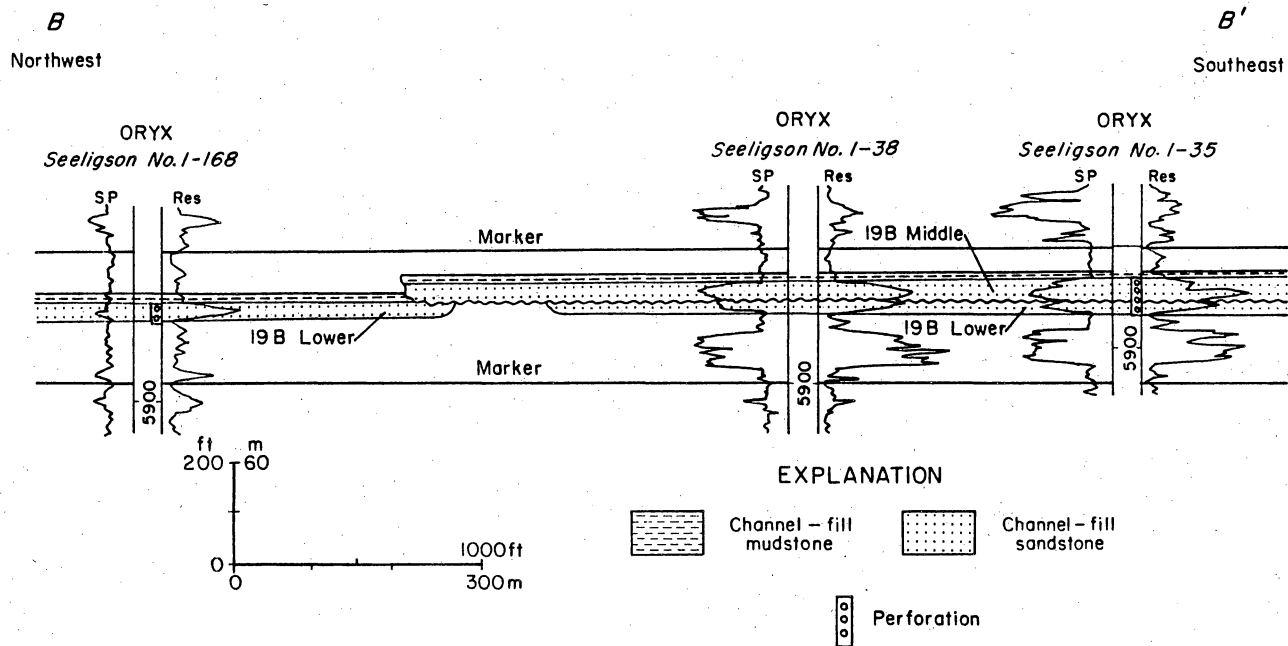


Figure 27. Net-sandstone thickness map of the middle Zone 19B genetic unit in east-central Seeligson field. Area of map shown in figure 2. Cross section B-B' shown in figure 28. Modified from Jirik and others (1991).



QA15225

Figure 28. Stratigraphic dip section B-B' in the lower and middle Zone 19B genetic units in east-central Seeligson field. Line of cross section shown in figures 26 and 27. Modified from Jirik and others (1991).

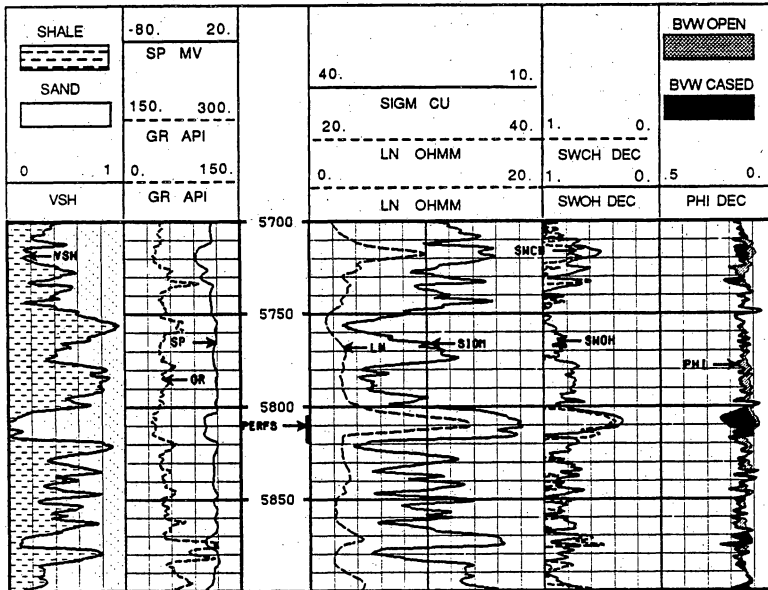
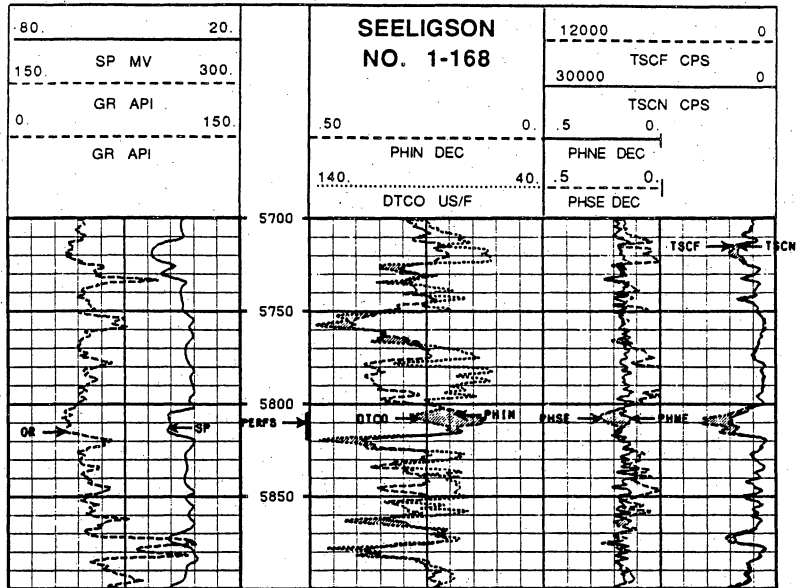


Figure 29. Combined cased-hole log suite, Oryx No. 1-168 Seeligson well, shown with porosity and water-saturation analyses. Well located in figures 26 and 27. From Jirik and others (1991).

Table 1. Successful recompletions in the Zone 14B and 19B reservoirs in east-central Seeligson field. Modified from Jirik and others (1991).

Well	Zone	Cumulative gas to March 1990 (Mcf)	Current rate (Mcf/d)	BHSIP (original)
1-94	14B	399,683	614	240
1-202	14B	298,900	743	240
1-236	14B	403,607	903	240
1-35	19B	212,411	230	210
1-168	19B	96,855	230	210

Zone 18A Reservoir

Depositional Environments

The Zone 18A reservoir consists of a system of south- and southeast-trending meanderbelt (channel-fill) deposits that are locally only 1,000 ft (305 m) wide (figs. 30 and 31). These channel-fill deposits, which are commonly flanked by crevasse-splay and levee deposits, merge eastward into composite belts that are up to 3,500 ft (1,067 m) wide. However, floodplain deposits are restricted to the southwest part of the map area (fig. 31). The crevasse-splay deposits in the east are inferred to be either compound overbank deposits or erosional remnants of older deposits that have been dissected by younger channels. The Zone 18A reservoir exhibits great variability in net-sandstone thickness in the 3.4-mi² (8.8-km²) area (fig. 30). The eastern area contains thick, multiple channel-fill sandstones, whereas the west part contains discrete, narrow meanderbelt deposits that are flanked by extensive, sand-poor levee deposits.

Potential for Reservoir Compartments

Cased-hole logs were obtained from the Zone 18A reservoir in the Oryx No. 1-85 Seeligson well, which is located approximately 5,000 ft (1,524 m) north of the northwest corner of the map area (fig. 30). This well encountered a 15-ft (4.5-m), upward-coarsening sandstone interpreted to be in either a proximal-splay or a channel-fill deposit by northwestward projection of the sinuous belt of channel-fill deposits in the northwest part of the map area (fig. 30). The cased-hole logs indicated a marginally gas productive sandstone with high water saturation (60 percent), and the reservoir was therefore inferred to be nearly depleted in this well (app. 1).

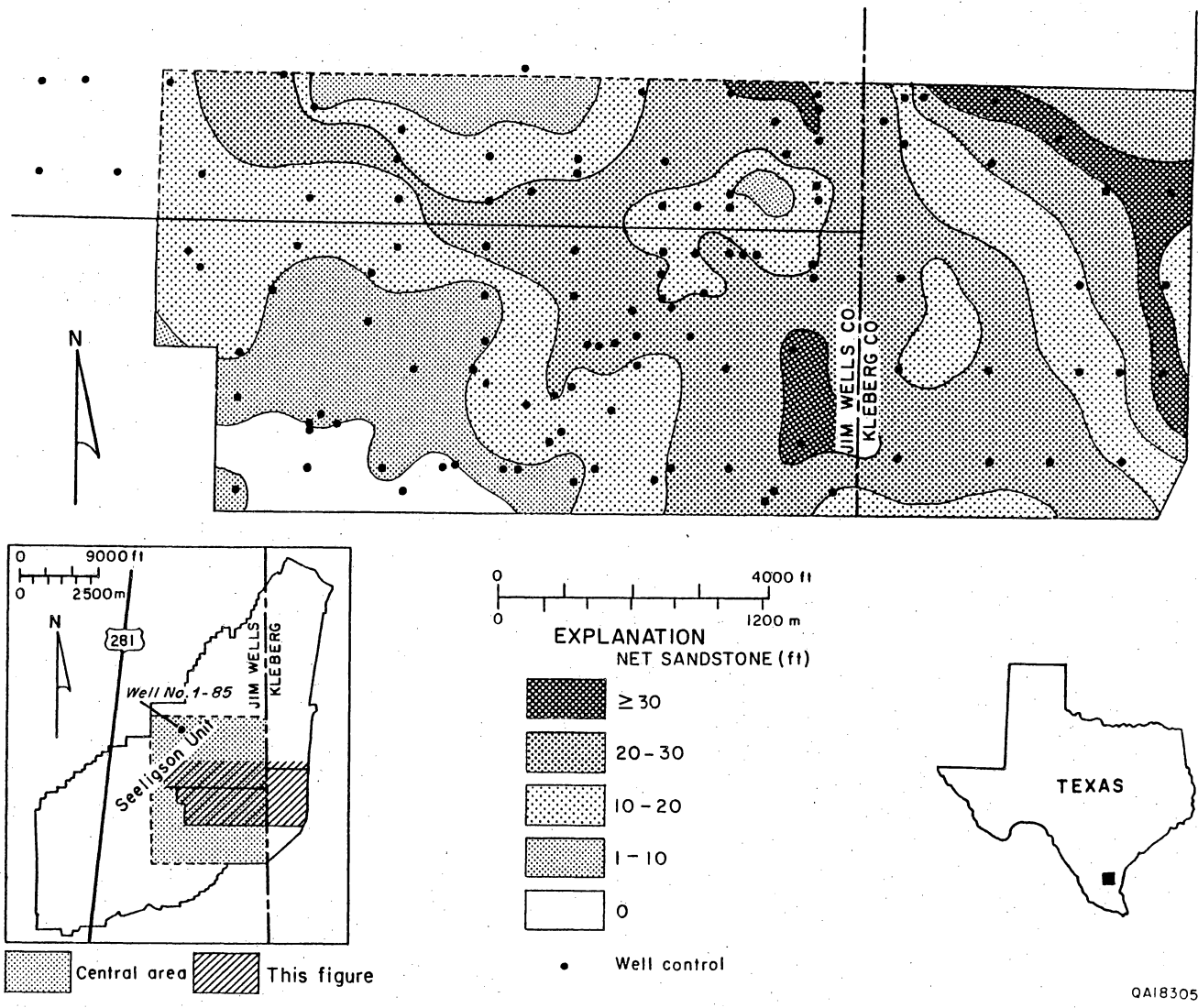


Figure 30. Net-sandstone thickness map of the Zone 18A reservoir in east-central Seeligson field.

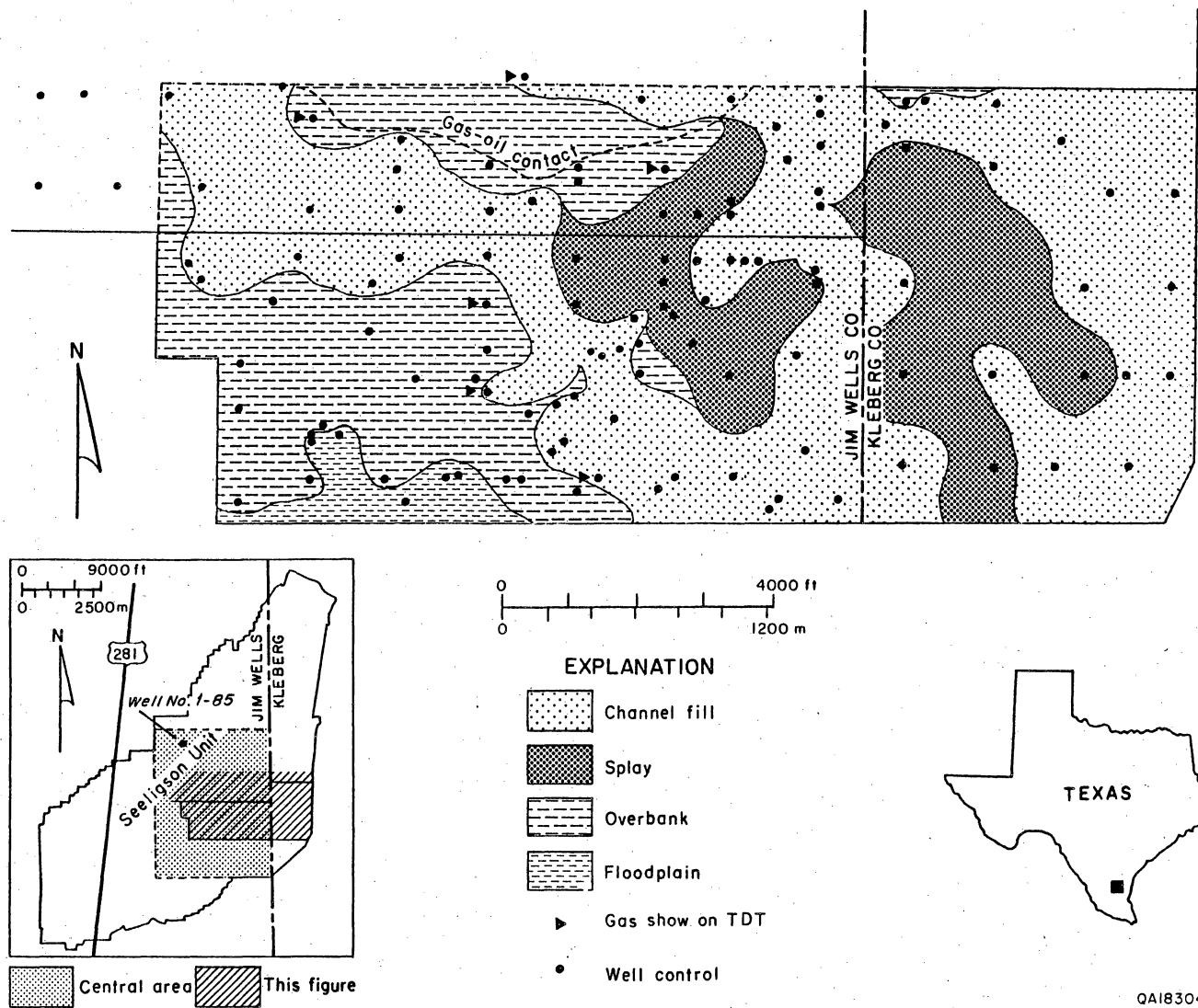


Figure 31. Inferred depositional environments in the Zone 18A reservoir in east-central Seeligson field.

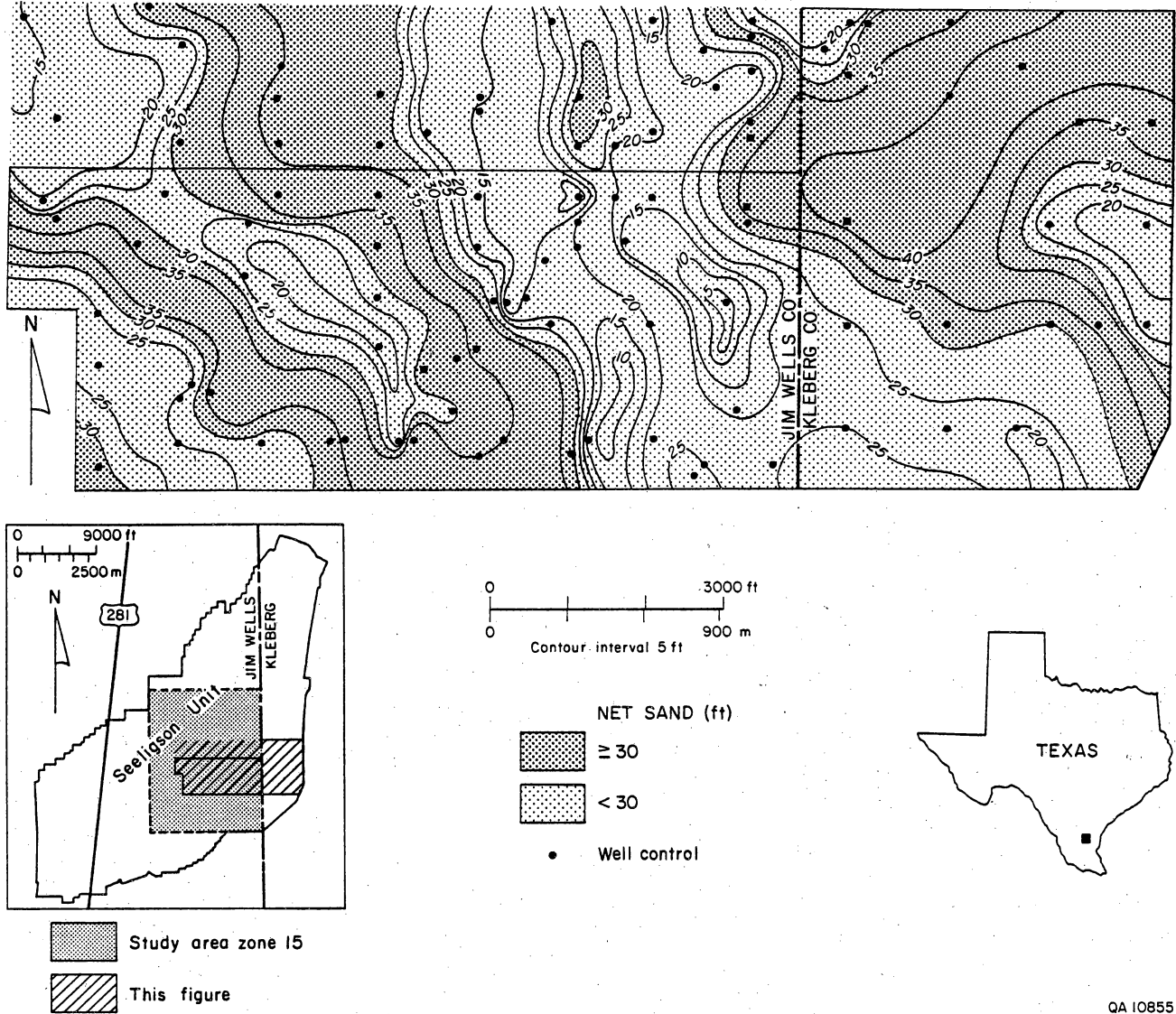
Zone 17 Reservoir

Depositional Environments

Zone 17 is a composite reservoir unit consisting of as many as five genetic depositional units. Net-sandstone thickness of the undivided Zone 17 reservoir ranges from 15 to 50 ft (4.5 to 15.2 m) (fig. 32). Zone 17 is a complex system of southeast-trending, dip-elongate channel-fill sandstones, inferred from blocky and upward-fining SP log response, that vary in width from less than 500 ft (152 m) to more than 4,000 ft (1,220 m) (fig. 33). This variance probably reflects the composite nature of the reservoir. Individual channel-fill sandstone deposits are inferred in the southwest part of the map area, whereas several combined channel-fill sandstone deposits occur in the wide (4,000 ft [1,220 m]) belt in the east.

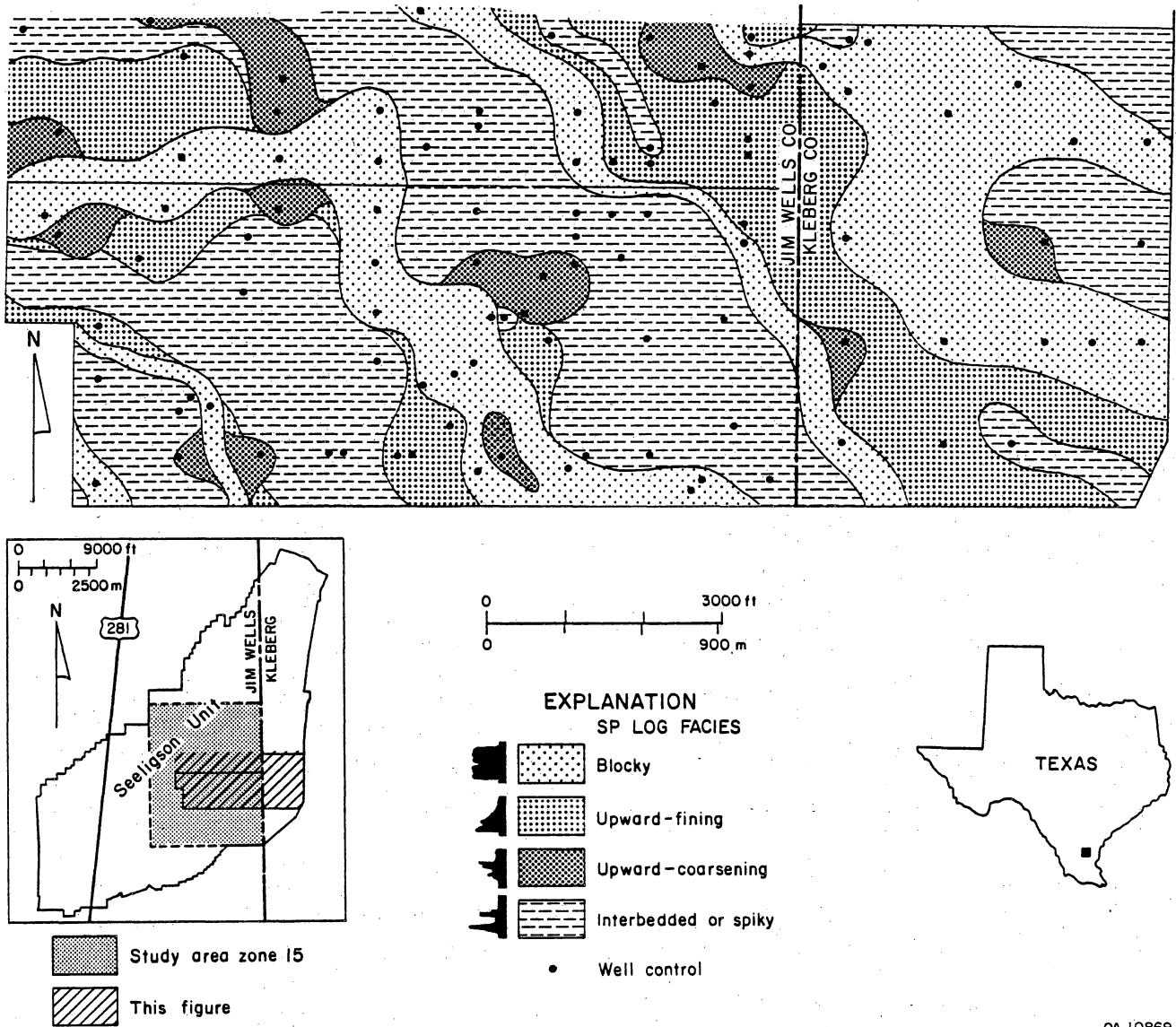
Potential for Reservoir Compartments

Because the Zone 17 consists of multiple sandstones rather than a single sandstone, this reservoir has potential for containing poorly contacted compartments. For example, crevasse-splay deposits in the Zone 17 reservoir occur as scattered, isolated pods of upward-coarsening sandstone commonly less than 1,000 ft (305 m) across (fig. 33). Crevasse-splay deposits in the Zone 17 reservoir have a limited areal extent, which suggests that potential reservoir compartments in this facies may not have been fully contacted at current completion spacing. Cased-hole logs were obtained from the Zone 17 reservoir in the Oryx No. 1-89 Seeligson well, located approximately 3,000 ft (915 m) north of the northwest corner of the map area (fig. 32). In this well, the Zone 17 reservoir consists of three genetic units (sandstones), with either upward-coarsening or spiky SP log responses, each separated by up to 5 ft (1.5 m) of mudstone.



QA 10855

Figure 32. Net-sandstone thickness map of the Zone 17 reservoir in east-central Seeligson field. Cased-hole logs were run in well 1-89 northwest of the map area. Modified from Jirik and others (1989).



QA 10869

Figure 33. SP log-facies map of the Zone 17 reservoir in east-central Seeligson field. Cased-hole logs were run in well 1-89 northwest of the map area. Modified from Jirik and others (1989).

The 1-89 well is inferred to occur in crevasse-splay or levee deposits adjacent to a system of channel-fill sandstones projected northwestward from the map area. Cased-hole logs indicated residual gas, although the high water saturation (60 percent) suggested that the reservoir is virtually depleted in the 1-89 well (app. 1).

Zone 15 Reservoir

At Seeligson field, the Zone 15 reservoir occurs at depths ranging from 5,100 to 5,400 ft (1,530 to 1,620 m) and is divided into four main genetic units (sandstones 15A through 15D). Sandstones 15B and 15C, which are locally separated by a thin (1 to 5 ft [0.3 to 1.5 m]) shale bed (fig. 34), have the widest distribution in the center of the field. The Zone 15 reservoir was the focus of a cooperative data-collection program between BEG and Oryx (Jirik and others, 1989). Wireline pressure tests in a cooperative well (Sun No. 141 P. Canales, located in figs. 2, 35, and 36) indicated higher pressure than anticipated from this supposedly nearly depleted reservoir.

Depositional Environments

Genetic unit 15B consists of elongate dip-parallel belts of channel-fill sandstones ranging from 2 to 20 ft (0.6 to 6 m) in thickness. Two main south-trending depositional axes in the east study area, consisting of channel-fill and splay deposits, merge southward into a wide (4,000 to 5,000 ft [1,220 to 1,524 m]) southeast-trending belt of sandstone (figs. 35 and 36). In contrast to overlying 15B sandstones, 15C channel-fill sandstones are thin (maximum thickness only 10 to 15 ft [3 to 4.5 m]) and distributed in narrow bands 1,000 to 2,000 ft (305 to 610 m) wide (figs. 37 and 38). These sandstones pinch out westward into mudstones. In addition, isolated areas of mudstone, possibly representing abandoned channel-fill deposits, occur between depositional axes.

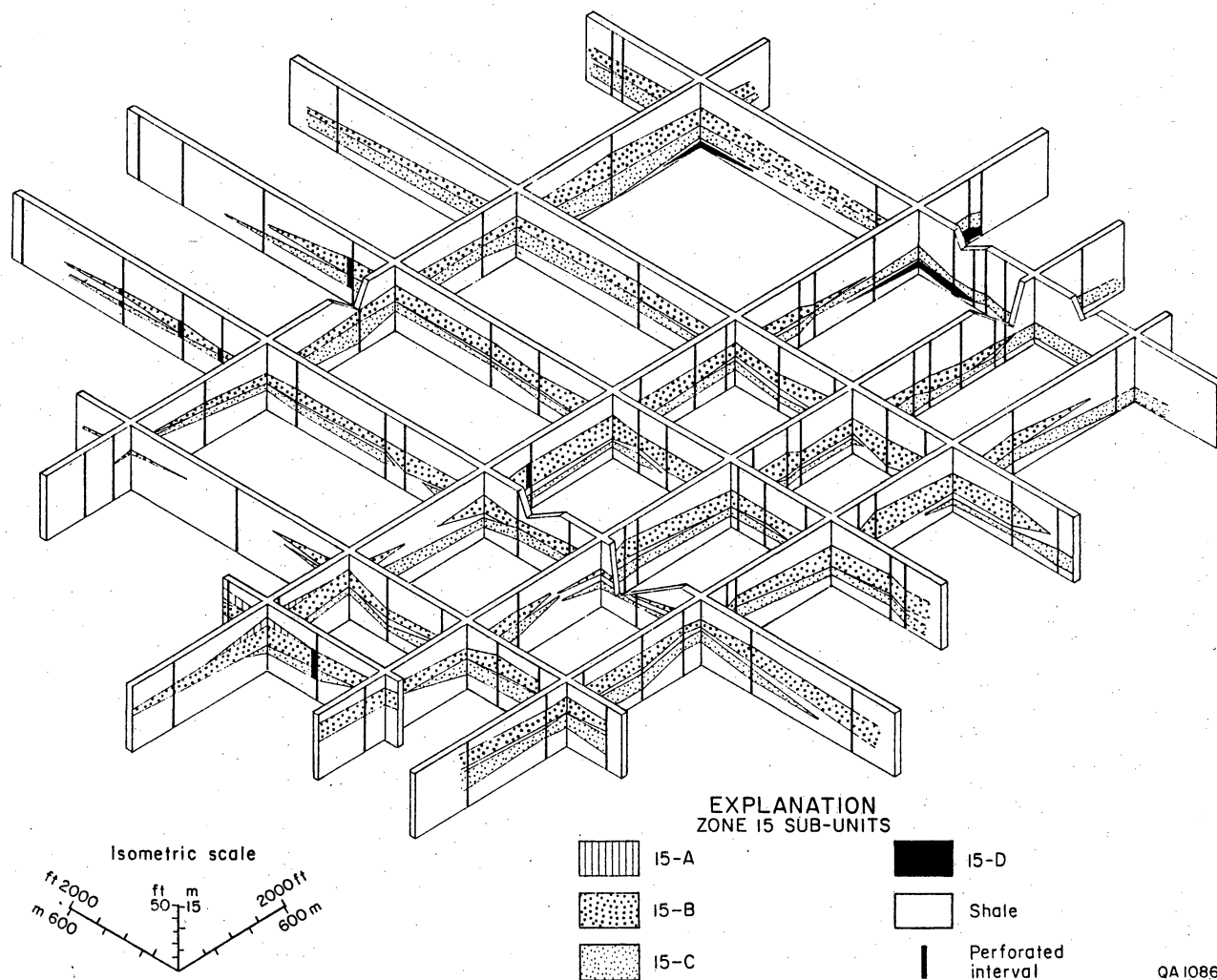
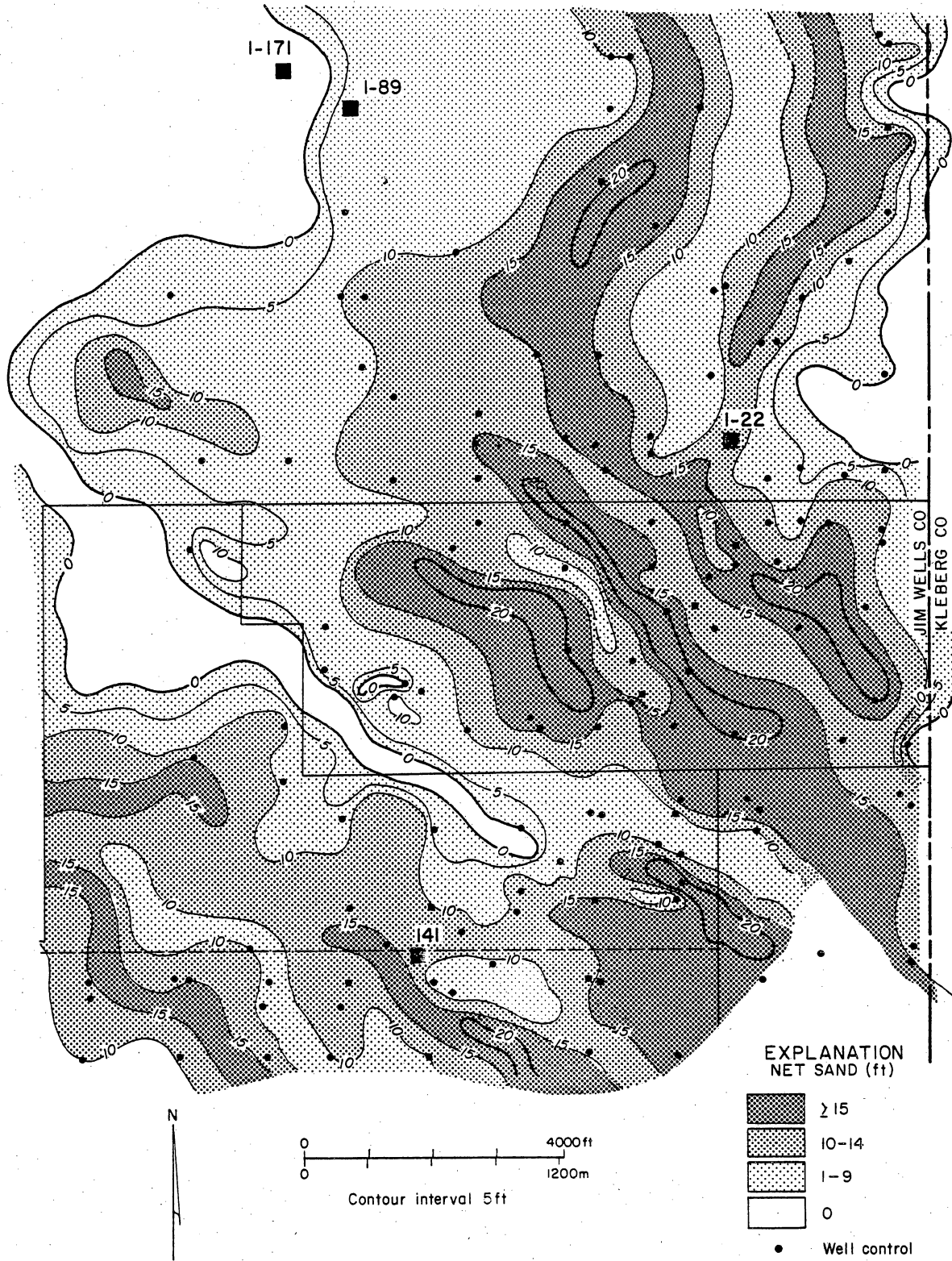


Figure 34. Fence diagram of the Zone 15 reservoir in central Seeligson field. The reservoir has been divided into four genetic sandstones, 15A through 15D. The 15B and 15C sandstones have the widest distribution and are commonly vertically isolated by a thin mudstone. From Jirik and others (1989).



QA10873

Figure 35. Net-sandstone thickness map of the Zone 15B genetic unit in north-central Seeligson field. Major southeast-trending depositional axes occur in the east-central and southwest parts of the area. Modified from Jirik (1990).

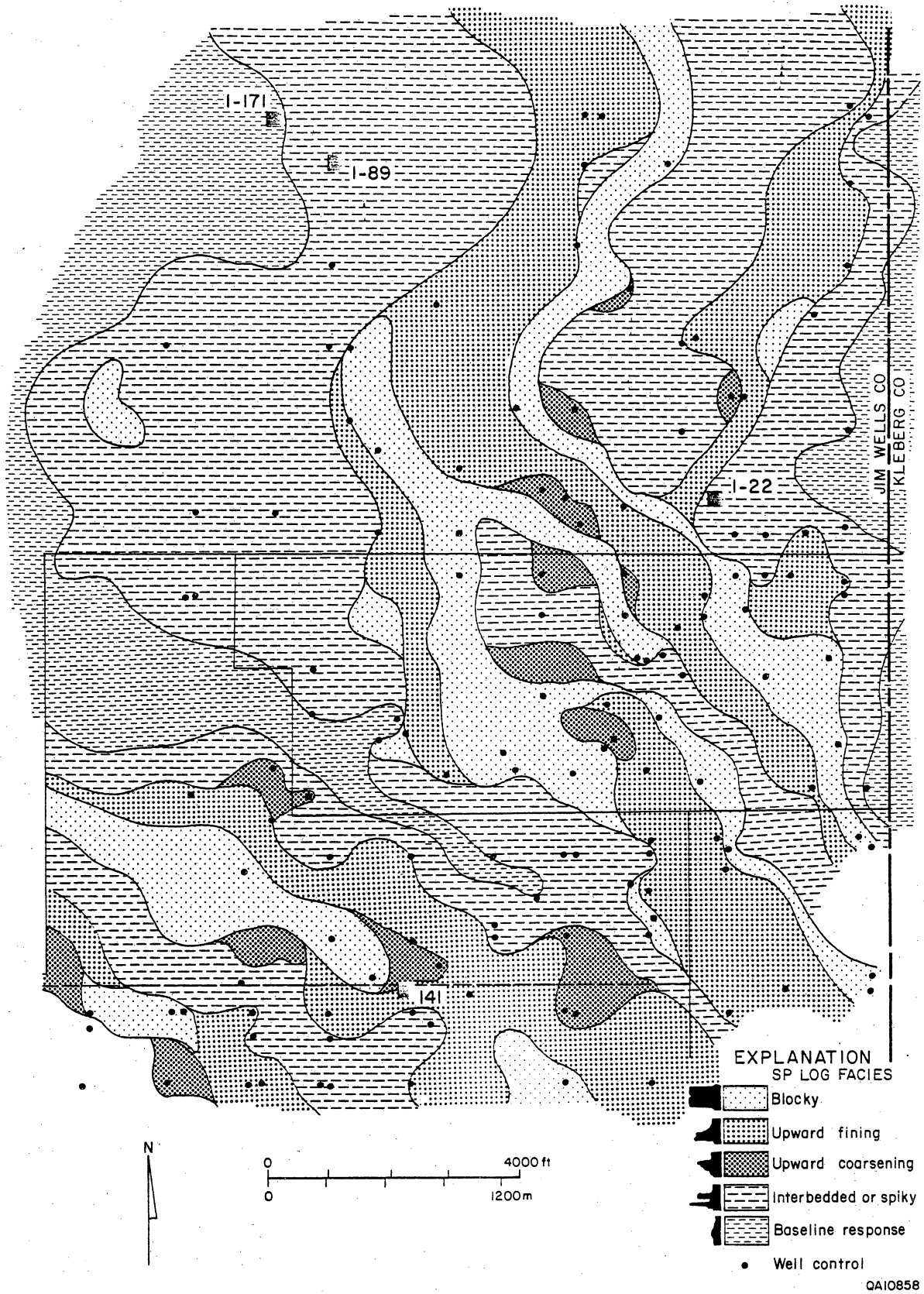
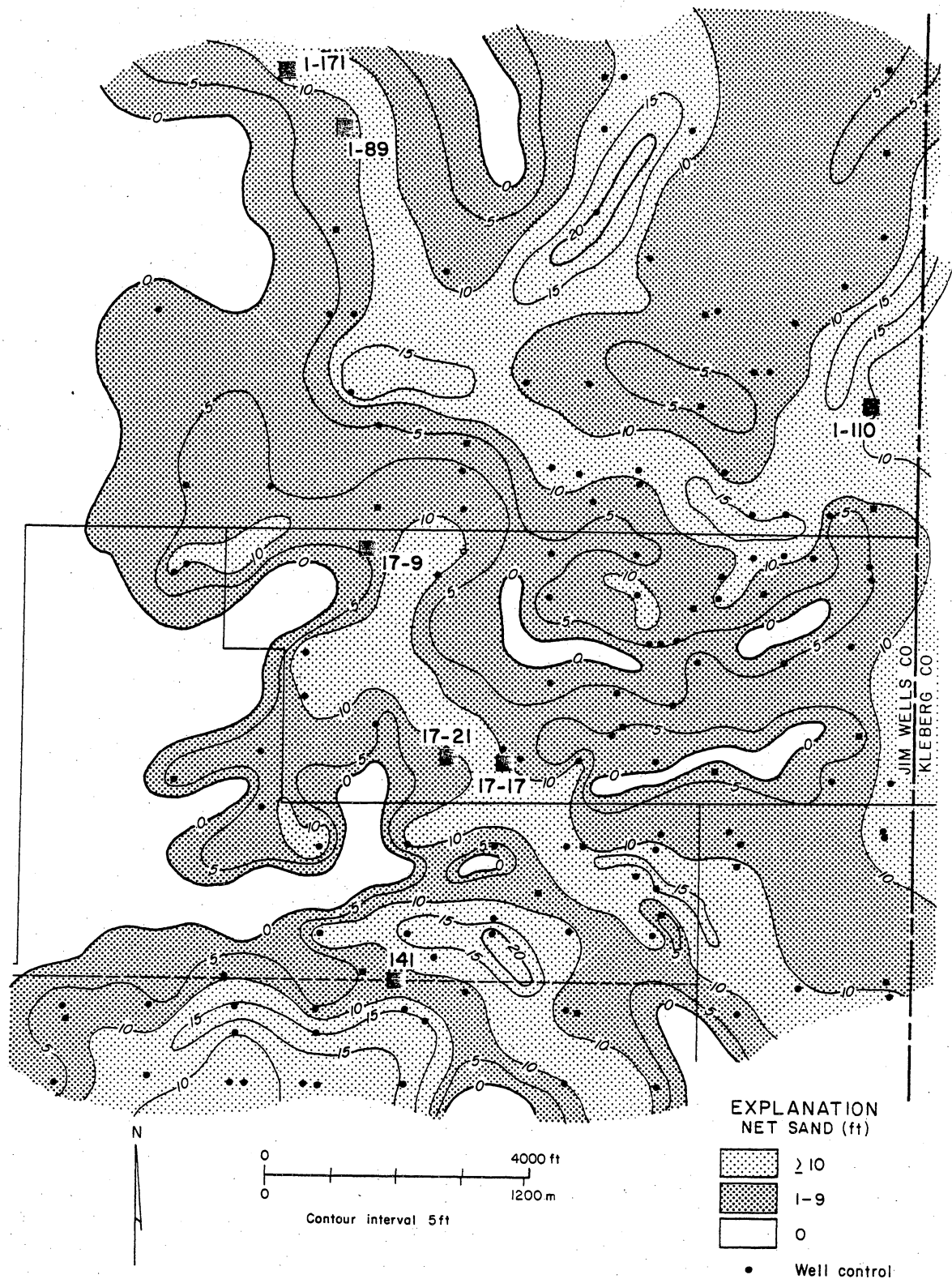


Figure 36. SP log-facies map of the Zone 15B genetic unit in north-central Seeligson field. Modified from Jirik (1990).



QA10857

Figure 37. Net-sandstone thickness map of the Zone 15C genetic unit in north-central Seeligson field. Primary depositional axes, defined by more than 10 ft (3 m) of net sandstone, occur throughout the area. However, sandstones pinch out in the west part of the area. Modified from Jirik (1990).

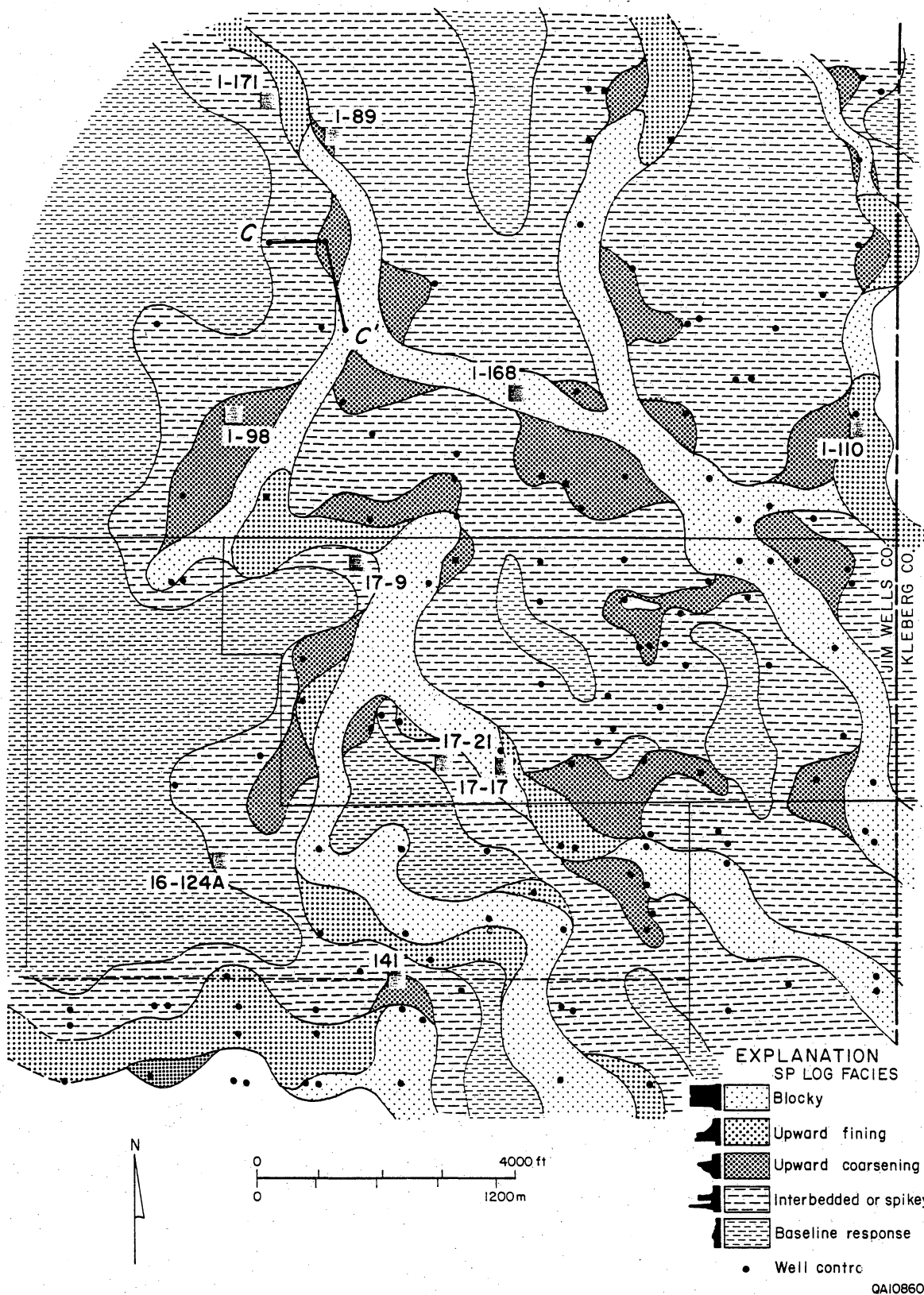


Figure 38. SP log-facies map of the Zone 15C genetic unit in north-central Seeligson field. Crevasse-splay deposits (upward-coarsening log response) are more widespread than in the Zone 15B genetic unit. Localized muddy areas may represent mudstone plugs in abandoned channel-fill deposits. Cross section C-C' shown in figure 45. Modified from Jirik (1990).

Potential for Reservoir Compartments

Production data from completions located in Tract 1 in north Seeligson field (fig. 39) were evaluated for evidence of reservoir compartments. These completions were made from 1966 through 1990. The cumulative production since production decline began in 1974 for Tract 1 Zone 15 completions was about 17.5 Bcf (fig. 40a). The trend of the pressure data indicates the average reservoir pressure was about 1,200 psi in 1974 and had declined to about 250 psi by 1990 (fig. 40b). The trend of pressure versus composite cumulative indicates a straight-line, which in turn indicates a volumetric depletion of the wells in a common reservoir without water-drive support.

Pressure Data

The pressure data for wells in the north part of the field were averaged to obtain annual pressures and establish trends. The cumulative production from all the completions in the Zone 15 reservoir in the north area of the field were added for a composite cumulative production from that part of the reservoir. The historical pressure data for the wells consists of shut-in wellhead pressures converted to bottom-hole pressures. Many of the reported data appear to be unreliable. The average annual pressure data plot a straight-line trend since 1974 (fig. 40a). Any reserve growth from the completion additions made since that time would have caused a flattening of the trend. Therefore, reservoir compartments are not inferred in the channel-fill complex number 1 in the Zone 15 reservoir.

Rate Data

The historical production data from wells completed in the Zone 15 reservoir in the north study area are plotted on figure 41a and b. The increase in producing rate after 1987 is the result of completions made in the Zone 15 reservoir in wells 1-98,

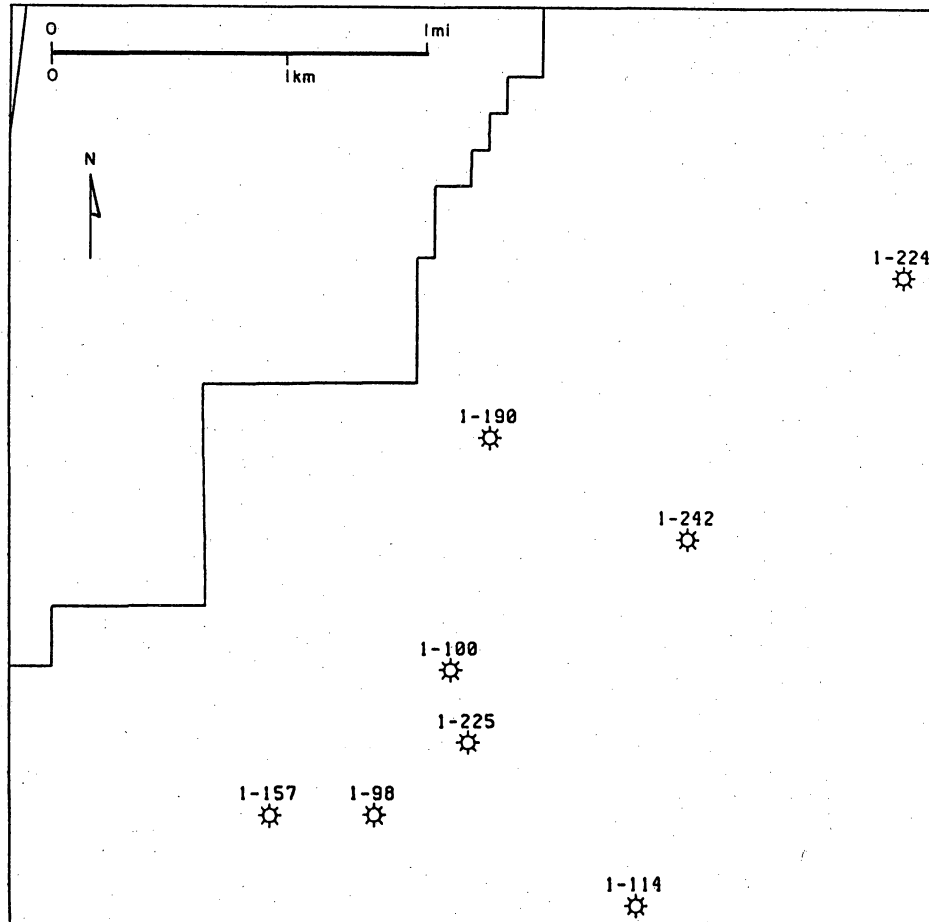


Figure 39. Completions in the Zone 15 reservoir in Tract 1 in north Seeligson field.

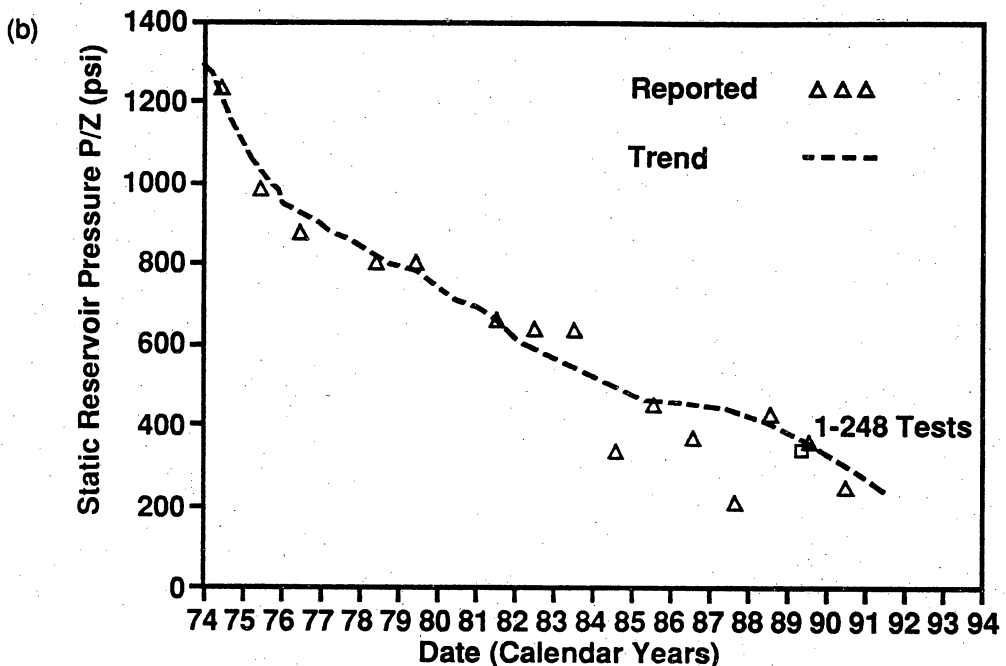
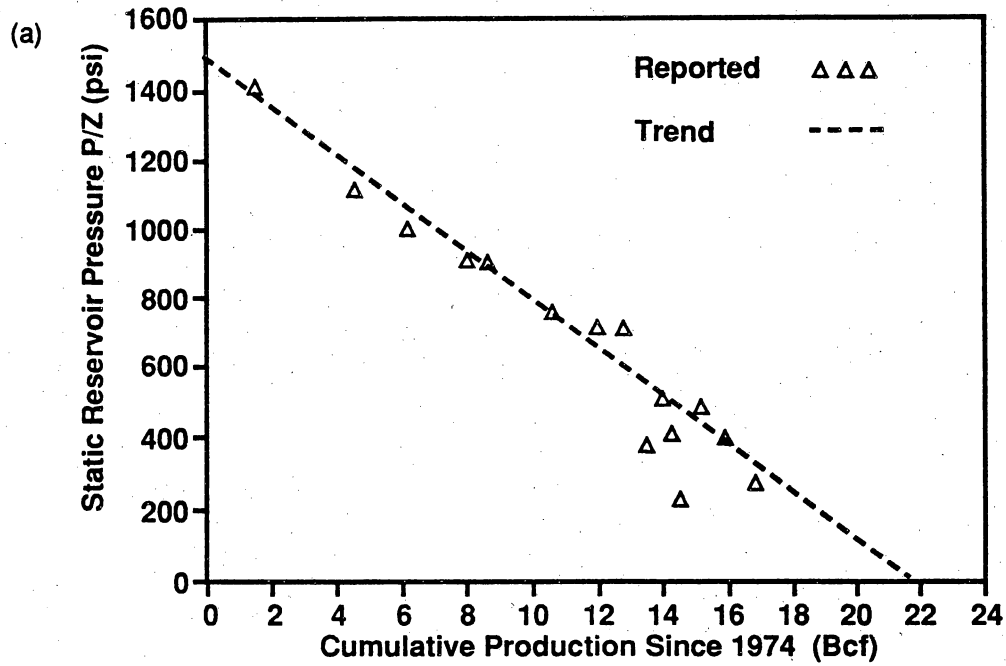


Figure 40. (a) Pressure versus cumulative production in wells in the Zone 15 reservoir shown in figure 39. (b) Post-gas-recycling (1974 to present) pressure-decline plot for the undivided Zone 15 reservoir.

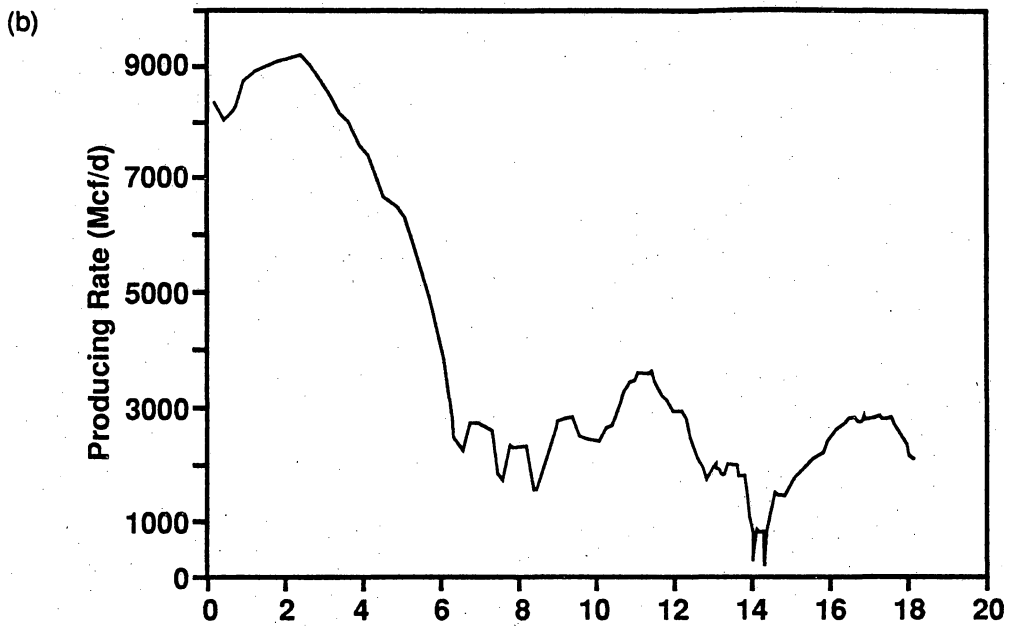
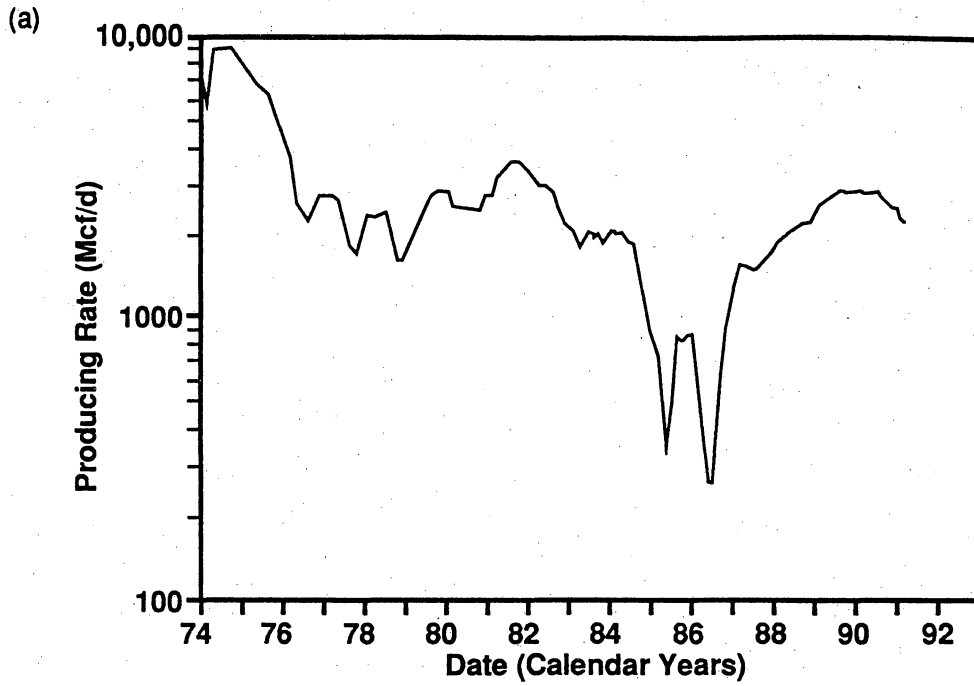


Figure 41. (a) Production rate versus time in Zone 15 wells in north Seeligson field. (b) Pressure versus cumulative production in these wells.

1-100, and 1-225, located in figure 39. A detailed plot of production from these wells since 1987 is shown in figure 42a. The production plots for these wells suggest the possibility of reserve growth; however, the pressure data from these wells and the composite pressure versus cumulative production (fig. 40a and b) show that no significant reserve growth occurred as a result of these additional completions in the reservoir. The production performance of a splay completion is shown by well 1-100 in figure 42a. The production-rate data from that well plot directly over the rate data from the 1-242 well (a channel-fill facies completion). This limited one-well example indicates that splay facies can have permeability and productivity similar to that of the channel-fill facies.

Most wells in the Zone 15 reservoir are inferred to be in pressure communication (fig. 40). Wells with low BHP's (300–600 psi) occur about 1 mi (1.6 km) from each other in sandy channel-fill and channel-margin deposits in a major channel-fill complex (number 1 in fig. 43). These wells (1-225, 1-114, and 1-163) have probably drained this major channel-fill complex; well 1-225 has produced 35 Bcf of the total 57 Bcf that has been produced from the Zone 15 reservoir in the southeast part of the field. Well 17-1 occurs in a proximal-splay deposit that is adjacent to the major channel complex and is apparently in communication with the reservoir. In addition, wells 1-157, 1-47, and 1-160 (northwest corner of map in fig. 43) are marginal to a narrow channel-fill deposit and exhibit low reservoir pressures, indicating that these wells are also in pressure communication.

Well Tests

Zone 15 was tested by wireline RFT measurements in the Mobil No. 248 Seeligson well in June 1989, located in channel-fill complex number 1 (fig. 43). Three valid RFT measurements were obtained in the 22-ft (6.7-m) sandstone interval to investigate vertical pressure differences of two channel-on-channel sandstones. Both the Zone 15B

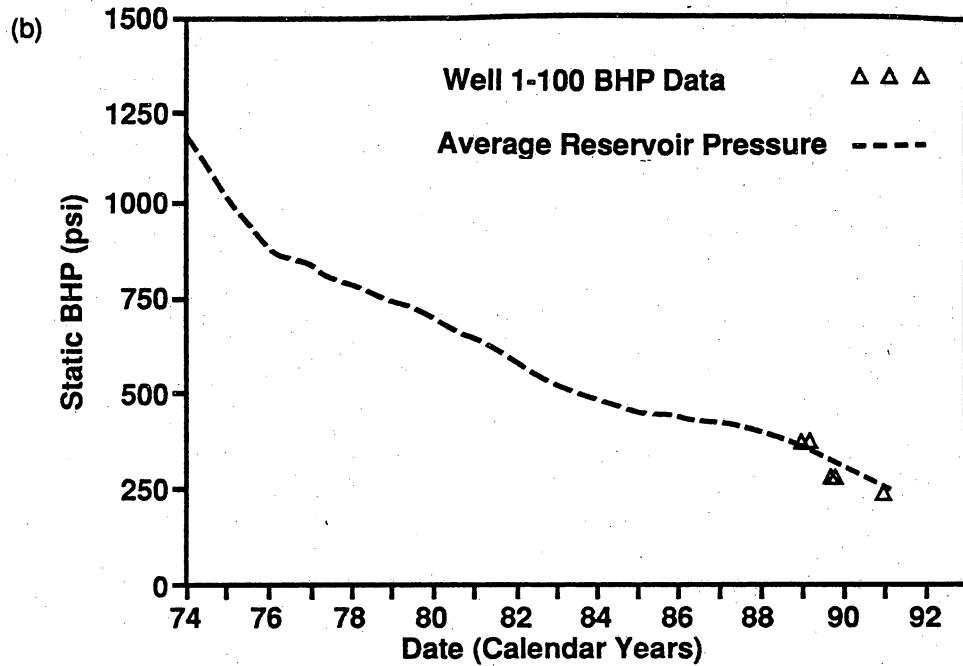
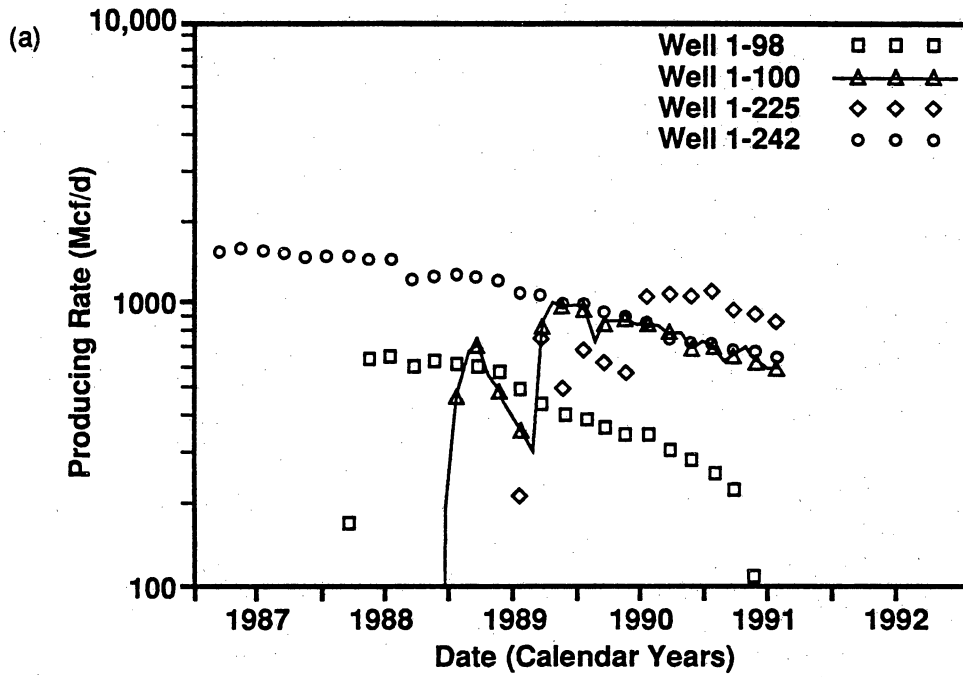
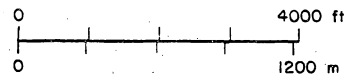
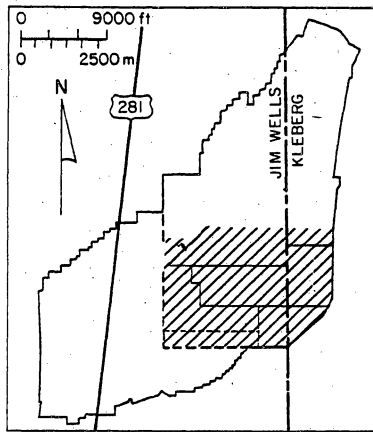
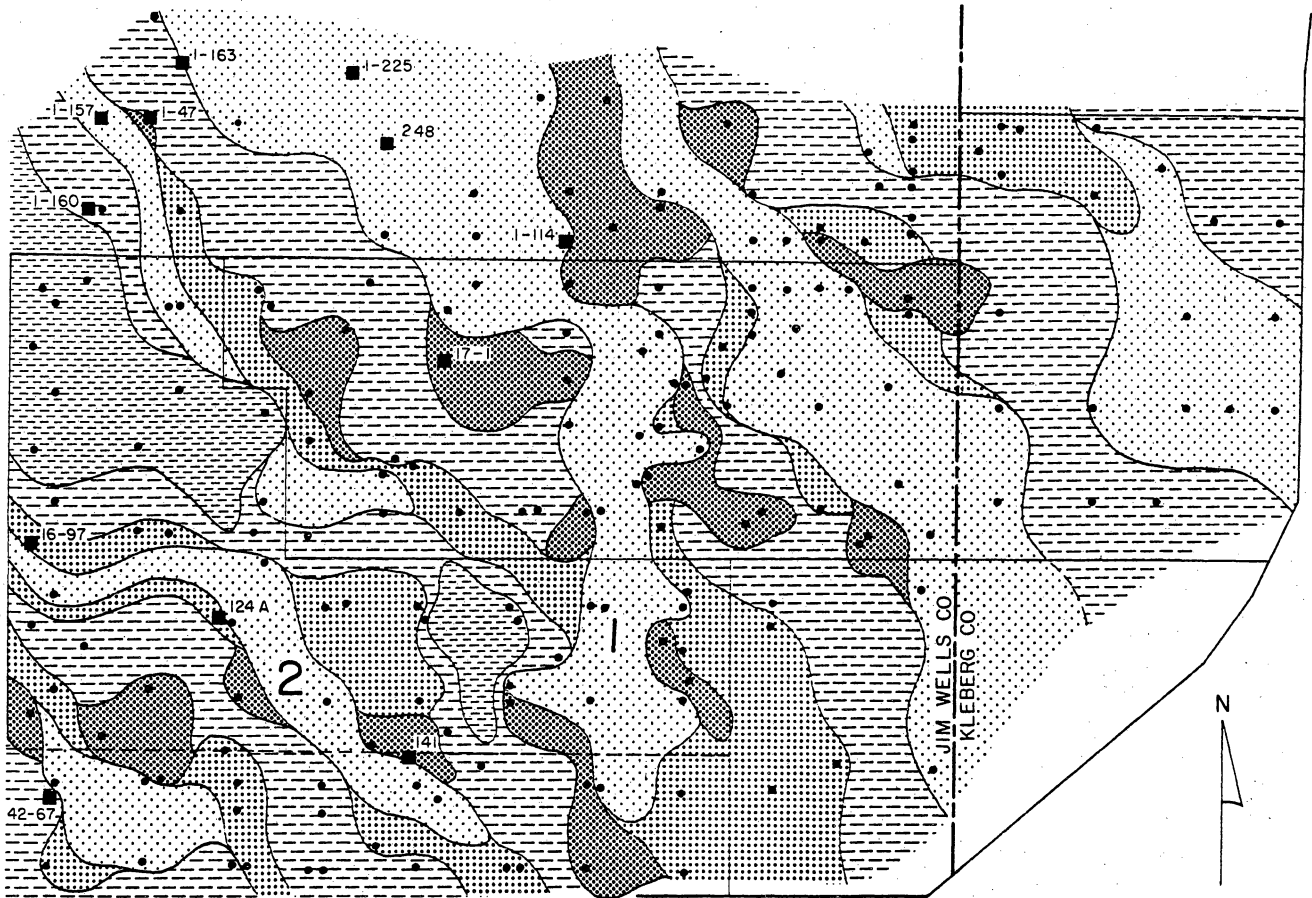
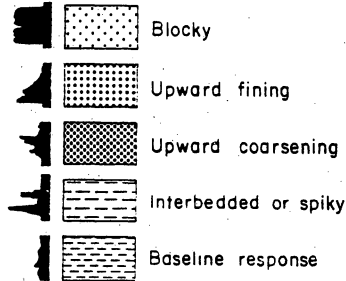


Figure 42. (a) Gas-production rate versus time in Tract 1 wells (shown in fig. 39) in the Zone 15 reservoir in north Seeligson field. (b) Pressure versus time in the Oryx No. 1-100 well.

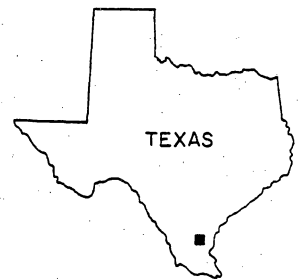


EXPLANATION
SP LOG FACIES



■¹⁴¹ Well with BHP data

• Well control



This figure

QA 10867

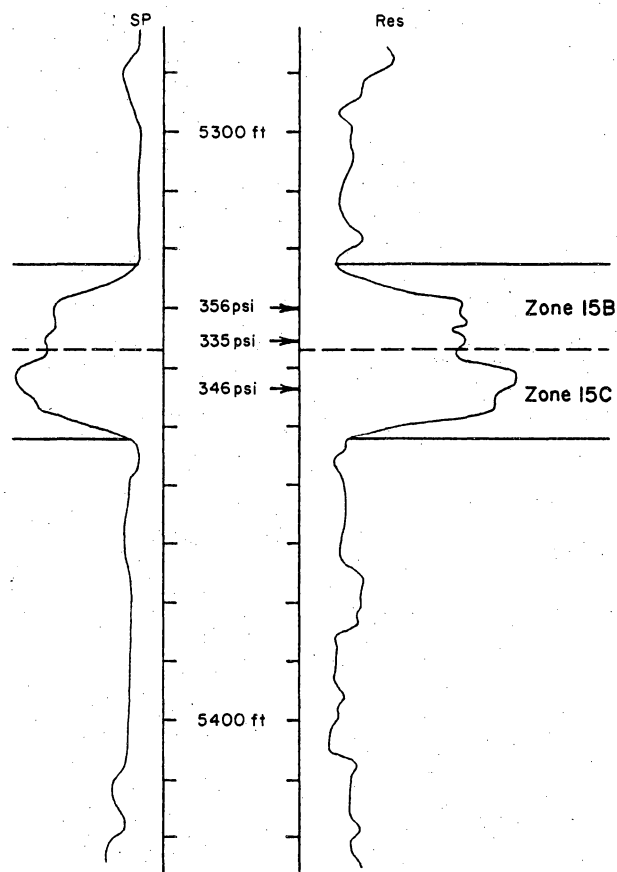
Figure 43. SP log-facies map of the undivided Zone 15 reservoir in north-central Seeligson field. Two major channel-fill complexes are separated by a tongue of floodplain mudstone. Higher-than-expected reservoir pressures were encountered in some recompleted wells (shown in fig. 46) in the southwest channel complex labelled number 2. Modified from Jirik (1990).

and 15C genetic sandstones were tested separately. The 15C genetic sandstone was measured to be at 346 psi, and the 15B genetic sandstone had an average pressure of 345 psi (fig. 44). These data indicate that the two channel-fill sandstones are in pressure communication at this well. The trend of the static bottom-hole pressure data in the Zone 15 reservoir from the nearby completions indicates an average of 353 psi in 1989 (fig. 40b) and closely matches the results of the wireline tests in well 1-248. The Zone 15 reservoir completions in the northern area (fig. 39) are probably in effective lateral and vertical pressure communication.

A pressure buildup test to evaluate lateral pressure variation in the Zone 15 reservoir was performed in November 1990 in the Oryx No. 1-100 Seeligson well. This well was tested because it was interpreted to occur in an incompletely drained proximal-splay deposit adjacent to a channel-fill deposit (Jirik and others, 1989), a completion made after a previous study of the Zone 15 reservoir (Jirik and others, 1989) (fig. 45). The well test was made to evaluate whether there was pressure discontinuity between the proximal-splay and channel-fill facies and whether these two facies have differences in permeability. The 1-100 well was successfully completed in the reservoir in December 1988, but it could not be determined from the existing data whether the reserves were incremental or were due to accelerated reservoir decline.

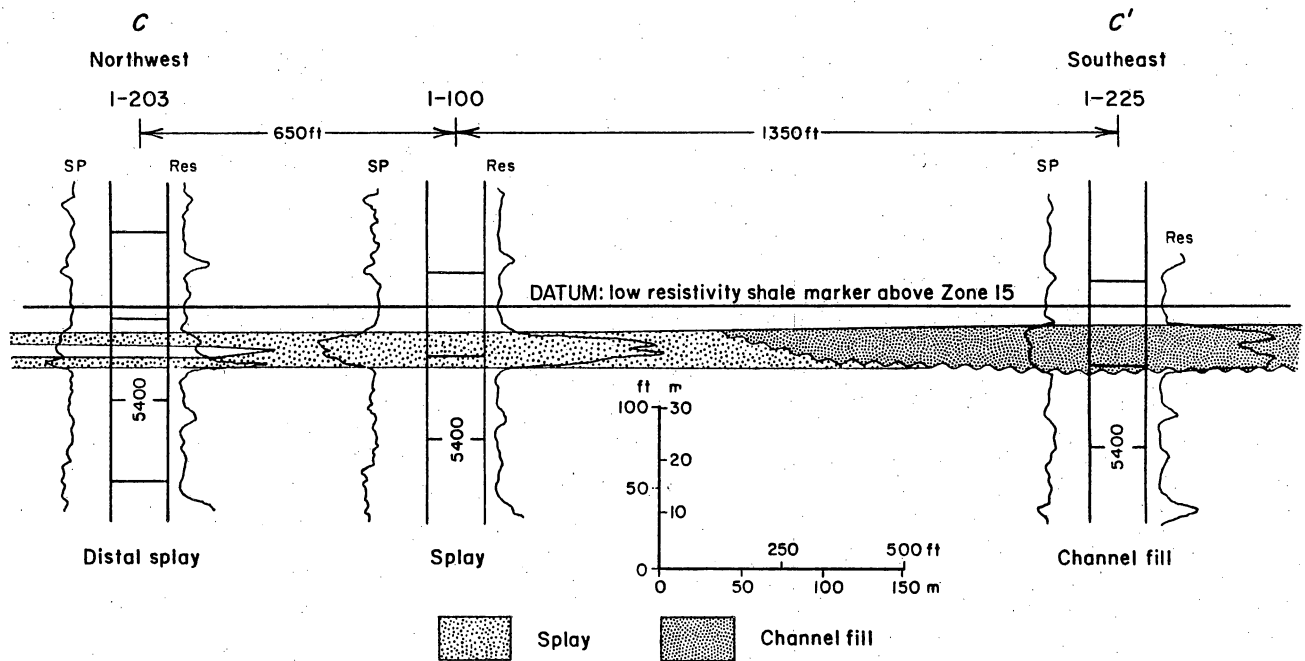
The 1-100 well was flowing at 726 Mcf/d with a flowing bottom-hole pressure of 188 psi at the time of shut-in. The well was shut in for 21 hr using a downhole shut-in tool, to minimize wellbore-storage effects, and the pressure data were obtained using a high-resolution electronic gauge. The radius of investigation of the test was 674 ft (205 m). The average permeability was found to be 184 md for the 18 ft (5.5 m) of net-sandstone thickness. This permeability is comparable to the channel-fill facies completions tested in Zone 19C. The Horner-plot extrapolated pressure was 245 psia. Although there was an indication of barrier effects in the plot of the pressure buildup data by a change in slope, the reservoir pressure was found to be similar to that in the

Mobil Seeligson Unit I-248



QA18509

Figure 44. Interval with wireline RFT measurements in the undivided Zone 15 reservoir in the Mobil No. 248 A. A. Seeligson well, located in figures 2 and 43.



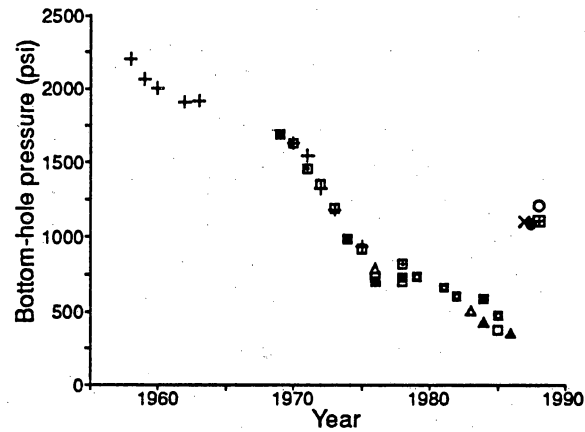
QA18507

Figure 45. Cross section C-C' in the Zone 15 reservoir. Pressure tests in the 1-100 well, located in a proximal-splay deposit, suggest that this well is in pressure communication with the channel-fill deposit in the 1-225 well. Line of section shown in figure 38.

surrounding wells in the Zone 15 reservoir. The boundary observed in the pressure buildup data may be the sandstone pinchout westward to mudstones between wells 1-100 and 1-203, or the channel-splay boundary between wells 1-100 and 1-225 as shown in figure 45. In either case, the boundary observed in the well test from well 1-100 is not an effective pressure barrier. The static reservoir pressure was on-trend with the regression fit of the average static pressure for completions in this part of the field.

The results of the pressure tests suggest that no effective permeability barriers exist between proximal-splay sandstone in the 1-100 well and channel-fill sandstone in the 1-225 well (fig. 45). The lack of flow barriers between these two facies is expected because proximal-splay and channel-fill sandstones (1) are commonly closely spaced and connected and (2) have similar rock properties (average grain size and mudstone content) because they are deposited in similar energy settings and flow-regime conditions. However, permeability barriers may exist over comparatively longer distances between channel-fill and distal-splay facies (1-225 to 1-203 wells in fig. 45). Across the transition from channel-fill to proximal-splay to distal-splay, the thickness of reservoir-quality sandstone commonly decreases and sandstones are interbedded with low-permeability mudstones where the edge of the distal-splay deposit pinches out into floodplain mudstone.

Although most wells in the Zone 15 reservoir are in pressure communication, especially where closely spaced wells are in proximal-splay and channel-fill deposits respectively, there are examples of incompletely drained reservoir compartments in channel-fill complexes that are laterally separated from other channel-fill complexes in the field. Bottom-hole pressures (1,100 to 1,200 psi) in the recently completed Sun 16-97, 16-124A, 42-67, and 141 Canales wells are anomalously high (fig. 46). These wells are located in channel-fill complex number 2 (fig. 43). A belt of mostly floodplain mudstone, averaging 2,000 ft (610 m) in width, separates these high-pressure wells in channel-fill complex number 2 from low-pressure wells in channel-fill complex



EXPLANATION		
WELL NUMBER		
□ 17-1	■ 1-47	× 16-97
+ 1-225	□ 1-160	● 16-124A
■ 1-114	▲ 1-157	■ P. Canales No. 141
△ 1-163	○ 42-67	

QA13980c

Figure 46. Bottom-hole pressure versus time for 11 wells that have produced from the Zone 15 reservoir at Seeligson field. Data from Oryx. Wells shown in figure 43. Modified from Jirik and others (1989).

number 1 (fig. 43). Three of the wells (16-97, 16-124A, and 141 Canales) are located in channel-fill complex number 2, whereas a fourth well (42-67) is located in a separate channel-fill complex approximately 2,000 ft (610 m) southeastward (fig. 43). Two of the wells (16-97 and 1124A) have produced 1.02 Bcf and 0.92 Bcf, respectively, since they were recompleted in 1987. The 16-97 well had an initial bottom-hole pressure of 1,111 psi, whereas the 16-124A well had a bottom-hole pressure of 928 psi. The average pressure of the completions in channel-fill complex number 1 in the north part of the study area (fig. 43) was about 430 psi at the time of these completions. The distance between the recompleted wells in the southern area and the more depleted wells to the north is between 1 and 2 mi (1.6 and 3.2 km). The production results from these completions show that successful reserve growth occurred by developing an incompletely drained reservoir compartment. The incompletely drained reservoir compartments found by these completions in the southern area suggests that the northern and southern channel-fill complexes are effectively separated by muddy levee and floodplain deposits shown in figure 43.

Results

It was concluded that the proximal-splay completion in the 1-100 well has permeability and production characteristics that are similar to the channel-fill facies completion in the 1-225 well (fig. 45). There appear to be few reservoir compartments between closely spaced wells (200 to 1,000 ft [61 to 305 m]) in the Zone 15 reservoir, even between wells in different facies (for example, proximal splay and channel fill). However, reservoir compartments in Zone 15 may be recognizable at a larger scale (for example, in channel-fill complexes that are separated from each other by thousands of feet of mudstone-rich floodplain and distal-splay deposits). The examples from the Zone 15 reservoir suggest that reservoir drainage has occurred between (1) small splay compartments that are well connected to channel-fill compartments and (2) along

depositional axes of channel-fill complexes. However, well-separated channel-fill complexes should be targeted for recompletions or infill wells because these complexes have been poorly drained by wells in other channel-fill complexes thousands of feet away, even though the distant completions are at the same stratigraphic level.

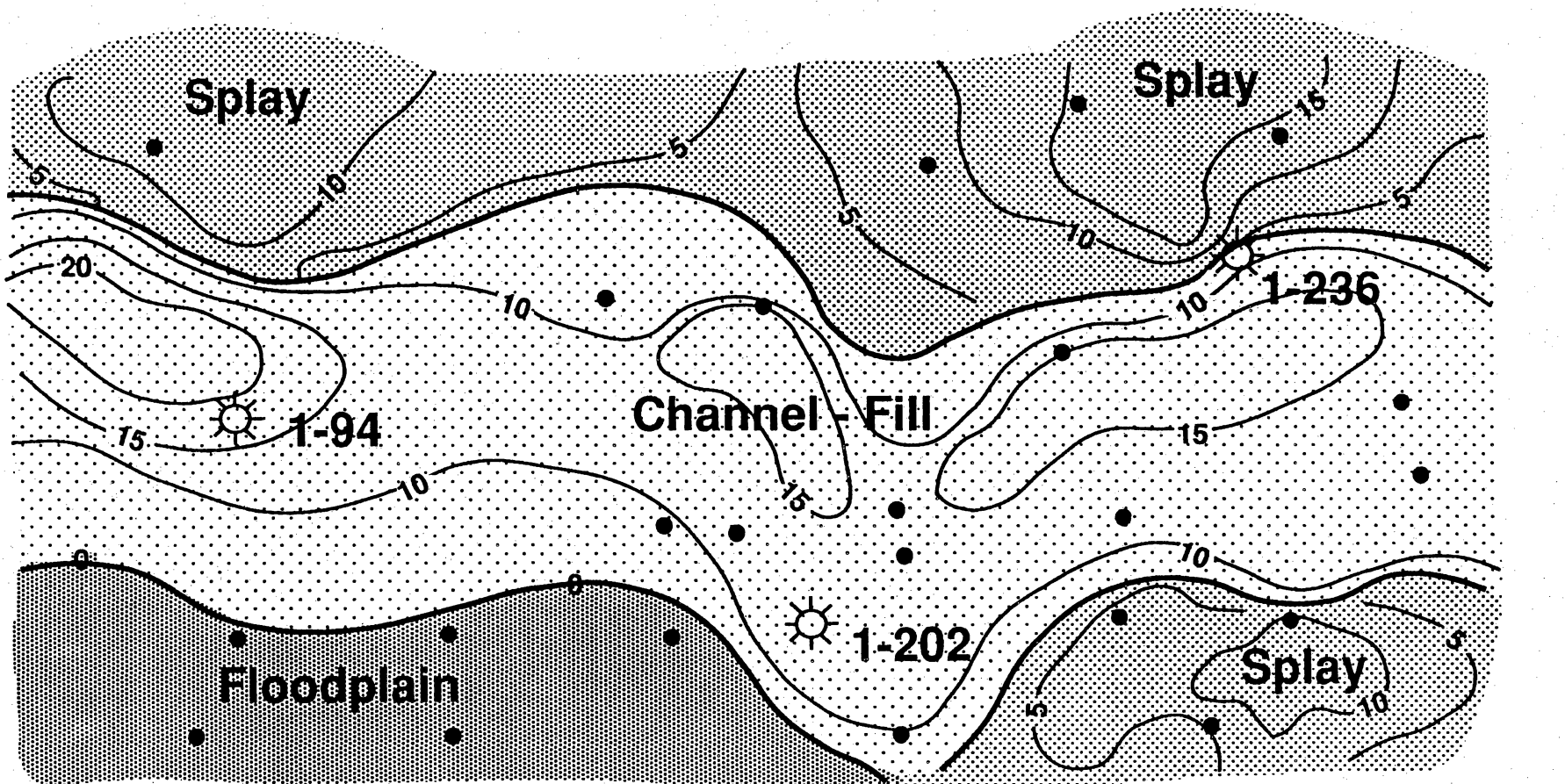
Zone 14B Reservoir

The Zone 14B reservoir occurs at depths ranging from 4,960 to 5,150 ft (1,488 to 1,545 m) in a 4-mi² (10-km²) area (fig. 2) in eastern Seeligson field and consists of three genetic units (lower, middle, and upper). Only the middle and upper genetic units are described because the lower genetic unit contains no reservoir facies in the east.

Depositional Environments

The middle genetic unit in the Zone 14B reservoir is composed primarily of channel-fill deposits that are flanked by levee and splay deposits. An east-trending belt of channel-fill deposits with more than 10 ft (3 m) of net sandstone is approximately 2,000 ft (610 m) wide (fig. 47). Splay sandstones range from 5 to 18 ft (1.5 to 5 m) in thickness.

The upper genetic unit, which is composed almost entirely of channel-fill deposits, directly overlies the middle unit throughout most of the area. Although the two genetic units are separated by shales that are too thin to vertically isolate the genetic units, sites where sandstones of the middle unit are truncated by channel-fill deposits of the upper unit may contain permeability barriers at zones of mud intraclasts at basal scour surfaces. Other permeability barriers at lateral pinch-outs of channel-fill and splay deposits into floodplain mudstones may also occur in the middle genetic unit.



-  **Successful Completion**
-  **Well Control**

0 2000 ft

CI = 5 ft

Figure 47. SP log-facies and net-sandstone thickness map of the Zone 14B genetic unit in east-central Seeligson field. Wells 1-94, 1-202, and 1-236 were recompleted in channel-fill sandstones. Area of map shown in figure 2. From Jirik and others (1991).

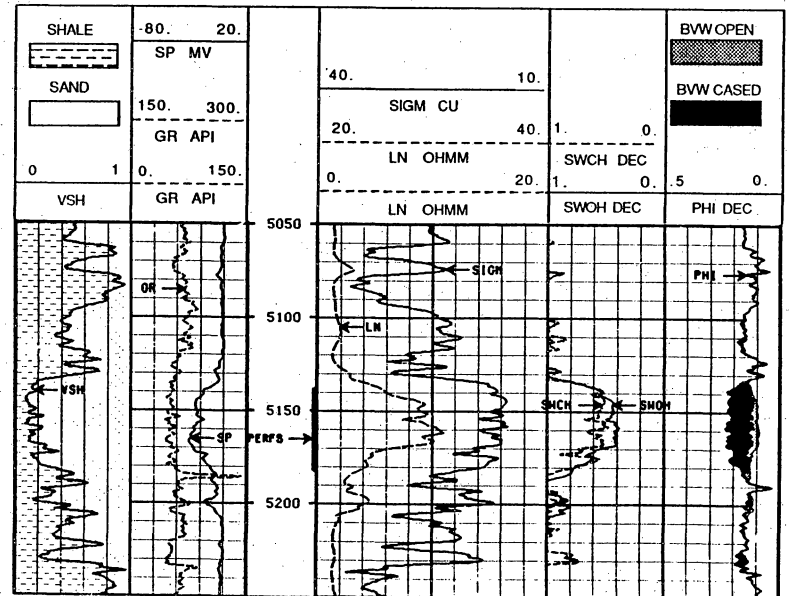
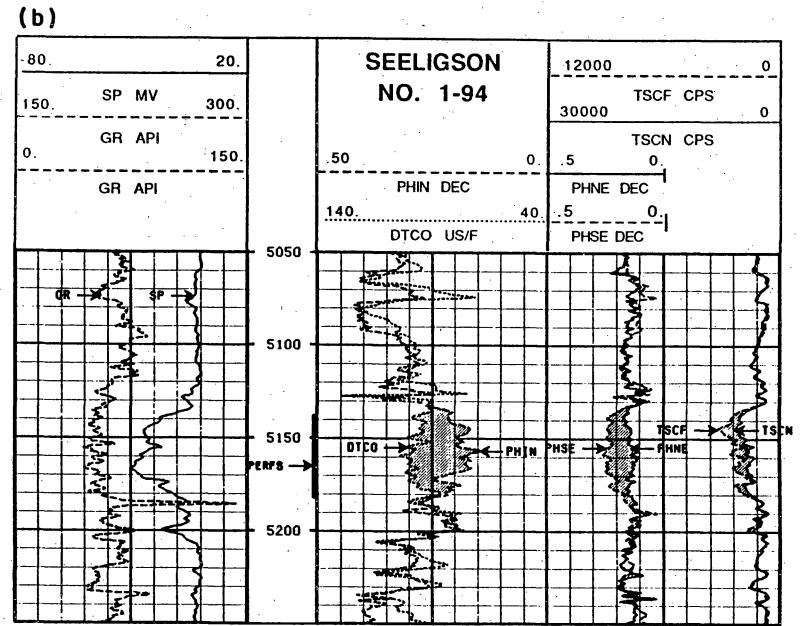
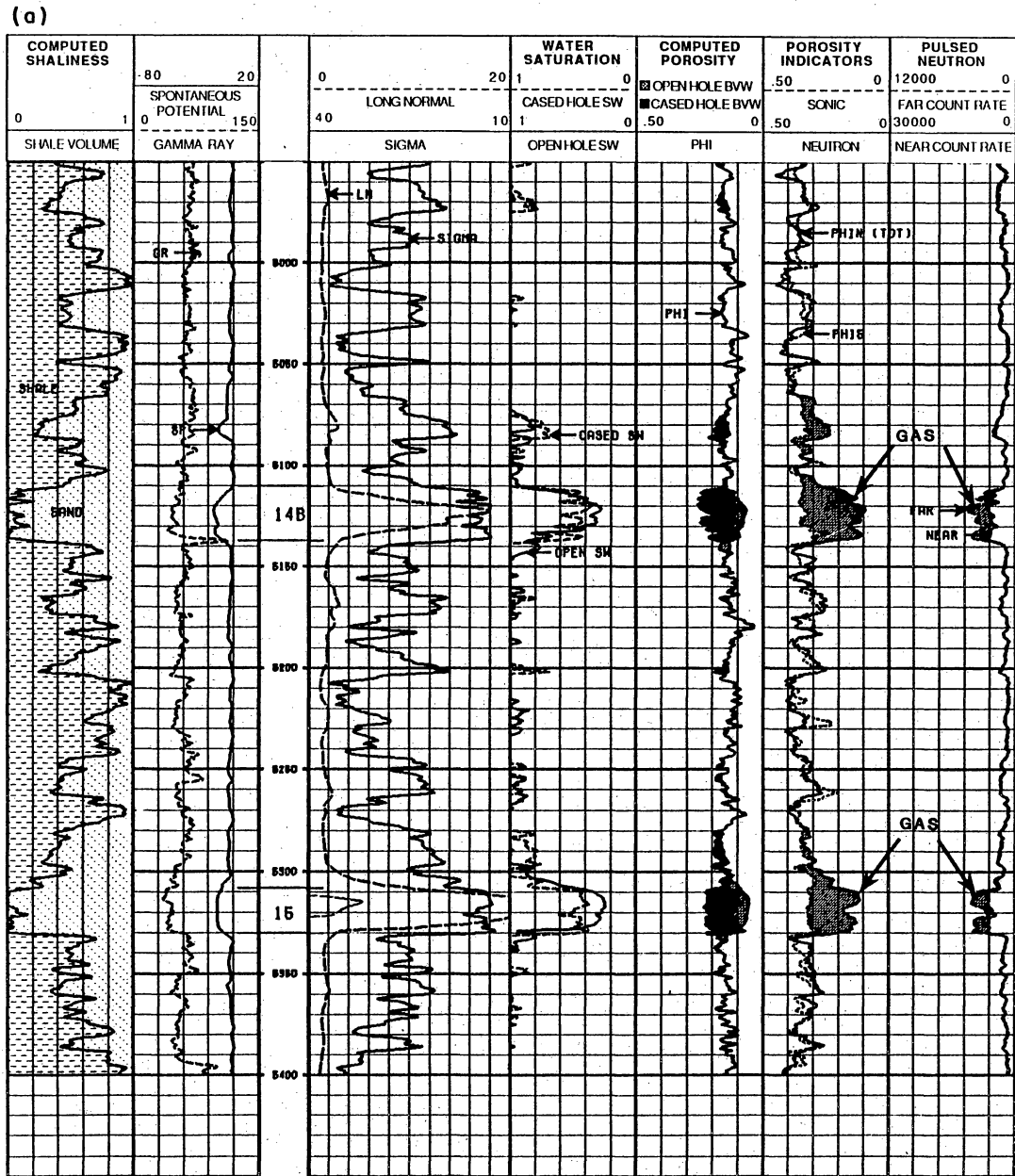
Potential for Reservoir Compartments

In the Zone 14B reservoir, cased-hole water saturation is not significantly higher than open-hole water saturation, which is an indication that hydrocarbons have not been thoroughly depleted. In this zone, gas effect is observed on the neutron sonic porosity overlay and the near- and far-count overlay (fig. 48a). Therefore, Zone 14B is a gas-productive reservoir if formation pressure is high enough. At Seeligson field, where a low-pressure gathering system is in place, this reservoir can be produced even when nearly depleted relative to conventional line pressure.

The 1-94 well (fig. 48b, located in fig. 47) was completed in the Zone 14B reservoir in a 14-ft (4.3-m) interval composed of superimposed channel-fill sandstones in both the middle and upper genetic units. The open-hole water saturation averages 42 percent, whereas the cased-hole water saturation averages 52 percent, indicating gas depletion from offset production. The indication of bypassed gas in the Zone 14B reservoir is mainly due to the location of the well, which is structurally higher than older producing wells in this zone. Two other successful completions were made in the Zone 14B reservoir from nearby wells in similar structural positions (wells 1-202 and 1-236 [table 1 and fig. 47]). More than 1.4 Bcf of gas was produced in approximately 18 mo from recompletions in three wells in the Zone 14B reservoir and in two other recompleted wells in the Zone 19B reservoir in the east part of the field (Jirik and others, 1991).

Summary of Facies-Related Production Performance

Zones 15 and 19C were examined for production performance of gas completions to determine facies controls on production. A total of 14 channel-fill and 3 splay completions in these two reservoirs were identified in the north part of the field. The



QA18751

Figure 48. (a) Combined logging suite of pulsed-neutron log and sonic log in the Oryx No. 1-168 Seeligson well, indicating gas in the Zone 14B and 15 reservoirs. (b) Combined cased-hole log suite in the Oryx 1-94 Seeligson well. Porosity and water-saturation analyses indicated on right side of these logs. Wells located in figures 2 and 47. From Jirik and others (1991).

limited number of splay facies completions is insufficient to conclude that they are different in terms of performance or reservoir connectivity from channel-fill facies completions. Moreover, the production performance of the splay completions exhibited no difference from the channel-fill completions.

The average net-sandstone thickness of the channel-fill completions in the Zone 15 and 19C reservoirs is 21 ft (6.4 m) and 13 ft (4 m) in the splay completions. It is impossible to determine whether only the thicker splay sandstones are productive or whether the thinner, distal parts of the splays were avoided in completion attempts.

In the Zone 15 reservoir, completions were compared in the 1-100 well (proximal splay) and the 1-225 well (channel fill) (fig. 45). These two wells have similar production-decline rates. The pressure of the splay completion at the 1-100 well is on trend with the previously established pressure decline of the other completions. Therefore, the splay facies of the 1-100 well is in effective communication to the main channel and is as productive as the channel-fill facies completions.

The Zone 19C reservoir in Tract 1 in the north part of the field has had only one gas completion (the 1-89 well) in a splay deposit (figs. 18 and 25). The 1-89 well produced from the Zone 19C reservoir from 1966 through 1977 and has a reported cumulative of 12.3 Bcf of gas from a 6-ft (1.8-m) sandstone. The 1-89 well produced during the time of gas recycling. The gas-injection well nearest the 1-89 well was the 1-125 well, which was utilized for gas injection until 1977. The large cumulative gas production from the 1-89 well is thought to be the result of the gas recycling and does not indicate a reservoir drainage volume. Three other channel-fill facies gas completions were producing from the Zone 19C in Tract 1 at the same time as the 1-89. However, the 1-89 well produced at a rate higher than did these wells. Pressure tests were unavailable to compare the static pressure of the 1-89 with the other completions. Excellent communication of the 1-89 with the main channel is indicated from (1) production during the time of gas recycling and (2) a production rate and cumulative

production higher than from surrounding wells. The productivity and permeability of the proximal-splay sandstone are inferred to be better than that in the channel-fill sandstones.

Facies-Related Permeability

Three well tests were performed in November 1990 to determine near-well permeability and static reservoir pressure of completions in Zones 15 and 19C. Two channel-fill and one splay facies completions were tested by pressure buildup. The permeability of the splay completion was found to be similar to that of the channel-fill facies completions (table 2). These tests support the conclusion that because production performance of the 1-100 splay completion was similar to that of the channel-fill completions in Zone 15, permeability will be similar.

Effective Drainage Area

The drainage volumes and effective areas were calculated from postinjection (1977) pressure and rate data for the eight postinjection gas producers in the Zone 19C reservoir in Tract 1. The effective drainage areas are large compared with the well spacing. The average drainage area is 750 ac/completion, although the average completion spacing of the gas wells is between 40 and 80 ac. The results of these calculations are limited because the complete production histories of the wells are unknown, the wells are irregularly spaced, and the wells did not produce at the same time.

Table 2. Permeability measurements in the Zone 15 and 19C reservoirs.

Reservoir	Well	Facies	h (ft)	k (md)	k (md-ft)
Zone 15	1-100	Splay	18	176	3,168
Zone 19C	1-41	Channel fill	26	97.6	2,537
Zone 19C	1-86	Channel fill	21	280	5,880

Drainage Volumes of Gas Completions in the Zone 15 and 19C Reservoirs

The drainage volumes for 17 completions in the Zone 15 and 19C reservoirs in the north part of the field were calculated from the most postrecycling production decline trend and the available pressure data. These calculations are limited because the spacing pattern of completions is irregular and all completions did not produce at the same time. The calculations provide an insight of general reservoir capabilities. The average drainage pore-volume per completion was found to be 67 MMcf. Converting the pore volume to an area for each completion resulted in an average drainage area of 670 ac/completion. The average spacing for these completions was found to be 100 ac/completion, on the basis of the distance to the nearest neighbor completed at the same reservoir level in Zones 15 or 19C. The majority of the completions were found to be spaced closer than 80 ac. The drainage areas for the completions in these reservoirs were found to be greater than the average completion spacing.

RESERVOIR SANDSTONE COMPOSITION AND POROSITY DISTRIBUTION

Sandstone Composition

Two distinct reservoir types (types I and II), differentiated on the basis of framework mineralogy, diagenetic history, and reservoir quality, have been defined in the middle Frio Formation in South Texas (Grigsby and Kerr, 1991). Type I reservoirs consist of sandstones that contain no volcanic glass detritus, have a strong positive correlation between porosity and permeability, and have a good primary intergranular pore system. Type II reservoirs consist of sandstones rich in volcanic glass detritus, which exhibit a weak correlation between porosity and permeability and have a poorly developed intergranular pore system. Type II reservoirs occur in the middle third of the

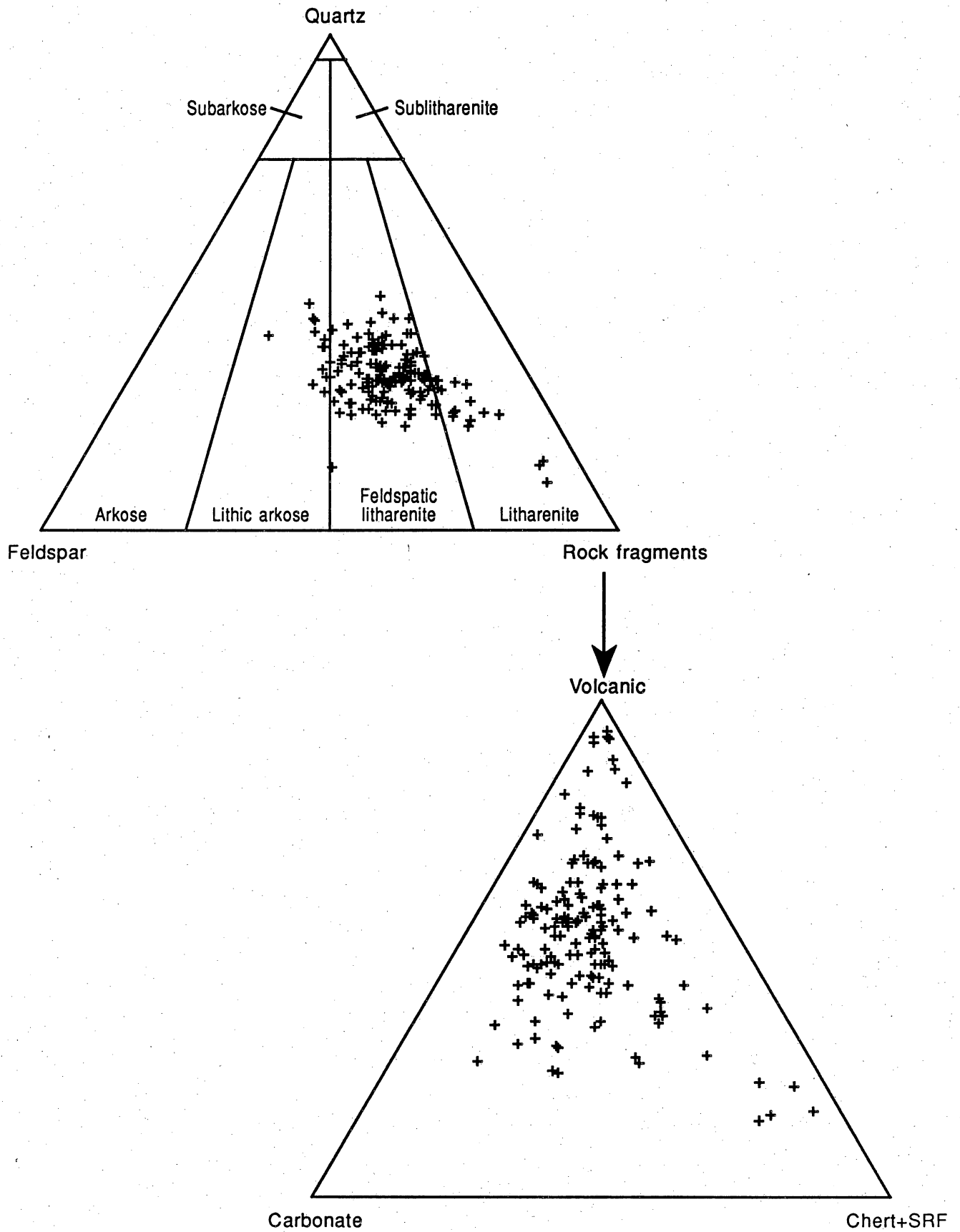
middle Frio Formation. However, in Seeligson field type I reservoirs are prevalent, and type II reservoirs are not widely developed. Even though volcanic glass detritus occurs in overbank mudstones between 4,900-ft (1,490-m) and 5,800-ft (1,763-m) log depth, it is absent or rare in middle Frio sandstones at this depth interval. This is in contrast to Stratton field where type II reservoirs are predominant in the glass-rich interval, possibly indicating differences in source material of different drainage basins of the Gueydan fluvial system (Kerr and Grigsby, 1991).

A total of 260 ft (79 m) of conventional core was available from two wells (see fig. 2). Core depths range from 5,180 ft (1,579 m) to 6,146 ft (1,874 m). In addition to conventional core, side wall core was available from two wells (fig. 2). These samples range in depth from 4,121 ft (1,256 m) to 6,599 ft (2,012 m). The composition of middle Frio sandstones in Seeligson field was determined from 116 thin sections. Data from an additional 97 thin sections were available from Sullivan (1988). Standard thin section petrography, scanning electron microscopy, and X-ray diffraction analysis were used to identify the framework and authigenic mineralogy. Electron probe microanalysis was used to determine the chemical composition of authigenic components.

The following sections will discuss the framework mineralogy, diagenesis, and porosity and permeability relationships of sandstone reservoirs in Seeligson field as important aspects of reservoir quality affecting reservoir heterogeneity and compartmentalization. These are typical examples of type I reservoirs.

Detrital Framework Mineralogy

Middle Frio sandstones in Seeligson field are poorly to moderately sorted feldspathic litharenites to litharenites having average compositions of $Q_{30}F_{24}L_{46}$ (fig. 49). Lithic fragments are predominantly volcanic, although carbonate rock fragments, which are predominantly microspar, are present in variable amounts (up to



QA18300c

Figure 49. Detrital composition of middle Frio sandstones in Seeligson field. Classification of Folk (1974).

16 percent). Plagioclase, which is the most abundant feldspar, is commonly leached and shows variable degrees of dissolution. Calcitization, seritization, and vacuolization also occur but in lesser quantities. Volcanic rock fragments are generally well preserved and contain readily recognizable feldspar laths. Partial alteration by silicification, pyritization, dissolution, argillization, or chloritization is common. Detrital quartz content is less than 30 percent and averages 19 percent. Volcanic quartz is the dominant variety, although plutonic and metamorphic quartz grains are present. Depositional matrix, which averages 4 percent, is a minor constituent in type I reservoirs; however, it can be important locally, constituting up to 30 percent of the rock volume.

Authigenic Mineralogy

Calcite is the most abundant authigenic mineral in Seeligson middle Frio sandstones, averaging 14 percent of the rock volume. It occurs as both a micritic cement precipitated during pedogenesis (fig. 50) and as a sparry cement that fills intergranular pores and replaces grains (fig. 51). The sparry cement is most abundant, and staining and electron probe microanalysis indicate that this calcite is nonferroan and corresponds with the early stage of calcite cement discussed by Loucks and others (1984). Sparry calcite precipitation is predated by formation of smectite grain coats, pedogenic calcite, and minor quartz and feldspar overgrowths. Following sparry calcite precipitation, secondary porosity developed by leaching feldspar, unstable rock fragments, and calcite cement. Secondary porosity is typically present as intragranular porosity or oversized pores (fig. 52); moldic porosity is rare. Absence of compaction and the presence of patchy remnants having corroded boundaries are evidence that calcite was once pervasive but later dissolved. Secondary porosity averages 5 percent and ranges from 0 to 18 percent. Intervals of no secondary porosity are tightly cemented by calcite.

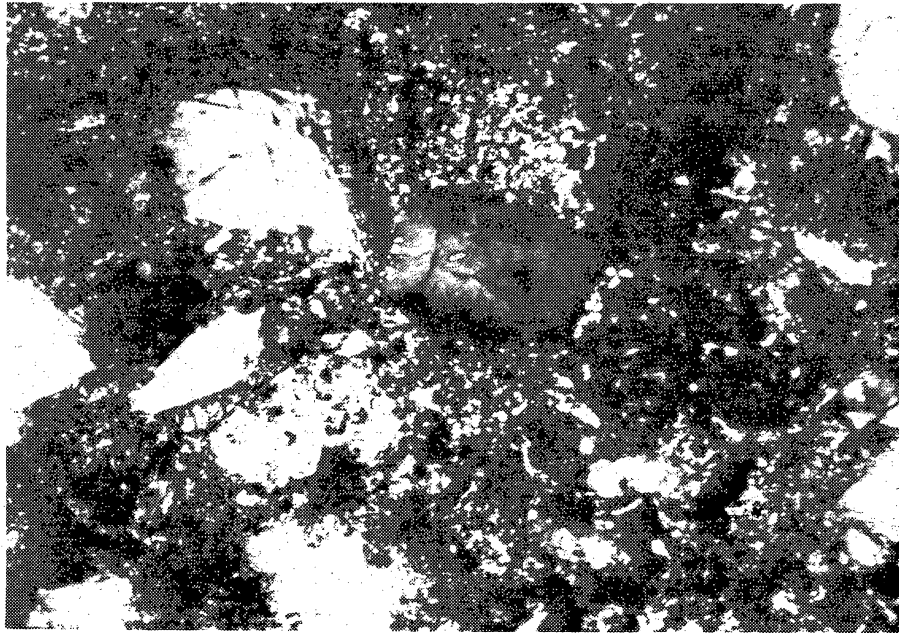


Figure 50. Photomicrograph of pedogenic calcite cement, c. Note the micritic nature of this calcite. Bar scale equals 250 μm .

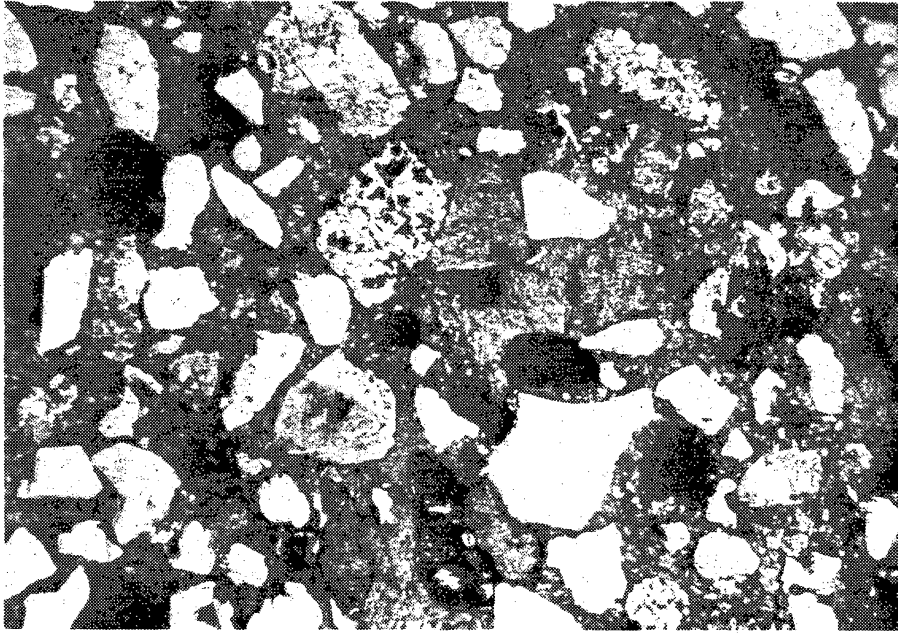


Figure 51. Photomicrograph of sparry calcite cement, c, filling intergranular porosity. Note lack of compaction. Bar scale equals 250 μm .

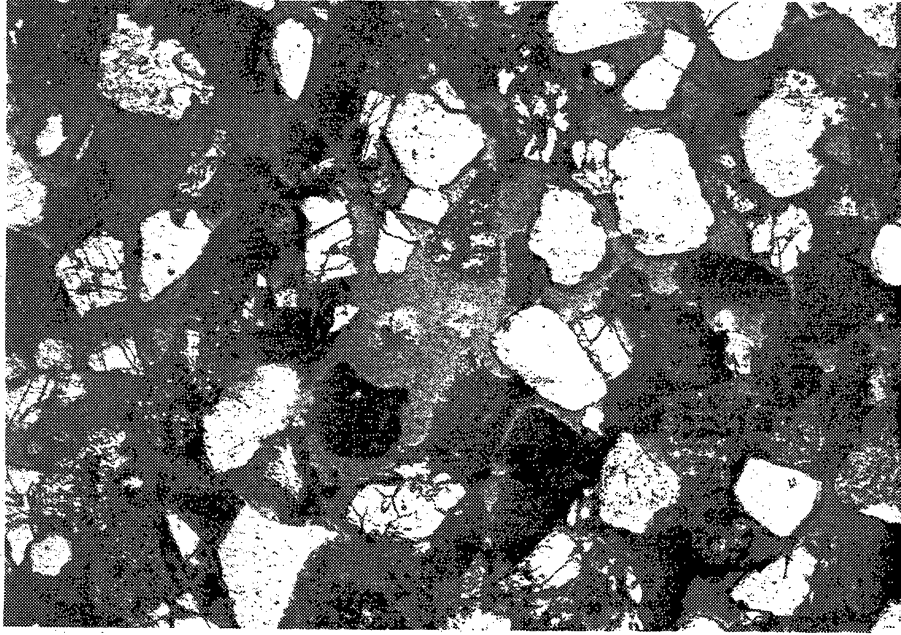


Figure 52. Photomicrograph showing the development of oversized, op, and intragranular, ip, secondary pores in middle Frio sandstones. Bar scale equals 250 μm .

The precipitation of kaolinite postdates creation of secondary porosity. Kaolinite is present in Seeligson field at depths between 4,300 and 5,900 ft (1,311 and 1,799 m). Kaolinite, which averages 1 percent and may constitute as much as 8 percent of the rock volume, most commonly fills secondary pores (fig. 53).

A minor stage of pyrite precipitation, which averages 2 percent of the rock volume, appears to postdate the development of secondary porosity. However, the exact timing of this event could not be determined. A general diagenetic sequence is illustrated in figure 54.

Reservoir Quality

In middle Frio sandstones at Seeligson field, porosimeter porosity averages 20 percent and ranges between 5 and 32 percent. Permeability averages 462 md and ranges between 0.2 and 4,766 md. These sandstones show a strong positive correlation between measured porosity and permeability ($r=0.82$) (fig. 55). This relationship is expected for an intergranular pore throat system and is typical of type I reservoirs. A crossplot of permeability versus point-count porosity results in a slight increase in the correlation coefficient ($r=0.84$). This indicates that point-count porosity may more accurately indicate effective porosity in these sandstones. The precipitation of calcite cement in intergranular pore spaces reduces porosity in type I sandstones (fig. 56a), and the preservation or dissolution of calcite directly affects permeability (fig. 56b). Calcite cementation in middle Frio sandstones has a highly irregular distribution, accounting for large variations in porosity and permeability measurements.

The distribution of kaolinite in secondary pores has a minor impact on reservoir quality because primary intergranular porosity largely controls permeability in these reservoirs. Pyrite, which can fill both primary and secondary pores, may influence porosity and permeability on a local scale.

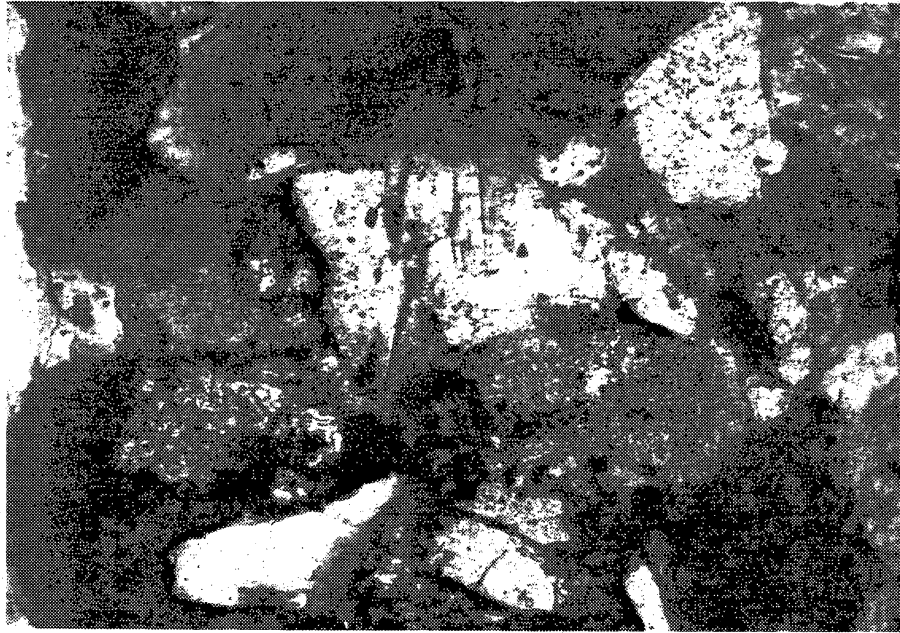
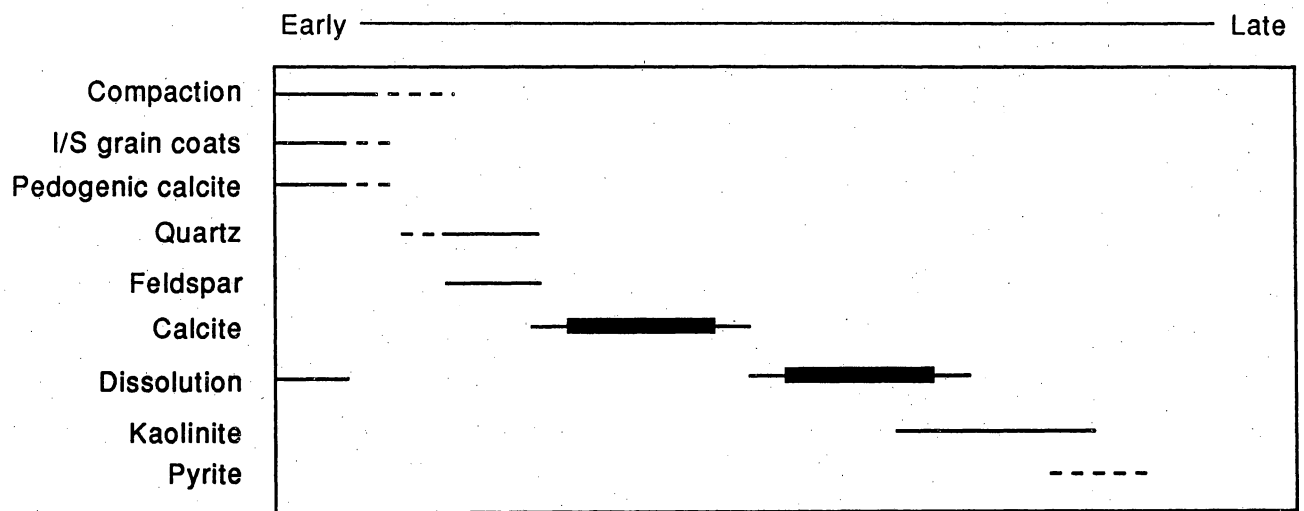
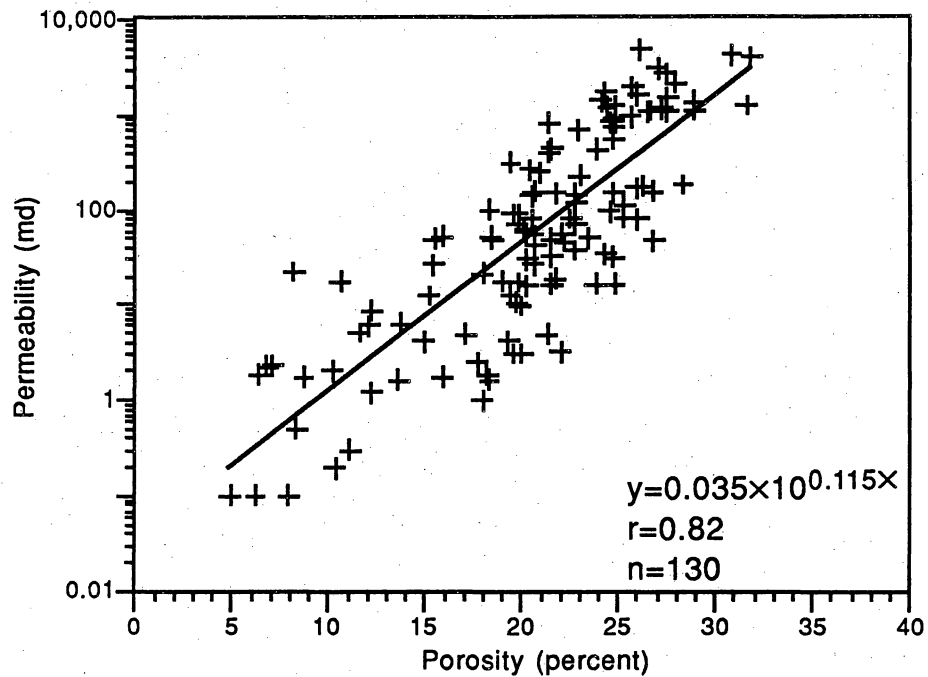


Figure 53. Photomicrograph of kaolinite, k, filling secondary pores. Bar scale equals 250 μm .



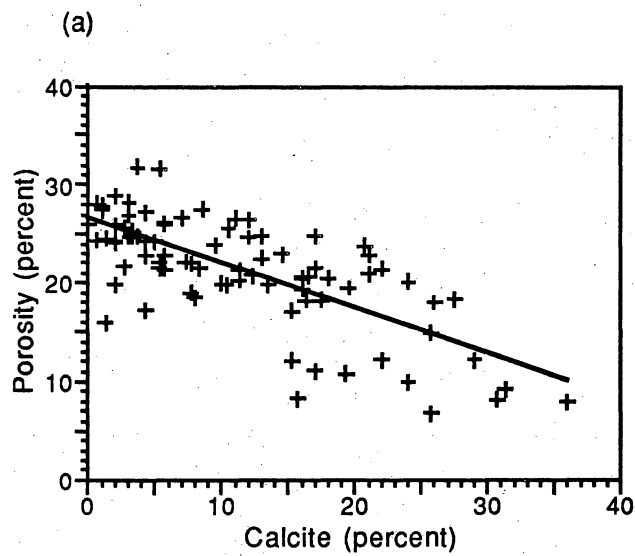
QA18393c

Figure 54. Generalized diagenetic sequence in middle Frio sandstones in Seeligson field. Thin lines indicate events of minor importance, thick lines events of major importance, in the diagenetic history of these sandstones.



QA18301c

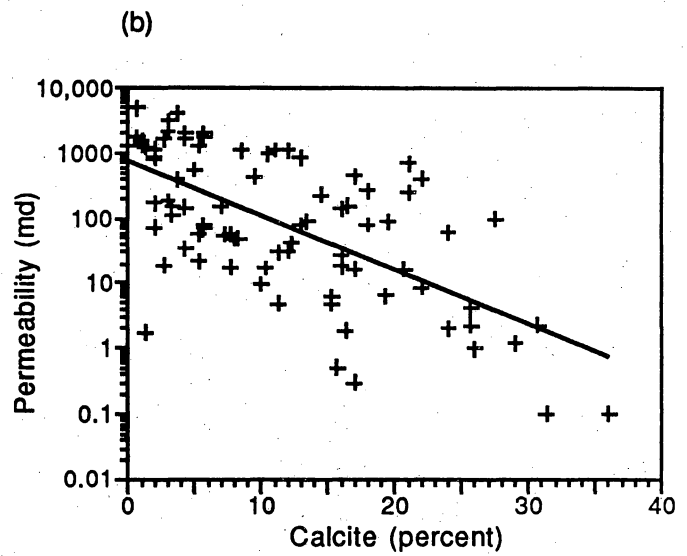
Figure 55. Cross plot of log permeability versus porosimeter porosity for sandstones of the middle Frio Formation. This strong positive correlation is typical of type I reservoirs and indicates a well-developed intergranular pore system.



$$y=26.56-0.46x$$

$$r=0.72$$

$$n=86$$



$$y=715.79 \times 10^{(-0.083x)}$$

$$r=0.65$$

$$n=86$$

QA18302c

Figure 56. Cross plot of calcite cement versus (a) porosimeter porosity and (b) log permeability for middle Frio sandstones in Seeligson field. Note strong negative correlations.

Porosity Distribution

During the evaluation of porosity distribution in middle Frio reservoirs, it is important to determine values for both total and effective porosity. For the purpose of this discussion, total porosity, \emptyset_t , is defined as the interconnective pore space occupied by water (both clay-bound water and free water) and hydrocarbons. Effective porosity, \emptyset_e , is defined as the pore space occupied only by free water and hydrocarbons. This is shown diagrammatically in figure 57.

Routine core analysis yields total porosity, and well log response must be modeled after this number. However, it is the effective porosity that will dominate the flow characteristics or permeability of a reservoir. For example, quantitative thin section point-count data will many times reflect changes in effective porosity and not total porosity because these data cannot resolve porosity of less than 5 microns. This is illustrated when a slightly improved correlation is obtained after thin section porosity is regressed against permeability rather than the core-measured total porosity. This effect was noted in the previous section. In addition, shale may contain porosity that must be accounted for when estimating the volume of gas in various Frio sandstone reservoirs. Core data from Seeligson field shows that in addition to having relatively large amounts of total porosity (19 to 20 percent), shales may also contain significant effective porosity (8 to 12 percent).

That porosity associated with shale probably contains only immobile or clay-bound water; that is, it cannot contain free hydrocarbons. As a result, many log computation models and programs used by service companies do not allow effective porosity in shales, and as a consequence, are in error (Cannon and Coates, 1990). In the Frio, if no attempt is made to determine the effective porosity associated with the shale in the shaly sands, or to compute this effective porosity from log analysis, the hydrocarbon

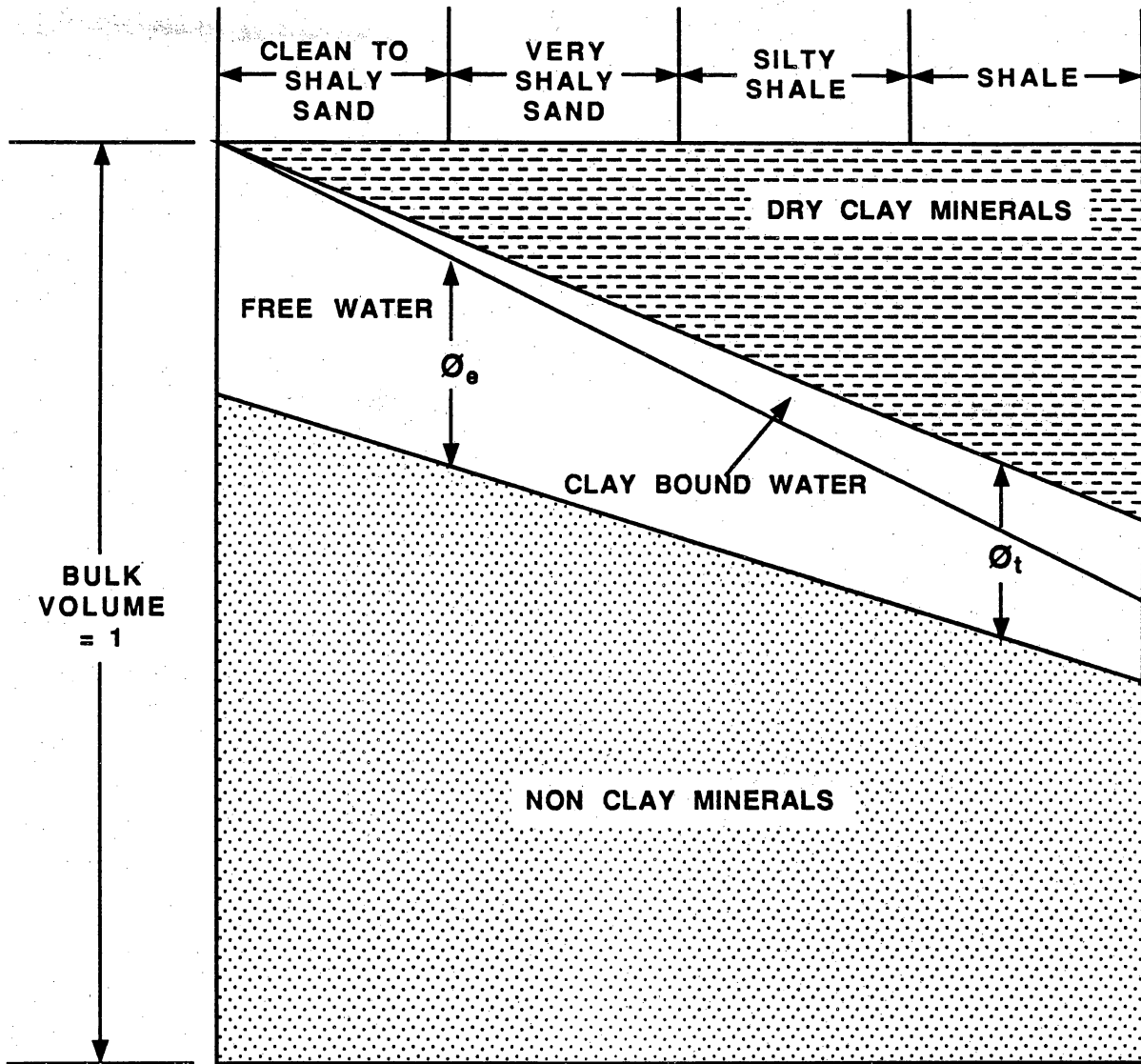


Figure 57. The bulk volume of the rock is divided into dry clay, pore space occupied by clay-bound water, pore space occupied by free water or hydrocarbons, and nonclay minerals. Shown is the distribution of porosity and minerals beginning with rock consisting of a clay-free sandstone reservoir and progressing to clay-rich shale.

pore volume will be in error. The effective shale porosity may be capable of storing hydrocarbons at reasonable capillary pressures or height above the free water level. Any underestimation of the effective porosity will directly reduce the bulk volume of hydrocarbons. The following sections discuss the determination of effective porosity in middle Frio sandstones and shales. In addition, a method of log analysis is discussed for the modeling of total and effective porosity.

Methods

Thirty-six feet of whole core, covering an interval from 5,406 ft (1,649 m) to 5,442 ft (1,659 m), was recovered from the P.C. Canales No. 141 well. In addition, a modern suite of well logs was acquired (see Truman and others [1989] for a complete description of this logging program). Thirty-seven core plugs were then obtained from both sandstone and shale throughout this interval. Total ambient porosity was measured for each core plug following conventional techniques. Effective porosity was determined using the methods of Hill and others (1979). Sandstone and shale compositions were determined from core plugs using X-ray diffraction and infrared absorption analysis.

Total and Effective Porosity from Core

Humidity-Dried Samples

Thirty-seven samples, twenty-three from sandstones and fourteen from shales, were selected for analysis. Two porosity measurements were made on each sample, and a summary of these porosity measurements is presented in table 3. Humidity-dried ambient porosity was obtained by drying the samples at 40 percent relative humidity and 140° F (60° C). This will leave at least one or two layers of absorbed water on the clay surface (Busch and Jenkins, 1970). The convection-dried ambient porosities were

Table 3. Humidity-dried and convection-dried core porosity results from shale samples, beginning with sample no. 1S.

Sample number	Depth (ft)	Humidity-dried porosity (%)	Convection-dried porosity (%)
1S	5406.3	21.7	22.0
1	5406.4	20.9	21.3
2S	5407.3	20.5	20.8
3S	5408.2	19.5	19.9
4S	5409.1	20.5	20.8
2	5410.1	23.0	23.5
3	5411.1	20.1	20.7
4	5412.1	20.6	20.6
5S	5413.4	20.4	20.5
5	5414.2	21.3	21.7
6S	5415.7	21.6	22.1
6	5416.3	18.3	20.4
7S	5417.2	26.5	26.7
7	5418.2	27.5	27.7
8S	5419.3	22.9	23.3
8	5420.2	26.6	26.8
9S	5421.3	23.9	24.2
9	5422.1	25.6	25.7
10	5423.1	24.8	24.9
11	5424.3	21.4	22.4
12	5425.6	19.8	21.2
13	5426.1	19.4	20.3
14	5427.4	21.5	22.5
15	5428.6	11.6	19.5
16	5429.8	11.2	19.4
17	5430.2	9.3	15.5
18	5431.5	12.2	19.8
19	5432.2	11.6	19.6
20	5433.1	10.9	19.8
21	5434.0	9.9	20.7
22	5435.0	7.8	19.3
23	5436.0	8.9	19.9
24	5437.0	9.0	19.4
25	5438.0	8.8	17.9
26	5439.0	9.0	18.0
27	5440.0	9.1	17.9
28	5441.0	8.2	15.8

determined by drying the samples at 230° F (110° C) to constant weight. In the sandstone interval (samples 1S to 14; table 3), which has an average clay volume of 6 percent (table 4), the humidity-dried porosity is slightly less than the convection-dried porosity. In contrast, in the shale interval (samples 15 to 28; table 3), which has an average clay volume of 31 percent (table 4), the humidity-dried porosity is approximately half of the convection-dried porosity. These results are surprising on two accounts. First, the convection-dried porosity in the shale is quite large and only 3.8 percent less than the convection-dried porosity in the sand. Second, the humidity-dried porosity in the shale is significant, averaging 9.8 percent. As suggested by Busch and Jenkins (1970) this humidity-dried porosity can be thought to reflect effective porosity, and the historical belief that shale contains only clay-bound water is in error.

Capillary Pressure

When a rock contains effective porosity, whether it occurs in sand or shale, the rock will be capable of storing hydrocarbons (Hill and others, 1979). According to Hill and others (1979), if the distribution of clay and therefore bound water is such that any particular void volume segment contains its proportional amount of bound water, then mercury saturation, S_{Hg} , is given by

$$S_{Hg} = S_g + S_{Hg} V_b/V_t, \quad (1)$$

and the gas saturation is given by

$$S_g = S_{Hg} (1 - V_b/V_t) = S_{Hg} \emptyset_e/\emptyset_t, \quad (2)$$

where

S_g = gas saturation from gas-brine capillary pressure tests,

S_{Hg} = mercury saturation from mercury capillary pressure tests,

V_b = bulk volume clay-bound water,

V_t = bulk volume clay-bound water + bulk volume pore water,

\emptyset_t = total porosity, and

Table 4. Summary of average bulk volumes for the cored interval.

	Average bulk volume sand (%)	Average bulk volume shale (%)
Quartz	29	20
Plagioclase	18	4
K-Feldspar	9	16
Calcite	15	10
Dolomite	1	0
Dry clay	6	31
Total porosity (convection dried)	22.6	18.8
Humidity-dried porosity	22.1	9.8

\emptyset_e = effective porosity.

Equation 2 shows that any rock with effective porosity greater than zero may contain hydrocarbons.

Three samples were selected for determination of air-brine capillary pressure curves, two sandstone and one shale. In addition, mercury injection capillary pressure curves were determined on these same three samples plus an additional two shale samples. All measurements were converted to equivalent height above the free water level in a gas reservoir.

The capillary pressure relationships for one of the sandstone samples is shown in figure 58. The relationship for the shale sample is shown in figure 59. Effective porosity from the air-brine and air-mercury capillary pressure data may be estimated from equation 3.

$$\emptyset_e = \emptyset_t S_g/S_{Hg} \quad (3)$$

This provides another means of estimating effective porosity in addition to humidity-dried porosity. Comparison of humidity-dried porosity with the porosity derived from capillary pressure is shown in table 5. The effective porosity derived from the capillary pressure data is generally lower than humidity-dried porosity for the three samples analyzed. The shale sample (sample no. 18) shows an effective porosity of 8.1 percent from the capillary pressure data. This effective porosity in the shale can store hydrocarbons. Results indicate that at 570 ft (173.8 m) above the free water level, an equivalent shale associated with a sandstone gas reservoir would contain approximately 14 percent of the gas a sandstone reservoir of equal thickness would hold.

Cation Exchange Capacity

Cation exchange capacity (CEC) was also investigated as a means of determining effective porosity (Truman and others, 1989). The cation exchange capacity method yielded unreasonable results in the form of negative porosity in the shales. The use of

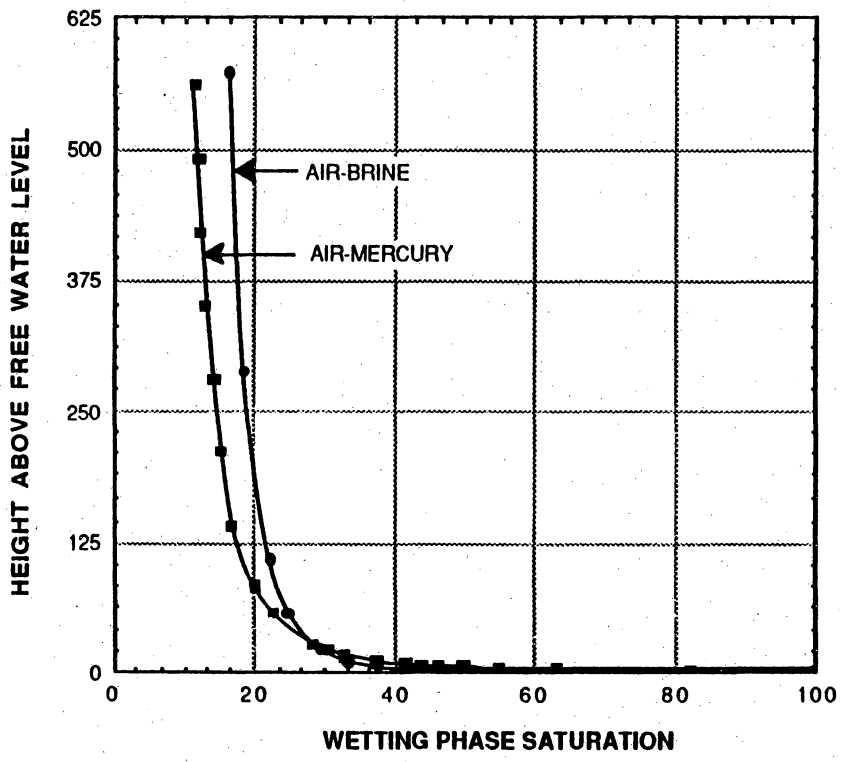


Figure 58. Comparison of capillary pressure data for air brine and air mercury in one of the sandstone samples (sample no. 2).

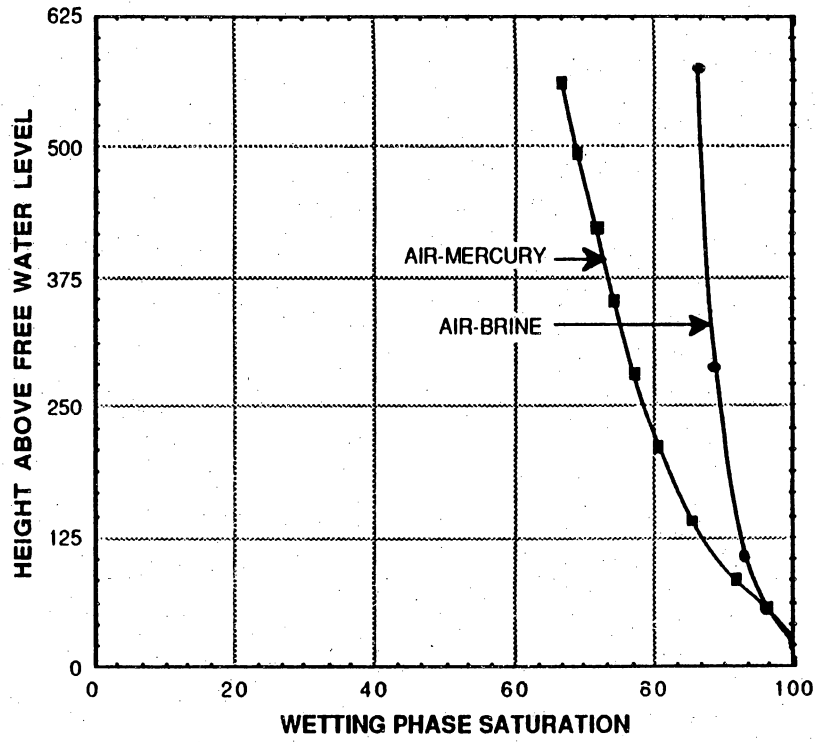


Figure 59. Comparison of capillary pressure data for air brine and air mercury in one of the shale samples (sample no. 18).

Table 5. Comparison of humidity-dried porosity with effective porosity from capillary pressure, including the resulting bulk volume mercury and air.

Sample number	Depth	Total porosity	Effective porosity		Bulk volume 570 ft above water contact Free water contact	
			Humidity-dried porosity	P _C -derived porosity	Mercury	Gas
6S	5415.7	22.1	21.6	21.9	0.181	0.179
18	5431.5	19.8	12.2	8.1	0.066	0.027
20	5433.1	19.8	10.9	—	0.057	—
24	5437.0	19.4	9.0	—	0.016	—

CEC to determine effective porosity may require the use of the membrane potential method to determine CEC. At present, membrane potential measurements are commercially unavailable.

Total and Effective Porosity from Logs

The following procedures were utilized in the determination of total and effective porosity from well logs. The well log clay indicators were calibrated to the clay content determined from the infrared absorption using previously published techniques (Truman and others, 1986). The clay indicators utilized were the density-neutron, neutron-sonic, neutron and SP. The minimum clay indicator from these multiple indicators was selected to determine the clay content. Porosity was determined from the density and the neutron using the following general relationships:

$$\emptyset = \frac{\rho_g - \rho_b}{\rho_g - \rho_f} - \frac{\rho_g - \rho_{cl}}{\rho_g - \rho_f} V_{cl} \quad (4)$$

and

$$\emptyset = \frac{\emptyset_n}{\emptyset_{nf}} - \frac{\emptyset_{nd}}{\emptyset_{nf}} V_{cl}, \quad (5)$$

where

V_{cl} = bulk volume clay,

\emptyset = porosity, either total or effective,

ρ_g = grain density,

ρ_f = fluid density,

ρ_{cl} = clay density,

\emptyset_{nf} = neutron fluid, and

\emptyset_{ncl} = neutron clay.

When total porosity is determined, the values for clay density, ρ_{cl} , and neutron clay response, \emptyset_{ncl} , will be the dry clay values, that is, no clay-bound water. When effective porosity is determined, the values for clay density and neutron clay response will be the

wet clay values, that is, with clay-bound water. Table 6 summarizes the parameters used in the above equations for the computation of total and effective porosity from the well logs. Figure 60 compares the total porosity and effective porosity computed from the well logs with the core total porosity and core humidity-dried porosity, respectively. There is good agreement between the well logs and the core analysis. Figure 61 compares total and effective porosity from the logs. The difference between the two is the volume of porosity filled with clay-bound water.

Discussion

Sandstones of the middle Frio Formation in Seeligson field are, in general, high porosity and high permeability gas reservoirs with a primary intergranular pore system. The presence or absence of pore-filling calcite cement strongly influences porosity and permeability distribution within these sandstones. Total porosity acquired from conventional core plug analysis closely estimates effective porosity within middle Frio sandstones. Because of the high clay content in middle Frio shales, total porosity acquired during conventional core plug analysis will greatly overestimate effective porosity. However, the fact that middle Frio shales may contain effective porosity, as high as 9.8 percent, indicates that these shales can store hydrocarbons. The occurrence of effective porosity in shales will have the largest impact in gas reservoirs without an active water drive. Gas stored in effective shale porosity could contribute to production as the reservoir is depleted and the pressure differential between the shale and sandstone beds increases. This could cause the migration of gas from shales into the sandstones.

The only commercially available method for determining effective porosity is use of capillary pressure data. Although the humidity-dried porosity yields higher values for effective porosity than the capillary pressure method, the results are in qualitative

Table 6. Parameters utilized for computation of the well logs.

ρ_g	=	2.67	\emptyset_{nm}	=	0
ρ_f	=	0.97	\emptyset_{nf}	=	0.97
ρ_{clwet}	=	2.21	\emptyset_{nclwet}	=	0.79
ρ_{cldry}	=	2.66	\emptyset_{ncldry}	=	0.53
m	=	1.89	n	=	1.79
R_w	=	0.11 @ 162° F			

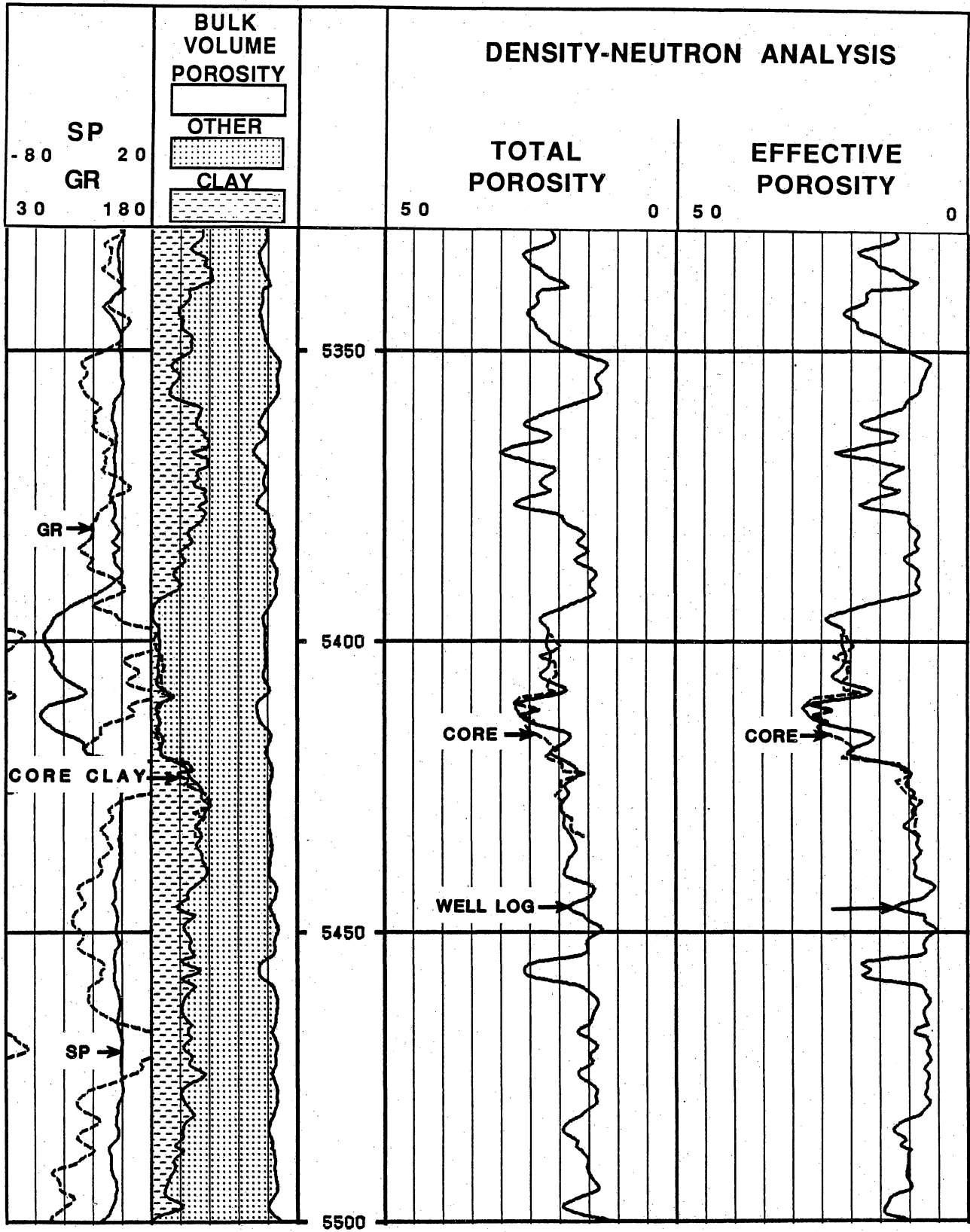


Figure 60. Total porosity, effective porosity, and clay content measured on cores and computed from log analysis.

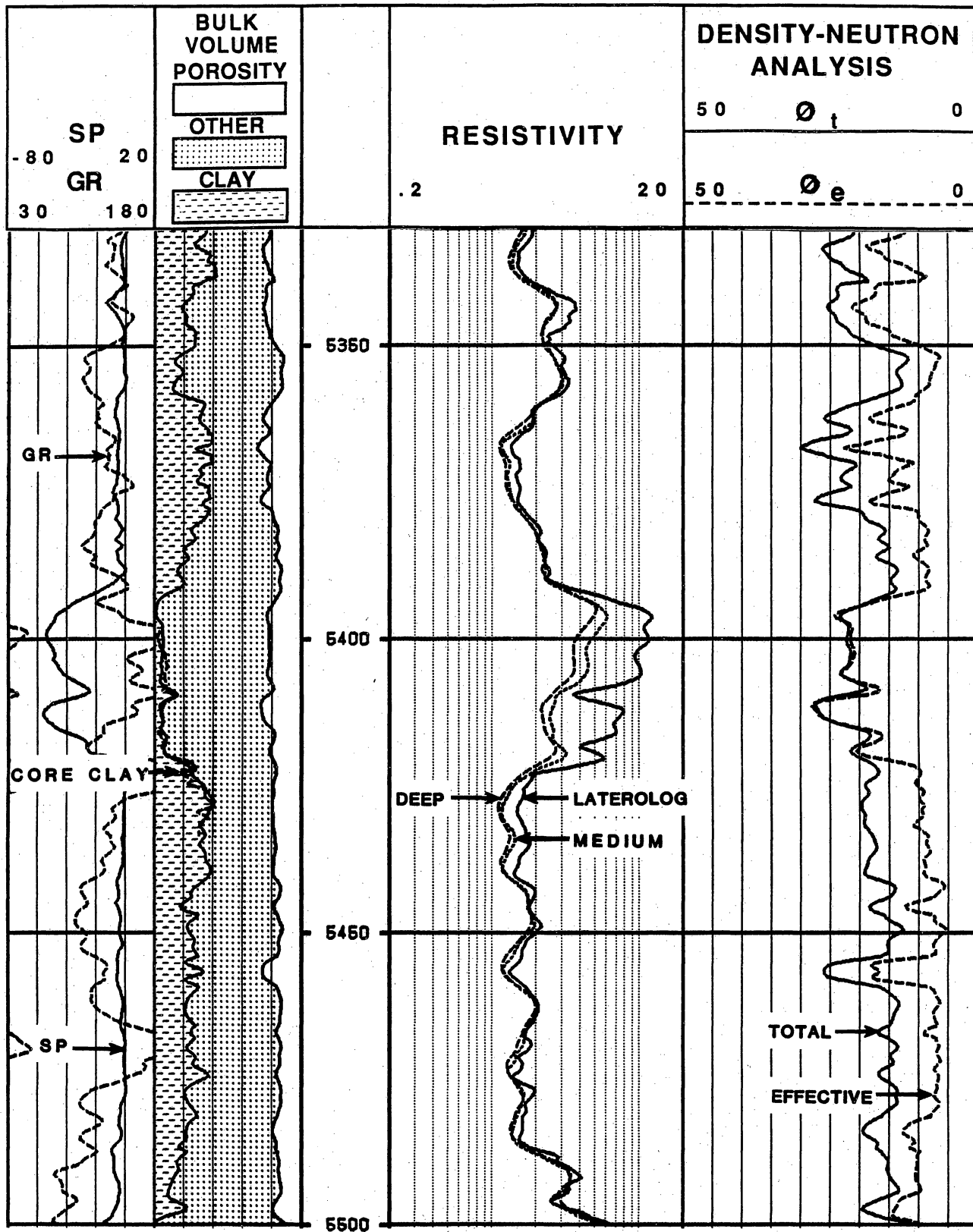


Figure 61. Total porosity, effective porosity computed from logs. The difference is clay-bound water.

agreement. Therefore, the use of humidity-dried porosity to model effective porosity for log analysis is certainly acceptable if these are the only available data.

If core is unavailable, it is important to model total and effective porosity from log analysis. The example discussed utilizes a log interpretation model based on clay volume. Similar results can be obtained using a shale-volume-based interpretation. When this is done the apparent grain density from the density and neutron logs is an excellent shale indicator. When hole conditions affect either one of these logging curves, other shale indicators can be used.

PETROPHYSICAL RESEARCH

As part of a previous contract with GRI (contract no. 5086-212-1426), ResTech developed a cost-effective method for finding bypassed gas in cased-hole wells using state-of-the-art logging technology. ResTech also developed an open-hole petrophysical interpretation model based on cores and geophysical logs in the Sun No. 141 Canales well. Under a new contract with BEG as part of the Secondary Gas Recovery Program, ResTech performed additional research in the following areas:

First, in cooperation with Mobil, the Mobil No. 247 and No. 248 Seeligson wells were drilled for deeper pool objectives to acquire additional data in lower and middle Frio reservoirs. These reservoirs were being investigated by GRI and BEG for additional gas research. The objective was to refine previous interpretations of data obtained in the open-hole No. 141 Canales well (Jirik and others, 1989). Second, three wells (the 1-85, 1-89, and 1-171) were made available by Oryx to continue the research in the cased-hole evaluation program in Seeligson field. Third, research was also performed in the No. 141 Canales well, where investigation of shale porosity and its impact on additional gas reserves was undertaken using special core analysis.

Open-Hole Petrophysical Research

The integrated open-hole petrophysical model combining core analysis with calibrated, log-derived parameters obtained in the No. 141 Canales well was used in the Mobil No. 247 and No. 248 Seeligson wells (located in fig. 2) to test its applicability to the Seeligson field area. As a result of the analysis performed, a shaly, low-resistivity pay sandstone was identified in the No. 247 well in the Vicksburg Formation.

Petrophysical problems encountered in Seeligson field are similar to those found in other shaly sandstone reservoirs. High-surface-area clays line the pores of sandstones causing high, irreducible water saturation. For example, in the No. 247 well a low-resistivity zone extends from 7,305 to 7,397 ft (2,227 to 2,255 m) (fig. 62). The log-derived petrophysical results show a zone of interest in the upper part with 30 percent shale and 70 percent water saturation. The interval from 7,308 to 7,332 ft (2,228 to 2,235 m) was perforated and produced gas at a rate of 1.618 MMcf/d on a 9/64-inch choke. The high apparent water saturation of 70 percent consists mostly of clay-bound water on the surface of clays and capillary bound water.

Data Acquisition

A logging program was designed for the No. 247 and No. 248 wells to complement other research in the project. The logging program recommended was open-hole dual induction, formation density, compensated neutron, gamma-ray, long spaced sonic, dipmeter, sequential formation tester, sidewall cores and cased-hole pulsed neutron-gamma ray, temperature, noise and cement bond logs (table 7). Several logs originally in the acquisition plan were cancelled because of adverse hole conditions caused by severe loss of circulation.

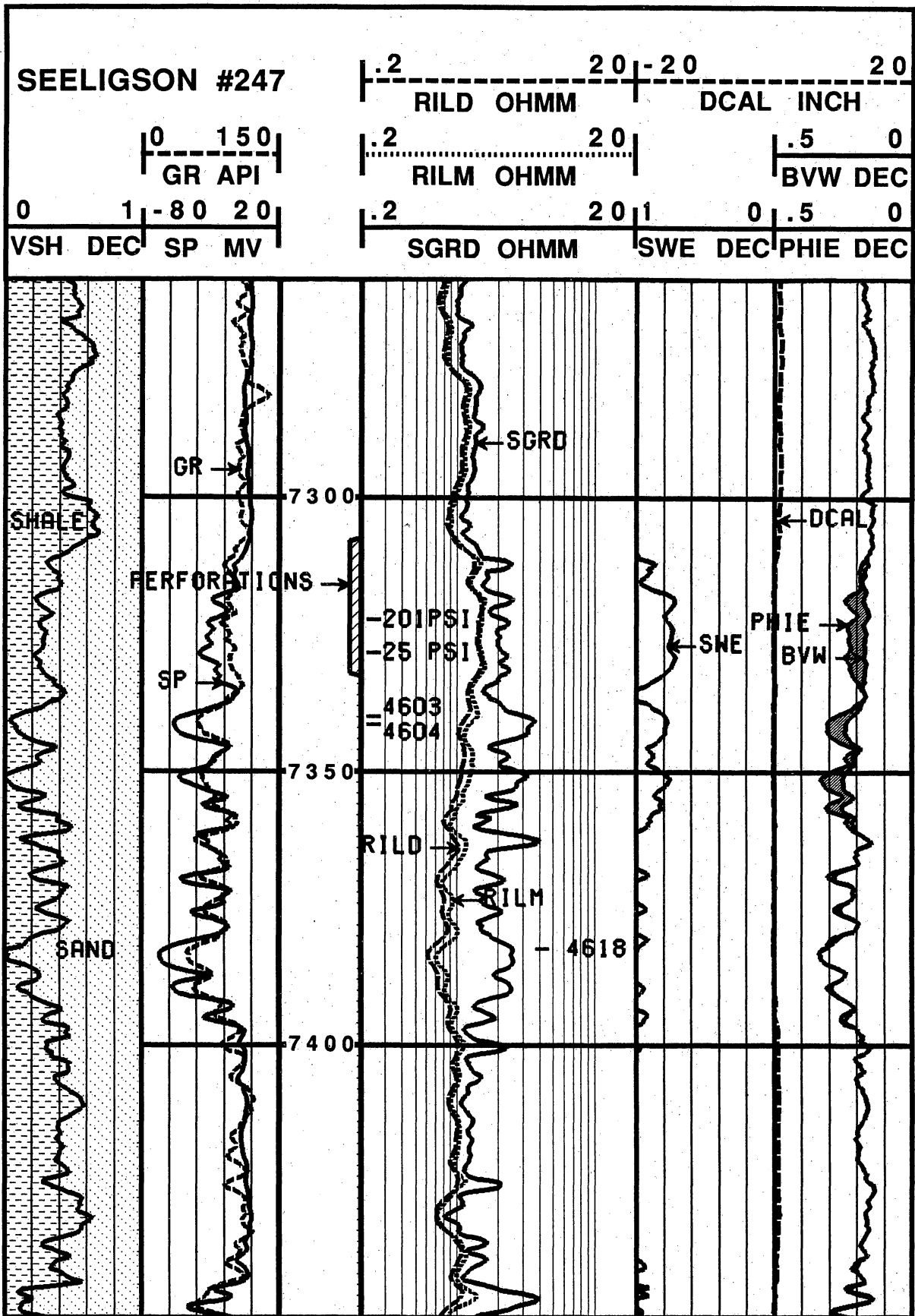


Figure 62. Induction log from the pay interval of the Mobil No. 247 Seeligson well. Calculated lithology, porosity, and water saturation also shown.

Table 7. Log types available for the 1-85, 1-89, and 1-171 wells at Seeligson field.

Logs obtained	1-171	1-89	1-85
Full-wave acoustic log	X	X	X
Pulsed neutron/GR	X	X	X
Noise	X	X	X
Temperature	X	X	X
CET	X	X	X
Borehole gravity (Edcon)		X	

The objective of the open-hole logs was to refine and test the application of the open-hole shaly-sandstone model previously developed in the No. 141 Canales well in order to identify potential gas-producing zones. The purpose of the program of sequential pressure tests was to assess pressure communication of permeability barriers in equivalent zones in nearby wells.

The cased-hole pulsed-neutron log was run to assess prediction of formation pressure behind casing using pulsed-neutron count rate ratio. The temperature, cement bond and noise logs were run as diagnostic logs for cased-hole VSP data acquisition.

Development of the Petrophysical Model

The acquisition of data in the No. 141 Canales well allowed development of a rock-based shaly sandstone petrophysical interpretation model, which combines core analysis with calibrated log-derived parameters to give an accurate description of reservoir properties from well logs (Truman and others, 1986). Up to 37 ft (11.3 m) of conventional core was cut across the Zone 15 reservoir (fig. 12) and the underlying shale in order to obtain representative values of mineralogy, porosity, and electrical factors "m" and "n" in the Frio Formation.

The shale was cored to provide mineralogy and porosity data to calibrate the shaly sandstone model. Porosities were measured both by drying in a convection oven at 230° F (110° C) (to obtain total porosity) and in a humidity-controlled oven (40 percent relative humidity and 140° F [60° C]) to estimate effective ambient porosity. Permeability was measured in the sandstones but not in the shales. The results of this research are described in the preceding section of the report (Truman and others, 1989).

Core Mineralogy

Thin-section analysis was used to calibrate the log-derived shale indicators and to confirm the mineralogy. Porosity from thin section point count ranges from 13 to 20 percent and is mainly primary intergranular porosity. Shards of volcanic glass were observed in the mudstones and may account for higher gamma-ray responses.

Analysis of mineral content from both infrared absorption and X-ray diffraction revealed that the primary mineral constituents of the rock are quartz, plagioclase, K-feldspar, calcite, illite and smectite (Truman and others, 1989.)

Determination of Shale Volume

Volume of shale can be obtained by calibrating log-derived shale indicators to volume of shale obtained from thin section point counts. In the Frio Formation a poor relationship exists between core shale volume and gamma-ray derived shale volume. Commonly, the gamma ray will overestimate the volume of shale. When this occurs, the apparent grain density from the neutron-density combination and the neutron log by itself provide secondary shale indicators. By using the minimum value of all three shale indicators, a more representative volume of shale is obtained.

Determination of Porosity

Total and effective porosity were determined from the density and neutron logs, after correction for shale content, utilizing the following relationships

$$\phi_{Dc} = \frac{\rho_g - \rho_b}{\rho_g - \rho_f} - \frac{\rho_g - \rho_{sh}}{\rho_g - \rho_{fl}} V_{sh}$$

and

$$\phi_{Nc} = \frac{\phi_N}{\phi_{Nf}} - \frac{\phi_{Nsh}}{\phi_{Nf}} V_{sh} ,$$

where

V_{sh} = volume of shale,

ϕ_{Dc} = density porosity, corrected either total or effective,

ϕ_{Nc} = neutron porosity, corrected either total or effective,

ρ_{gr} = grain density,

ρ_{sh} = shale density,

ρ_{fl} = fluid density,

ϕ_{Nf} = neutron fluid, and

ϕ_{Nsh} = neutron shale.

A grain density of 2.67 g/cm³ derived from core measurements was used for porosity determination from the density log. A sandstone matrix was used for neutron porosity derivation. After calculating the density and neutron porosities, a straight average is made in nongas zones to obtain porosity. In gas zones the density and neutron porosities are affected in opposite ways. A weighted average is used to account for the gas effect on the two measurements. Generally more weight has to be given to the density porosity. Good agreement with core porosity is found using these techniques (ResTech, 1988).

Determination of Formation Water Resistivity

Knowledge of the proper formation water resistivity is important in order to obtain a representative water saturation for the formations being analyzed. At Seeligson Field the formation water resistivity ranges from 0.18 to 0.24 ohmmeters at 75° F [24° C]. These resistivity values were measured from several water samples collected at Seeligson. These same values are found in nearby Stratton and TCB fields in Frio sandstones and are representative of many Frio sandstones along the Vicksburg Fault Zone. In the low-resistivity Vicksburg pay sandstone in the No. 247 and No. 248 wells, an R_w of 0.18 ohmmeters at 75° F [24° C] was used.

Cementation Exponent "m" and Saturation Exponent "n"

Other important factors needed to obtain a representative water saturation are the values of the cementation exponent "m" and the saturation exponent "n" at reservoir conditions. The values of cementation exponent "m" = 1.89 and saturation exponent "n" = 1.79 were measured in the Zone 15 reservoir in the No. 141 Canales well. These same values were used to interpret the other Frio reservoirs at Seeligson field. Because these values are very close to parameters found in most sandstone-shale sequences they were also applied to the No. 247 and No. 248 wells.

Determination of Formation Water Saturation

The dual-water method was used to calculate water saturation in the area of Seeligson field. This shaly sandstone model effectively accounts for the high surface area of clays lining the pores of shaly sandstones in Frio Formation. As applied by ResTech, the model also accounts for any additional gas stored in the shale porosity. Another method that should apply equally well in the shaly sandstones is the Waxman-Smiths saturation equation, which uses the CEC measurements obtained from special core analysis in clays. A check on the log-derived water saturations, in pay zones, can be made by comparison with both preserved core water saturations and saturations from capillary pressure measurements if the water table level is known. These measurements were unavailable from any of the cores from Seeligson field.

Application

The shaly sandstone log-evaluation model described earlier for the No. 141 Canales well was applied to the No. 247 and No. 248 wells to provide a description of reservoir properties from logs. This evaluation model, specific to Seeligson, allowed us to identify the shaly pay zone in the No. 247 well. This model has several advantages over conventional interpretation models. First, the model accounts for the presence of

effective porosity in shales, and therefore a better estimation is made of hydrocarbon volume in shaly sandstones (hydrocarbon volume may be underestimated by conventional models, which do not allow for porosity in shale). Second, this model has been calibrated with results from core analysis of Seeligson sandstones and is therefore more representative of reservoir properties. Third, the model can be extrapolated to other wells in Seeligson field.

Quick-Evaluation Techniques

Reasonable results can be obtained using some quick-look techniques to find zones of interest in the field. Use of apparent water resistivity, neutron density and neutron-sonic crossover analysis, and porosity and water saturation calculations using dual induction, compensated neutron, formation density, repeat formation tester, and sidewall cores, are common in the evaluation of Seeligson wells (ResTech, 1988).

The apparent water resistivity (R_{wa}) is determined from the Archie saturation relationship where:

$$S_w^2 = \frac{.81 R_w}{\phi_w^2 R_t}$$

Assuming $S_w = 1$, the relationship becomes

$$1 = \frac{.81 R_w}{\phi_d^2 R_t},$$

$$R_{wa} = \frac{\phi_d^2 R_t}{.81}, \quad \text{and} \quad S_w^2 = \frac{R_w}{R_{wa}},$$

where

ϕ_d = density porosity,

R_w = formation water resistivity or R_{wa} minimum, and

S_w = water saturation.

Using this relationship, water saturations can be estimated by drawing a line on the log at the known R_w (or R_{wa} minimum) and determining the deflection of the

R_{wa} curve. The ratio of $R_{wa} : R_w$ can be used to predict water saturation. A ratio of $1/1 = 100$ percent S_w , $2/1 = 71$ percent S_w , $3/1 = 58$ percent S_w , and $4/1 = 50$ percent S_w .

Any shows better than $3/1$ are productive, assuming that pressure is not depleted. Any shows better than $2/1$ are significant and should be evaluated further. An example of the R_{wa} technique is shown in figure 63 in the Zone 15 reservoir.

Gas affects neutron and density oppositely. The low hydrogen content causes the neutron porosity to read low, and the lower fluid density causes the density porosity to read high (Schlumberger, 1987). These two log readings will cross over in clean sandstones when gas is present (fig. 64). Sonic and neutron porosities can be used in the same manner, with even greater sensitivity to gas. Shale affects the neutron log severely, causing it to read high and masking some shaly gas productive zones. Sonic and neutron data are affected by shale in the same direction, thus allowing gas identification in the shaly sandstones as well as clean sandstones (Schlumberger, 1987). Figure 65 illustrates use of the neutron-sonic log as a gas identifier.

Porosity can be read directly from the density log if the density porosity is run using a 2.65 g/cm^3 grain density. Recommendations are to use density porosity directly off of the density log for log calculations as opposed to a neutron-density crossplot. If not corrected for shale, the crossplot will determine porosities that are much too high in the shales and shaly sandstones.

The formation tester is used to monitor formation pressure and to determine fluid type. In the unitized section, pressures are reduced as a result of offset production. If pressure depletion is only partial, sandstones are still candidates for recompletion when offset wells are no longer producing. Pressure monitoring may be the most critical evaluation requirement of all.

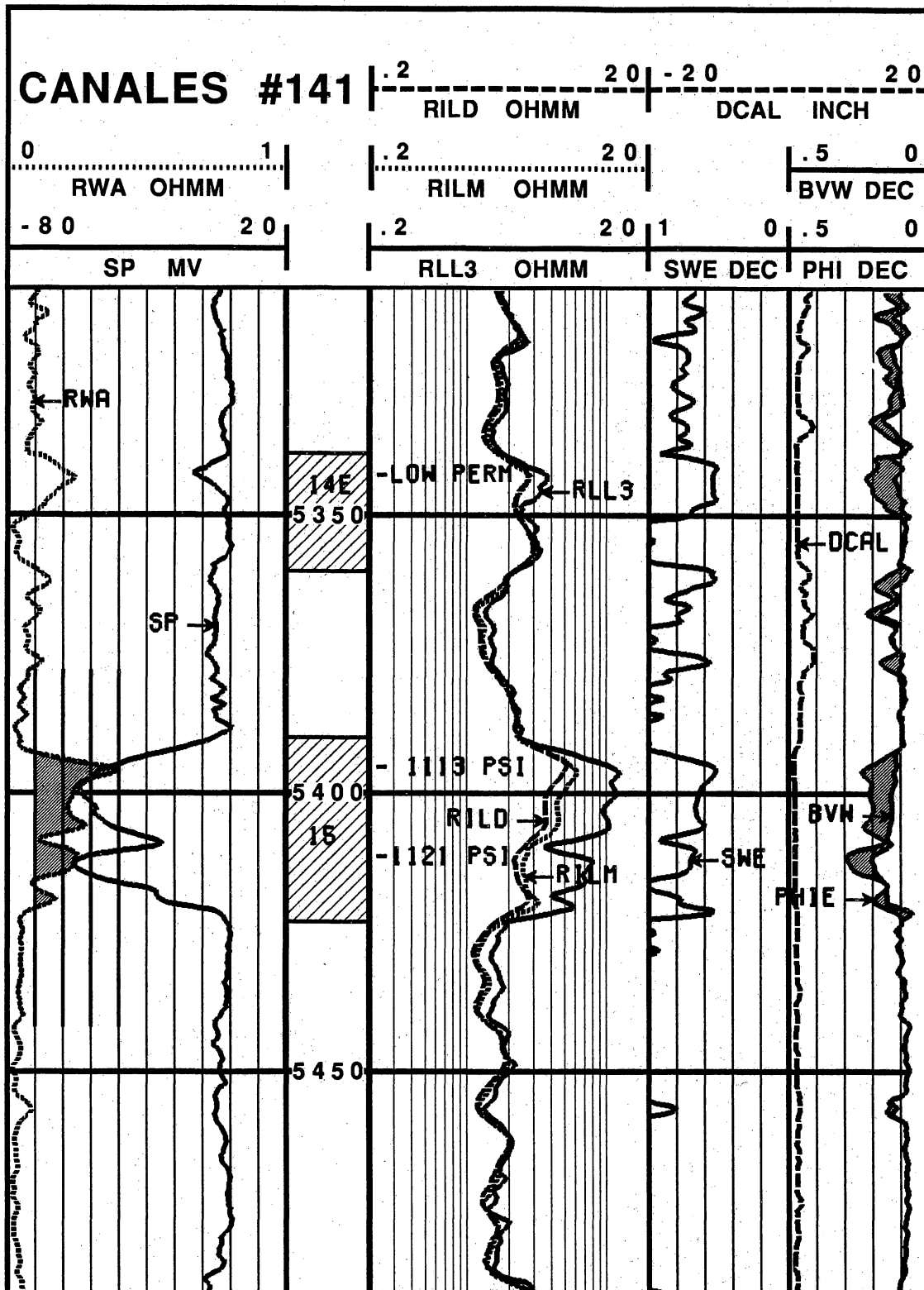
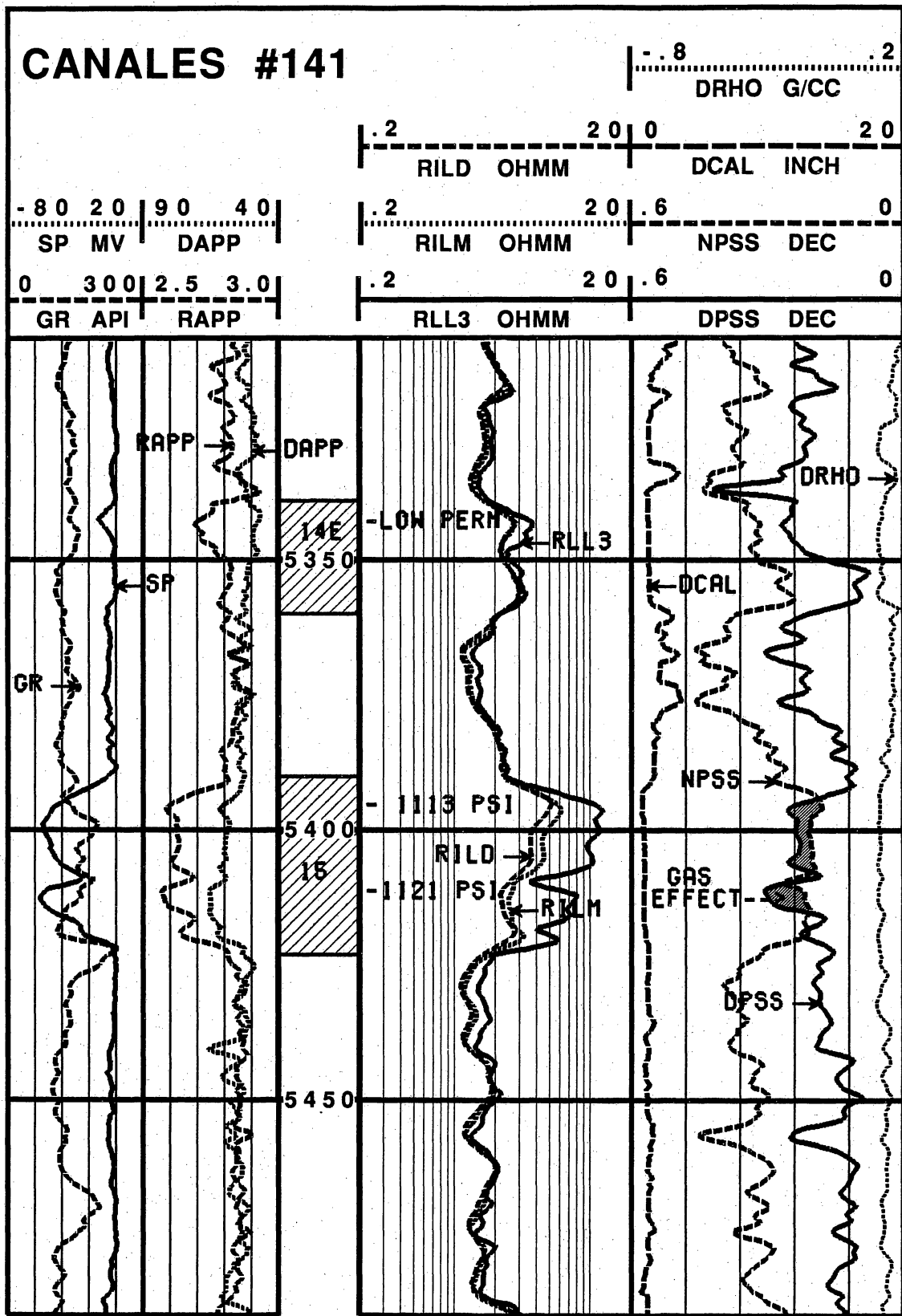


Figure 63. Illustration of R_{wa} interpretation in the Sun No. 141 Canales well.



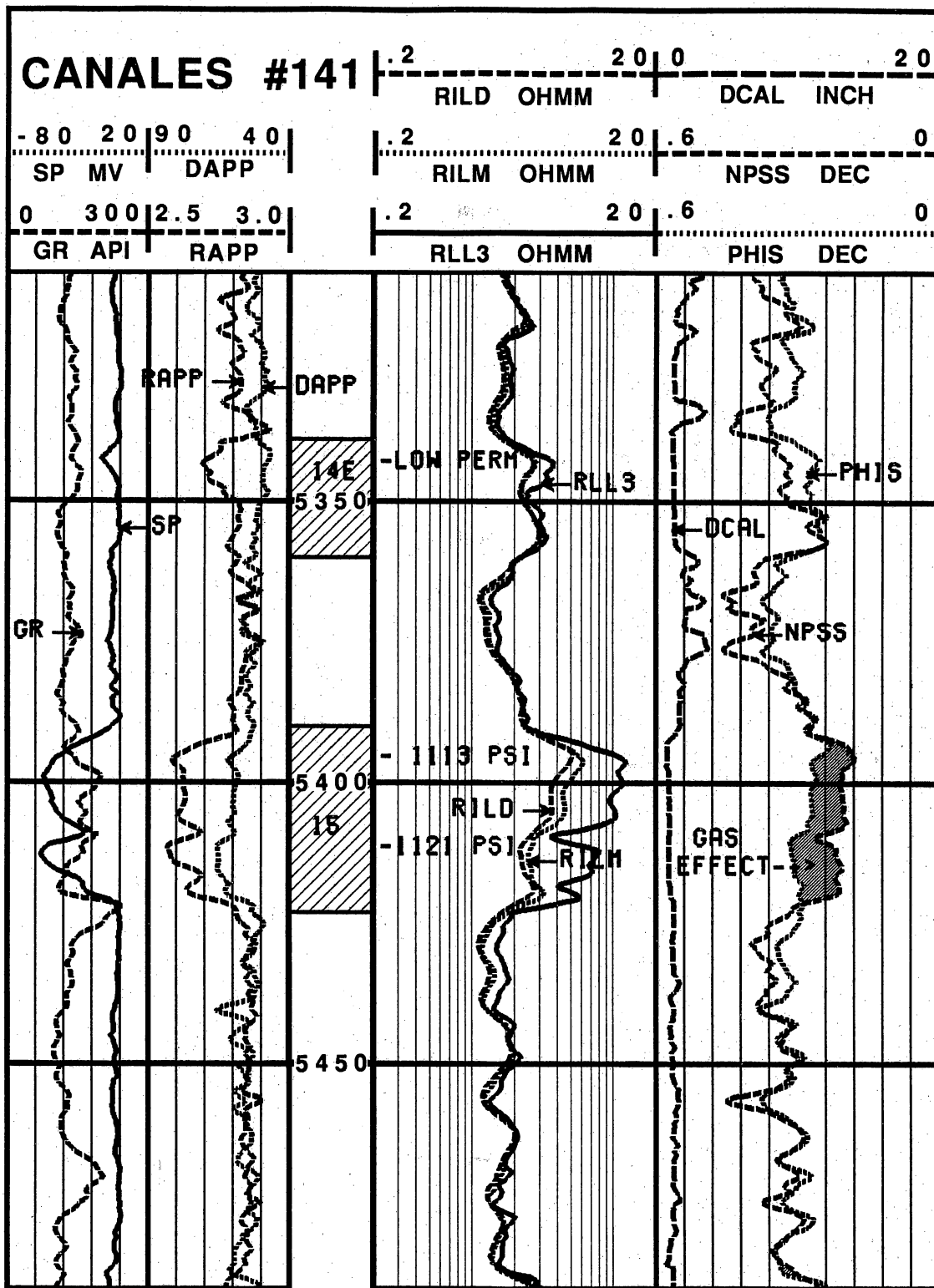


Figure 65. Gas effect from neutron-sonic log in the Zone 15 reservoir in the Sun No. 141 Canales well.

Sidewall cores are used for porosity and permeability information and to determine hydrocarbon shows. The information is only qualitative because percussion shattering affects the answers significantly. They may also be used to help distinguish oil from gas.

Problems Encountered

Two wireline data acquisition problems were found that also apply to other areas. First, it was impossible to obtain shear velocities in Frio sandstones from the full-wave acoustic log. Second, 50 percent of the sequential formation pressure tests were unrepresentative of formation pressures.

Figure 66 illustrates the problem encountered with the full-wave acoustic log. Whereas the instrument is able to obtain high-quality values for compressional velocity, it is virtually unable to distinguish the shear arrivals from the tube or mud waves. To solve this problem a shear source must be used. At the time of the data acquisition a tool with a shear source was unavailable from wireline companies. Since then, service companies have developed a new type of full-wave acoustic log with a shear source able to measure a shear velocity in acoustically slow formations.

Problems were also encountered during acquisition of sequential formation pressure data in the low-permeability shaly sandstones. The time necessary to obtain valid shut-in pressures using the tool may be prohibitive. However, a significant number of tests can be salvaged by knowing whenever the tool has been set in a low-permeability, restricted-flow zone or in a partially depleted zone. Many times a few minutes more of set time is all that is necessary for the tool-indicated pressure to build up to formation pressure. Therefore, either taking additional time during data acquisition of sequential pressures to assure that the pressures are stabilized or repeating a set in a tight zone will improve the percentage of representative shut-in pressures.

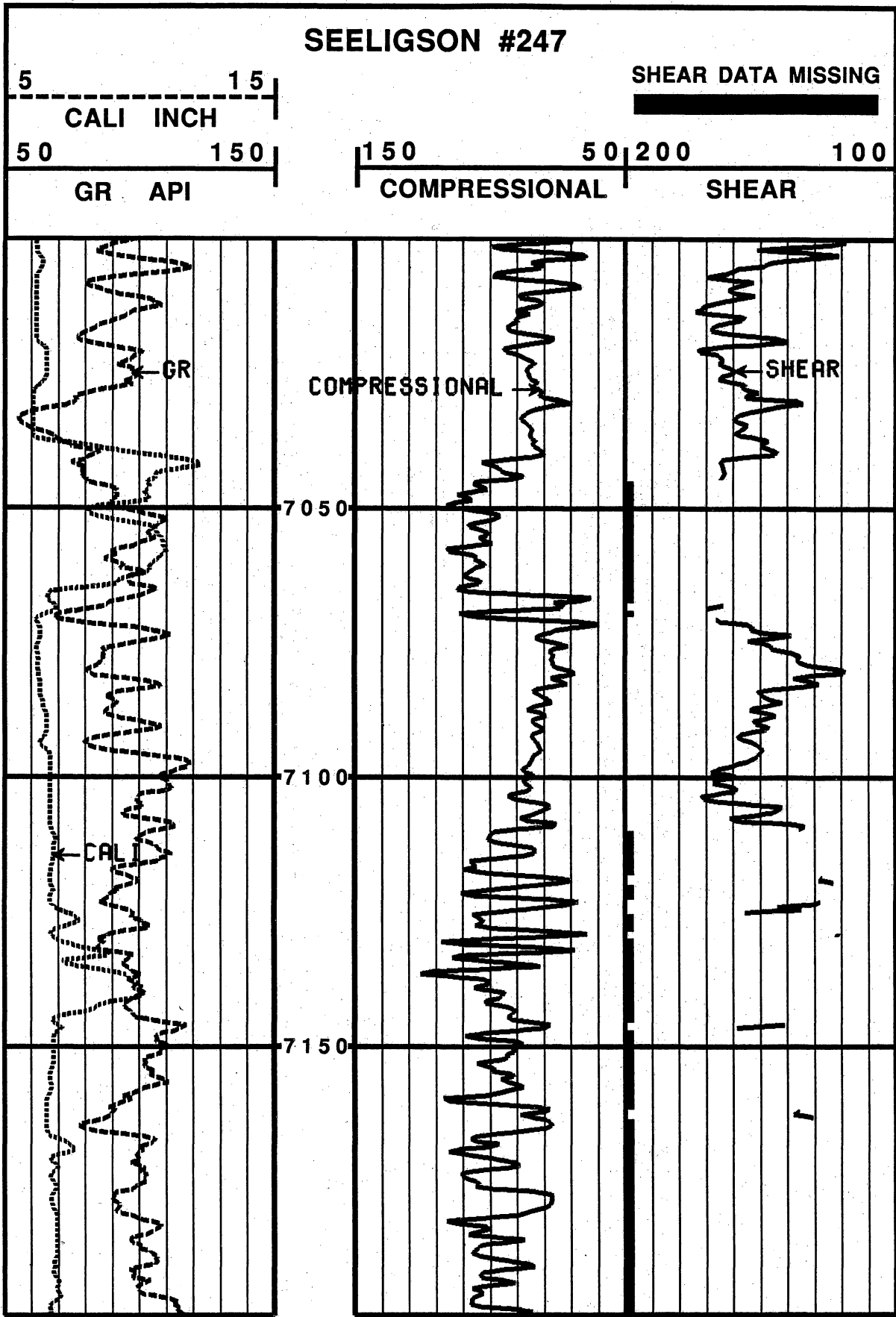


Figure 66. Full waveform sonic log of the Mobil No. 247 Seeligson well.

In the No. 247 well, the low-resistivity, high-water saturation sandstone was completed from 7,308 to 7,332 ft (2,228 to 2,235 m). The formation-pressure test data across the zone indicated a pressure of 201 psi. Subsequent production tests after perforations indicate the zone had a formation pressure of 4,300 psi. Two sequential pressure tests taken just below the zone at 7,341 and 7,342 ft (2,238 and 2,238.4 m) indicate more than 4,600 psi formation pressure. The higher pressure is obviously the correct one for the completed zone. Figures 67 and 68 are the field recordings of the two tests taken. The test at 7,323 ft (2,233 m) indicates 201 psi. The other test at 7,341 ft (2,238 m) indicates 4,603 psi. The latter (fig. 68) builds up rapidly to 4,603 psi. The former (fig. 67) was in the process of building up slowly when it was terminated. Failure to identify the fact that this test was prematurely terminated could have resulted in the zone not being completed. In the No. 248 well, 40 pressure measurements were taken and assumed to be valid by the field engineer. After careful examination, 20 of those tests were found to be prematurely terminated and thus only the remaining 20 tests were valid (ResTech, 1989).

The problems associated with the formation tester obviously need to be addressed. One solution is to modify the tool mechanically to increase the speed at which pretest chambers in the formation pressure-tool fill (necessary for formation pressure). This can be accomplished by decreasing the size of the pretest chamber or by increasing the surface area of the sampling port. Both techniques would improve the efficiency of the pressure test allowing a faster buildup in low-permeability formations. A complete knowledge of the capabilities of each service company, as well as close supervision of the operation at the wellsite, is needed to obtain accurate results.

Pressure Prediction from Pulsed-Neutron Logs

Sequential formation pressure tests were correlated with pulsed-neutron measurements from the No. 248 well. A correlation was found with the pulsed-neutron

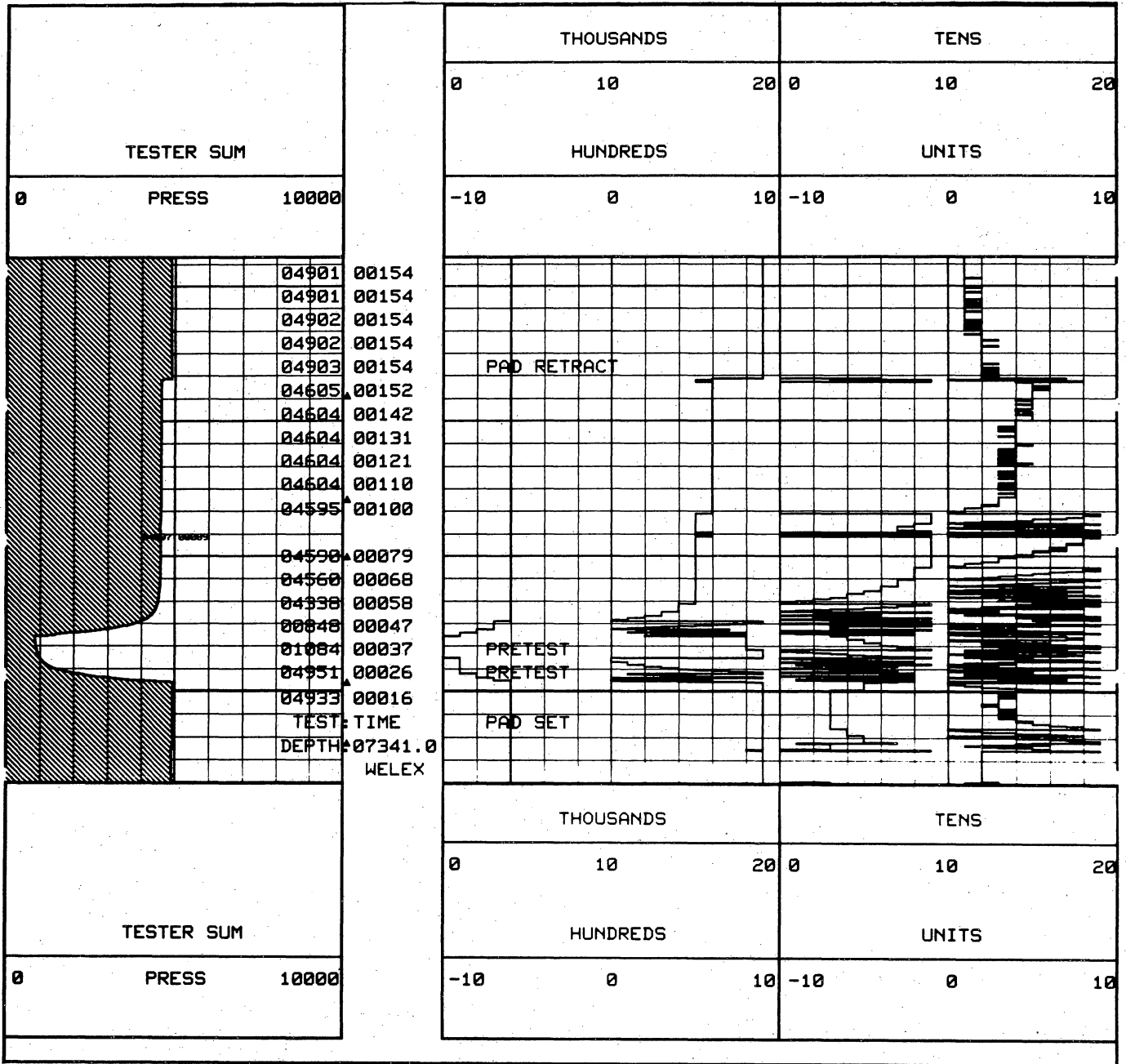


Figure 68. Formation pressure test at 7,341 ft (2,238 m) in the Mobil No. 247 Seeligson well. Pressure builds up to 4,603 psi within 110 seconds of setting the tool.

count ratio (fig. 69). The correlation is good in the clean gas sandstones. However, other effects such as shaliness and reservoir fluid type reduce the accuracy. The technique holds some promise and is being developed in Stratton field.

Cased-Hole Petrophysical Research

Cased-hole evaluation techniques were used to identify and quantify gas-bearing zones in existing wellbores at Selligson field by assessing gas presence; determining lithology, porosity, and water saturation; and inferring the degree of pressure depletion. In order to identify gas zones in old cased wells, additional cased-hole logs must often be run to complement the available open-hole data. At Seeligson field, the original open-hole data consists mostly of old electrical surveys, micrologs, and some sidewall core analysis. A cased-hole logging program must be designed to complement the available data. The pulsed-neutron with gamma-ray and the full-wave acoustic log can be used to obtain the parameters of interest and to identify gas zones. The borehole gravity survey has also been tried in Seeligson to obtain density and porosity through casing (the No. 1-89 well).

Previous Research

Formation-pressure test data were used to document reservoir heterogeneity between well pairs and to demonstrate pressure communication or permeability barriers in equivalent zones between two relatively closely spaced wells. Fourteen wells were selected in the east-central part of the field for pulsed-neutron logging (Jirik and others, 1989). These wells, selected on the basis of availability, lithological heterogeneities of unit reservoirs, and comparison of offset-well production, were evaluated for water saturations on the basis of estimated porosity. Gas shows in the fourteen wells were compared, and the wells were ranked to select intervals for cased-hole sonic logs. Data

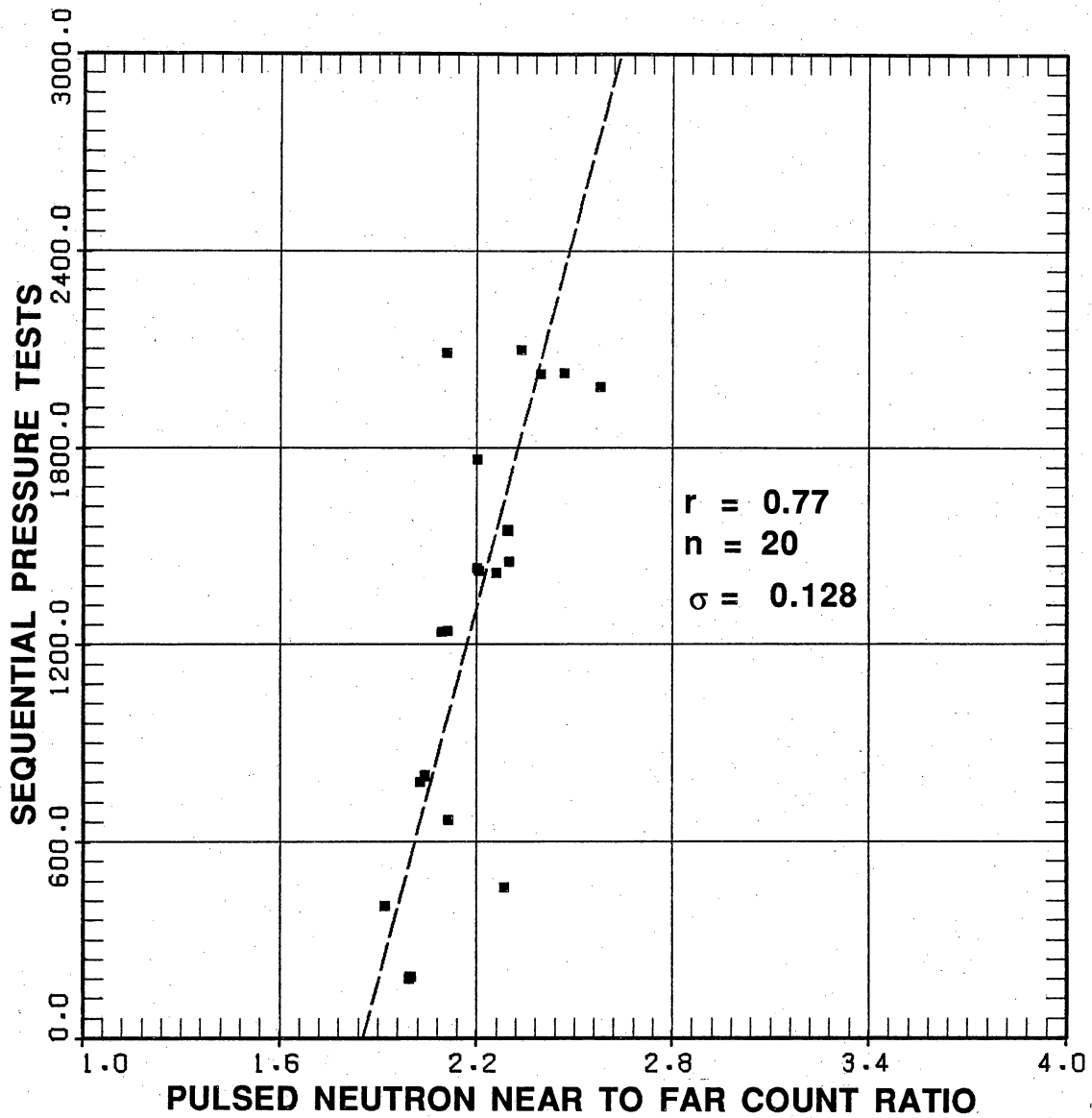


Figure 69. Relationship between pulsed-neutron and formation pressure in the Mobil No. 248 Seeligson well.

from five cased-hole sonic logs were compared with data obtained from pulsed-neutron logs to calculate porosity and to determine gas effect on the logs. These two porosity values were used in conjunction with capture cross-section (σ) data to calculate cased-hole water saturation. Long-normal curves from old electric logs were used to estimate resistivity and were combined with newly acquired porosity data to calculate open-hole water saturation. The results were plotted to include both original open-hole water saturation and cased-hole water saturation in conjunction with porosity from the sonic and neutron logs. Gas-productive sandstones were identified from the log plots.

Open-hole water saturation was computed from a combination of long-normal curve values from the electric log and porosity values from the neutron and sonic log curves. This allowed use of the pre-1960 technology (electrical survey without a porosity log) and modern through-casing sonic tools to calculate original open-hole water saturation. The cased-hole water saturation was calculated from the capture cross-section (σ) curve of the pulsed-neutron log and the neutron and sonic porosity data.

Oryx Three-Well Project

Several gas-bearing zones were identified on three cased wells as a result of a cooperative data collection and cased-hole evaluation plan conducted in conjunction with Oryx operations in Seeligson field. The program focused on unitized (Zones 7-20) Frio reservoirs. The objective was to use cased-hole logs, a borehole gravity survey, and a cased-hole interpretation package (ResTech, 1988) to find bypassed gas zones, predict pressure and determine cement integrity. The research was performed on the No. 1-85, No. 1-89, and No. 1-171 wells.

Before data acquisition, the wells were reentered, cleaned of any obstructions, and the casing was pressure tested. A complete suite of cased-hole logs including full-wave acoustic, pulsed neutron, cement evaluation tool (CET), noise, and temperature logs was run for borehole information and formation evaluation, as well as to assist in the

planning and interpretation of VSP surveys. In the No. 1-89 well a borehole gravity survey was run to test the application of this tool in Gulf Coast sandstone-shale sequences.

Several gas-bearing zones were identified using the cased full-wave acoustic and pulsed-neutron logs. The combination of these two measurements provide porosity, water saturation, and type of hydrocarbon. Compressional travel time using an acoustic device was obtained through casing when bonding was 50 percent or better (Jirik and others, 1991). The cement-evaluation log was used to establish zone isolation and to determine whether sufficient cement in the annulus was available for accurate full-waveform acoustic results. The temperature and noise logs were obtained to determine wellbore integrity and to identify possible noise problems that could affect VSP data acquisition.

An example of the application of this method is illustrated in figure 70. In the No. 1-89 well, the Zone 15 reservoir is gas bearing. Notice the gas crossover in the porosity logs and pulsed-neutron count rates, indicating gas presence. The pressure-prediction program developed in the No. 248 well (see Open-Hole Interpretation section) indicates that this zone may be partially depleted as observed in figure 71. This prediction is also confirmed from a sequential formation pressure of 356 psi measured in the Zone 15B reservoir in the nearby No. 248 well. The open-hole and cased-hole water saturations are low in this zone, also indicating that gas is present. However, a water zone can be observed in figure 70 from 5,458 to 5,470 ft (1,664 to 1,668 m). Notice here the lack of gas indication in the porosity logs and count ratio and the high calculated cased-hole water saturation. Therefore, the log-derived parameters suggest that the Zone 15 reservoir is gas-bearing.

SEELIGSON 1-89

BVG OPEN



BVG CASED

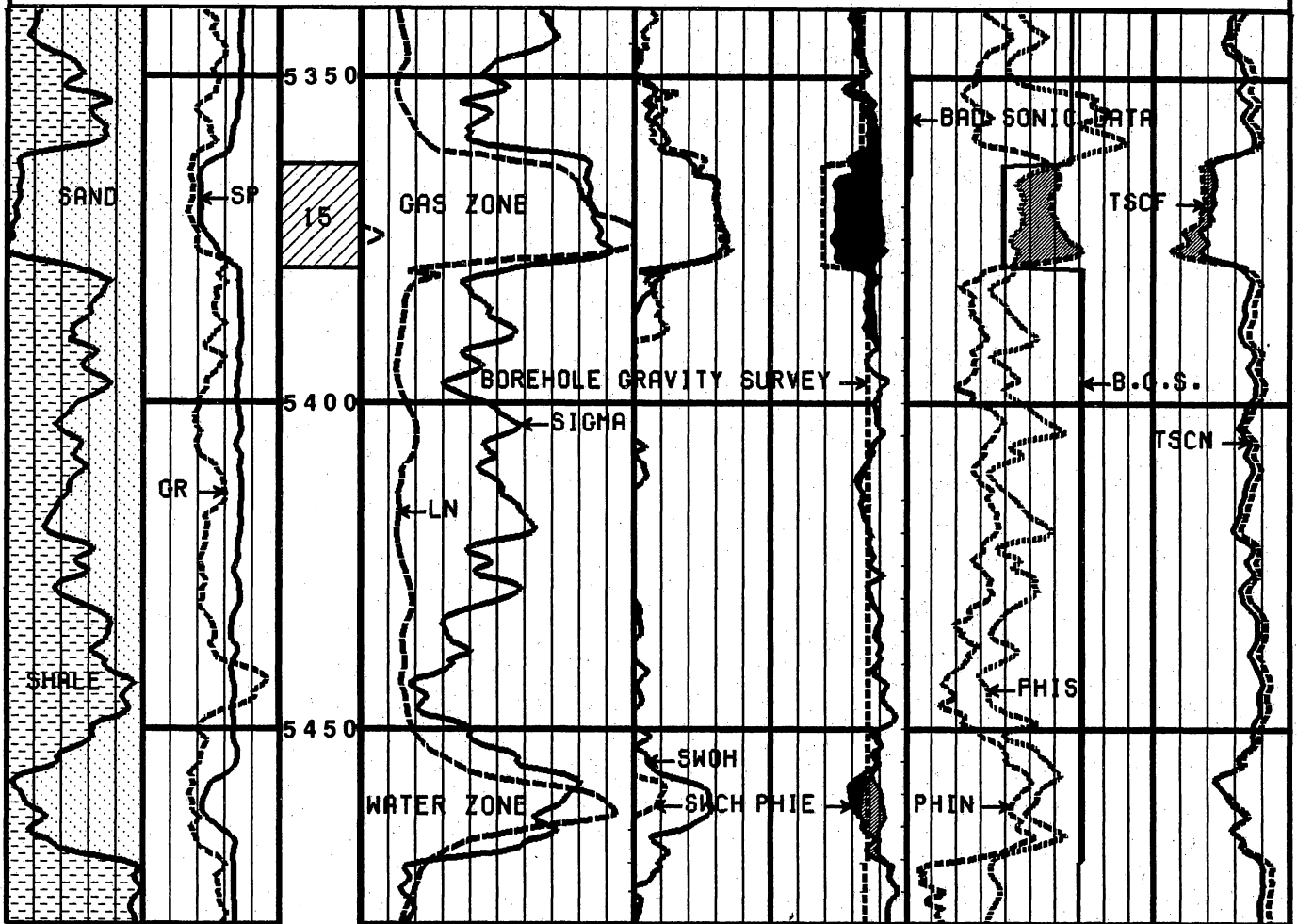
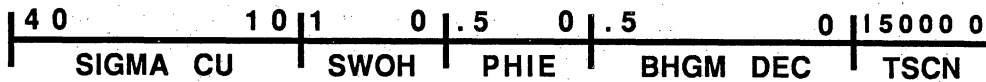
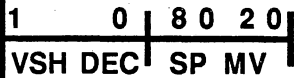
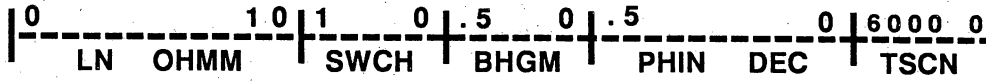
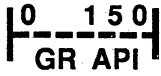
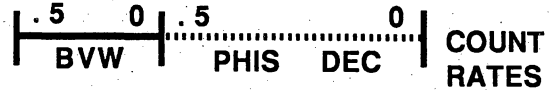


Figure 70. The Zone 15 reservoir is gas bearing in the 1-89 well, as indicated by porosity logs and borehole gravity survey and pulsed-neutron count rates.

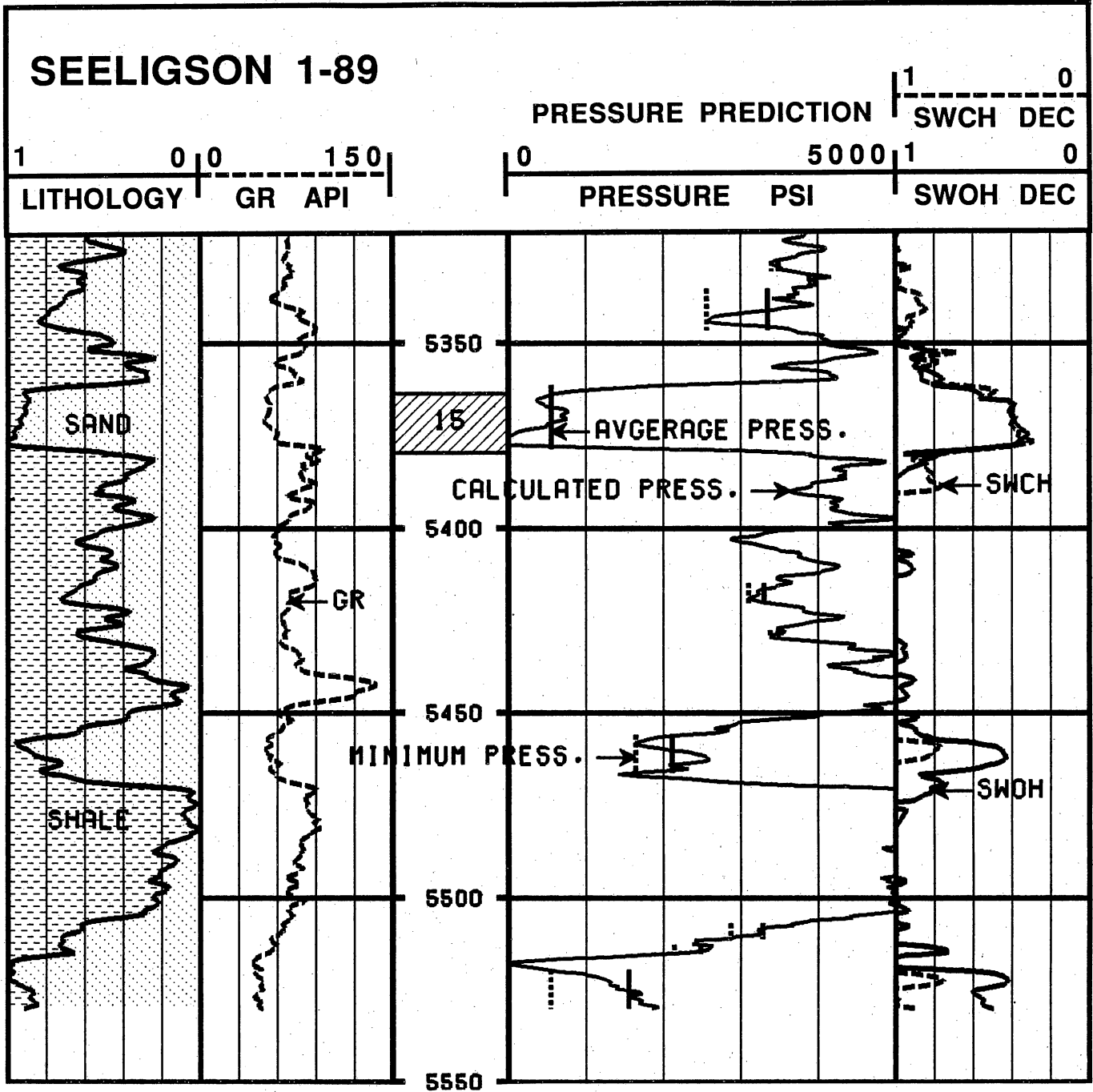


Figure 71. Pressure prediction from pulsed-neutron count rates indicates that the Zone 15 reservoir may be partly depleted in the 1-89 well.

Determination of Shale Volume and Lithology

As in the open-hole analysis, the simple lithology determination is based on the input of several shale indicators. The volume of shale is calculated from the minimum value of the cased-hole gamma-ray log and sigma from the pulsed-neutron log (ResTech, 1988). The gamma-ray log is not a good indicator of shale volume because of high readings in sandstones, which are probably caused by radioactive volcanic rock fragments. Using the minimum of the two indicators results in a shale volume calculation that is representative of core descriptions from other wells in the field.

Determination of Porosity

Although many old wells have unavailable porosity logs, it is possible to obtain a porosity measurement from cased-hole measurements such as the pulsed-neutron and full-wave acoustic log. The pulsed-neutron log provides a cased-hole neutron porosity that is similar to a conventional compensated neutron log. The pulsed-neutron porosity is obtained from the ratio of the near and far counts. At Seeligson field, a sandstone matrix was used to calculate pulsed-neutron porosity.

The acoustic log porosity is calculated from the compressional travel time of the full-wave acoustic log. A reliable compressional travel time can be obtained through casing when cement conditions are adequate (Jirik and others, 1991). The Raymer-Hunt equation was used to calculate sonic porosities:

$$\phi_s = \frac{\Delta_t - \Delta_{tma}}{\Delta_t} 0.625,$$

where

Δ_t = compressional travel time, and

Δ_{tma} = travel time of matrix = 55.5 μ sec/ft.

Total and effective porosities can now be obtained by correcting pulsed-neutron and sonic porosity for shale volume using the following general relationships:

$$\phi_{Nc} = \frac{\phi_N}{\phi_{Nf}} - \frac{\phi_{Nsh}}{\phi_{Nf}} V_{sh}$$

and

$$\phi_{Sc} = \phi_S - \phi_{Ssh} V_{sh}$$

where

V_{sh} = volume of shale,

ϕ_{Nf} = neutron fluid,

ϕ_{Nsh} = neutron shale, either wet or dry,

ϕ_{Nc} = neutron porosity corrected, either total or effective,

ϕ_{Sc} = sonic porosity corrected, either total or effective, and

ϕ_{Ssh} = porosity sonic shale, either wet or dry.

In sandstones where the sonic porosity is reliable, the weighted average of ϕ_{Sc} and ϕ_{Nc} is used. However, when cement conditions are marginal and a sonic porosity cannot be obtained, the neutron porosity alone is used. These porosities are then used for calculation of water saturation and to observe gas crossover. An example of the quality that can be expected from a full-wave acoustic compressional log through casing is shown in figure 72. Here, a comparison of open-hole and cased-hole compressional travel time in a Seeligson well indicates that reliable cased-hole compressional travel times can be obtained when cement bonding is 50 percent or better (Jirik and others, 1991).

Gas Indicators

Gas presence can easily be identified by observing sonic and neutron porosities on a compatible scale. Sonic and pulsed-neutron porosities respond in a similar manner in oil, water, and shaly zones. However, in gas-bearing zones the porosities separate ($\phi_S >$

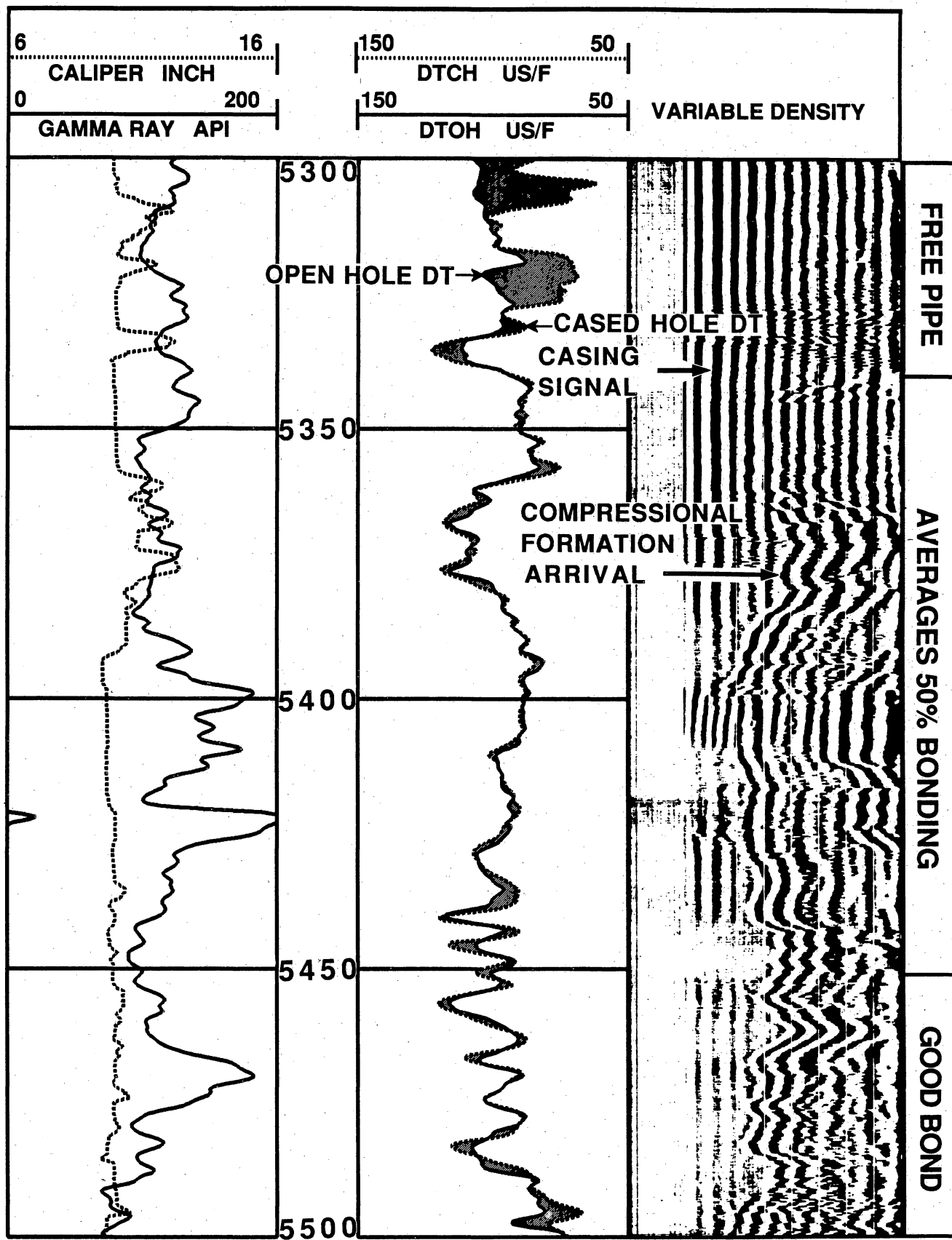


Figure 72. Reliable compressional travel times obtained through casing (when bonding is 50 percent or better).

σ_N), thus indicating gas (Jirik and others, 1991). An additional gas indicator is the near- and far-count rates of the pulsed-neutron log, which, when observed in a compatible scale, also separate in gas bearing zones (Jirik and others, 1991). When combining those two indicators, gas zones are identifiable on the composite displays.

Water Saturation

Water saturation can also be calculated using the pulsed-neutron log. Sigma, or formation capture cross section, is used as an input, along with the porosity previously determined to obtain saturation using an equation that corrects for structural shale (ResTech, 1988). Notably, a reliable quantitative analysis of cased-hole water saturation is possible using sigma and porosity since the gas-bearing Frio sandstones exhibit a contrast between sigma gas (10), and sigma water (38). Also, sigma water of 38 capture units is higher than expected for the low-salinity formation waters in the Frio ($R_w = 0.11$ ohm-meters) because of the presence of boron and lithium in the waters (MacPherson, 1989; MacPherson and Land, 1989).

Open-hole water saturation can also be computed using available electrical logs and cased-hole porosity. In this three-well study, only electrical logs were available. The thin sandstones make the 18-ft-8-inch lateral difficult for water saturation calculation (Hilchie, 1979). However, the short and long normals can be used to compute an approximate open-hole water saturation. The cementation factor of 1.89 and the saturation exponent of 1.79 (derived in the No. 141 Canales well) were used in the formation water saturation equation.

Borehole Gravity Survey

A borehole gravity survey was run in the No. 1-89 well to test its applicability at finding gas zones in the Frio Formation and to determine formation density through

casing. This tool is important because the measurement is unaffected by casing or hole washout. Results show that the borehole gravity survey can be used to both determine porosity and identify gas in Seeligson reservoirs, whether or not the well is cased. In the Zone 15 reservoir in Seeligson No. 1-89 well (fig. 70), the borehole-gravity-survey-derived porosity clearly identifies gas ($\rho_d > \rho_n$) in the interval 5,363 to 5,379 ft (1,635 to 1,640 m). In this interval the tool reads 2.18 g/cm (30-percent porosity), whereas the pulsed-neutron porosity is lower because of the decrease of hydrogen in gas zones.

The tool measures the earth's gravity at each station, where the tool is stopped and a gravity reading is made. A formation density is calculated from the vertical gradient of gravity between two stations. Deviation of the surrounding rock from uniformity will cause differences with the density measured from the wireline gamma-gamma density tool, thus indicating rock heterogeneity or changes in porosity (Exploration Data Consultants, 1991).

In gas-bearing formations the measurements of the borehole gravity density will normally be lower than the gamma-gamma density because the borehole gravity measurements are unaffected by the invaded zone. Borehole gravity measurements are also practically unaffected by casing and hole washouts because the tool has a large radius of investigation. A remote body with sufficient density contrast may be detected at a distance of between one and two times the height of the body (Edcon-Schlumberger, 1991; Exploration Data Consultants, 1991).

The accuracy of the borehole gravity survey measurement depends on uncertainties in depth and gravity differentials. For a set level of gravity and depth uncertainty, increased density accuracy is achieved by using larger depth increments. Useful accuracy with the current tool (used in the No. 1-89 well) is difficult for depth increments of less than 6.5 ft (2 m) (Edcon-Schlumberger, 1991). A new tool known as the Shuttle Sonde is being developed in the SGR project, which overcomes the 6.5-ft (2-m) limitation. The borehole gravity report (app. 2) lists the bulk densities at all

stations recorded in the well. Two other methods are described in appendix 2 that confirm the earlier interpretation of the Zone 15 reservoir in the No. 1-89 well.

Temperature, CET, and Noise Log

The temperature, noise log, and cement evaluation tool were run to diagnose potential mechanical and well-integrity problems and to indicate zones where sonic and VSP surveys may be unreliable. For example, figure 73 shows some problems in well 1-89 in the interval 5,165 to 5,210 ft (1,575 to 1,588 m). The CET acoustic caliper indicates casing damage in a previously perforated and squeezed zone. Notice that the internal casing size has increased because of damage caused during the life of the well. In fact, casing may not even exist there. The cement-quality display (figure 74) shows that the squeeze is adequate in front of the perforations but is marginal above and below. The temperature log (fig. 73), run in static conditions, indicates a cooling anomaly near 5,210 ft (1,588 m). This anomaly is caused by gas expansion and indicates communication behind casing with nearby zones. The conclusion is that this squeeze was not successful.

Some doubts arose about the quality of cement calculated at the wellsite, and the CET results confirmed these doubts. After we met with wireline representatives, a final recomputation was made using the proper calibration values. Until more experience is gained by wireline operators in the field on proper calibration values for the CET, we recommend using the conventional cement bond tool with variable density waveform display to test for cement quality because the field calibration procedures are well established and provide reliable answers about the cement condition.

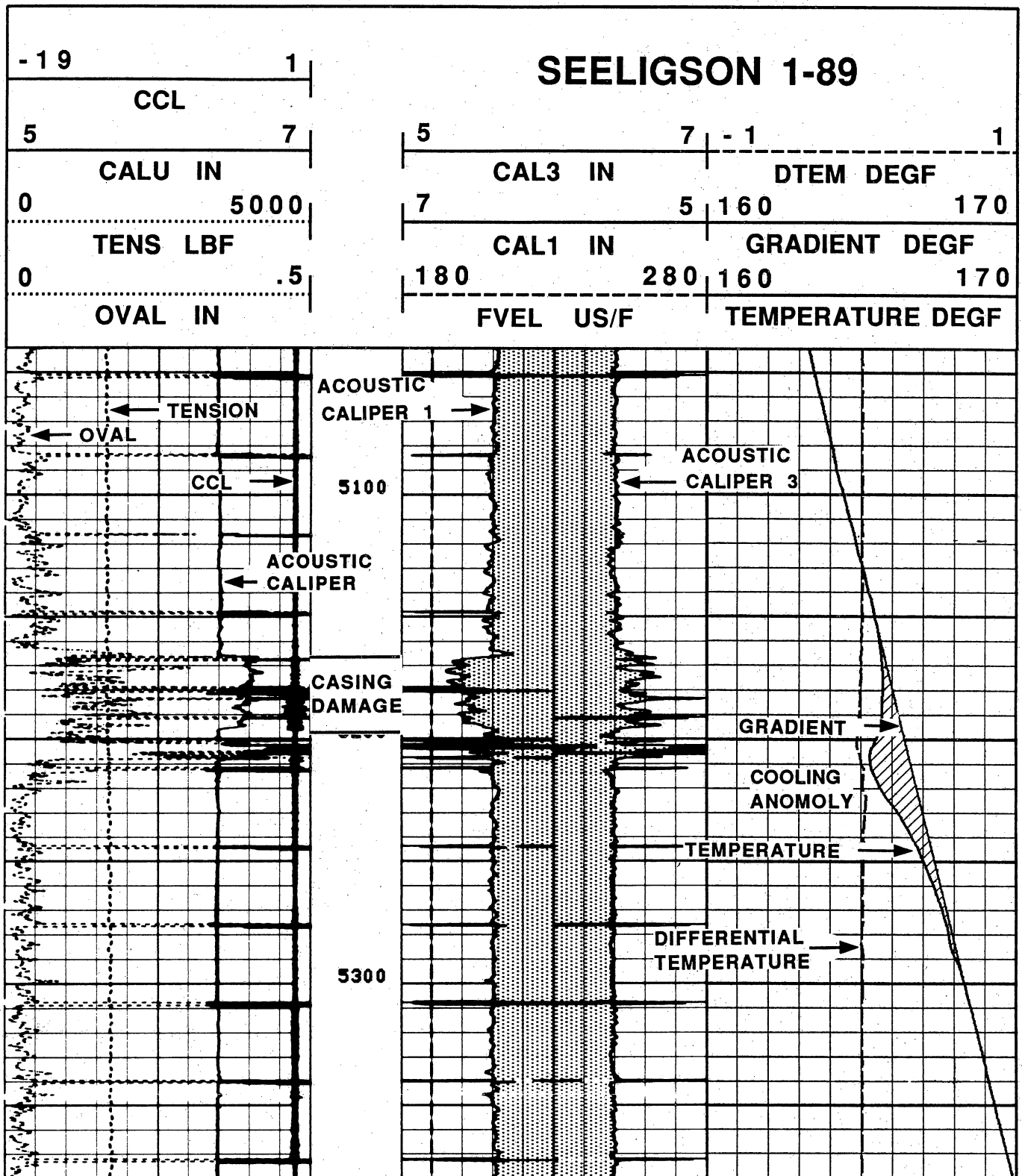


Figure 73. The CET acoustic caliper showing casing damage from 5,165 to 5,210 ft (1,575 to 1,588 m) in the 1-89 well. The temperature log shows a cooling anomaly.

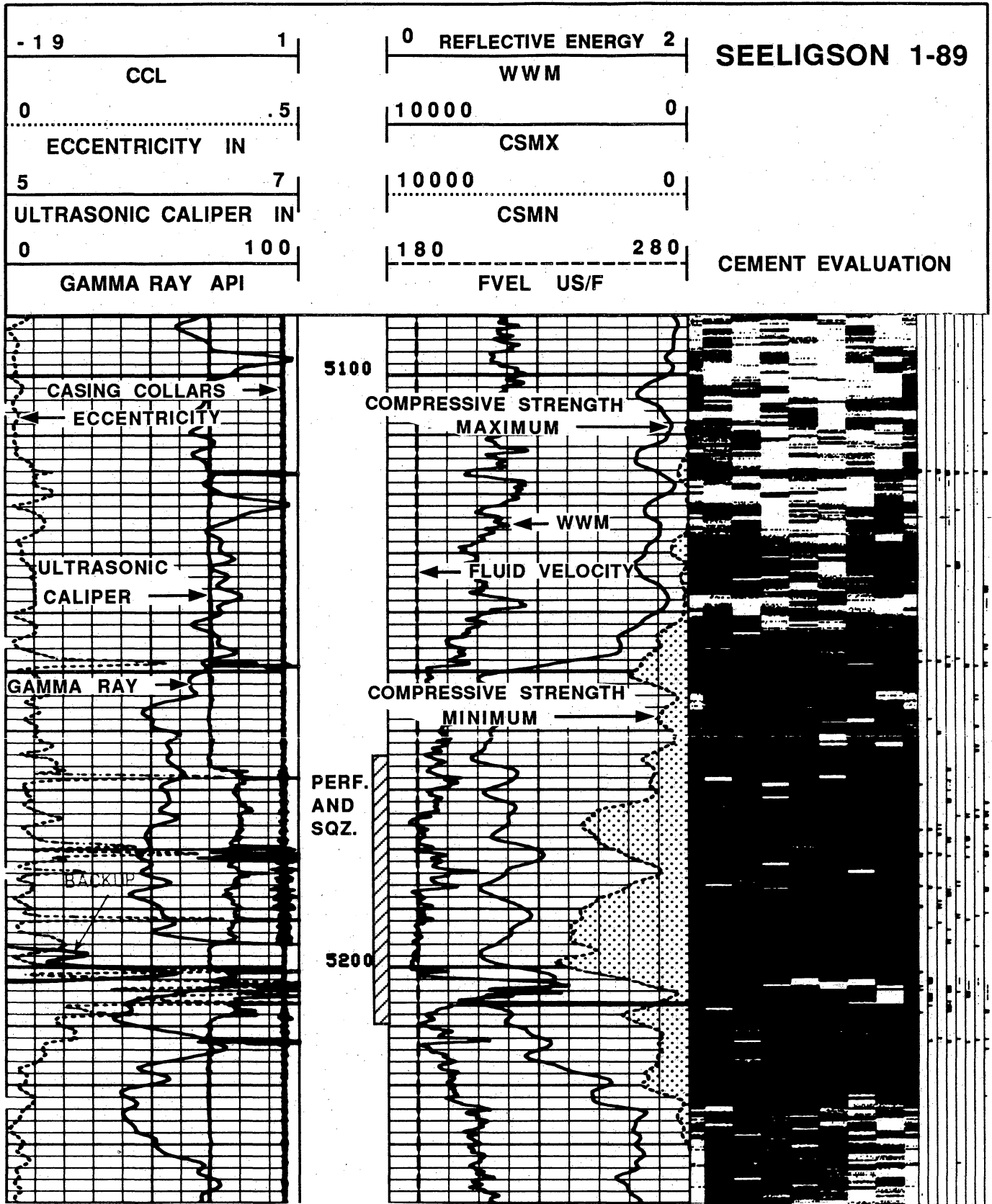


Figure 74. The CET cement evaluation log showing that the perforated and squeezed interval from 5,165 to 5,210 ft (1,575 to 1,588 m) is adequate but marginal above and below the squeeze.

Limitations

Several limitations exist when obtaining logs through casing. First, one of the limitations is related to the outside diameter of the tools currently available for logging. All the cased-hole tools, including pulsed neutron, temperature, noise, gamma ray, and the CET, have 1 11/16-inch outside diameter. However, the full-wave acoustic and the cement bond logs have larger outside diameters of 2 3/4 to 3 5/8 inches, whereas the borehole gravity survey is 4 1/2 inches. This may limit the acquisition of these logs in some wells using smaller casings or tubing. Second, the tubing needs to be pulled out to run the larger diameter tools. Third, the well must be dead, with no perforations open, and full of brine water in order to get valid cased-hole interpretation parameters.

Results of Petrophysical Research

(1) In the Mobil No. 247 Seeligson well, the combination of state-of-the-art open-hole logs and the use of an interpretation model developed in the Sun No. 141 Canales well identified a low-resistivity, shaly pay zone, which was tested and which produced gas in commercial quantities. This shaly sandstone would have been bypassed if proper allowance was not made for the presence of shale laminae in the reservoir.

(2) In the Mobil No. 248 Seeligson well, a comparison of wireline formation pressures with cased-hole pressure tests revealed the need to confirm wireline-formation-tester pressures before they are used for interpretation. It was found that up to 50 percent of the wireline pressure tests taken in the No. 248 well, assumed to be valid by the wireline operator, were in fact prematurely terminated and did not represent true formation pressures. Close supervision of the operation at the wellsite is needed to obtain more representative wireline-formation-tester pressure tests.

(3) In gas-depletion drive reservoirs like the ones in Seeligson field, estimation of formation pressure in old cased-hole wells will be needed to find the most promising pay zones. In the No. 248 well, the sequential formation pressures were correlated with several cased-hole log measurements; consequently, a correlation was found between pulsed-neutron count rates and pressures in gas-bearing zones.

(4) Additional gas zones were identified as a result of analysis of cased-hole logs acquired in No. 1-85, 1-89, and 1-171 wells. These zones were identified by using a cased-hole interpretation methods previously developed in Seeligson. This method combines the information obtained from a pulsed-neutron and full-wave acoustic log through casing to obtain porosity, water saturation, and lithology.

(5) The core data available in the No. 141 Canales well were used to calibrate the log-derived parameters used for evaluation in Seeligson field. Furthermore, core analysis results were used for a study of effective and total porosity in shale to estimate the impact of shale porosity on additional reserve calculations, which if not accounted for, will cause underestimation of reserves.

(6) The pressure prediction method developed in the No. 248 well predicted that the Zone 15 reservoir in the No. 1-89 well may be partially depleted.

(7) The borehole gravity survey was tested for applications in the Frio Formation and identified a gas-bearing sandstone in the Zone 15 reservoir in the No. 1-89 well. However, the identified gas zones have not yet been tested.

(8) Finally, the full-wave acoustic log was used to obtain porosity in cased-hole wells. It was found from previous experiments that even with only 50-percent cement bonding it is possible to obtain reliable porosities through casing from the compressional travel time. Determination of reliable shear travel time was not possible due to limitations of current tool design. Temperature and cement-quality logs were also run in the cased-hole wells to find zones with potential recompletion problems.

THREE-DIMENSIONAL SEISMIC PROGRAM

Introduction

Three-dimensional seismic imaging of subsurface stratigraphy is a standard, well-structured technology and is a particularly important tool for delineating oil reservoirs. However, the three-dimensional seismic technique is not yet widely used to evaluate onshore gas reservoirs. The first three-dimensional seismic data base used at BEG for gas reservoir characterization was recorded at Seeligson field, Jim Wells County, Texas (fig. 75) in late 1990 as part of the Secondary Gas Recovery Project. Three-dimensional seismic data in an area encompassing approximately 1 mi² (2.59 km²) in the north part of the field (figs. 1 and 2) were acquired to better define dimensions of gas reservoirs and identify the topology of genetic sandbodies at the Seeligson experimental test site.

At Seeligson field, gas is produced from a stacked sequence of fluvial-deltaic Frio sandstones extending from a depth of about 5,750 ft (1,753 m) to approximately 4,750 ft (1,448 m). Oryx operates the wells that produce from this interval, and Mobil has the mineral rights for deeper reserves. Consequently, the Seeligson three-dimensional seismic data acquisition and processing costs were shared equally by Mobil, Oryx, and BEG. Most of the technical decisions related to how to carry out the data acquisition and processing were made by Mobil and Oryx.

Three-Dimensional Seismic Amplitude Maps

By slicing across a three-dimensional seismic data volume along selected depositional surfaces, the areal topography of individual reservoirs can often be revealed in surprising detail. Consequently, this horizon slice technique was used to interpret the Seeligson three-dimensional migrated data. Because BEG had no

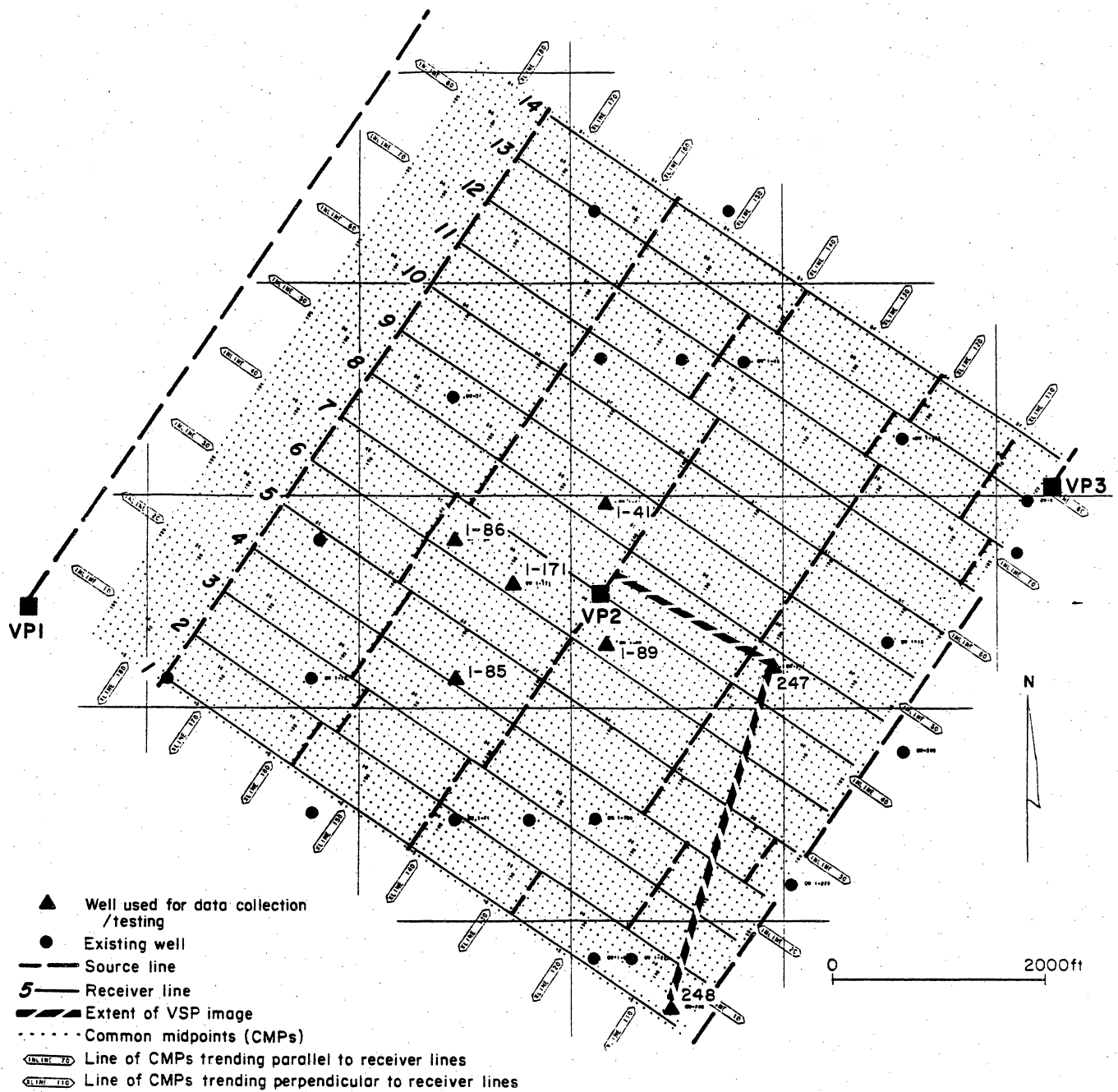


Figure 75. Field geometry used to record a three-dimensional surface seismic grid in part of Seeligson field, Jim Wells County.

interactive geophysical workstation, the horizon interpretation was contracted to Halliburton Geophysical Services, and BEG scientists monitored and adjusted the interpretation using well control throughout the seismic data grid.

A horizon slice generated at the Zone 19C reservoir level is shown in figure 19. In seismic terms, the Zone 19 reservoir is considered a thin bed because the reservoir thickness (typically 10 to 30 ft [3 to 9 m]) is less than one-fourth the dominant seismic wavelength. (The dominant wavelength at the 19C level is approximately 200 ft [60 m].)

In a sandstone-shale sequence, an important principle of seismic thin-bed stratigraphy is that the amplitude of a thin-bed reflection is directly proportional to the amount of net sandstone in the thin-bed interval (Mechel and Nath, 1977). Based on this principle, the darker amplitude responses on the map in figure 19 correspond to thicker amounts of sandstone.

AVO Maps

Rather than simply slicing through a three-dimensional volume of stacked seismic reflection amplitudes as is shown in figure 19, an alternate interpretation technique, which relates seismic reflection behavior to reservoir stratigraphy, is to display how reflection amplitude varies with angle of incidence at a selected reservoir level. This interpretation approach is commonly called AVO (amplitude versus offset).

Oryx used the Seeligson data to generate a three-dimensional image of AVO behavior and then calculated synthetic AVO responses to determine how to interpret the field-measured AVO values. A slice across the Oryx AVO data volume, which follows a horizon interpreted to be at the Zone 19C reservoir, is shown in figure 20.

On the basis of Oryx's synthetic model calculations, the darker (more positive) responses in this display should map the higher gas saturations. The oval distribution of

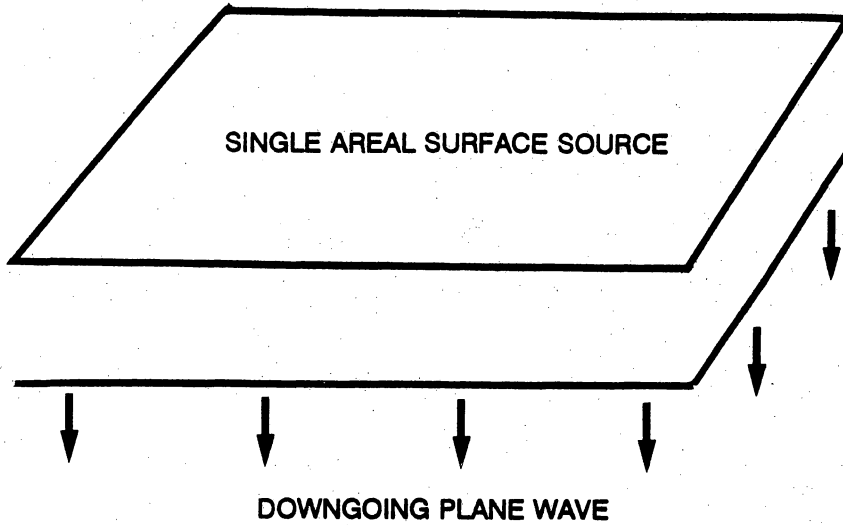
the higher gas saturations is reasonably similar to the oval topology of the net sandstone shown in figure 19.

Fundamental Assumptions and Approximations

The fundamental source and receiver objectives required for three-dimensional imaging are illustrated in figure 76. Basically, the energy source(s) must produce a downgoing illumination wavefield equivalent to the wavefield that would be produced by an areally continuous source overlaying the entire image area, and the receiver(s) used to record the subsurface image must capture the reflected wavefield in exactly the same manner as would an areally continuous antenna overlaying the complete data collection area. Geophysicists are forced to approximate these assumptions of an areally continuous source and an areally continuous receiver antenna using a finite number of discretely positioned point sources and point receivers. In the three-dimensional source approximation, a time-delayed sequence of discretely positioned, spherically spreading wavefields is created across the survey area rather than a single, laterally extensive, downgoing, plane wavefield emanating uniformly and simultaneously from every surface point. The term "time-delayed" refers to the time pause that occurs between the recording of successive vibrator outputs (or explosive shots) from individual shot points across the data grid. Because of this shot-to-shot time pause, adjacent small portions of the areally continuous source (fig. 76) are constructed at time intervals of 5 to 60 min, depending on field conditions such as equipment performance and weather. In the three-dimensional receiver approximation, individually recorded, spherical wavefields from each shotpoint are converted into upward-traveling, laterally extensive plane waves and summed to produce a single upward traveling plane wave encompassing the entire receiver grid.

(a)

SOURCE OBJECTIVE - CREATE A SINGLE, LARGE, AREAL SOURCE COVERING THE ENTIRE SURVEY GRID AND CAUSE THIS SOURCE TO ILLUMINATE THE UNDERLYING SPACE WITH A SINGLE, DOWNGOING, PLANE WAVE.



(b)

RECEIVER OBJECTIVE - CREATE A SINGLE, LARGE, AREAL ANTENNA COVERING THE ENTIRE SURVEY GRID TO RECEIVE THE REFLECTED WAVEFIELD GENERATED BY THE SOURCE DESCRIBED ABOVE.

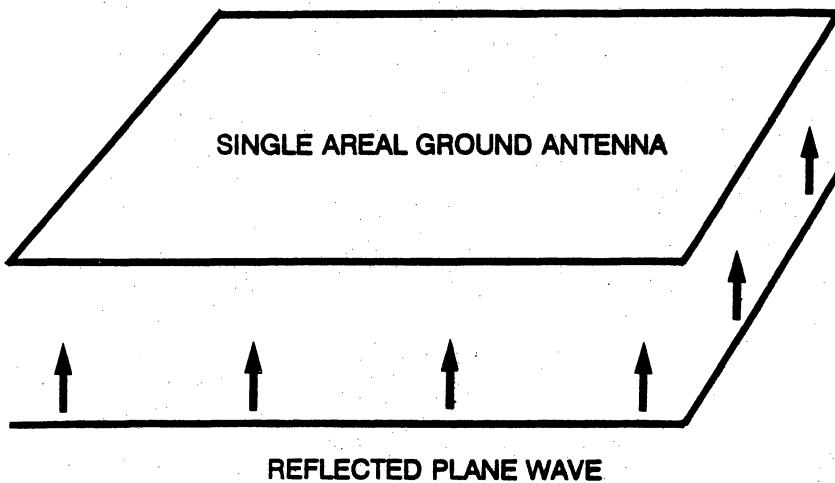


Figure 76. (a) The fundamental source assumption involved in three-dimensional seismic data acquisition and (b) the fundamental receiver assumption.

These approximations can be reasonably accurate implementations of the assumptions illustrated in figure 76 if budget restraints allow a proper number of source points to be occupied and a proper number of receiver sites to be recorded. As expenditures are reduced, compromises must be made, which cause the approximating steps to deviate farther from the assumptions. A reasonable balance between technical validity and budget expenditure (about \$75,000 for acquisition and processing) appears to have been achieved in the Seeligson three-dimensional seismic program. References will be made to these fundamental assumptions as the three-dimensional data collection and analysis are discussed in the following sections of this report.

Field Geometries Used in the Seeligson Three-Dimensional Seismic Survey

The specific source-receiver geometry that was used to record the three-dimensional seismic data volume at Seeligson field will now be described by referring to figure 75. The data recording was performed by Western Geophysical, Party Number V-3, in December 1990. The receiver, source, and common depth point attributes resulting from this field geometry can be described as follows:

Receiver Lines

Fourteen parallel receiver lines (shown as solid lines in fig. 75) were deployed in a northwest-southeast orientation, which is the approximate direction of structural dip. The line-to-line spacing is 495 ft (151 m). Each line was composed of 36 receiver groups, spaced 165 ft (50.3 m) apart, which will be described in the next section. A total of 504 receiver groups (14 lines by 36 groups per line) were thus laid out to create a rectangular antenna measuring 6,435 by 5,775 ft (1,962 by 1,761 m). The reflected wavefields arriving at all 504 receiver groups were simultaneously recorded for every illumination wavefield inserted into the subsurface during the data acquisition program.

At Seeligson, recording data simultaneously at all points in this 504-element rectangular receiver pattern is assumed to adequately represent the assumption of the areally continuous ground antenna depicted in figure 76.

Receiver Arrays

Each of the 504 receiver groups was constructed by planting 12 in-line geophones to form a linear array. Specifically, GS2OD 10-Hertz geophones were used. The element-to-element spacing was 7.5 ft (2.3 m), which produced an array 82.5 ft (25.2 m) long. A gap of 82.5 ft (25.2 m) was left between adjacent receiver groups, so complete ground coverage was not constructed. This array geometry and the resulting surface coverage along each receiver line are diagrammed in figure 77.

Recording System

Western Geophysical used a Geosource MDS-16 system to record these three-dimensional data. This system is built on a modular concept in which eight-channel remote units (RU's) are distributed along the receiver lines. Data from eight geophone groups feed into each RU in traditional analog form via standard twisted-pair cables. The RU digitizes the eight channels of information and sends the data on to a central recorder in digital form via a fiber optics cable. A total of 63 RU's were required to simultaneously record all 504 receiver groups.

Source Arrays

Six source lines (fig. 75) were oriented perpendicular to the receiver lines. The source-line-to-source-line spacing was typically 1,485 ft (453 m), but numerous line

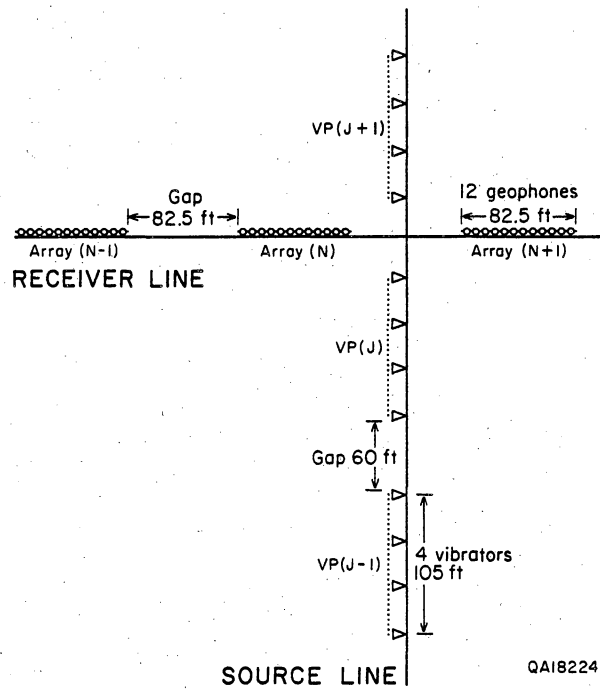


Figure 77. Geometrical parameters used to construct individual source and receiver lines in the Seeligson three-dimensional seismic data grid.

offsets had to be made to avoid well pads and production facilities in this active gas field. These variations in line spacing are accurately depicted in figure 75.

Vibration points were surveyed at intervals of 165 ft (50.3 m) along each source line so the source spacing would be identical to the receiver group interval. A complete seismic line contained 41 vibration points unless proximity to surface production equipment forced a source location to be skipped. Each source line extended 6,600 ft (2,012 m), or 40×165 ft (12.2×50.3 m), providing a rectangular source array measuring 6,600 ft (2,012 m) by approximately 7,425 ft (2,264 m) overlaying the 504-element receiver antenna pattern.

This six-line source pattern is assumed, at Seeligson, to adequately represent the assumption of the areally continuous source shown in figure 76. If there is a technical weakness in the Seeligson three-dimensional seismic program, it can probably be traced to the failure of adequately approximating an areally continuous source. In this instance, the technical benefit of adding more source lines to improve the areal source approximation was judged to be not worth the costs of additional permitting, bulldozing more lanes through the mesquite, and adding extra days of crew time to the acquisition program. A reasonable compromise between cost and data validity has been made.

At each surveyed vibration point, four LRS Model 315 vibrators were stationed in line and centered on the shot flag with their pads separated a distance of 35 ft (10.7 m), to produce a source array 105 ft (32.0 m) long with a gap of 60 ft (18.3 m) between adjacent arrays. This source array geometry and the resulting ground coverage along each source line are illustrated in figure 77. A Model 315 vibrator can produce a peak force of 47,000 pounds (209,066 n) at full drive, but Western Geophysical reduces the peak force to 41,000 pounds (182,377 n). Thus, a total peak force of 164,000 pounds (729,508 n) could be applied at each source location during each sweep. Ground force phase locking was used to keep the vibrators synchronized and to ensure that a consistent basic wavelet could be extracted for each source wavefield. Ground force

phase locking was an important requirement because significant variations in the pad-to-earth coupling existed at the 246 source locations owing to changes in soil type.

This four-element source array executed six 10-85 Hz upsweeps at each vibration point, allowing the equivalent of 24 sweeps from a single Model 315 vibrator to be summed to produce each source wavefield. Each sweep length was 14 s followed by a 6-s listen time.

Modern vibrator electronics allows the sweep drive signal to adjust the amount of energy produced by a vibrator in certain portions of the frequency band. This flexibility can be helpful when the higher frequency components need to be amplified to ensure that high frequency data will be recorded at long travel distances. A nonlinear 6-dB/octave drive signal was selected for the Seeligson survey, which is to say the amount of cumulative energy produced by the vibrator pad motion increases by a factor of 4 each time the sweep frequency doubles. The graphs in figure 78 illustrate how the pad moves when controlled by this type of drive signal and how the pad motion energy is distributed over the frequency band. Unfortunately, Western Geophysical provided plots for a 16-s sweep for this figure rather than for the 14-s sweep actually used at Seeligson, but the graphs still illustrate the principles of a nonlinear vibroseis sweep.

The nonlinear amplification of energy in the higher frequency part of the sweep results from a continuous increase of the length of time required for the pad motion to span a selected frequency interval (curve C) rather than by an alteration of the magnitude of the driving force (curve D). The result is the energy distribution shown by curve B, labeled "percent of sweep energy above frequency." The numbered points 1, 2, and 3 on this function show that only 4.25 percent of the total energy is produced in the first octave (10–20 Hz); an additional 17 percent of the output energy is created during the second octave (20–40 Hz); and the bulk (68 percent) of the energy associated with the pad motion occurs during the third octave (40–80 Hz).

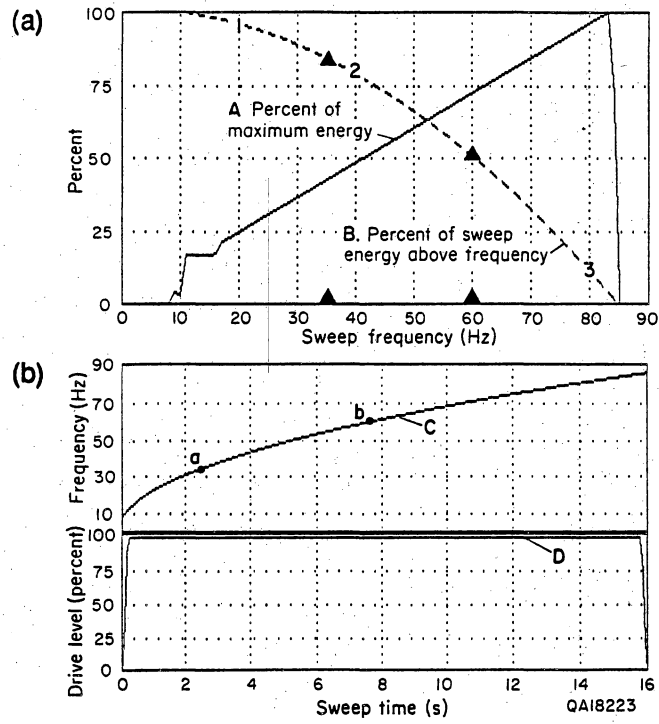


Figure 78. (a) Distribution of vibrator sweep energy as a function of frequency and (b) the nonlinear time functions controlling the pad frequency and the hydraulic drive level that produces the frequency-dependent energy distribution in (a).

An additional visualization of the manner in which the energy content of the vibrator wavelet is weighted toward the higher frequency components results when the 75-Hz bandwidth (10–85 Hz) at Seeligson is divided into three equal portions as shown by the solid triangles in figure 78a. Curve B shows that only 15 percent of the total energy is produced in the lowest third of the spectrum. This relatively small amount of energy generation results because the vibrator pad is forced to make a smooth transition from a 10-Hz oscillation to a 35-Hz oscillation in less than 3 s, as shown by arrow point labelled "a" in the frequency-versus-time curve, C. In contrast, 50 percent of the energy is produced in the upper third of the spectrum because the length of time used to drive the pad over the 25-Hz interval from 60 Hz to 85 Hz is increased to more than 8 s (that is, the time interval from arrow point b to the end of sweep at 16 s).

The energy distribution described here represents only what the drive signal causes the vibrator pad motion to be. The actual energy distribution within the propagating vibroseis wavelet varies from this description because some energy is lost and some phase shifting of certain frequency components occurs because of inefficient and variable pad-to-earth couplings across the survey area.

Analysis of the Three-Dimensional Receiver and Source Array Responses

Two tacit assumptions in three-dimensional seismic data acquisition and processing are: (1) All sensor groups throughout the surface receiver grid have identical antenna patterns, and (2) identical radiation patterns are generated at all source positions.

The validity and implications of these assumptions will be analyzed before discussing the three-dimensional seismic data processing at Seeligson field is discussed.

For the receiver antenna analysis, seismic wavefields will be allowed to arrive at a typical 12-element Seeligson surface sensor array from a variety of directions in three-dimensional space, and the resulting array responses will be compared. For the source

radiation analysis, the shape of the radiation pattern emitted by the four-element Seeligson source array in a large number of three-dimensional vector directions will be calculated and compared.

The three-dimensional coordinate system used in these calculations is illustrated in figure 79. In the receiver analysis, the 12-element inline sensor group diagrammed in figure 77 is assumed to be centered about the origin of this coordinate system and aligned along the X axis. The angles ϕ and θ shown in this figure are used to define the direction in three-dimensional space along which the wavefield is traveling, upon arriving at the receiver array. When calculating three-dimensional source radiation patterns, the four-element source array diagrammed in figure 77 is also centered at the origin and aligned along the X axis. The energy radiated in the three-dimensional direction defined by angles ϕ and θ is then calculated for a large range of angles.

Examples of the three-dimensional characteristics of Seeligson receiver array antenna patterns and three-dimensional pictures of Seeligson source array radiation patterns are provided in figures 80, 81, 82, and 83.

Source Radiation Patterns

The shape of the radiation pattern produced by the four-vibrator source array is described by the polar coordinate plots in figure 80. Each plot shows how the radiated energy is spatially distributed in a single, vertical plane for a particular frequency component. Analyses are presented for the low end of the source spectrum (10 Hz), for the middle of the source spectrum (40 Hz), and for the upper end of the spectrum (70 Hz).

The flat top of each polar plot in this series of figures represents the earth's surface, and the shaded area describes the shape of the radiation pattern traveling into the earth. The coordinate where the shaded area intersects the flat top of each

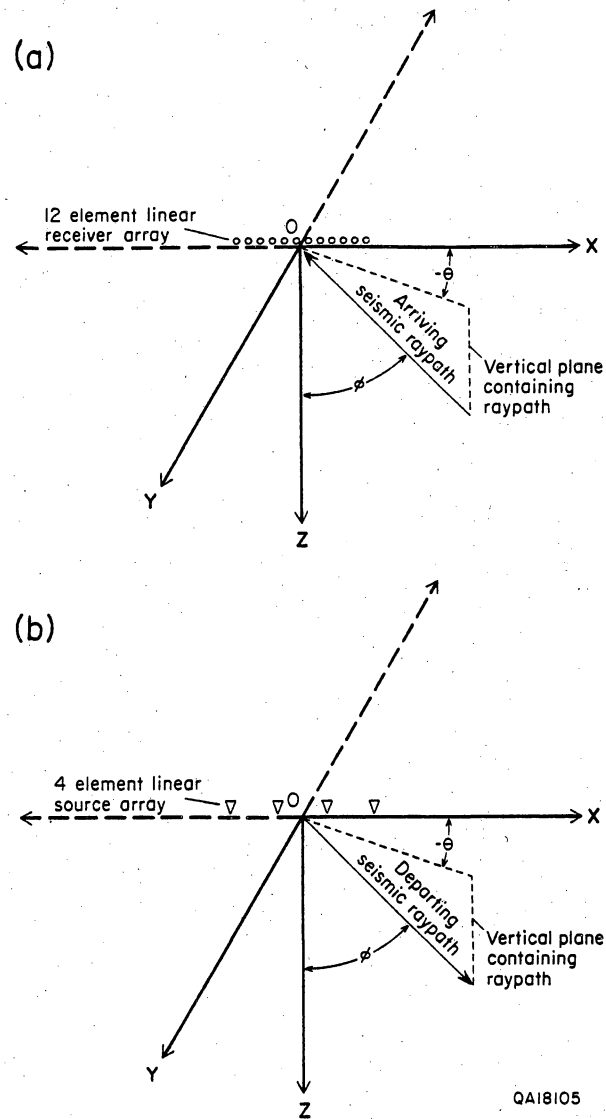


Figure 79. Mathematical models used to investigate the three-dimensional directional properties of the Seeligson receiver and source arrays. The earth's surface is the XY plane, and the positive z axis extends into the earth. In (a), a 12-element Seeligson receiver array is centered at the coordinate origin O and distributed along the X axis. The receiver array response is then calculated when a wavefield approaches the array in a direction specified by angles ϕ and θ . In (b), the Seeligson source array is centered at O and the radiation pattern is calculated for arbitrary directions specified by ϕ and θ .

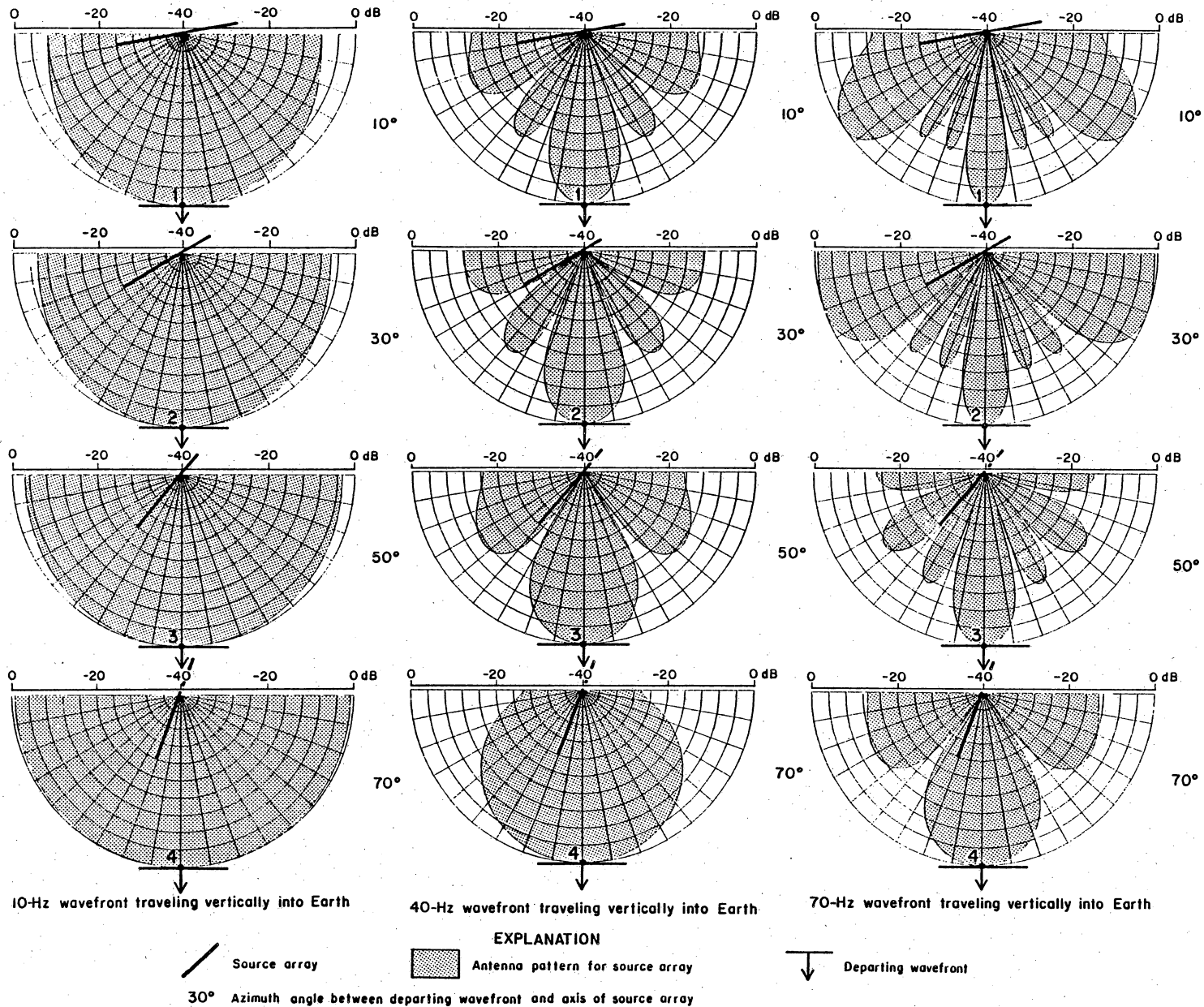
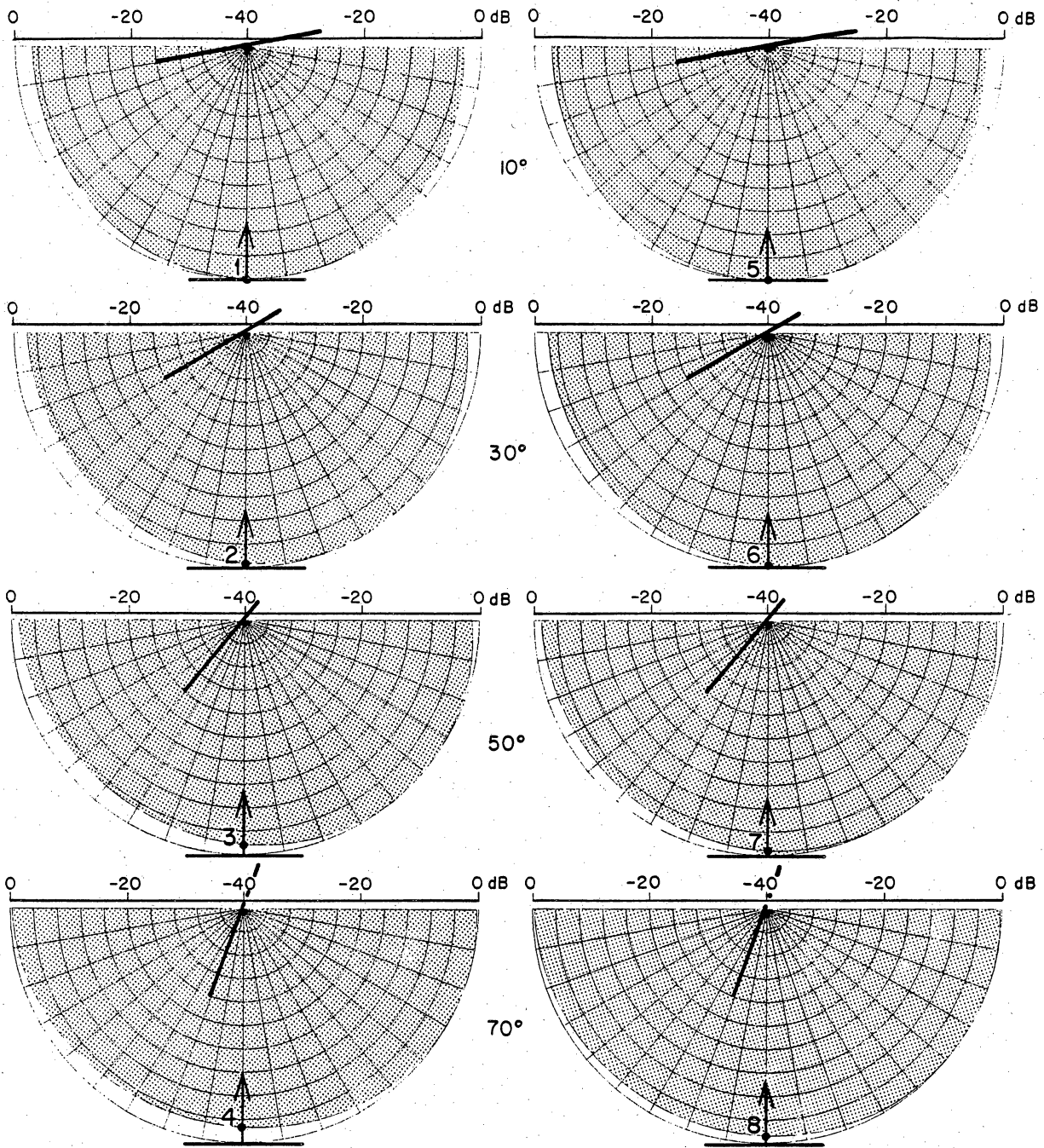



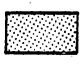

Figure 80. The shaded areas describe the shape of the radiation pattern produced by the 4-vibrator source array used for the Seeligson three-dimensional seismic program. Vertical slices are taken through the radiation pattern at azimuth angles $\phi = 10^\circ, 30^\circ, 50^\circ,$ and 70° (see fig. 79 for a definition of ϕ) in order to give a sense of the three-dimensional nature of the radiation geometry.



10-Hz wavefront traveling horizontally on Earth's surface

10-Hz wavefront traveling upward at 45° to Earth's surface

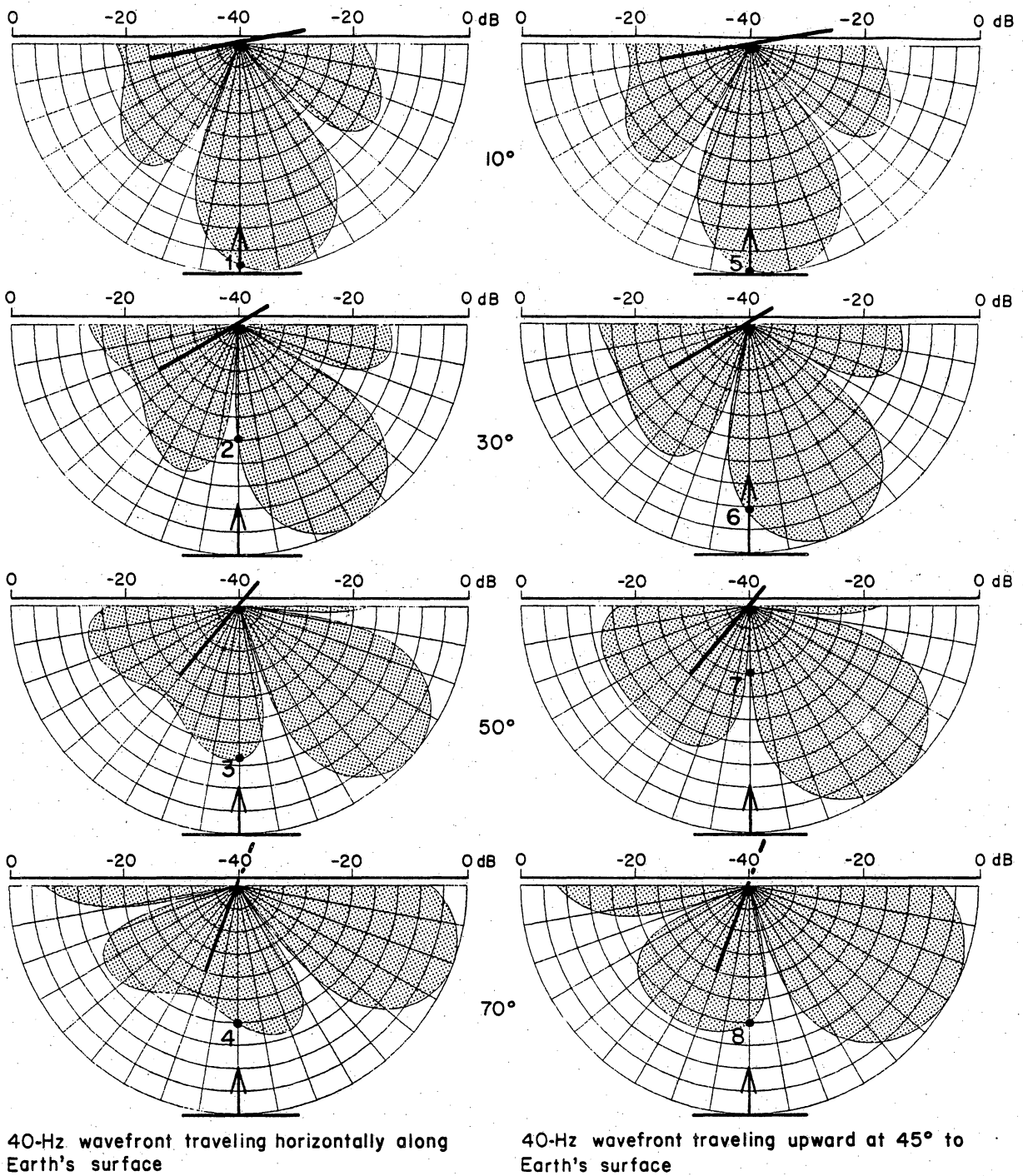
EXPLANATION

 Receiver array
  Antenna pattern for receiver array
  Approaching wavefront

30° Azimuth angle between approaching wavefront and axis of receiver array

QA18089a

Figure 81. The shape of the 10-Hz antenna pattern provided by the 12-element receiver arrays.

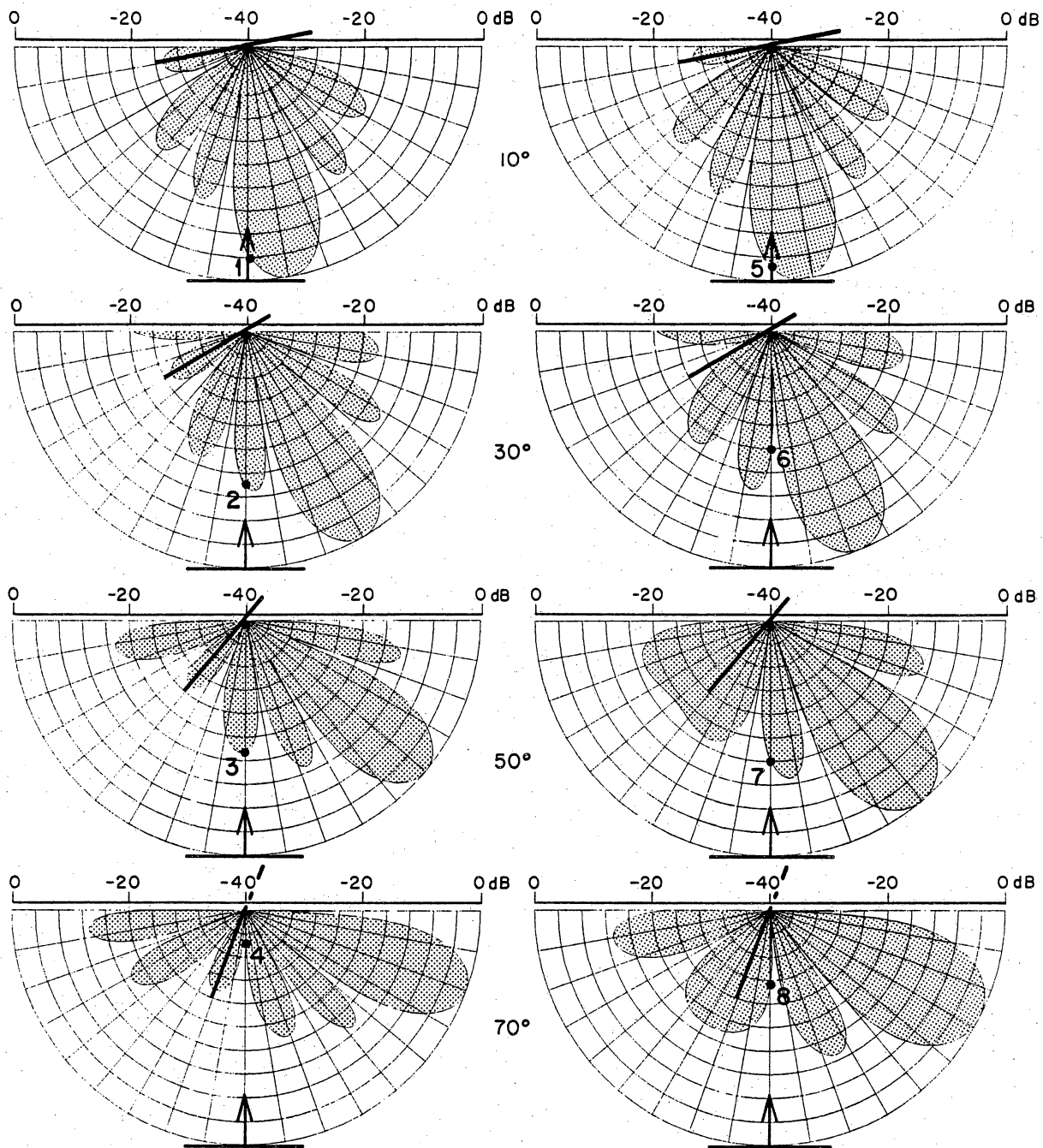


EXPLANATION

- Receiver array
 - Antenna pattern for receiver array
 - Approaching wavefront
- 30° Azimuth angle between approaching wavefront and axis of receiver array

QA18089b

Figure 82. The shape of the 40-Hz antenna pattern provided by the 12-element receiver array.



70-Hz wavefront traveling horizontally along Earth's surface

70-Hz wavefront traveling upward at 45° to Earth's surface

EXPLANATION

- Receiver array
 - Antenna pattern for receiver array
 - Approaching wavefront
- 30° Azimuth angle between approaching wavefront and axis of receiver array

QA18089c

Figure 83. The shape of the 70-Hz antenna pattern provided by the 12-element receiver arrays.

semicircle defines the amplitude of the wavefront traveling horizontally away from the source. The position of the boundary of the shaded area on each radial line defines the amplitude (in decibels) of the wavefront propagating into the earth at an angle, θ , equal to the inclination of the radial line, where θ is shown in figure 79. The wavefront traveling downward at an inclination angle $\theta = 90^\circ$ (again refer to fig. 79 for a definition of θ) is indicated by the symbol labeled "departing wavefront" in each polar plot.

The source array is centered at the origin of the radial lines, and the short, heavy line drawn through the origin shows the orientation of the source array relative to the vertical plane containing the polar plot. This azimuth angle between the axis of the source array and the vertical analysis plane is the angle θ shown in figure 79. Four azimuth directions are analyzed and specified as 10° , 30° , 50° , or 70° in the center of each figure.

The principal point illustrated by these polar plots is that no frequency component of the seismic wavefield propagating away from the four-vibrator array can be represented by a simple spherical wavefront—a common assumption. Instead, each frequency component has a radiation shape, which is not uniform in all directions, and which is comprised of a sequence of lobes and nulls positioned at specific orientations. This source radiation pattern differs significantly from the fundamental three-dimensional source assumption shown in figure 76.

Receiver Antenna Patterns

A similar sequence of polar plots is used in figures 81, 82, and 83 to describe the three-dimensional character of the antenna pattern associated with the 12-element receiver arrays used to record the Seeligson data. The notation in the figures and the interpretations of the polar plots are explained in the preceding section's discussion of the source radiation patterns.

Inspection of the receiver plots leads to the conclusion that the receiver array does not create an antenna having a uniform response in all directions. Instead, the antenna exhibits high gain (lobes) and low gain (nulls) in specific directions and does not behave like the three-dimensional antenna model assumed in figure 76.

Common Midpoint Coverage

The common midpoint (CMP) reflection coverage produced by the Seeligson source-receiver geometry is shown by the grid of small black dots in figure 75. Each dot is positioned at the center of a stacking bin encompassing an area 82.5×82.5 ft (25.2×25.2 m) in the subsurface. Once the data are processed, the total image volume spanned by these CMP's can be described in terms of 80 southeast-northwest reflection profiles and 82 southwest-northeast profiles. The lateral spacing between these profiles is 82.5 ft (25.2 m), so the imaged volume is a vertical block having a rectangular cross-sectional area of 6,600 ft (2,012 m) (SE-NW) by 6,765 ft (2,063 m) (SW-NE) and extending straight down below this midpoint grid. A horizontal slice through this data volume will always contain 6,560 (that is, 82×80) data bins.

Stacking Fold

The number of seismic traces falling within each of the 82.5×82.5 ft (25.2×25.2 m) stacking bins varies both laterally and vertically throughout the Seeligson data volume. The maximum number of source-receiver pairs that cause a reflection point to fall inside a specified midpoint bin is indicated in figure 84. This map is a tracing of only a few contours from a detailed color display of stacking fold, which showed the maximum stacking fold can vary from a value of 1 trace per bin at the edges of the image to a high of almost 60 traces per bin in a few cells near the center of the grid. A black-and-white copy of this color map is displayed in figure 85.

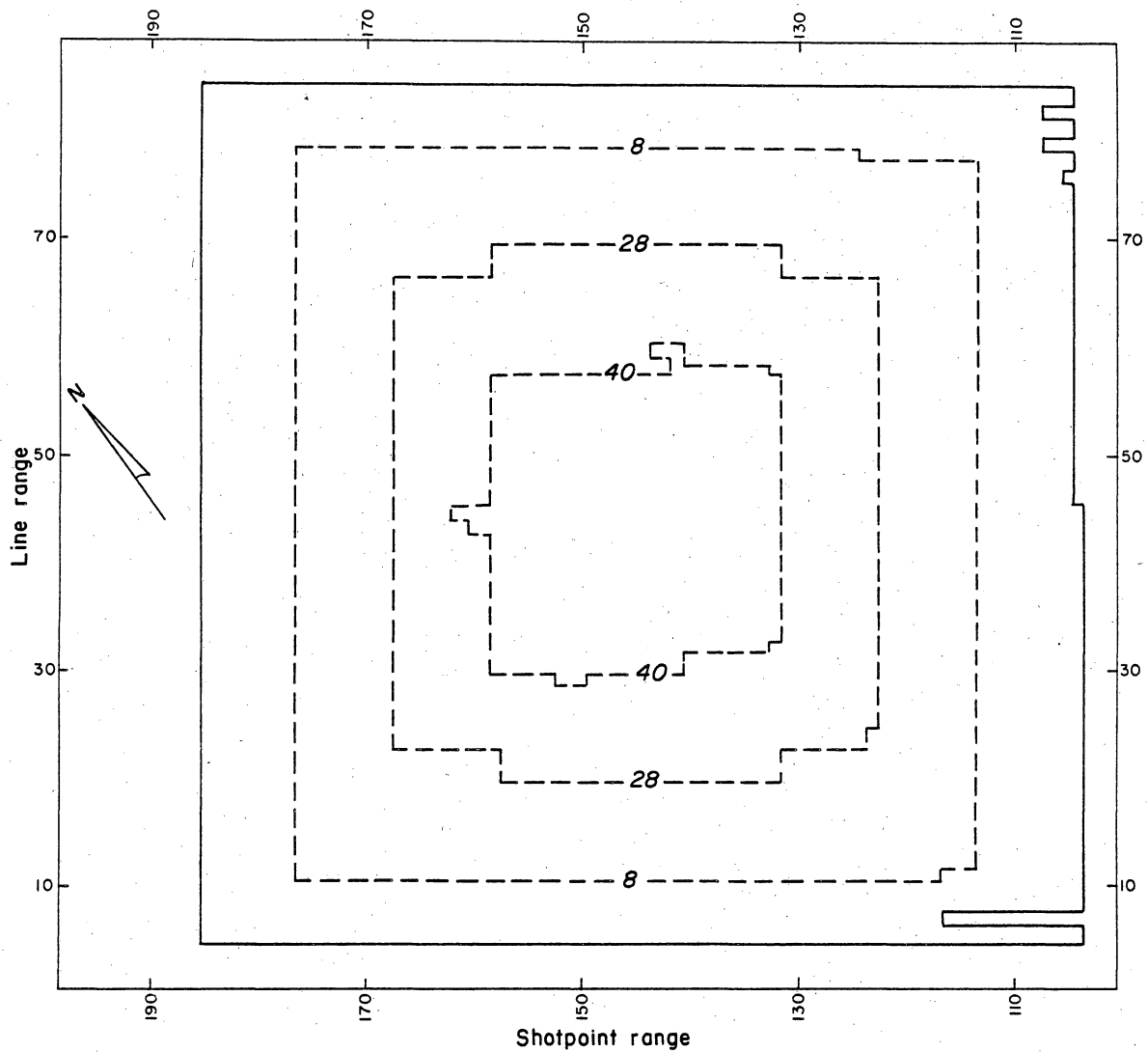


Figure 84. Simplified picture of the maximum stacking fold achieved in the Seeligson three-dimensional seismic survey. The original stacking fold map was a detailed color display showing that the stacking fold varied from 1 trace/bin at the edges of the image to almost 60 traces/bin in a few cells at the center of the grid. Black-and-white copy of this color map shown in figure 85.

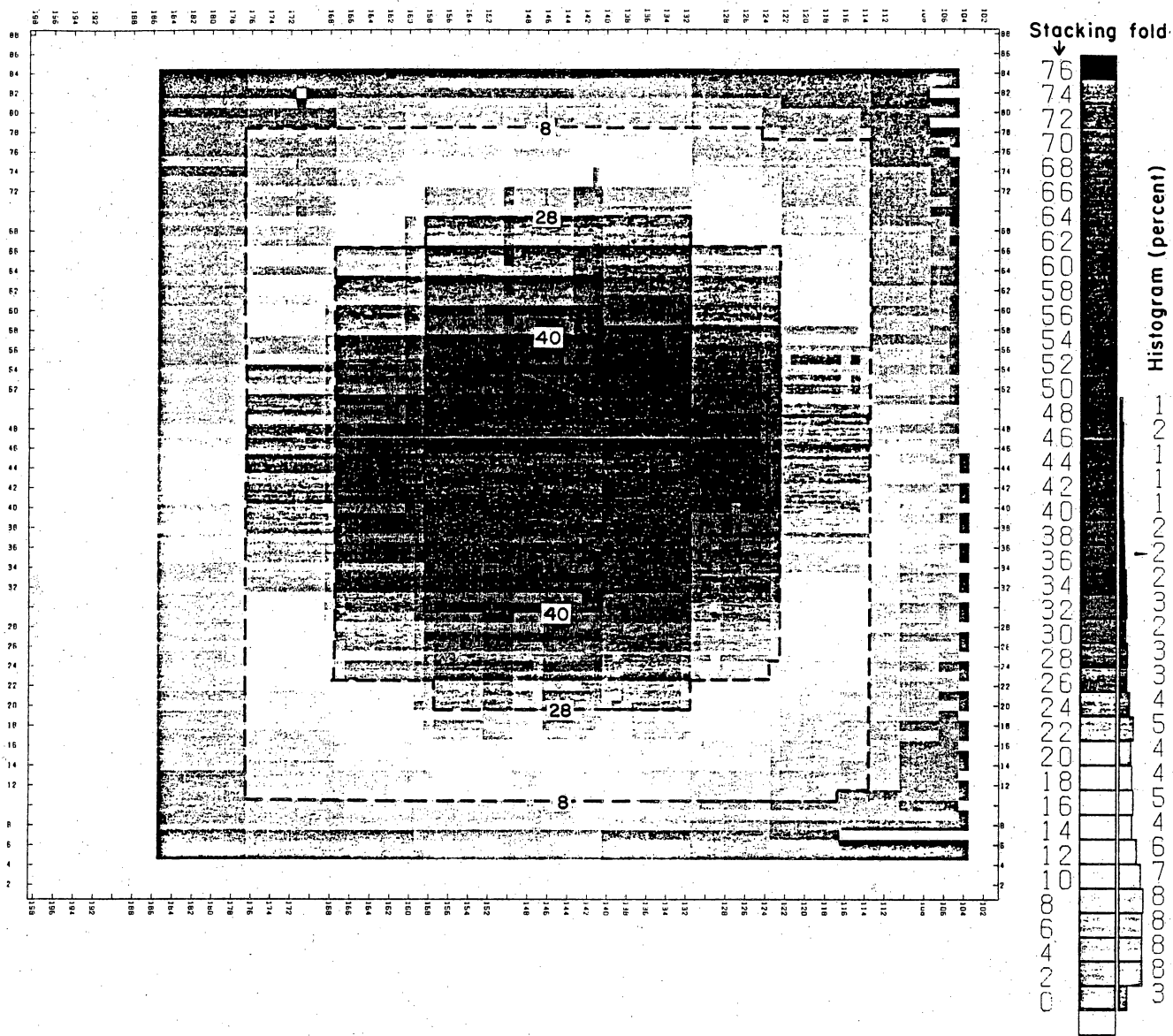


Figure 85. Black-and-white copy of the original color display of stacking fold within the Seeligson grid. The contours in figure 84 are reproduced here.

The stacking fold behavior depicted in these charts is the maximum possible fold, which is a condition valid only at late reflection times in which traces with the largest source-receiver offsets can be included in the stacking summation. As reflectors approach the earth's surface, only traces at shorter offsets satisfy the assumptions for midpoint stacking, and the stacking fold is necessarily reduced from what is implied in figure 84.

The geometry used in the Seeligson data acquisition program causes the stacking fold to exhibit abrupt changes in magnitude, which parallel the source and receiver lines. This behavior is exhibited by the series of bands crisscrossing the stacking fold map in figure 85. The bands parallel to the source lines (the vertical bands in this map orientation) are more obvious because the source lines are more widely separated than the receiver lines and because the stacking fold discontinuity is greatest in a direction perpendicular to the source lines.

Even when conditions for maximum stacking fold exist at late reflection times, the stacking fold in much of the data volume is not large. The histogram at the right side of figure 85 defines the percent of total data bins that can have certain magnitudes of stacking fold and shows that 35 percent of the bins have a stacking fold of 8 or less. This amount of stacking fold is low for present-day seismic acquisition standards. Only the central 17 percent of the image space can have a stacking fold of 30 or more, which represents a more preferred stacking objective. (The histogram percentages do not sum to 100 percent, owing to round off. For example, no stacking bins are shown to have a stacking fold greater than 48, although several such bins exist).

Data Processing

Western Geophysical was contracted to process the three-dimensional seismic data. The objective of the processing is to convert these wavefields, which are generated and

recorded at discrete spatial points, into the areally continuous downgoing and upgoing plane waves shown in the three-dimensional illumination assumption summarized in figure 76. The processing steps followed by Western Geophysical to accomplish this transformation are listed in table 8 which is directly copied from a Western-processed seismic display.

Examples of unprocessed field data recorded at all 504 receiver stations are shown in figures 86, 87, and 88. These wavefields were produced when the vibrators were positioned at the west corner, the east corner, and the center, respectively, of the SE-NW receiver grid. The source location is specified as VP1, VP2, or VP3 in each wavefield display, and these vibration points are shown in figure 75.

The 36-trace groups labeled 1 through 14 in figures 86, 87, and 88 represent the data recorded by the fourteen receiver lines used to construct the Seeligson areal receiver antenna. Each receiver line comprised 36 receiver arrays; hence, the 36-trace grouping. The receiver line notation starts with 1 at the south edge of the grid and increments to 14 at the north edge (fig. 75).

These areal wavefields have a reasonably wide frequency band and are relatively noise free. The most obvious noise is the air wave produced by the diesel engines of the vibrators, which travels downwind from each vibrator position at a velocity of 1,100 ft/s (335 m/s), the speed of sound in air. Since the receiver lines are separated by 495 ft (151 m), this propagation velocity means the air wave is delayed 450 ms between adjacent receiver lines as documented in figures 86 and 87.

Surface-Consistent Processes

The adjective "surface consistent" is often used by geophysicists to describe certain data procedures applied to seismic data. This terminology appears in step 7 of table 8 and is implicit in steps 4, 9, and 11. At Seeligson field, the concept of seismic surface

Table 8. Data processing sequence used to produce three-dimensional imagery at Seeligson field.

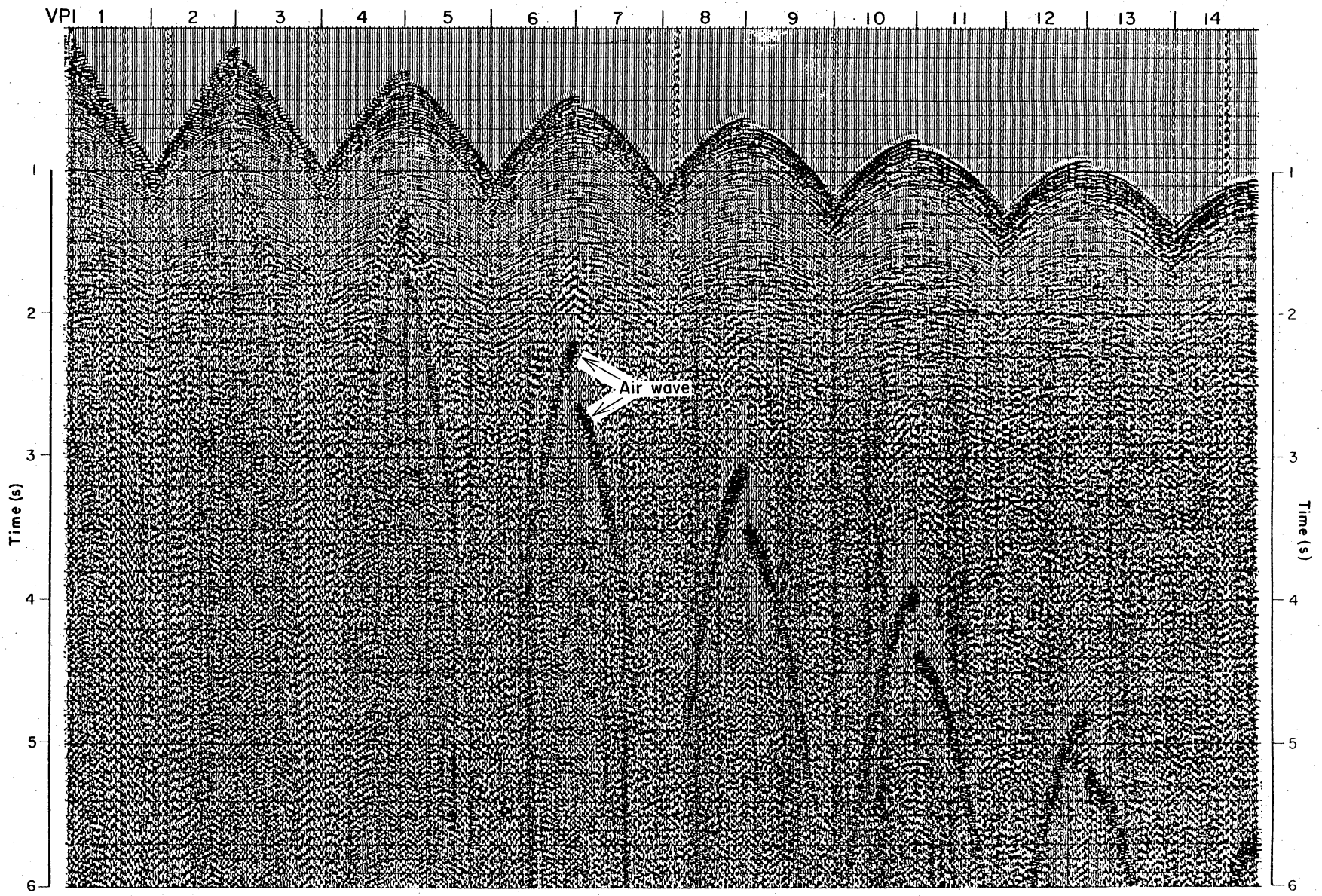
Processing sampling interval: 2 ms

1. Convert SEG-D to WGC code 4
2. Compute subsurface geometry and statics
3. Sort to CDP order
4. Zone anomaly processor (Z.A.P.)
5. Geometric spreading compensation
6. Apply min. phase shaping operator
7. Surface consistent deconvolution
 - Three windows
 - Operator length: 140 ms
 - Prediction distance: 2 ms
8. Trace balance
9. Zone anomaly processor (Z.A.P.)
10. Velan® (Velocity analysis)
11. Miser® (Auto statics)
12. Time variant spectral whitening
13. Apply model-based wavelet compensation
14. Common offset DMO on selected profiles
15. Velan® (Velocity analysis)
16. Dip moveout correction
17. Final stack
18. Inline migration—cascaded finite difference

Time (s)	Velocity (ft/s)	Time (s)	Velocity (ft/s)	Time (s)	Velocity (ft/s)
0.00	4,659	0.30	6,364	0.60	6,698
0.90	7,549	1.20	7,789	1.50	8,202
1.80	8,787	2.10	9,000	2.70	9,200
4.10	9,600	6.00	10,000		
19. Crossline sort
20. Crossline migration—cascaded finite difference

Time (s)	Velocity (ft/s)	Time (s)	Velocity (ft/s)	Time (s)	Velocity (ft/s)
0.00	4,659	0.30	6,364	0.60	6,698
0.90	7,549	1.20	7,789	1.50	8,202
1.80	8,787	2.10	9,000	2.70	9,200
4.10	9,600	6.00	10,000		
21. Time variant filter

Time	Hz/dB	-	Hz/dB
0	14/24	-	75/48
1,000	12/24	-	65/48
1,700	8/24	-	60/48
3,000	8/24	-	50/48
6,000	8/24	-	40/48
22. RMS gain
 - Window: 56 – 1,024 ms

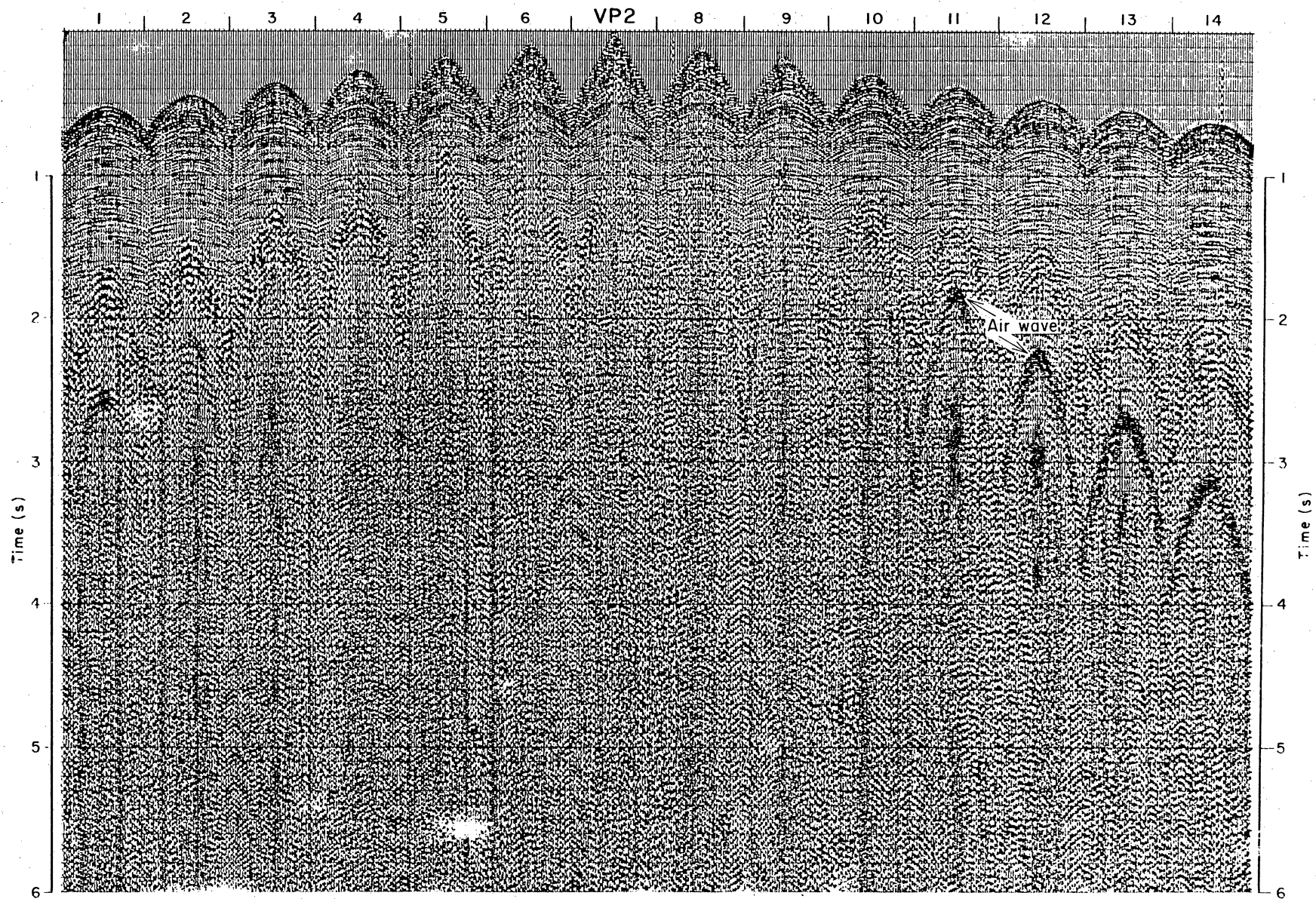


EXPLANATION

| 9 | Receiver line

QA17976a

Figure 86. Wavefield recorded by all 504 Seeligson receiver arrays when the vibrators were positioned at the westernmost source point of the data grid.

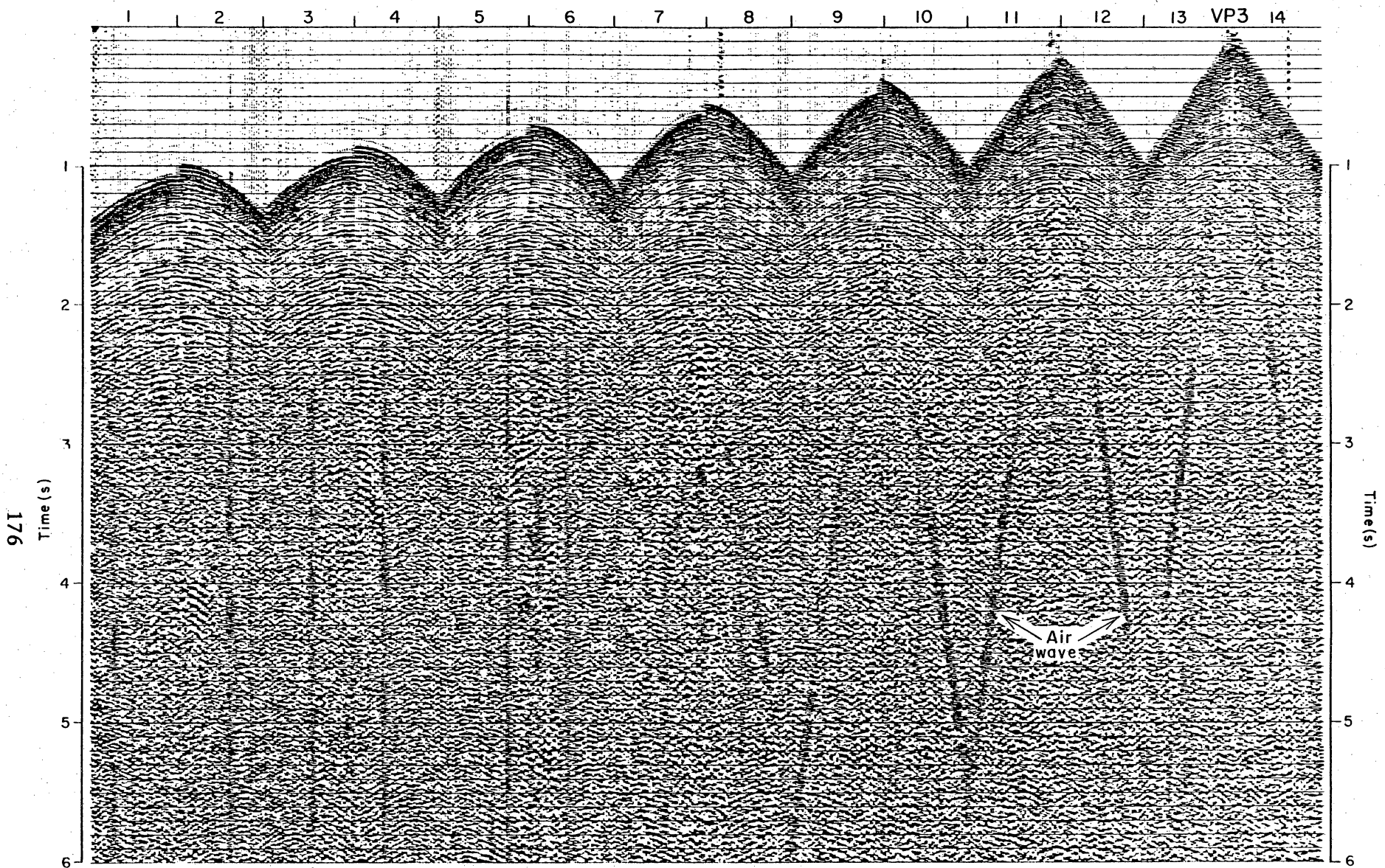


EXPLANATION

1 9 1 Receiver line

04172764

Figure 87. Wavefield recorded by all 504 Seeligson receiver arrays when the vibrators were positioned at the center source point of the data grid.



EXPLANATION

| 9 | Receiver line

QA17976c

Figure 88. Wavefield recorded by all 504 Seeligson receiver arrays when the vibrators were positioned at the easternmost source point of the data grid.

consistency means the statistically averaged phase and amplitude properties of all the wavefields recorded at each receiver group location, all the wavefields generated at each source position, and all the wavefields observed at each source-receiver offset distance are numerically adjusted not to deviate too far from a set of chosen standard values. As a result, the seismic source wavefield is, in an average statistical sense, consistent across the entire survey area as required by the uniform areal source assumption in figure 76. Similarly, the 504 distinct receivers tend to behave like a continuous, uniformly consistent antenna overlaying the entire data grid, as also emphasized in figure 76. In the Western processing, surface consistent corrections were performed for the following numerical properties of the field data, listed in table 8: (1) wavefield amplitude (steps 4 and 9), (2) wavefield phase shifts and time delays (step 11), (3) wavelet shape and spectrum (step 7), and (4) intrabed multiples (step 7).

By applying these surface-consistent operations to the data, any wavefield characteristics introduced into the data set as a result of anomalous surface conditions at a particular receiver site are minimized, as are anomalous behaviors produced at a given source location or observed for one particular source-receiver offset distance. The result of these surface-consistent processes is that the phase and amplitude variations remaining in the Seeligson data can be more confidently associated with geological conditions occurring along the subsurface travel path.

Dip Moveout

The dip moveout (DMO) correction done in processing step 16 of table 8 is a powerful technique for creating correct images in seismic data windows, where there are conflicting structural dips. The technique will not be described here, and interested readers are referred to Yilmaz (1987). A situation of conflicting seismic dips commonly

occurs in the immediate vicinity of rotated fault blocks and significant growth faults, and DMO is now often used to improve image quality when the section of interest is faulted.

The DMO technique was used in the Western processing sequence because Mobil wanted to achieve optimum fault resolution in the deeper section below the Frio (where Mobil has the mineral rights). In the shallower Frio interval where the objectives of the Secondary Gas Recovery project are focused, DMO processing is unnecessary because no conflicting seismic dips occur. Since DMO has sometimes enhanced rather than attenuated intrabed multiples, Oryx processed the Seeligson three-dimensional seismic data independently and omitted the DMO step because their interests are also focused on the Frio interval. Examining the imagery produced by Oryx and Western Geophysical led to the conclusion that the DMO corrections carried out by Western Geophysical did not seriously degrade image quality in the Frio interval.

GAS RESERVOIR HETEROGENEITY AND RESERVE GROWTH POTENTIAL

Stratigraphic Architecture

Varying architectural styles in middle Frio fluvial reservoirs in South Texas resulted partly from relative rates of coastal plain aggradation (Kerr and Jirik, 1990). Relatively slow aggradation resulted in laterally stacked (connected) channel systems, whereas rapid aggradation resulted in vertically stacked (isolated) channel systems (fig. 89). Connected sandstones form wide, sand-rich channel systems and predominate in the 2,000-ft (600-m) thick unitized middle Frio section at Seeligson field (fig. 10). These relatively continuous sandstones are internally complex, commonly contain abundant channel-on-channel contacts, and are typically rich in mud rip-up clasts. Contrasts in permeability as great as four orders of magnitude exist between these mud-clast zones and adjacent sandy channel-fill deposits. In contrast, isolated sandstones form discrete channel systems. This architectural style is characterized by narrow belts of channel-fill

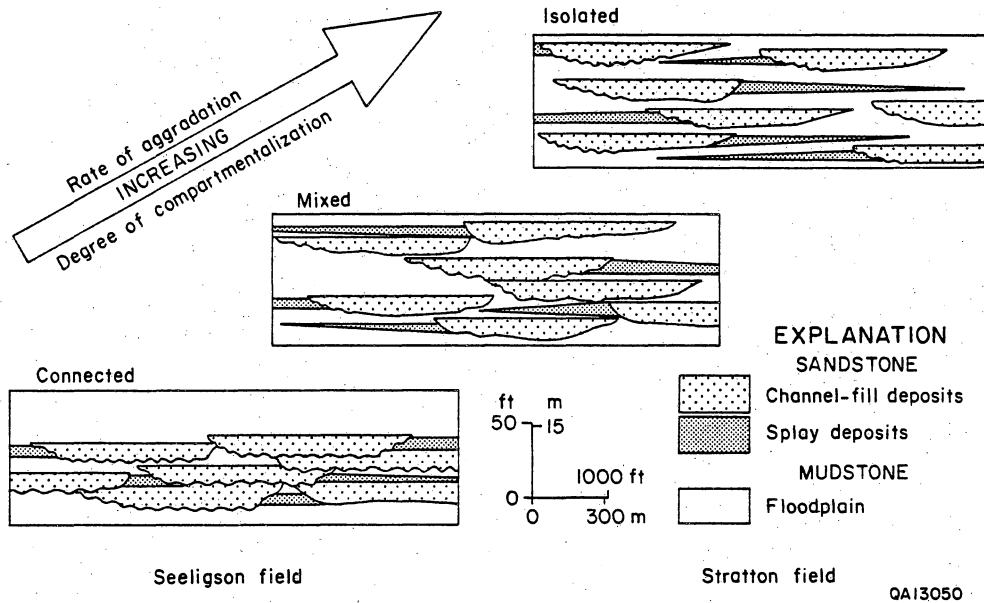


Figure 89. Fluvial architectural styles in the middle Frio Formation in the FR-4 play. Modified from Kerr and Jirik (1990).

deposits flanked by splays that are encased in extensive floodplain mudstones. Architectural style has important implications for reservoir compartmentalization. Connected sandstones may contain incompletely drained reservoir compartments because internal permeability contrasts act as partial, leaky barriers. However, isolated sandstones may contain compartments that are virtually untapped by conventional well spacing.

Correlations of middle Frio strata between Seeligson, Stratton, and Agua Dulce fields in the Frio FR-4 play (fig. 4) indicate that the spatial distribution of channel-fill and splay sandstones forms a continuum (fig. 89). One end of the continuum is the connected architectural style where sandstone bodies of the channel-fill and splay facies laterally and/or vertically contact one another or are vertically separated by only a few feet of the floodplain mudstone facies. At the other end of the continuum is the isolated architectural style, in which sandstone bodies are poorly connected and are vertically separated by at least 10 ft (3 m) of floodplain mudstone.

Individual channel-fill sandstones in the connected architecture are poorly preserved because they were commonly eroded by laterally accreting channels on a weakly subsiding coastal plain. These erosional processes limited the original depositional lateral continuity of floodplain mudstone that otherwise encases channel-fill sandstones. As a result, the sand-to-mud ratio is high in connected architecture (fig. 89).

In contrast, isolated fluvial architecture resulted from relatively greater rates of subsidence that preserved complete channel-fill and splay deposits encased in floodplain mudstones. The resulting spatial configuration is one with a low sand-to-mud ratio (fig. 89).

Seeligson field contains both types of fluvial architecture. In the 2,000-ft (610-m) thick middle Frio interval, the architectural style alternates 10 times from connected to isolated (Kerr and Jirik, 1990). The connected sandstones are continuous across the field

for 15 mi (24 km) along depositional strike (northeastward). A typical well may contact two to three discrete genetic intervals in each of the 50- to 100-ft (15- to 30-m) thick connected sandstones, whereas the probability of contacting the isolated sandstones is lower.

Stratton and Agua Dulce fields also contain both types of fluvial architecture that alternate 13 times in the 2,500-ft (762-m) thick middle Frio section. However, these fields contain a higher proportion of the isolated architecture than does Seeligson field. In contrast to Seeligson field, connected sandstones are not continuous across the 20 mi (32 km) extent of Stratton and Agua Dulce fields. Instead, these sandstones grade locally into isolated sandstones near normal faults where connected sandstones in the footwall block become isolated sandstones in the hanging wall block.

Fluvial architecture patterns in the middle Frio Formation in Seeligson and Stratton–Agua Dulce fields were compared for variation in stacking patterns of the fluvial facies. The comparison was performed by analyzing cross sections oriented in a similar direction relative to structural position and depositional trends. Results indicate that the variation in facies architecture between these two fields in the Frio Formation is significant (fig. 90). Approximately 50 percent of Seeligson field contains the laterally connected fluvial architecture compared with 33 percent at Stratton–Agua Dulce field. In addition, Seeligson field has only 12 percent of the vertically isolated fluvial architecture compared with Stratton and Agua Dulce fields, which contain 43 percent. This contrast in fluvial architecture between these fields strongly suggests that development plans should be modified to account for different degrees of reservoir connectedness. Fields that contain isolated reservoirs require closer completion spacing to maximize recovery.

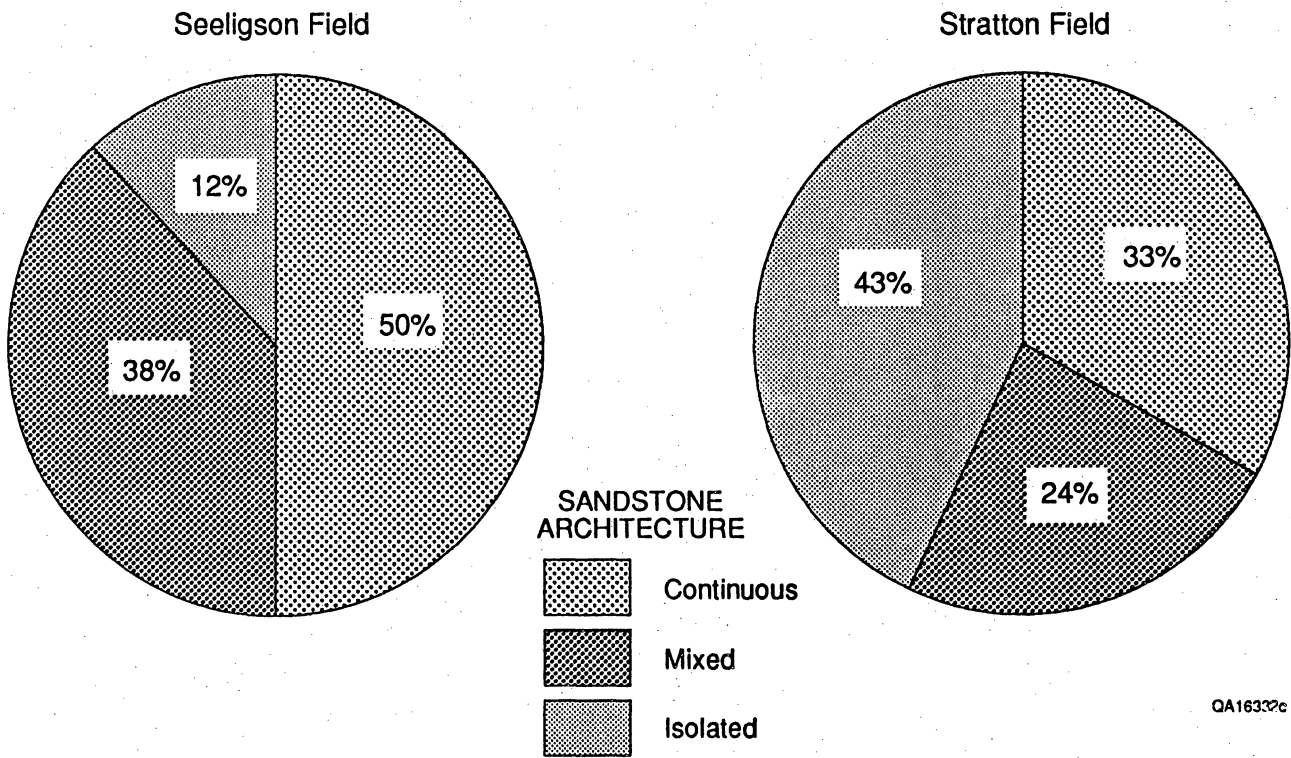


Figure 90. Comparison of fluvial architectural style between Seeligson and Stratton fields.

Scales of Heterogeneity

Four main levels of heterogeneity, ranging from microscopic to megascopic, control reservoir geometry and affect hydrocarbon recovery (fig. 91 [Tyler, 1988]). Microscopic heterogeneity, governed by diagenetic processes, occurs at the pore-throat scale and partly controls hydrocarbon saturation. Mesoscopic heterogeneity is related to variations in bedforms within facies, whereas macroscopic heterogeneity occurs at the level of facies or genetic sandbodies such as point-bar and crevasse-splay deposits. This is the critical scale of interwell heterogeneity that controls secondary recovery opportunities and is, in turn, a function of the specific depositional system of each reservoir. Megascopic heterogeneity is at the largest possible scale and encompasses large-scale relations between reservoirs (for example, connected versus isolated fluvial architecture [fig. 89]).

Similar scales of heterogeneity in fluvial sandstones exist in a six-fold hierarchy based on bounding surfaces (fig. 92 and table 9 [Miall, 1988]). Although most of these surfaces can be recognized in cores, they are difficult to correlate between wells because of their limited lateral extent (<25 ac; <0.039 mi² [<0.101 km²]). However, fifth-order surfaces, which correspond to the macroscopic level of heterogeneity of Tyler (1988), define major channel bodies that can be inferred from net-sandstone, log-facies, and three-dimensional seismic maps (for example, fig. 19). At Seeligson field, ribbon channel sandstones, which define fifth-order bounding surfaces, are isolated sandstone bodies that form reservoir compartments (for example, channel-complex number 2 in fig. 43). Sixth-order surfaces define large-scale units comparable to connected or isolated fluvial architectural systems.

At Seeligson field, microscopic heterogeneity is primarily controlled by authigenic calcite and kaolinite cements. The precipitation of calcite cement in intergranular pore

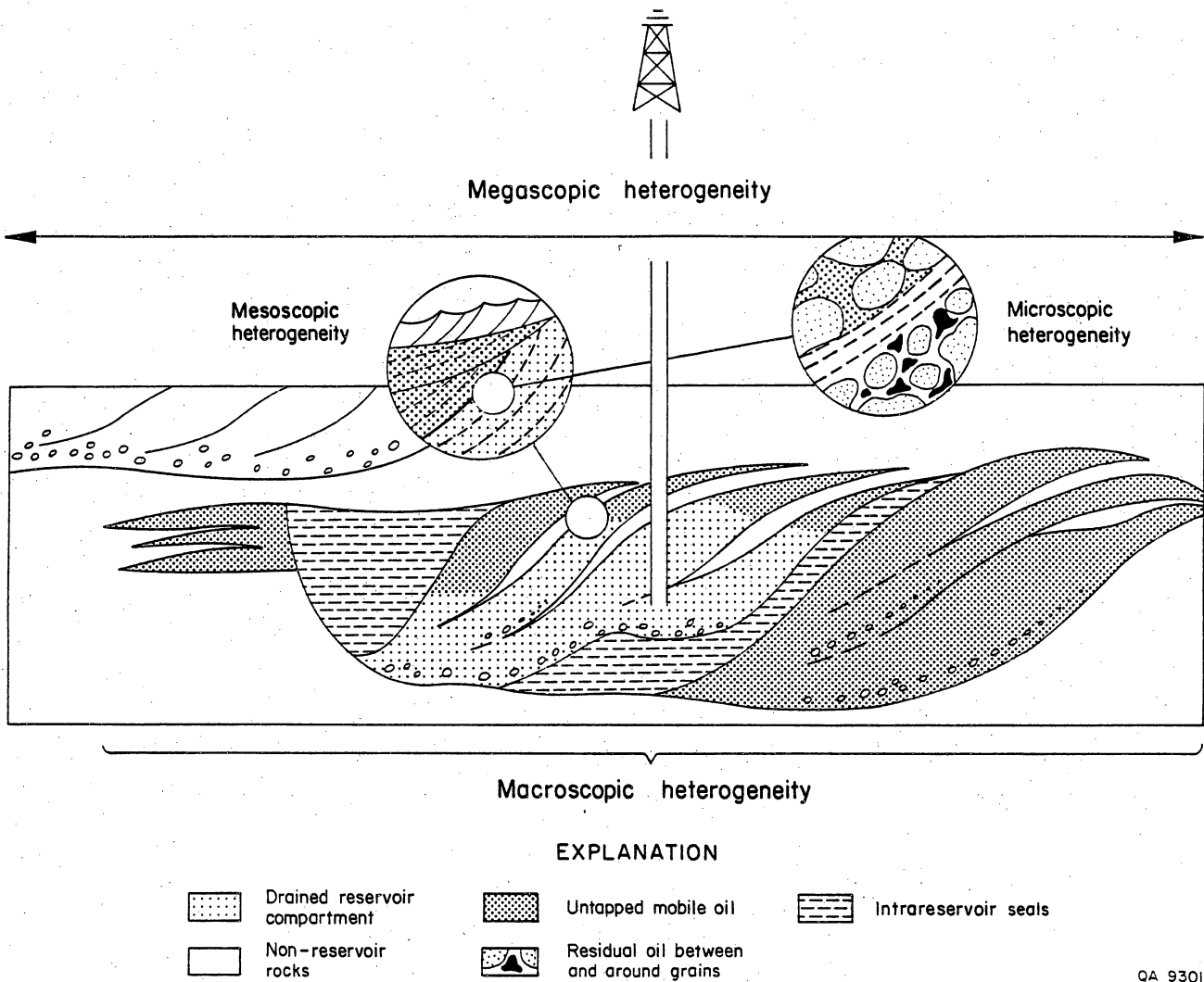


Figure 91. Four scales of reservoir heterogeneity. At Seeligson field, poorly drained reservoir compartments that occur at the megascale level of heterogeneity are inferred from net-sandstone and log-facies maps. Sizes of these compartments are best resolved in three-dimensional seismic maps. From Tyler (1988).

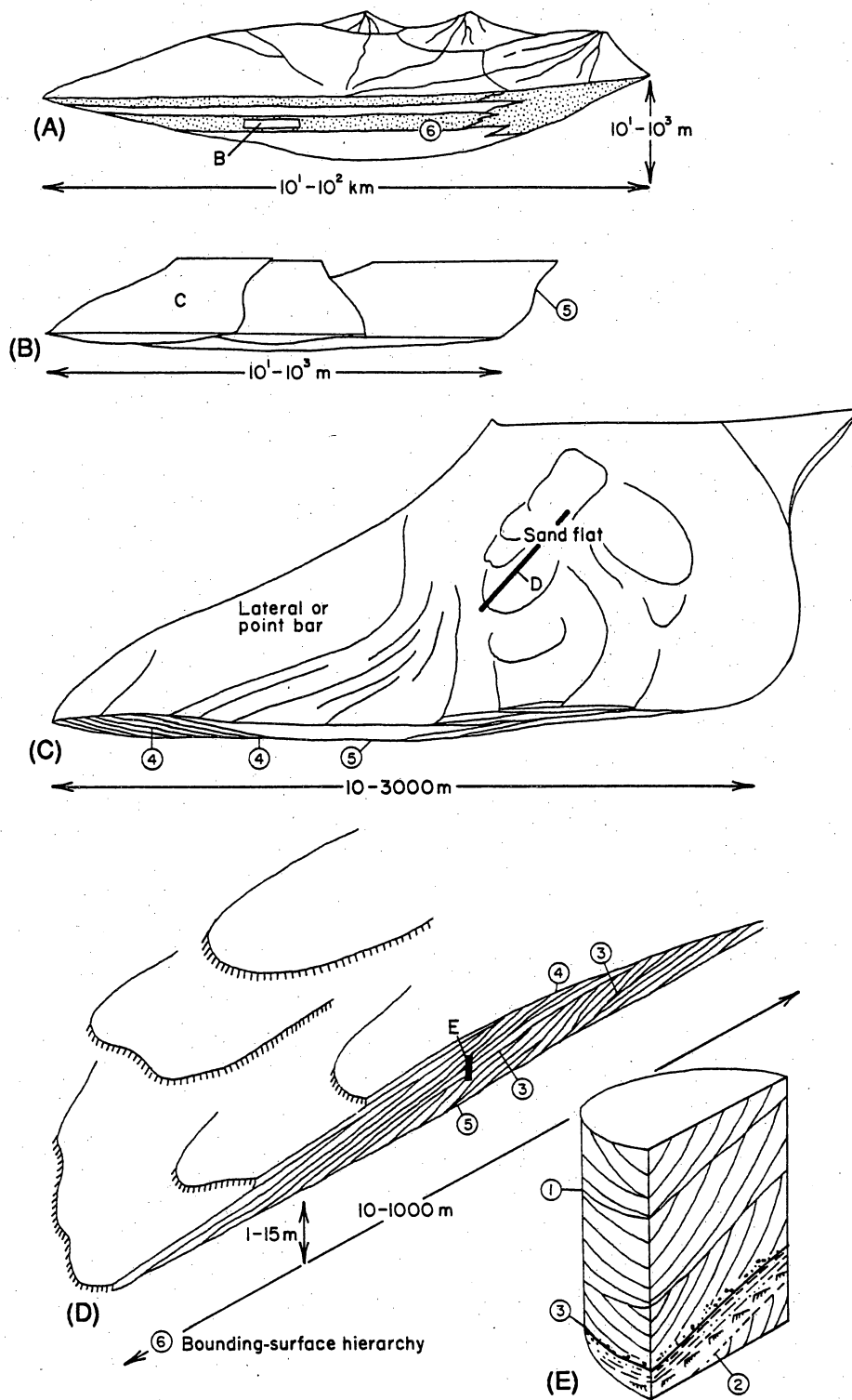


Figure 92. Six-fold hierarchy of heterogeneity in fluvial systems. Circled numbers 1 through 6 indicate ranks of bounding surfaces. Scales of heterogeneity range from small-scale, identified in cores (E), to large-scale architecture of stacked channel-fill deposits (A). This hierarchy also listed in table 9. Modified from Miall (1988).

Table 9. Range of scales of reservoir heterogeneities in fluvial sandstones illustrated in figure 91. Modified from Miall (1988).

Rank of bounding surface	Lateral extent of unit	Thickness of unit (m)	Area of unit (ha)	Origin	Subsurface mapping methods
6	200 × 200 km	0-30	4 × 10 ⁷	Members or submembers, subtle tectonic control	Regional correlation of wireline logs
5	1 × 10 km	10-20	10 ⁴	Sheet sandstones of channel origin	Intrafield correlation of wireline logs, 3-D seismic
5	0.25 × 10 km	10-20	2,500	Ribbon channel sandstone	Mapping difficult except with very close spacing, 3-D seismic
4	200 × 200 m	3-10	40	Macroform elements	Dip of 4th- and 3rd-order surfaces may be recognizable in core
3	100 × 100 m	3-10	10	Reactivation of macroforms	Dip of 4th- and 3rd-order surfaces may be recognizable in core
2	100 × 100 m	5	10	Cosets of similar crossbed facies	Facies analysis of core
1	100 × 100 m	2	10	Individual crossbed sets	Facies analysis of core

spaces strongly controls permeability and porosity, whereas kaolinite is restricted to secondary pores and has only a minor effect on reservoir quality. However, these cements do not coincide with facies types at Seeligson field, and therefore their impact on large-scale, between-well reservoir heterogeneity at Seeligson field is negligible.

At Seeligson and Stratton fields, the features that primarily control reservoir heterogeneity at the mesoscopic scale are intraclast zones at the bases of channel-fill and splay-channel deposits. These intraclast zones exhibit significant changes in permeability and porosity over small distances (<0.1 inch [<2.5 cm]), where permeability values can range from less than 0.1 to almost 10 md (Levey and others, 1991). However, mesoscopic heterogeneity at Seeligson field extends over small distances (tens to hundreds of feet) and its influence on reservoir compartmentalization cannot be determined at common gas-well spacings of 320 and 640 ac.

Contrasts in reservoir quality between facies are recognized at the level of macroscopic heterogeneity. At Seeligson and Stratton fields, lower and middle channel-fill and proximal-splay subfacies contain the highest permeabilities (locally more than 1,000 md), whereas upper channel-fill and distal-splay subfacies commonly have permeabilities <10 md (Jirik and others, 1989; Levey and others, 1991). These high-permeability facies segment large-scale composite channel-fill and splay sandstone complexes into reservoir compartments that are extensive enough to be inferred from three-dimensional seismic, net-sandstone, and log-facies maps. However, some compartments (for example, abandoned-channel fill or proximal-splay channel) have limited sizes and may not extend across many wells at 320- or 640-ac spacing and therefore their occurrence between wells may be difficult to predict. Moreover, individual channel-fill sandstones can have widths as narrow as 1,000 ft (305 m), have sinuous trends (fig. 19), and may therefore have a sufficiently limited areal extent to be only partly contacted at lesser well spacing of less than 320 ac.

The relative occurrence and magnitude of reservoir compartments at Seeligson field versus other fields in the FR-4 play (for example, Stratton and Agua Dulce fields) is ultimately a function of large-scale, megascopic heterogeneity. The major reservoir compartments at this scale are characterized by either connected or isolated fluvial architectural styles, which control the nature and frequency of channel-on-channel contacts and the extent of composite sandstone bodies (Kerr and Jirik, 1990). In isolated fluvial architecture, many potential reservoir compartments may exist as bypassed or untapped zones. In contrast, it is less apparent that connected fluvial architecture contains reservoir compartments at a scale smaller than conventional gas-well spacings (320 to 640 ac). Channel-on-channel contacts are common in this architectural style and partial communication between sandstone bodies is expected. However, evidence suggests that bypassed or poorly drained compartments can exist in sandstones of connected architecture. For example, the Zone 15 reservoir at Seeligson field exhibited a reservoir-pressure decline from 2,200 to 300 psi after 30 yr of production, and yet pressure values at nearly 50 percent of expected original reservoir pressure were recently observed in some wells (fig. 46).

Channel-on-channel contacts in a system of connected channels such as those in the Zone 19C reservoir may serve as permeability barriers that partly compartmentalize the reservoir. These contacts segment what may appear as a continuous belt of sandstone into poorly connected reservoir compartments. For example, the middle Zone 19C genetic unit is truncated by sandstones in the upper Zone 19C genetic unit throughout the north part of Seeligson field. Significant low-permeability zones associated with channel-on-channel contacts may result in incomplete drainage of the reservoir. An additional example is from the Ferron Sandstone (Upper Cretaceous) in east-central Utah, where basal distributary-channel-lag deposits consist of 4- to 30-cm-thick, poorly sorted, medium to granule sandstone, clay-pebble conglomerate. The clay clasts in these channel-lag deposits, which were derived from channel-bank mudstones

eroded and redeposited at the base of channels, are inferred to represent fluid-flow barriers where local reduction of permeability is more than an order of magnitude (Tyler and others, 1991).

Thus, lithologic heterogeneity at different scales in connected fluvial architecture or between facies in a discrete genetic interval should produce leaky barriers to gas flow, creating the potential for opportunities to exploit partially drained compartments. In contrast, lithologic heterogeneity in isolated fluvial architecture should produce more effective barriers to natural gas, resulting in higher potential for bypassed or poorly drained compartments.

Secondary Gas Recovery Potential of Seeligson Field and Related Fluvial-Deltaic Reservoirs

The potential for secondary gas recovery in reservoirs in fluvial-deltaic plays such as the Frio of South Texas is controlled by fluvial architectural style and operator drilling and development history. The thickness of individual sandstones in Seeligson and Stratton fields is similarly distributed (fig. 93), indicating that reservoir compartments in these fields may be of similar size. However, these sandstones are arranged in different architectural styles; at Seeligson and La Gloria fields, connected fluvial architecture is the most common style of reservoir geometry in middle Frio strata, resulting in a high degree of communication between reservoir sandbodies (Jackson and Ambrose, 1989; Kerr and Jirik, 1990). In contrast, fluvial architecture in middle Frio reservoirs at Stratton and Agua Dulce fields is dominantly of the isolated style with consequent high degree of reservoir compartmentalization (Kerr, 1990). Because connected sandstone bodies result in separate but potentially "leaky" compartments and isolated sandstone bodies represent untapped compartments, a relatively low potential for secondary gas recovery in middle Frio reservoirs exists in Seeligson and La Gloria fields, whereas a good

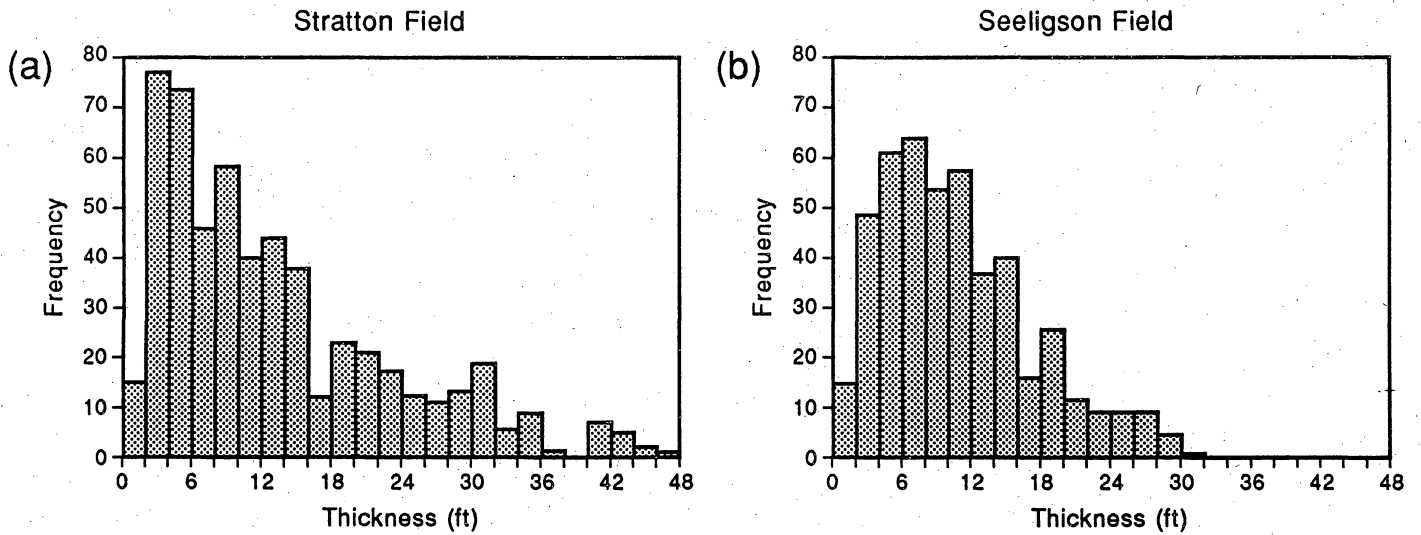
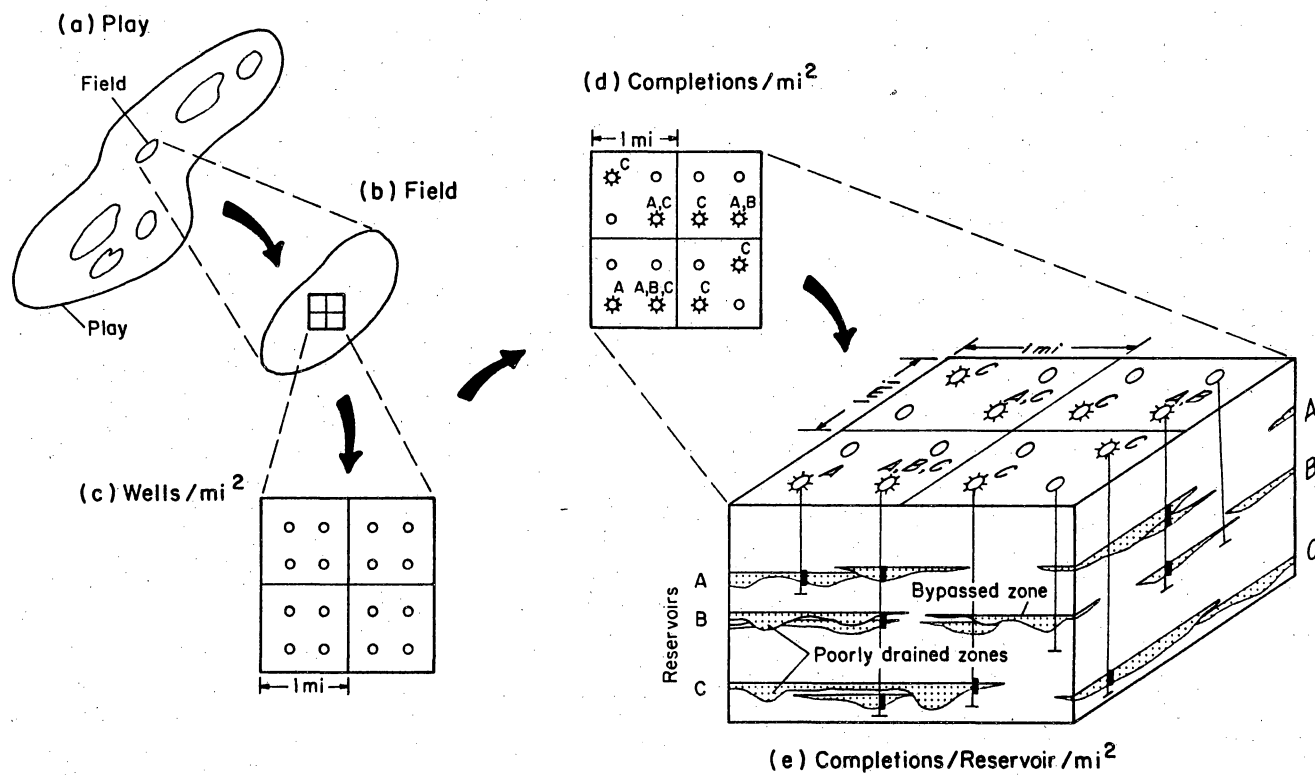


Figure 93. Distribution of thickness of individual sandstones in (a) Stratton field and (b) Seeligson field. Similarities in sandstone thickness in these fields suggest that variations in recovery efficiency can possibly be attributed to differences in fluvial architecture, completion practices, or both.

potential exists in Stratton and Agua Dulce fields. Differences in fluvial reservoir architecture must therefore be taken into account as part of infield exploration strategies for each field.

Another factor controlling the potential for secondary gas recovery in mature fields is the level of development or completion and perforation spacing (fig. 94). Many of the fields in the FR-4 play were discovered in the 1940's and 1950's and have almost been depleted (Kosters and others, 1989). Compared with other Frio gas plays in the Texas Gulf Coast, the FR-4 play has some of the greatest numbers of infill wells (Jackson and Finley, 1991). However, significant variations in number of reservoirs/mi², completions/reservoir/mi², and cumulative gas/completion exist even in these fields. Additionally, reservoirs are defined differently for each field in the FR-4 play. For example, at Seeligson field many individual sandstone bodies less than 30 ft (9 m) thick are defined as a reservoir (figs. 11 and 95), whereas at Agua Dulce and Stratton fields many reservoirs are defined as composite intervals referred to a reservoir series, commonly over 100 ft (30 m) thick and consisting of multiple, isolated sandstone bodies interbedded with mudstone (fig. 96 [Kerr, 1990]). At Stratton field, most of the new reserve growth has come from thin sandstone stringers that are partly or completely isolated from the main body of the reservoir. Many individual sandstones in these complex intervals at Agua Dulce and Stratton fields have not been perforated or have been poorly drained and are therefore inferred to contain relatively more reservoir compartments/mi² than does Seeligson field.

Of the major fields in the FR-4 play, only Brayton field has more completions/reservoir/mi² (1.85) than does Seeligson (0.88) (table 10). Reservoirs in other fields (Agua Dulce, La Gloria, and Stratton) have been relatively sparsely completed (less than 0.30 completions/reservoir/mi²). In addition, Seeligson field leads the FR-4 play in numbers of reservoirs/mi², has a relatively high number of wells/mi², but has a gas cap with a small areal extent (table 10). As a result of high number of



EXPLANATION

- Perforation interval
- Well
- ⊛ Completed well
- ▨ Sandstone reservoir

Reservoir	No. of Completions	No. of Completions/mi ²
A	4	1.00
B	2	0.50
C	6	1.50

QA18506

Figure 94. Generalized illustration of field- and reservoir-development parameters listed in table 10. (a) Hypothetical play containing fields. (b) Area of gas cap of a selected field (see column 3 in table 10 for examples in the FR-4 play) with representative 4-mi² (6.4-km²) area. (c) Wells drilled/mi² (column 4 in table 10). (d) Gas-well completions/mi² (column 6 of table 10). (e) Completions/reservoir and completions/reservoir/mi² (columns 7 and 8 in table 10). In this example, there is (c) an average of 4 wells drilled/mi², of which there is (d) an average of 3.2 completions/mi². Distribution of these completions/reservoir is shown in (e), where reservoir C has a relatively high completion density (1.50 completions/mi²). In contrast, reservoir B has a low completion density (0.50 completions/mi²) and contains uncompleted, bypassed zones.

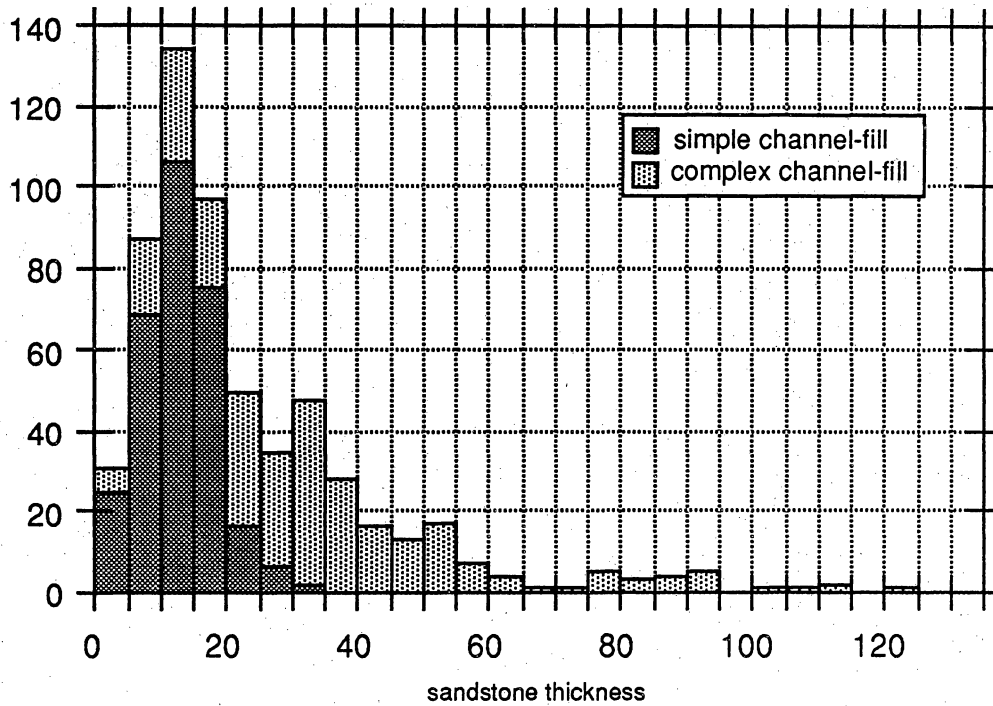
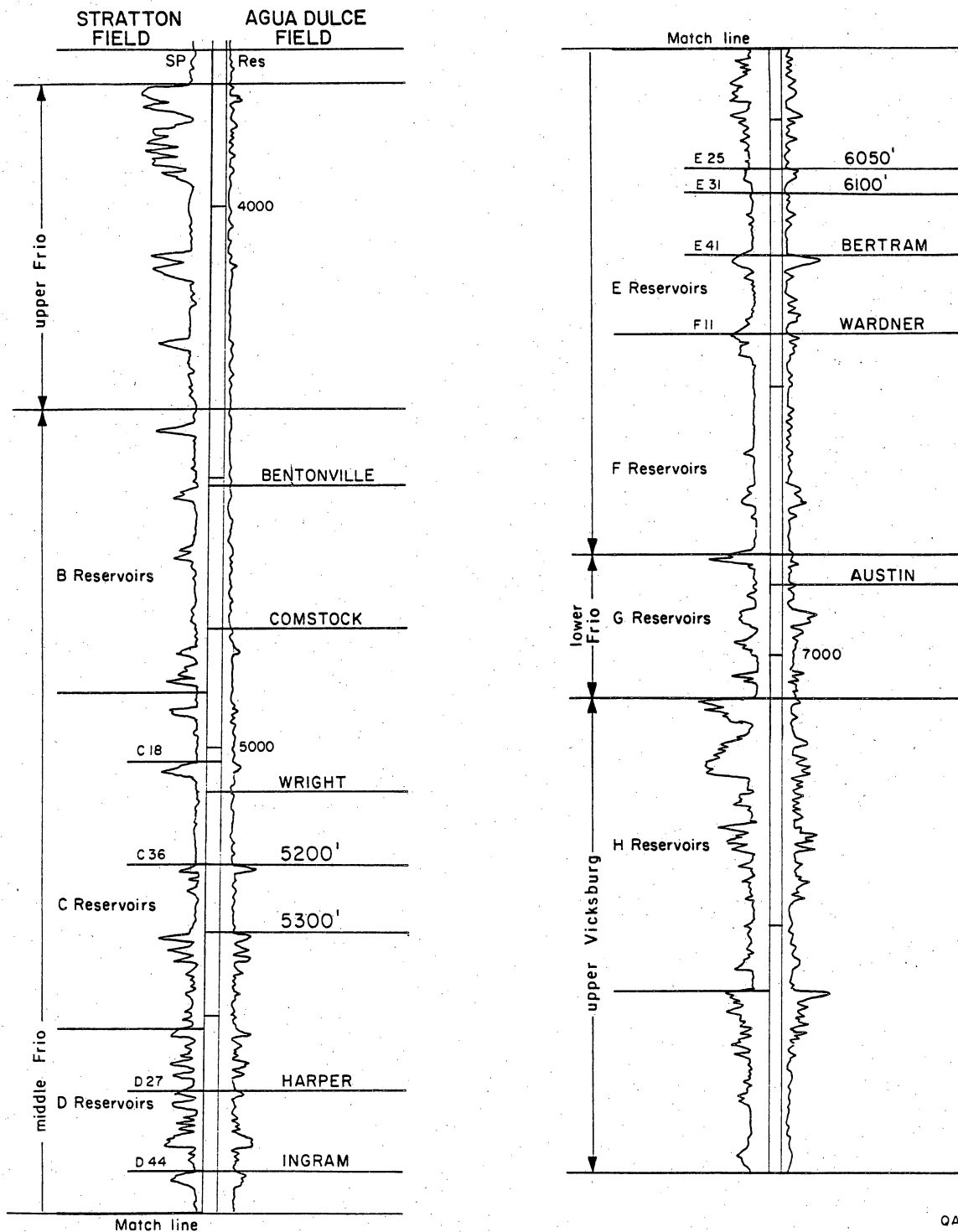


Figure 95. Distribution of individual-sandstone thickness (simple channel fill) and composite-sandstone thickness (complex channel fill) in selected middle Frio reservoirs in Seeligson field. Many reservoirs in Seeligson field (for example, Zones 19B, 18A, 15, and 14B) consist of one or two genetic sandstone bodies that commonly are each <20 ft (<6 m) thick, whereas other reservoirs (for example, Zones 19C and 17) contain several genetic sandstone bodies that commonly have an aggregate thickness of >40 ft (>12 m).

UNION PRODUCING CO.
Driscoll No.7A



QA 12633

Figure 96. Reservoir nomenclature at Stratton field in the FR-4 play. At Stratton field, many reservoirs are defined as composite intervals consisting of multiple, isolated sandstones interbedded with mudstone. Because individual sandstones at Stratton field are not commonly defined as a reservoir (in contrast with Seeligson field where individual sandstones are commonly defined as reservoirs [fig. 11]), many of these sandstones have not been contacted at present levels of completions. From Kerr (1990).

Table 10. Field-size, drilling, completion, and production data from the major fields in the FR-4 play. Important parameters (gas-cap area, number of wells drilled/mi², number of completions/mi², and number of completions/reservoir/mi²) are illustrated for a hypothetical field in figure 94. Data from files of the Texas Railroad Commission.

Field	No. of reservoirs	Gas cap area (mi ²)	Wells (mi ²)	No. of completions	No. of completions (mi ²)	No. of completions/reservoir	No. of completions/reservoir (mi ²)	Cumulative gas (Bcf)	Cumulative gas/reservoir (Bcf)	Cumulative gas/reservoir (mi ²) (Bcf)
Agua Dulce	208	26.25	8.91	930	35.43	4.47	0.17	2,092.6	10.1	0.38
Borregos	178	30.50	6.89	1,003	32.89	5.63	0.18	1,871.6	10.5	0.34
Brayton	19	3.75	7.47	132	35.20	6.95	1.85	231.5	12.2	3.25
Cage Ranch	17	15.25	3.15	48	3.15	2.82	0.19	89.6	5.3	0.35
Cortez	11	7.25	4.97	44	6.07	4.00	0.55	64.3	5.8	0.81
Kelsey	15	11.25	10.84	117	10.40	7.80	0.69	131.2	8.7	0.78
Kelsey Deep	159	13.00	4.08	290	22.31	1.82	0.14	194.9	1.2	0.09
Kelsey South	82	7.50	6.80	164	21.87	2.00	0.27	158.0	1.9	0.26
La Gloria	63	20.25	5.23	359	17.73	5.70	0.28	2,480.8	39.3	1.94
La Reforma	56	13.25	8.23	115	8.68	2.05	0.15	211.2	3.8	0.28
Minnie Bock No.	30	8.50	4.59	72	8.47	2.40	0.28	113.5	3.8	0.45
Pita	45	5.25	7.81	85	16.19	1.89	0.36	129.4	2.9	0.55
Rincon	60	25.50	6.82	148	5.80	2.47	0.10	89.4	1.5	0.06
Rincon No.	117	16.75	6.81	264	15.76	2.26	0.13	302.8	2.6	0.15
Seeligson	131	8.50	7.06	977	114.94	7.46	0.88	2,460.8	18.8	2.21
Stratton	277	35.50	8.96	931	26.23	3.36	0.09	5,008.0	18.1	0.51
Sun	49	14.50	6.76	157	10.83	3.20	0.22	121.0	2.5	0.17
Sun North	108	9.25	7.14	200	21.62	1.85	0.20	125.2	1.2	0.13
TCB	80	17.50	5.83	341	19.49	4.26	0.24	577.1	7.2	0.41

completions/mi² at Seeligson field, cumulative gas/completion (approximately 2.5 Bcf) is much less than that in Stratton field (5.3 Bcf) (table 10), suggesting that relatively high numbers of completions/mi² (114.9/mi² in Seeligson reservoirs versus 26.2/mi² in Stratton field) have already contacted large volumes of gas (2.21 Bcf/mi² in Seeligson field versus 0.51 Bcf/mi² at Stratton field [table 10]) and that recent completions in Seeligson field produce relatively less remaining gas.

In summary, Seeligson field is considered to have a lower potential for secondary gas recovery in comparison with other fields in the same play because the reservoir sandstones are well connected laterally, resulting in leaky compartments that have been drained by a relatively greater number of completions. Because many reservoirs at Seeligson field are defined as individual sandstone bodies rather than composite intervals of multiple sandstones separated by mudstones, many of these reservoirs have already been contacted and effectively drained by existing wells. However, a limited number of poorly drained reservoir compartments still exist at Seeligson field; the location and extent of these remaining compartments can be inferred from comparison of three-dimensional seismic, net-sandstone, and log-facies maps and their reserve-growth potential can be evaluated using improved cased-hole logging techniques.

CONCLUSIONS

Exploration for incompletely drained compartments or bypassed gas zones in old fields can be improved by using detailed geologic studies that integrate engineering and petrophysical methods. Isolated or incompletely drained hydrocarbon-bearing zones can be tested through well recompletions or geologically based infill drilling. At Seeligson and other fields in the Frio Formation, complex fluvial reservoirs represent opportunities for identifying potentially undrained reservoir compartments. Similar reservoirs also exist in other plays of the Gulf Coast basin and in other gas-producing regions.

Zones 15 and 19C in Seeligson field are complex, connected fluvial channel systems comprising channel-fill and crevasse-splay sandstones, levee siltstones, and floodplain siltstones and mudstones. These sand-rich zones appear to be relatively continuous and therefore have been developed as essentially homogeneous reservoirs. However, they have a high degree of internal architectural complexity and contain a limited number of compartments with uncontacted gas reserves. Anomalous bottom-hole pressures observed in recompleted wells in Zone 15 are related to facies heterogeneities; incompletely drained channel-fill deposits in a fluvial complex are contacted in these wells. This channel complex is separated by silty and muddy floodplain facies from adjacent channel systems that have depleted reservoir pressures. The lateral barrier to flow is provided by the low-permeability levee and floodplain facies, resulting in the higher-than-expected reservoir pressures.

The integration of reservoir-characterization methods with state-of-the-art petrophysical techniques is effective in identifying bypassed-gas zones. The reserve-growth potential of bypassed and untapped zones can be evaluated with an advanced cased-hole logging program using pulsed-neutron and acoustic logs. At Seeligson field, reservoirs were studied for bypassed gas potential and evidence of incomplete drainage due to compartmentalization. Middle Frio sandstones were described and mapped; reservoir-quality facies identified. Pulsed-neutron, gamma-ray, and acoustic logs were recorded in selected cased holes and interpreted using new techniques that demonstrate their effectiveness in identifying gas-bearing zones. Five successful recompletions were made in two zones that have produced more than 1.4 Bcf of gas in about 18 mo.

Although Seeligson field contains poorly contacted reservoir compartments, its potential for secondary gas recovery in the middle Frio Formation is less than that of other fields in the FR-4 play. Seeligson field contains connected fluvial sandstones that have been well drained by relatively greater numbers of completions. In contrast, many other fields in the play (Stratton and Agua Dulce) contain less intensively completed,

isolated fluvial sandstones that represent uncontacted reservoir compartments. Differences in fluvial reservoir architecture and completion practices must be considered as an important part of an infield exploration program for fields in the Frio Formation within the Gulf Coast Basin Tertiary stratigraphic section as a whole.

ACKNOWLEDGMENTS

This work was performed for and funded by the Gas Research Institute under contract no. 5084-212-0924. The cooperation of Oryx Energy Company and Mobil Exploration and Producing, U.S., Inc., is gratefully acknowledged. Discussions with R. P. Langford, M. L. W. Jackson, and D. R. Kerr were extremely helpful. Research was assisted by L. L. Brock, T. N. Diggs, N. Baghai, L. Sparlin, and R. Remington. T. F. Hentz and R. J. Finley critically reviewed the manuscript and added to the clarity of the presentation. Figures were drafted by Edwin Banks, Jana Robinson, and Susan Krepps under the supervision of R. L. Dillon. Editing was by Lana Dieterich.

REFERENCES

- Ambrose, W. A., and Jackson, M. L. W., 1989, Geologically based infill potential of fluvial gas reservoirs, La Gloria (Frio) field, South Texas: Bulletin of the South Texas Geological Society, v. 29, no. 5, p. 13-21.
- Busch, B. C., and Jenkins, R. E., 1970, Proper hydration of clays for rock property determinations: Journal of Petroleum Technology, v. 22, July, p. 800-804.
- Cannon, D. E., and Coates, G. R., 1990, Applying mineral knowledge to standard log interpretation: Society of Professional Well Log Analysts 31st Annual Logging Symposium, June 24-27, Paper V, p. 1-10.
- Connolly, W. M., Denham, M., Peterson, M., Ritter, C., and Mazzullo, J., 1986, Seasonal variations in the morphology and sedimentology of a point bar on the Brazos River of Central Texas (abs.): Gulf Coast Association of Geological Societies Transactions, v. 36, p. 429.
- Edcon-Schlumberger, 1991, Deep density BHGM: sales brochure example, 7 p.
- Exploration Data Consultants, Inc., 1991, Borehole gravity survey, Seeligson No. 1-89, Jim Wells County, Texas: Report on Data Acquisition, 8 p.
- Finley, R. J., Fisher, W. L., Seni, S. J., Ruppel, S. C., White, W. G., Ayers, W. B., Jr., Dutton, S. P., Jackson, M. L. W., Banta, Nancy, Kuuskraa, V. A., McFall, K. S., Godec, Michael, and Jennings, T. V., 1988, An assessment of the natural gas resource base of the United States:

The University of Texas at Austin, Bureau of Economic Geology Report of Investigations
No. 179, 69 p.

Finley, R. J., Guevara, E. H., Jirik, L. A., Kerr, D. R., Langford, R. P., Wermund, E. G., Zinke, S. G.,
Collins, R. E., Hower, T., Lord, M., and Ballard, J. R., 1990, Secondary natural gas recovery:
targeted technology applications for infield reserve growth: The University of Texas at
Austin, Bureau of Economic Geology, annual report prepared for the Gas Research
Institute under contract no. 5088-212-1718, 194 p.

Folk, R. L., 1974, Petrology of sedimentary rocks: Austin, Texas, Hemphill Publishing Company,
182 p.

Galloway, W. E., 1977, Catahoula Formation of the Texas Coastal Plain—depositional systems,
composition, structural development, ground-water flow history, and uranium distribution:
The University of Texas at Austin, Bureau of Economic Geology, Report of Investigations
No. 87, 59 p.

_____ 1982, Depositional architecture of Cenozoic Gulf Coastal Plain fluvial systems, *in*
Ethridge, F. G., and Flores, R. M., eds., Recent and ancient nonmarine depositional
environments: models for exploration: Society of Economic Paleontologists and
Mineralogists, Special Publication No. 31, p. 127–155.

Galloway, W. E., Hobday, D. K., and Magara, K., 1982, Frio Formation of the Texas Gulf Coast
basin—depositional systems, structural framework, and hydrocarbon origin, migration,
distribution, and exploration potential: The University of Texas at Austin, Bureau of
Economic Geology, Report of Investigations No. 122, 78 p.

Gournay, L. S., 1991, Seeligson No. 1-89 wellbore gravity log analysis and interpretation:
Prepared for ResTech, Houston, February, 6 p.

Grigsby, J. D., and Kerr, D. R., 1991, Diagenetic variability in middle Frio Formation gas
reservoirs (Oligocene), Seeligson and Stratton fields, South Texas: Gulf Coast Association of
Geological Societies Transactions, v. 41, p. 308-319.

Han, J. H., and Scott, A. J., 1981, Relationship of syndepositional structures and delatation,
Vicksburg Formation (Oligocene), South Texas: Society of Economic Paleontologists and
Mineralogists, Gulf Coast section, 2d annual research conference, Program and Abstracts,
p. 33-40.

Hilchie, D. W., 1979, Old electrical log interpretation: Colorado School of Mines, Department of
Petroleum Engineering, p. 57-87.

Hill, H. J., Shirley, O. J., and Klein, G. E., 1979, Bound water in shaly sands—its relationship to
Qv and other formation properties: The Log Analyst, v. 20, p. 3-19.

Jackson, M. L. W., and Ambrose, W. A., 1989, Influence of reservoir heterogeneity on gas-
resource potential for geologically based infill drilling, Brooks and I-92 reservoirs, Frio
Formation, South Texas: Gulf Coast Association of Geological Societies Transactions, v. 39,
p. 127-140.

Jackson, M. L. W., and Finley, R. J., 1991, Extrapolation of gas reserve growth potential:
development of examples from macro approaches: The University of Texas at Austin,
Bureau of Economic Geology, contract report prepared for the Gas Research Institute
under contract no. 5090-212-2076, 108 p.

- Jirik, L. A., 1990, Reservoir heterogeneity in middle Frio fluvial sandstones: case studies in Seeligson field, Jim Wells County, Texas: Gulf Coast Association of Geological Societies Transactions, v. 40, p. 335-352.
- Jirik, L. A., Ambrose, W. A., Kerr, D. R., and Light, M. P. R., 1989, Coordination of geological and engineering research in support of the Gulf Coast co-production program: The University of Texas at Austin, Bureau of Economic Geology, final report prepared for the Gas Research Institute under contract no. 5084-212-0924, 118 p.
- Jirik, L. A., Howard, W. E., and Sadler, D. L., 1991, Identification of bypassed gas reserves through integrated geological and petrophysical techniques: a case study in Seeligson field, Jim Wells County, South Texas: Society of Petroleum Engineers, Gas Technology Symposium, SPE paper no. 21483, p. 7-16.
- Kerr, D. R., 1990, Reservoir heterogeneity in the middle Frio Formation: case studies in Stratton and Agua Dulce fields, Nueces County, Texas: Gulf Coast Association of Geological Societies Transactions, v. 40, p. 363-372.
- Kerr, D. R., and Grigsby, J. D., 1991, Recognition and implications of volcanic glass detritus in fluvial deposits of the middle Frio Formation: Gulf Coast Association of Geological Societies Transactions, v. 41, p. 353-358.
- Kerr, D. R., and Jirik, L. A., 1990, Fluvial architecture and reservoir compartmentalization in the Oligocene middle Frio Formation, South Texas: Gulf Coast Association of Geological Societies Transactions, v. 40, p. 373-380.

- Kosters, E. C., Bebout, D. G., Seni, S. J., Garrett, C. M., Jr., Brown, L. F., Jr., Hamlin, H. S., Dutton, S. P., Ruppel, S. C., Finley, R. J., and Tyler, Noel, 1989, Atlas of major Texas gas reservoirs: The University of Texas at Austin, Bureau of Economic Geology Special Publication, 161 p.
- Levey, R. A., ed., 1991, Infield gas reserve growth potential: Gulf Coast sandstone reservoirs (Frio, Vicksburg, Wilcox): The University of Texas at Austin, Bureau of Economic Geology, short course prepared for the Gas Research Institute under contract no. 5088-212-1718, unpaginated.
- Levey, R. A., Grigsby, J. D., Langford, R. P., Kerr, D. R., Guevara, E. H., Scott, A. R., and Finley, R. J., 1991, Core and log analysis of depositional systems and reservoir properties of Gulf Coast natural gas reservoirs: an integrated approach to infield reserve growth in Frio, Vicksburg, and Wilcox sandstones: The University of Texas at Austin, Bureau of Economic Geology, guidebook prepared for the 1991 Gulf Coast Association of Geological Societies Transactions convention in Houston, Texas, 60 p.
- Loucks, R. G., Dodge, M. M., and Galloway, W. E., 1984, Regional controls on diagenesis and reservoir quality in Lower Tertiary sandstones along the Texas Gulf Coast, *in* McDonald, D. A., and Surdam, R. C., eds., *Clastic diagenesis: American Association of Petroleum Geologists Bulletin, Memoir 37*, p. 15-45.
- MacPherson, G. L., 1989, Sources of lithium and barium in Gulf of Mexico Basin formation waters, USA, *in* Miles, D. L., ed., *Proceedings of the 6th Symposium on Water-Rock Interaction: Rotterdam, Balkama*, p. 453-456.

MacPherson, G. L., and Land, L. S., 1989, Boron in saline brines, Gulf of Mexico sedimentary basin, USA, *in* Miles, D. L., ed., Proceedings of the 6th Symposium on Water-Rock Interaction: Rotterdam, Balkama, p. 457-460.

Mechel, L. D., and Nath, A. K., 1977, Geologic considerations for stratigraphic modeling and interpretation: American Association of Petroleum Geologists, Memoir 26, p. 417-438.

Miall, A. D., 1988, Reservoir heterogeneities in fluvial sandstones: lessons learned from outcrop studies: American Association of Petroleum Geologists Bulletin, v. 72, no. 6, p. 682-697.

Nanz, R. H., 1954, Genesis of Oligocene sandstone reservoir, Seeligson field, Jim Wells and Kleberg Counties, Texas: American Association of Petroleum Geologists Bulletin, v. 38, no. 1, p. 96-117.

ResTech, 1988, Improved logging behind casing and technology support for advanced formation evaluation: final report prepared for the Gas Research Institute under contract no. 5086-212-1426, 106 p.

_____ 1989, Secondary natural gas recovery: targeted technology applications for infield reserve growth: annual report prepared for the Gas Research Institute under contract no. 5088-212-1718, p. 58-75.

Schlumberger Limited, 1987, Log interpretation principles/applications: Schlumberger Educational Services, p. 32-60.

Sullivan, K. B., 1988, Sandstone and shale diagenesis of the Frio Formation (Oligocene), Texas Gulf Coast: a close look at sandstone/shale contacts: The University of Texas at Austin, Master's thesis, 242 p.

Truman, R. B., Davies, D. K., Howard, W. E., and Vessell, R. K., 1986, Utilization of rock characterization data to improve well log interpretation, Society of Professional Well Log Analysts 27th Annual Logging Symposium, June 9-13, Paper V, p. 1-10.

Truman, R. B., Howard, W. E., and Luffel, D. L., 1989, Shale porosity—its impact on well log modeling in interpretation, Society of Professional Well Log Analysts 30th Annual Logging Symposium, June 11-14, Paper Q, p. 1-9.

Tyler, Noel, 1988, New oil from old fields: *Geotimes*, v. 33, p. 8-10.

Tyler, Noel, Barton, Mark, Fisher, R. S., and Gardner, M. H., 1991, Architecture and permeability structure of fluvial-deltaic sandstones: a field guide to selected outcrops of the Ferron Sandstone, east-central Utah: The University of Texas at Austin, Bureau of Economic Geology Guidebook, 80 p.

Yilmaz, Ozdogan, 1987, Seismic data processing: Tulsa, Oklahoma, Society of Exploration Geophysicists, 526 p.

APPENDIX 1

EVALUATION OF RESULTS

The following analysis identifies potential gas-productive zones found using the pulsed-neutron full-wave acoustic log analysis method and borehole gravity survey results. These zones are presented on a well-by-well basis with relevant comments.

Seeligson 1-89

In the 1-89 well three sandstones show gas indications from cased-hole logs. Sandstone No. 15 is the best recompletion zone in this well. Gas presence is confirmed by the borehole gravity survey, but the sandstone may be partially depleted.

Sandstones No. 17 and 19c show some residual gas; however, they were previously produced and squeezed in this well.

Reservoir	Depth	Ø (%)	Sw (%)	Gas effect	Comments
15	5360-78	26	50	Yes	Gas
17	5550-57	30	60	No	Marginal
19C	5855-60	22	62	Moderate	Marginal

Seeligson 1-171

In the 1-171 well three sandstones show gas indications from cased-hole logs. Sandstones No. 15 and 19c appear gas productive. These zones have not been tested.

Sandstone No. 14 B shows some residual gas. It was previously produced and squeezed.

Reservoir	Depth	Ø (%)	Sw (%)	Gas effect	Comments
15	5400-07	25	58	Yes	Gas
19C	5910-40	18	59	NA	Gas
14B	5200-15	23	63	Yes	Marginal

Seeligson 1-85

In well 1-85 there is only one marginal gas sandstone (18A) with high water saturation. No other gas zones are evident from cased-hole logs.

Reservoir	Depth	Ø (%)	Sw (%)	Gas effect	Comments
18A	5730-39	25	60	Moderate	Marginal

APPENDIX 2

The research reported herein is self-contained; that is, although page numbers consecutively follow those of the rest of this report, the figure, table, and appendix numbers do not.

**SEELIGSON No. 1-89 WELL
BOREHOLE GRAVITY LOG
ANALYSIS AND INTERPRETATION**

**PREPARED FOR
RESTECH, HOUSTON**

FEBRUARY, 1991

**by:
LUKE S. GOURNAY, Ph.D.**

**HY-TECH SERVICES, Inc.
P.O. BOX 1145
GRANBURY, TX 76048**

I. SUMMARY

A borehole gravity log (BHGL) was run in the S.U. 1-89 well, Seeligson Field, Jim Wells County, Texas on January 4-5, 1991. EDCON provided the logging services and supplied their report with drift corrected gravity data, and derived formation bulk density. Twenty one intervals were logged in this survey.

The logging operation went smoothly with no obvious downhole malfunctions. Logging had to be terminated early because of earth vibrations generated by an earthquake in Burma of magnitude 7.5 on the Richter scale. However, most of the intervals of interest had been investigated before this incident occurred.

BHGL data were examined separately, in conjunction with the 1945 lateral log, and together with a recent PNC (TDT) log.

These three logs, individually, show some indication of hydrocarbons in the depth interval 5363 to 5379 feet, but with a degree of ambiguity.

The Barchie method, which uses a combination of BHGL and Lateral log data, strongly predicts the presence of hydrocarbons in this interval.

The combination BHGL and PNC data also strongly predicts the presence of hydrocarbons in this interval.

On the basis of these results, a test of the interval from 5363 to 5379 feet is clearly and definitely recommended.

II. OBJECTIVES AND DESCRIPTION OF THE BHGL

The Seeligson 1-89 was drilled and initially completed in 1945. Resistivity logs and S.P. logs were run at that time.

Over time, several zones were tested and completed. Results of these tests are summarized in TABLE 1. Probably in 1989, a CIBP was set at 5350 ft. There is no evidence from well history that the interval 5363 to 5379 was ever tested.

The objectives of the BHGL were to obtain formation bulk density data and to look for remaining gas-bearing formations. The BHGL can log through casing, is not affected by near wellbore conditions, and has a large radius of investigation. The BHGL log was only a part of a much larger effort to develop means for locating gas-behind-casing.

On the basis of the original 1945 well logs, numerous sands from 5850 feet to 4000 feet were selected for the BHGL. A recent TDT log was used to slightly modify these selections prior to logging.

EDCON provided the gravity survey, made the needed corrections to the data, and computed the formation bulk density for each interval. Field operations went smoothly but had to be terminated prior to intended completion. An earthquake in Burma of Richter magnitude 7.5 generated strong earth vibrations that persisted for hours. Fortunately, data had already been obtained on the most important intervals before this event occurred. EDCON's data are given in TABLE 2.

ResTech, Houston provided this analysis with parameters such as matrix density, formation water resistivity, and Archie constants. They also supplied mean values of formation resistivity, TDT porosity, and calculated water saturation for each BHGL interval. The parameters used were:

Matrix density = 2.65 gm/cc,
Water density = 1.015 gm/cc
Water resistivity = 0.11 ohm-m at 162 degrees F,
Archie constants: $a = 1$, $m = 1.89$, $n = 1.79$

BHGL data and analysis are given in the next section of this report.

III. BHGL ANALYSIS AND RESULTS

Formation bulk densities derived from gravity data are given in Table 2. The gravity measurements underwent all applicable corrections including those for meter drift and for solar and lunar effects. The last column identifies each interval alphabetically to enable its location on crossplots.

The mean density of this group of 21 sands is 2.39 gm/cc. One interval, labeled F and which extends from 5363 to 5379 feet, departs significantly from this value. It has a bulk density of 2.18 gm/cc with measurement error limits of ± 0.022 gm/cc. (See EDCON final report for this derivation). This large departure of density from the mean suggests that interval F contains something other than water. However, this evidence alone is not unambiguous and other methods for examining the data are necessary.

BARCHIE METHOD

Values of porosity and water saturation were computed using the BARCHIE method described in Appendix 1. Formation resistivity, R_f , as measured by the original electric logs was used in this computation as well as the BHGL bulk density. The mean value of R_f for each interval was provided by ResTech, Houston along with the formation parameters listed in Part II of this report.

Figure 1 displays the results of these computations in the form of a crossplot of the BARCHIE computed porosity versus BHGM bulk density. With the exception of the interval labeled F, all intervals plot on or near the water line. Given perfect logs, all water-filled sands should plot on the water line. Any sand that contains fluids with a density less than water should plot below this line, as does F.

It is noteworthy that those intervals that have been produced fall on or near the water line. These are: A, C, E, and G. The intrusion of water as a consequence of production has caused an increase in their bulk density and has apparently "pushed" their plotting position towards the water line.

These effects can be graphically exaggerated by plotting the product of BARCHIE porosity and water saturation versus BHGM bulk density as shown in Figure 2. If a sand has 100% water, this multiplication will not change its position in the crossplot, as is demonstrated by intervals L, T, U, N, and O for example. However, interval F is now positioned well away from the others as a strong indication of some fluid content other than water.

In this context, interval H might be considered as being slightly suspect of containing something other than water.

COMBINED PNC AND BHGL LOGS

This method for cross-plotting PNC (pulse capture neutron) porosity versus BHGL density is described in Appendix 2. A TDT log was run in this well immediately prior to the BHGL; mean values of TDT porosity were provided by ResTech Houston. A cross-plot of TDT porosity vs. BHGL density is given in Figure 3.

Although significantly different physical methods are employed in this method, interval F again displays strong evidence of the presence of gas. Interval H which had shown a slight possibility in the BARCHIE method loses this possibility in this approach.

The displacement of all points other than F to positions above the water line can most likely be attributed to lithological effects on the TDT log, i.e., shaly sands with limey cementation. This effect does not pose a great hindrance to this method since only a

relative displacement of gas-bearing intervals is of interest.

These results again lead to a strong recommendation that interval F be perforated and tested.

TABLE 1

WELL DATA, SEELIGSON No. 1-89

<u>Perf. Interval,</u> <u>feet</u>	<u>-----CUMULATIVE-----</u>		<u>Approx</u> <u>BHGM zone</u>
	<u>Oil,</u> <u>Barrels</u>	<u>Gas,</u> <u>MCF</u>	
5202 5206	23743	180622	G
5535 5540	84101	1053879	C
6041 6054	30601	4095066	No BHGM log
5855 5862	51495	8215719	A
5456 5466	7861	23632	E

TABLE 2

BHGM DATA, SEELIGSON No. 1-89

<u>Depth Interval,</u> <u>feet</u>		<u>BHGM Density,</u> <u>gm/cc</u>	<u>Zone</u> <u>ID</u>
5850	5862	2.36	A
5680	5700	2.35	B
5530	5556	2.43	C
5516	5530	2.51	D
5455	5470	2.43	E
5363	5379	2.18	F
5180	5200	2.40	G
5002	5014	2.28	H
4872	4885	2.37	I
4830	4846	2.32	J
4750	4760	2.37	K
4690	4700	2.48	L
4630	4640	2.47	M
4510	4540	2.41	N
4431	4443	2.42	O
4409	4420	2.29	P
4383	4398	2.32	Q
4361	4371	2.42	R
4338	4349	2.44	S
4266	4278	2.48	T
4225	4235	2.47	U

FIGURE 1

SEELIGSON No. 1-89

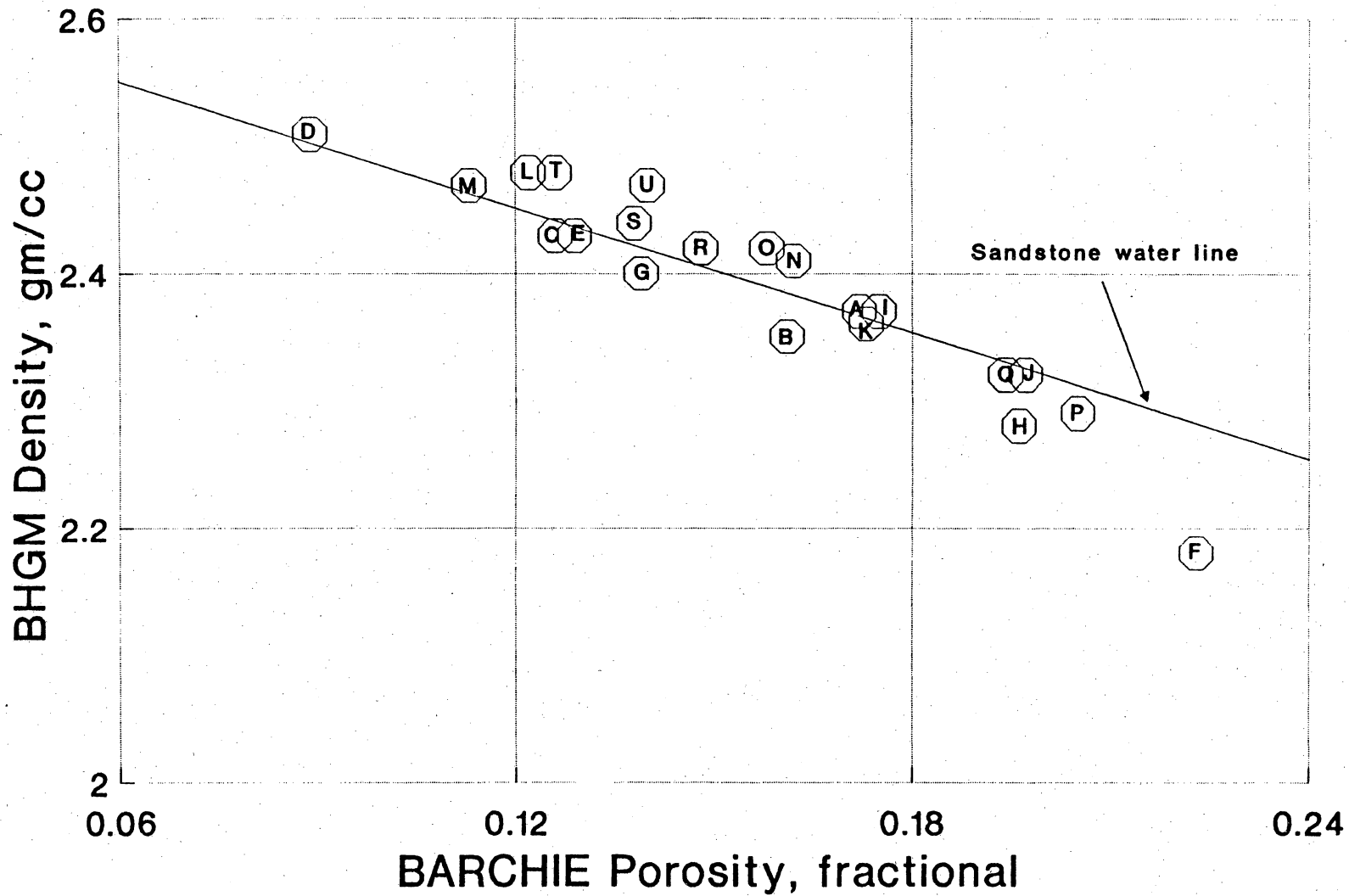


FIGURE 2

SEELIGSON No. 1-89

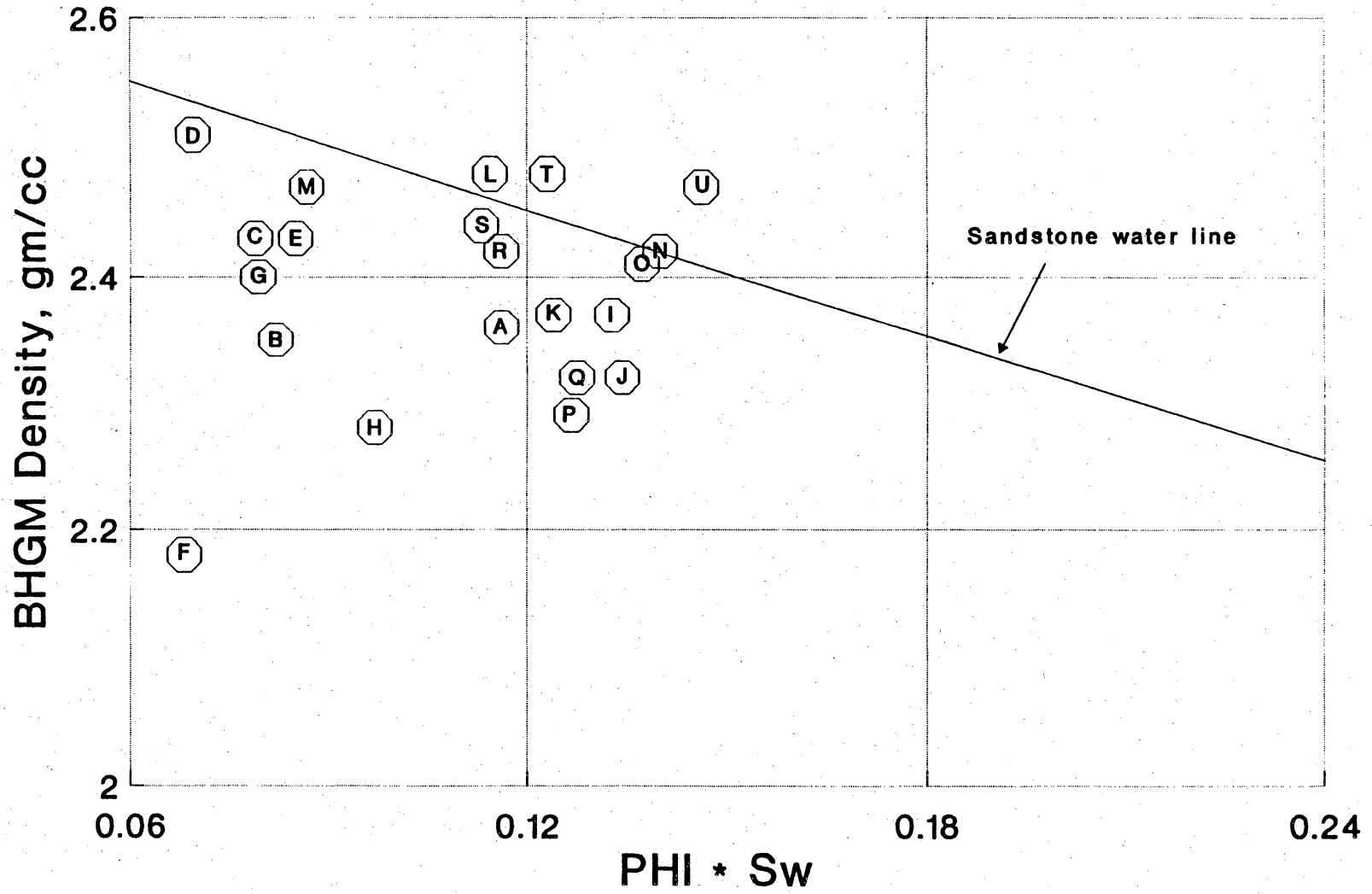
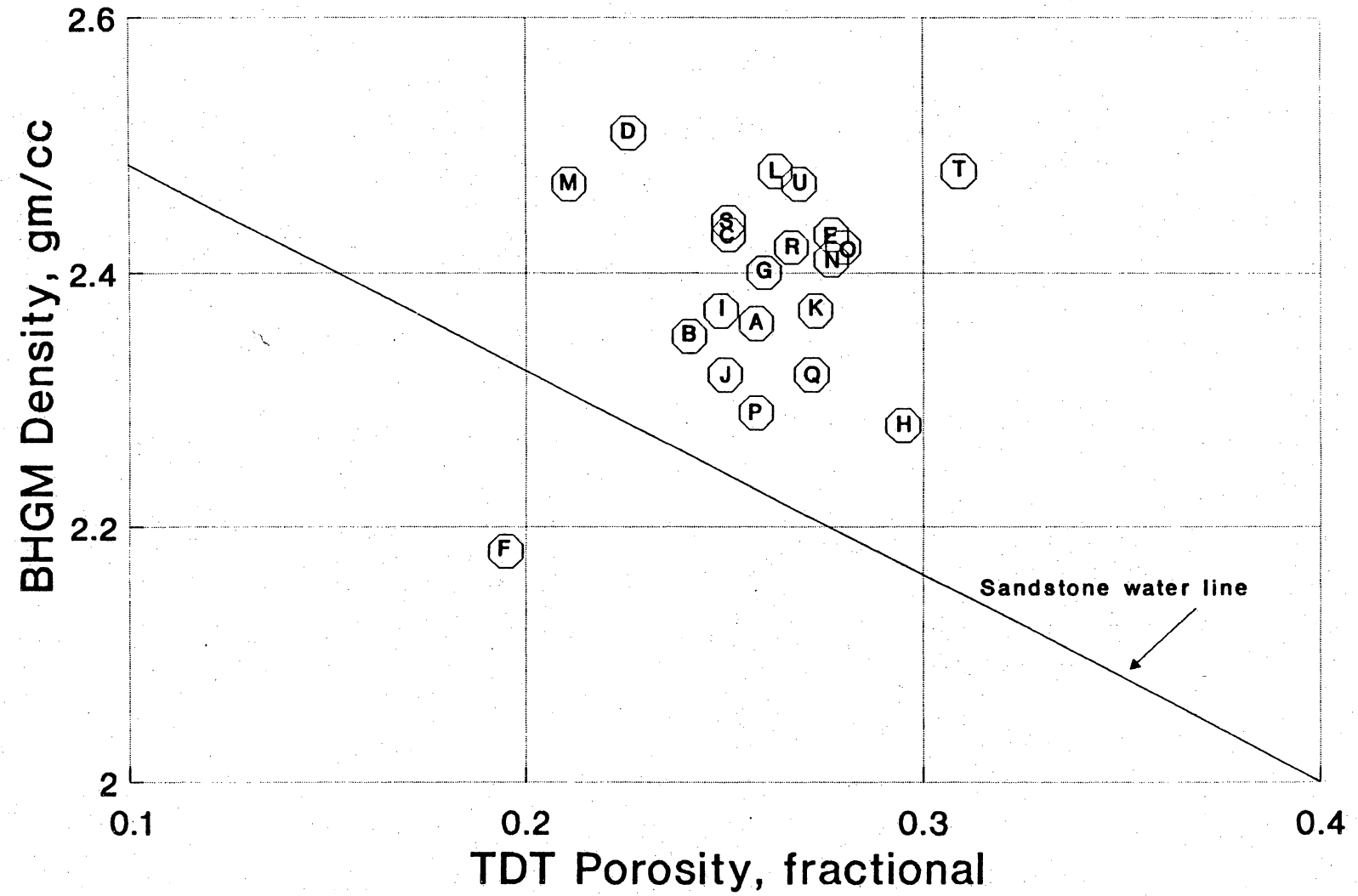


FIGURE 3

SEELIGSON No. 1-89



APPENDIX 1

BARCHIE METHOD

The method described here, and which was used in this analysis, employs two deep reading logging tools that sample a large volume of rock well away from the wellbore. The borehole gravity log has this inherent capability as does the lateral log and induction log. Together, these logs provide the capability for detecting gas away from the wellbore with reduced influence of near wellbore conditions. This combination also has value because the open hole lateral log was generally run in most wells drilled in the 40's to 60's and the BHGM can be used through casing as these same wells are re-entered today.

The name of this method derives from the combination of the BULK DENSITY equation (B) with the ARCHIE equation (ARCHIE).

The materials balance equation that relates BHGM-derived bulk density of a zone to its formation parameters is:

$$\rho_b = (1-\phi) \rho_{ma} + \phi [S_w(\rho_w - \rho_h) + \rho_h], \quad (1)$$

where

- ϕ = porosity
- ρ_{ma} = matrix density
- S_w = water saturation
- ρ_w = water density
- ρ_h = hydrocarbon density.

Archie's equation relating formation resistivity, porosity, and water saturation is given by Eqn. (2) as

$$S_w = [aR_w/R_t]^{1/n} \phi^{-m/n}, \quad (2)$$

where

- $aR_w\phi^m$ = formation factor
- R_t = formation resistivity
- m = cementation factor
- n = saturation index
- R_w = formation water resistivity.

If parameters such as a , m , n , ρ_{ma} , etc. are known with a reasonable degree of accuracy, one is left with two equations and two unknowns, i.e., porosity and water saturation. A simultaneous solution is now possible for these two factors if suitable density and resistivity logs are available. Eqn.(2) can be rearranged in the form

$$\phi = [aR_w/R_t]^{1/m} S_w^{-n/m}. \quad (3)$$

Substitution of Eqn. (3) into Eqn.(1) leads to:

$$0 = (\rho_{ma} - \rho_b) - [aR_w/R_t]^{1/m} S_w^{-n/m} [\rho_{ma} - S_w(\rho_w - \rho_h) - \rho_h] \quad (4)$$

in which porosity does not appear. Various methods can be employed to find a value of S_w that satisfies this equation. This value of S_w can then be substituted in Eqn. (1) to solve for porosity.

When deep reading logs such as the BHGM and the Lateralog are combined in this manner, a large volume of rock is examined at a distance well away from the wellbore.

Previous field results based on this technique were reported in the PROCEEDINGS TWENTY FIFTH ANNUAL MEETING AND SYMPOSIUM OF THE SOCIETY OF PROFESSIONAL WELL LOG ANALYSTS: NEW ORLEANS, JUNE 10-13, 1984, L.S. Gournay and W.D. Lyle.

APPENDIX 2

COMBINED PNC AND BHGM LOGS

Detection of gas within a formation with the BHGM is indirect since the tool only measures gravitational acceleration. It is from these measurements that the formation bulk density can be derived. Thus, an ambiguity in interpretation can result since the bulk density is influenced by both porosity and fluid saturation. This conclusion is clearly shown by the following materials balance equation:

$$\rho_b = (1 - \phi) \rho_{ma} + \phi [S_w (\rho_w - \rho_h) + \rho_h], \quad (1)$$

where

- ϕ = porosity
- ρ_{ma} = matrix density
- S_w = water saturation
- ρ_w = water density
- ρ_h = hydrocarbon density.

This equation contains two unknowns and consequently poses an ambiguity. A low BHGM density value could arise equally from a high porosity, water filled zone or from a low porosity, gas bearing zone.

The PNC log likewise has its limitations and faces some ambiguities. Porosity derived from this log generally assumes a water filled formation. However, if the formation contains gas, the PNC derived porosity will be lower than the true porosity. Thus a low PNC porosity value could be attributed equally to a water filled, low porosity zone or to a higher, gas-saturated porosity.

Other PNC gas indicators are hampered by a similar ambiguity: some tight zones give the same indication as higher porosity gas zones.

A combination of the BHGM and PNC logs can be useful for the removal of these ambiguities and for the enhancement of interpretation. A plot of BHGM bulk density vs. PNC porosity in Figure 1A of this appendix demonstrates this potential. The point "a" falls on the water line and represents a water filled sand of approximately 25% porosity and a corresponding bulk density of 2.24 gm/cc. Given perfect logs, all wet sands would fall on this water line.

If hypothetical sand "a" contains gas, the log data point will not plot at "a" but will be displaced to a lower PNC porosity such as "b" and to a lower BHGM density such as "d". Therefore, any intervals that fall significantly below the water line can be considered as suspect gas-bearing zones.

Conversely, if the interval has a low porosity the PNC value would again be shifted towards "b", but the BHGM density value should be high and shifted towards "c". Such zones should plot on or near the water line.

Details on corrections and field examples are given in THE LOG ANALYST, MAY-JUNE 1982, L.S. Gournay and R.E. Maute.

FIGURE 1A

